University of Huddersfield Repository

Leung, Pak Hung

Investigation on the Deformation of Cutaneous Blood Vessel in Relation to Pressure Ulcer Formation by Computational Modelling

Original Citation

Leung, Pak Hung (2019) Investigation on the Deformation of Cutaneous Blood Vessel in Relation to Pressure Ulcer Formation by Computational Modelling. Doctoral thesis, University of Huddersfield.

This version is available at http://eprints.hud.ac.uk/id/eprint/35198/

Investigation on the Deformation of Cutaneous Blood Vessel in Relation to Pressure Ulcer Formation by Computational Modelling

Pak Hung Leung

A thesis submitted to the University of Huddersfield in partial fulfilment of the requirements for the degree of Doctor of Philosophy

The University of Huddersfield

July 2019

Abstract

Pressure ulcer is a serious injury which affects the skin integrity of patients and is a financial burdens to healthcare providers worldwide. Pressure ulcers are usually caused either by excessive stress or ischemia which appears as deep tissue injury and superficial pressure ulcers respectively. Some of the pressure ulcers are known to be caused by the application of medical devices. These medical device related pressure ulcers are usually superficial and contribute to a significant numbers of the total number of pressure ulcers. The engineering community often focuses on the aetiology of excessive stress by developing computational models and investigating the *in vivo* conditions when a patient is subject to high loads. Limited attempts have been made on developing computational models for the aetiology of ischemia. Hence, it is the aim of the study to develop computational model to investigate the deformation of the cutaneous blood vessels in relation to the formation of superficial pressure ulcers.

This study provides information on the magnitudes of interface pressure experienced by patients in clinical setting experimentally by using pressure mapping system on both static and dynamic mattresses. Computational models are developed to demonstrate the *in vivo* cutaneous conditions and the relationship of mechanical loadings and the deformation of cutaneous blood vessels is established. The computational results is further correlated to a set of physiological data acquired by using laser Doppler technique to enhance the clinical relevance. The computational models and the established correlation is applied in three situations including; evaluating the effect of oxygen facial delivery masks on patients' skin; understanding the effect of same magnitude mechanical load on different skin conditions, and converting an external parameter, interface pressure from mattresses testing, into a physiological parameter. The overall study provides a novel tool for the medical device developers in evaluating the effects of their devices on patients' skin in relation to the formation of superficial pressure ulcers. The computational models and the established correlation with the physiological data allows the clinicians to understanding the *in vivo* cutaneous conditions of patients rather than just evaluating an external parameter.

Acknowledgement

Firstly, I would like to express my sincere gratitude to my supervisors Dr. Leigh Fleming, Dr. Karl Walton and Prof. Karen Ousey for their continuous support, motivation and patience through my Ph. D study. Their guidance helped me in all the time of research and writing of this thesis.

Beside my supervisors, I would like to thank the application engineer of the research centre, Mr. Chris Dawson, for his support and technical assistants.

I would also like to thank my friends including Chrystal, Kenny, Vincent, Ming and James for their support and motivation especially throughout the writing up period.

My biggest thanks to my parents William Leung and Wai Sau Au for their continuous support. I cannot imagine the differences I would have without their endless contributions.

Table of Contents

List of Figures

List of Tables

List of Equations

Chapter 1   Introduction

1.1.   Background of Study

Skin is the largest organ in human body, however, skin health is often neglected by the public. Failure of skin integrity is often perceived as minor health issue with insignificant effect on general health. In fact, skin serves its function in order to maintain health. It protects the inner organs, prevents the pathogens or chemicals from entering the body and maintains thermal balance. The failure of skin results in losing skin integrity and incapable of serving its functions.

Pressure ulcers, loss of integrity of skin due to application of mechanical loads which can range from slight discoloured skin to serious full thickness tissue loss, are one of the commonly found causes of losing skin integrity in any clinical settings including acute hospital wards, community hospital wards, mental health communities, nursing homes and residential care homes (Safety_Thermometer, 2018). Pressure ulcers are categorised by the wound depth and the affected tissues. The expose of bones can be the results of a Category IV, the most severe type, pressure ulcer which is the highest category. The Category III and IV pressure ulcers are susceptible in blood poisoning, bone and joint infection, necrotizing fasciitis, and gas gangrene which are all fatal.

Two aetiologies are associated with the formation mechanism of pressure ulcers, the first is excessive stress caused by distortion and the second is ischemia. Interface pressure applied on skin surface would result in non-uniformed distortions in deep tissue and results in internal stress due to the irregular shape of the bones (Menon, Cleary, & Lane, 2012). Maximum stress was found in the deep tissue, i.e. muscle and fat, when significant interface pressure is applied to the skin surface (Elsner & Gefen, 2008) and that explained the formation of Category III and IV pressure ulcers and deep tissue injury. Ischemia is another aetiology for the formation of pressure ulcers in

which interface pressure results in obstruction in the cutaneous blood flow. The oxygen and nutrient supply consequently become insufficient, the metabolic removal is impaired, pH values of tissue are decreased resulting in cell death ultimately. Although pressure ulcers caused by ischemia are often superficial and fall into Category I and II they are relatively minor compared to the Category III and IV. Category I and II pressure ulcers contribute to a significant portion of the total prevalence of pressure ulcers. Medical devices related pressure ulcers (MDRPU) are often caused by the aetiology of ischemia.

Efforts from the engineering society to the field of pressure ulcer prevention is significant especially during the last couple of decades. Computational models were developed to demonstrate the *in vivo* conditions and contribute to the understanding of the formation of the deep tissue injury. Computational models allow the approximations of the internal stress distributions when interface pressure is applied on the skin surface. This fills the gaps of incapability in recognising stress distributions in clinical practice. These developed computational models are also utilised for evaluating the effect of a medical devices and the results are more scientific than just statistical analysis for live human trials. However, the engineering society mainly focuses on the aetiology of excessive stress caused by distortion. Limited attempts have been made to understand the formation of pressure ulcers caused by ischemia. Hence, there is a lack of computational models or tools to understand or evaluate the *in vivo* conditions in relation to the formation of ischemic pressure ulcers.

The aim of the project is to develop a computational model to demonstrate the effect of applied mechanical loads on the formation of superficial pressure ulcers. Objectives listed below are set for achieving the aim of the project:

I)   To gain better understanding in pressure ulcers preventions and the current input from the engineering society to the field. This allows to discover the needs of the field and methods of developing related tools for pressure ulcer preventions.

II)   To acquire the relevant mechanical properties and physical dimensions of the cutaneous layers which serve as the foundations and bases of the developed computational models.

III)   To investigate and acquire the commonly found magnitudes of interface pressure in clinical setting to be a reference of the working range of the developed computational model. Also, to be used as an application of the developed model.

IV)   To investigate and demonstrate, by utilising the developed model, the percentage change of the cross-sectional area of the cutaneous blood vessels (CBV) under a range of magnitudes of the applied mechanical loads.

V)   To establish a correlation between the computational data produced by the developed model with a set of physiological data, percentage change of the cutaneous blood flow velocity, acquired by utilising Laser Doppler technique.

VI)   To conduct three applications including physiological data for oxygen delivery mask and mattresses and alternate skin conditions. And to demonstrate the usages of the developed computational model as well as the established correlation with a set of physiological data.

The culmination of results from all the component studies and achievement of the objectives provided an initial tool for evaluating the effect of mechanical loads on the formation of superficial pressure ulcers. This is a novel tool in the field of pressure

ulcer prevention for superficial pressure ulcers which is often caused by ischemia. The lack a related tool results in inadequate determining the effects of medical devices on the formation of superficial pressure ulcers. The developed model in this study has similar aims as other developed computational models in the field which demonstrate the *in vivo* conditions and evaluate the effect of medical devices on the formation of pressure ulcers.

1.2.   Overview of Thesis

The thesis comprises eleven chapters including the introduction.

Chapter 2

Chapter 2 focuses on the physiological and anatomical structure of human skin and background research on the mechanical properties and dimensions of the cutaneous layers. All the information from this chapters contributes to the computational modelling.

Chapter 3

Chapter 3 is dedicated to review the existing scientific researches on the formation of pressure ulcers and discover the needs of more engineering input in the field of pressure ulcer prevention. Previous computational models are discussed.

Chapter 4

Chapter 4 is relating to the methodologies adopted in the current studies including the main techniques applied, Finite Element Method (FEM), pressure mapping measurement and laser Doppler Velocimetry. These methods are inter-related and affect the results produced in different components of the study.

Chapter 5

Chapter 5 consists of two pressure mapping measurements on static and dynamic mattresses respectively. The peak pressure is recorded in each of the measurement and the ranges of magnitudes were analysed. The results of this chapter are the reference as the working range of the newly developed computational model in later chapters. The findings in this chapter will also be used as the last application of the developed model in Chapter 8.

Chapter 6

Chapter 6 presents the "quartered model" which is a first of its kind computational model capable of demonstrating the deformation of CBV. This model is utilised and demonstrates the effect of the mechanical loads on the CBV of a healthy volunteer in sitting positions. A numerical data is provided in terms of the percentage change of the cross-sectional area of the CBV which is never acquired before.

Chapter 7

Chapter 7 consists of two parts including the presentation of "halved model" with the advancements from the quartered model and the effect of a range of magnitudes of mechanical loads on the CBV simulated by the halved model. This application of the halved model generates a set of computational data of a range of magnitudes of applied pressure to the percentage change of the cross-sectional area of the CBV. This is unable to achieve without a relevant computational model as it would be impossible to measure the percentage change of CBV *in vivo* while applying mechanical loads despite the advancement of medical imaging techniques.

Chapter 8

Chapter 8 consists of two parts including the acquisition of the physiological data by utilising Laser Doppler technique and establishment of the correlation between the computational and physiological data. A set of computational data is not clinically and physiologically relevant if it is not validated or correlated to a set of physiological data. Hence, the aims of chapter 8 is to acquire the effect of a range of magnitudes of applied mechanical loads on the percentage change in the cutaneous blood flow velocity and correlate it to the computational data. This allows the computational data to be clinically and physiologically relevant and an external parameter, i.e. applied pressure, to be converted to a physiological parameter, cutaneous blood flow velocity. This allows more meaningful evaluation of the effect of applied mechanical loads on the formation of superficial pressure ulcers. The effect of a commonly used medical devices, oxygen delivery mask, on the cutaneous blood flow velocity is demonstrated by the halved model and the established correlation. The second application in the study is demonstrating the effect of same magnitude mechanical load on the cutaneous blood flow velocity when the mechanical properties of the cutaneous layers are varied. This shows that the developed model and the established correlation are a good tool in analysing the effect of different mechanical properties on the formation of pressure ulcers. The final application is to evaluate the effectiveness of the static and dynamic mattresses in terms of a physiological parameter, percentage change in the cutaneous blood flow velocity. This is the first attempt in evaluating the effectiveness of a pressure redistribution mattress by analysing not only the interface pressure but also the physiological effect on skin.

Chapter 9 and 10

Chapter 9 and 10 are the discussion and conclusion chapters respectively. They discuss on all the components conducted in the study and emphasise the contribution to the

field of pressure ulcer prevention by the developed model and the established correlation for clinical and physiological relevance. The limitations of the developed model are discussed which is also the direction of further study.

Chapter 11

Chapter 11 reviews the project so far and proposes further developments which include enhancing the physiological relevancy of the computational model and the accuracy of the acquired physiological data as well as increasing the functionality of the computational model.

Chapter 2   Human Skin

2.1. Introduction

Skin is a versatile organ which is a barrier of the human body providing direct contact and protection from the external environment. Millington and Wilkinson commented that a healthy and intact skin is required as it is vital to maintain a healthy and intact skin to serve its functions including, thermoregulation and prohibiting pathogens and chemicals from entering the body (Millington & Wilkinson, 2009).

Dermatology, the study of skin health is an extensive and complex field. Many parameters and factors are associated with, and have an impact upon skin integrity, for instance, pigmentation, appendages, viscoelastic property, young's moduli, configurations of cutaneous blood vessel and topology. One of the conditions which can affect skin integrity is "pressure ulcers" which occur due to different loads being applied on skin through a number of different mechanisms. The formation of pressure ulcers can be investigated from both the mechanical engineering and the physiological perspective, and some variables in the system which causes pressure ulcers are more related to the formation of the pressure ulcer than others; for instance, the thicknesses of skin, the vascularisation of cutaneous layers and various mechanical properties of the skin which can be influenced by a wide variety of factors. This chapter will explore, from a mechanical engineering perspective: general skin properties which are relating to the formation of pressure ulcers including the key cutaneous properties and the information related to computational modelling.

2.2. Nature and Functionality of Skin

Skin is the largest organ which is approximately 4 kg in weight contributing 5.5% - 8.33% of the total weight of a human body (Edwards & Marks, 1995; Millington &

Wilkinson, 2009). The surface area of skin is very difficult to be measured precisely due to the presence of the folds on the skin surface but Millington et. al. estimated that the skin surface area was approximately 1.2 to 2.0 square metres (Millington & Wilkinson, 2009). Skin is the periphery of a human body contacting the external environment which serves a number of important functions. The thermoregulatory function of skin enables the human body to maintain a constant temperature. Aside from the little heat loss contributed by the respiratory system, a human body mainly losses heat to maintain a thermobalance by controlling the cutaneous blood flow and thermal sweating on skin. Higher temperature differences are achieved by allowing higher cutaneous blood flow rate when the human body needs to be cooled down. Sweating is also an effective method of losing large amount of heat energy by evaporation (Cranston, 1989). Humans are exposed to a range of physical and chemical stimuli in daily life, for instance, pathogens in the environment, soaps for cleaning the body, interaction and friction between skin and textiles at the interface with clothing or other materials. The structures and the self-repairing function of skin enable it to be a robust barrier to these harmful stimuli. As the main periphery between the human body and the environment, skin facilitates one of the five basic senses of perception (somatosensation) while the other four senses are vision, audition, gustation and olfaction. Sibbald deemed that skin can also be an indicator of the general state of a human body, for instance, changes in skin colour, turgor or integrity resulting from the dying process (Sibbald, Krasner, & Lutz, 2010).

2.3. Structure of Skin

Skin is a three-layered organ with the dermis being regarded as the primary structure. The dermis layer of skin is overlaid by a layer named epidermis as shown in Figure 2.1. Although this epidermis is also multilayer, only the superficial layer named stratum

corneum (SC) at the outermost of epidermis was taken separately into account to the computational modelling of the formation of pressure ulcers on skin in this study because the SC is a layer of dead cells and significantly stiffer than the rest of the epidermis named "viable epidermis".
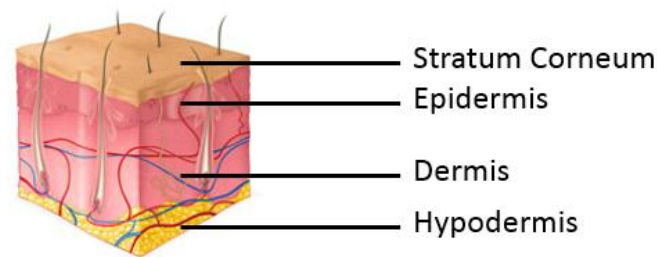
Figure 2.1   Histological diagram of the cutaneous layers (ISIIP, 2016)

2.3.1. Epidermis

Epidermis is the outermost layer of the cutaneous structure which is the first contact with the environment. The epidermis consists of stratum corneum, stratum lucidum, stratum granulosum, stratum spinosum and stratum germinativum from the outermost layer to the innermost layer respectively (Millington & Wilkinson, 2009). Stratum corneum which is the outermost layer of the epidermis is identified by its distinctive formation mechanism and mechanical properties. The formation process of the stratum corneum is regarded as the dying progress of the inner layers of the epidermis, cells of the epidermis move toward the external environment and the cells are flattened and dead. The layers of dead coenocytes provide the structure of the stratum corneum (Millington & Wilkinson, 2009). This layer of dead cells is much stiffer than the rest of the layers of the epidermis named viable epidermis. Kendall and Chong et al. study concurred that the general stiffness of the stratum corneum was distinctively higher compared to the other layers of the epidermis, especially at the outer side of the stratum corneum despite the mechanical properties of the stratum corneum varying dramatically with the influence of temperature, relative humidity,

hydration and chemicals. (Kendall, Chong, & Cock, 2007).

2.3.2. Dermis

Dermis layer which is the primary structure of the human skin is hard to be defined as it merges into the sub-cutaneous layer, hypodermis. Dermis consists of two layers which are papillary and reticular. The papillary layer is located in between the epidermis and reticular layer. The papillary layer consists of fine connective tissue fibres, fine capillaries loops and nerve endings. Thick, coarse and densely interlacing collagenous fibres are presence at the reticular layer of dermis in which they are mostly parallel to the skin surface. (Millington & Wilkinson, 2009).

2.3.3. Hypodermis

Theoretically, the hypodermis is not part of the cutaneous structure, it is an extension of the dermis layer. However, the behaviours of skin are different with the presence of the hypodermis layers in computational modelling. Hence, it would be appropriate to consider the hypodermis layer in the construction of any cutaneous computational model. Major blood vessels are located in the hypodermis layer, hence, the hypodermis layer is deemed to be highly vascularised (Saladin, 2007) with the thickness of hypodermis varying considerably depending on the anatomical locations and age. Taking the abdomen as an example, this layer could be 10 centimetres or even thicker (Millington & Wilkinson, 2009) while the hypodermis at the triceps was only 2.96 ± 2.35 millimetres in a study conducted by Akkus et al. (Akkus, 2012). The presence of the hypodermis layer in the computational model enables the simulations of more realistic behaviours of the cutaneous layers.

2.3.4. Thickness of the Cutaneous Layer

The thickness of skin is a key parameter to the computational modelling as it directly affects the geometry of the computational models and ultimately the accuracy and level of clinical and physiological relevancy of the analysis. However, the thickness of the cutaneous layers depends on a range of factors such as the anatomical locations, genders, ages etc. It is difficult to have an absolute thickness to represent members of the general public. However, some research findings regarding the thickness of skin is summarised in Table 2.1. Owing to the thicknesses of the different layers of skin shown in Table 2.1 are depending on gender, age, anatomical location as well as the types of testing methods, the values of the thickness in different studies are not directly comparable. The existing studies found and presented in Table 2.1 were mostly layer specific and as such, none of the studies focused on every layer of the skin. Nevertheless, a systematic computational model of skin by Leveque et al. in 2013 provided a set of thicknesses and mechanical properties to the key layers of the skin which is discussed in detail in Section 2.4.2 (Lévêque & Audoly, 2013).

Table 2.1 Summary of the thicknesses of skin

Testing Environment	Type of Examination	Layer of Skin	Anatomical Location	Thickness (µm)	Reference
In vitro	Biopsy from live patients	Whole skin	Eyelid, prepuce, back, palm, sole	521 - 1,977	(Lee & Hwang, 2002)
		Epidermis		31 - 637	
		Dermis		469 - 1,942	
In vitro	Biopsy from volunteers	Stratum Corneum	Forearm, shoulder, scapula, buttock	11.0 - 18.3	(Sandby-Moller, Poulsen, & Wulf, 2003)
		Epidermis		74.9 - 96.5	
In vivo	Ultrasound	Whole skin	Upper arm, abdomen anterior, anterior of upper leg	1,930 - 2,350	(Akkus, 2012)
		Hypodermis		3,650 - 17,870	
In vitro	Biopsy from cadavers	Epidermis	Head	29.6 - 62.6	(Chopra et al., 2015)
		Dermis		758.9 - 1,969.2	

2.4. Mechanical Properties of Skin

2.4.1. Testing Methods of Skin

Skin is the largest organ of the human body with the mechanical properties being investigated in an attempt to develop new technologies and techniques to understand

behaviour of skin under different types of mechanical loading regimes. Panzer's (2018) study identifying the mechanical properties of skin served different purposes including understanding the effect of ageing, evaluating the effects of cosmetic products, developing better procedures for treatment of skin or skin closure, designing and manufacturing humanoid dummies for different tests. Testing methods of evaluating the mechanical properties of skin are categorised as *in vivo* and *in vitro*. The *in vitro* tests include tensile, nano-indentation and compression while the *in vivo* tests include torsion, tension, suction and indentation.

Skin is a live organ obtaining a supply of nutrients and water through the blood circulation and as such skin loses its metabolic supply once the sample of skin is detached from live donors. The skin samples excised from cadavers also do not give a true representation of the skin *in vivo* due to the metabolic supply through blood circulation ceases immediately following the death of the donor. The *in vivo* test captures the actual behaviours and performance of skin whereas *in vitro* tests can give a comparative evaluation of skin behaviours, but will never give a fully quantitative evaluation due to the rapid deterioration in condition. The use of *in vivo* test to determine mechanical properties of the skin are usually conducted by means of applying specific mechanical loading to live human skin with the behaviours of the skin under different magnitude of loading being observed and recorded. The limitations of i*n vivo* test methods are significant due to the damage which can be caused by loading skin, the range in which skin can be tested therefore is narrow and does not give a huge amount of scope for data collection. *In vivo* tensile testing is a measure of the force required to elongate a certain area of skin. The magnitudes of the force causing a prescribed magnitude of displacement on skin is recorded by the *in vivo* tensile test machine. *In vivo* torsion test on skin is performed by attaching solid disc to the human skin with applied torque. Hence the anisotropic mechanical properties of skin are

evaluated. These *in vivo* tensile and torsion testing methods are applied in plane mechanical loadings to evaluate mechanical properties of the superficial layers with minimum effects of the deeper layers including dermis and hypodermis. *In vivo* suction and indentation are two methods which apply mechanical loadings perpendicular to the skin surface. Hence, the presences of the deeper tissues contribute to the overall mechanical properties of the whole skin (Groves, 2012). The suction test creates a decrease in pressure on the surface of skin resulting in deformation of skin in vertical direction to analyse the magnitude of the deformation and ultimately the elasticity of skin affected by the skin layers. As opposite to the *in vivo* suction test, the *in vivo* indentation test is applying a mechanical load using a probe applied to the skin surface. The displacement of the probe is recorded and analysed to evaluate the elasticity of the skin. In order to evaluate the mechanical properties at different scales, a range of different sized probes and suction cups can be used. Smaller and larger sized indentation probes and cups were utilised for evaluating the mechanical properties of superficial layers and deeper layers of skin respectively (Hendriks, Brokken, Oomens, & Baaijens, 2004).

The *in vitro* test methods are another strategy for evaluating the mechanical properties of skin. *In vitro* tests are similar to the standard engineering methods for quantifying the mechanical properties of materials. However, *in vitro* tests provide opportunities for understanding the behaviours of skin under different extreme conditions, for instance, the ultimate tensile strength of skin (Gallagher, Ní Annaidh, Bruyère, & al, 2012). The orientations of the *in vitro* test are more fixable. Skin is known to be anisotropic and the orientation of test affects the magnitude of the mechanical properties (Panzer, 2018). Wang in 2013 discovered that the anatomical locations did have significant influences on the mechanical properties of the skin by examining the skin samples excised from mice (Wang, Marshall, Baba, Gerling, & Lumpkin, 2013). The

tests of extreme conditions are not ethical to be conducted on live humans or animals. Thus, *in vitro* test is the method of understanding skin under various conditions including under the influence of extreme magnitudes of mechanical loads. Skin is also a multi-layered organ and the mechanical properties of skin are distinctive across the layers. For *in vitro* tests, different layers can be isolated before testing to evaluate the mechanical properties of individual layers without the influences of other layers. Therefore, it provides better understanding of the mechanical properties of individual layers of skin. Two common *in vitro* methods are tensile and nano-indentation tests. Unlike the *in vivo* tensile test, the magnitude of the applied displacement is predetermined before conducting an *in vitro* test. There is no limit to the displacement as the skin sample is detached and the displacement does not cause any harm to the donors or cadavers. The mechanism of the *in vitro* tensile test is, the same as the *in vivo*, to record the magnitude of force required to cause a certain displacement in order to deduce the mechanical properties. The *in vitro* and *in vivo* indentation testing methods are similar. The *in vitro* indentation testing is to indent into excised skin samples as opposed to live human participants as for *in vivo* indentation test. Grant (2012) measured the viscoelastic behaviour of skin by utilising atomic force microscopy (AFM) as a tool for nano-indentation. Also, the static moduli of normal skin and scar skin were determined (Grant, Twigg, & Tobin, 2012). This study showed scar skin has weaker viscoelastic creep and capability to orientate fibres but more importantly AFM is an effective tool for evaluating different mechanical properties of skin.

2.4.2. Mechanical parameters of skin

The mechanical properties of cutaneous layers are very difficult to be discerned due to the different methods adopted as mentioned before in Section 2.4.1. It was found

that the values of the mechanical properties also vary for a range of factors including age, anatomical location, test methods, test apparatus, hydration levels and the period of the sample being excised from the donors or cadavers (Kalra & Lowe, 2016). Hence, a wide range of values of the mechanical properties in the literature is found. The values of the mechanical properties of skin are summarised in Table 2.2. The values of the parameters are in a range rather than a specific value because of the multiple sample evaluated or number of measurements. This posed a challenge in the computational modelling of skin, typically in selecting the relevant values for the simulations.

Table 2.2 Table of the mechanical properties of skin

Testing Enviornment	Mechanical Testing	Layer of Skin	Parameters	Reference
In vivo	Torsion	Whole skin (dorsal forearm)	Young's Modulus: 0.42 - 0.85MPa	(P. G. Agache, Monneur, Leveque, & De Rigal, 1980)
In vitro	Tensile	Whole skin	Young's Modulus: 5 - 30MPa Ultimate Tensile Strength: 15 - 150MPa	(Edwards & Marks, 1995)
In vitro	Indentation	Stratum Corneum	Young's Modulus: 2.6 ± 0.6MPa	(Geerligs et al., 2011)
		Epidermis	Young's Modulus: 1.1 ± 0.2MPa	
	Others	Stratum Corneum and Epidermis	Young's Modulus 1MPa	
In vitro	Tensile	Whole skin (backs of cadavers)	UTS: 27.2 ± 9.3MPa Young's Modulus: 98.97 ± 97MPa	(Gallagher et al., 2012)

Table 2.2 summarised the Young's moduli and Ultimate Tensile Strength (UTS) found by researchers which showed various tests were conducted to understand the magnitudes of the young's moduli and UTS of skin. The studies focused on the influence of mechanical properties of a specific layer of skin and a whole layer of skin. Luebberding conducted an evaluation of the mechanical properties of skin in related to ageing (Luebberding, Krueger, & Kerscher, 2014). This study highlighted the decline of the values of the elasticity of skin with ageing. A better understanding of skin in relating to age was established. Gallagher conducted tensile tests for the skin samples excised from cadavers which determined a young's modulus of 98.97± 97MPa (Gallagher et al., 2012). These two studies demonstrated classic dermatological measurement to obtain mechanical properties of skin under various measurement conditions, such as anisotropic nature of skin and the sensitivity of biological samples to measurement conditions. Both Luebberding et al., and Gallagher's research results concluded a lack of a comprehensive study on the mechanical properties of skin for all layers. The studies either focused on the complete skin (overall effects across the layers) or specific layers in relating to specific factors. There is little (if any) understanding on the influence of the individual cutaneous layers to the global skin mechanical properties.

Lévêque and Audoly (2013) developed a three-layered two-dimensional finite element computational model for investigating the influence of the thickness and stiffness of the stratum corneum (SC) to the global mechanical properties of skin and the amplitudes and periodicity of fold formation in 2013 (Lévêque & Audoly, 2013). The study also identified difficulties in determining the influence of individual cutaneous layers to the global skin mechanical properties by *in vivo* methods as the epidermis

and dermis layers are both soft and complex bio-composite materials with distinctive dimension and structure. Hence, a three-layered computational model with respective mechanical properties assigned to the individual layer was developed by Lévêque and Audoly to understand the fold formation of skin influenced by the stratum corneum layer. In Lévêque and Audoly's model, the mechanical properties of the stratum corneum was set from 1 to 12 MPa in which the range of the stiffness was acquired from The "Hand book of non-invasive methods and the skin" (Jorgen Serup). The young's moduli of the epidermis and dermis was set to be 0.05MPa and 0.6MPa respectively based on the assumption of softness of the living epidermis and *in vitro* observation. The thicknesses of the cutaneous layers of 10 to 20μm for the stratum corneum, 50μm for epidermis and 1,285μm for dermis were determined through calculation. The authors concluded that the layer of the stratum corneum contributed considerably to the global mechanical properties of skin because of the significantly stiffer properties of the SC layer. The developed model in Lévêque and Audoly's study was proven to be a numerically efficient and a straightforward application. Indeed, the study was a versatile tool and knowledge for various applications, such as for evaluating the effectiveness of cosmetic products which were mainly focused on the influence on the change in the properties and dimensions of SC layers. The study filled the gap of knowledge in the understanding of the individual cutaneous layers by providing a full set of mechanical properties and dimensions of cutaneous layers. This had a significant impact of the later research on the computational modelling of cutaneous layers. This set of mechanical properties of human skin is also adopted in the current study.

2.5. Properties of Skin

2.5.1.   Anisotropic properties of skin

Skin has been recognised as an anisotropic material since early tests on the mechanical properties of skin were conducted (Dupuytren, 1836; Langer, 1978a, 1978b). The early tests were mainly conducted by observations of the changes on punched cadavers' wounds. Langer (1978) discovered that the skin was pre-stressed in specific direction by observing the punctures created by the awl on cadavers' skin. The circular punctures became elliptical holes, commonly known "Langer Lines" (Figure 2.2). A and B of Figure 2.2 show the Langer lines on the anterior and posterior side of a human body respectively. The discovery of Langer lines had significant impact to different medical fields, for instance, surgical wounds were found to heal better with less scaring if incisions were made parallel to the Langer lines (MXP, 2017). Langer also investigated the mechanical properties of skin by hanging weight on the strips of skin samples which were harvested from cadavers along and perpendicular to the Langer lines. More extensions were found on the strips of skin samples harvested perpendicular to than along the Langer lines (Langer, 1978b). However, Millington and Wilkinson deemed that patterns of Langer lines could change at different physiological situations, for instance the pattern of Langer lines changed at the abdominal skin to allow the pregnancy or from mainly circumferential to adult pattern for infants below the age of two (Millington & Wilkinson, 2009).
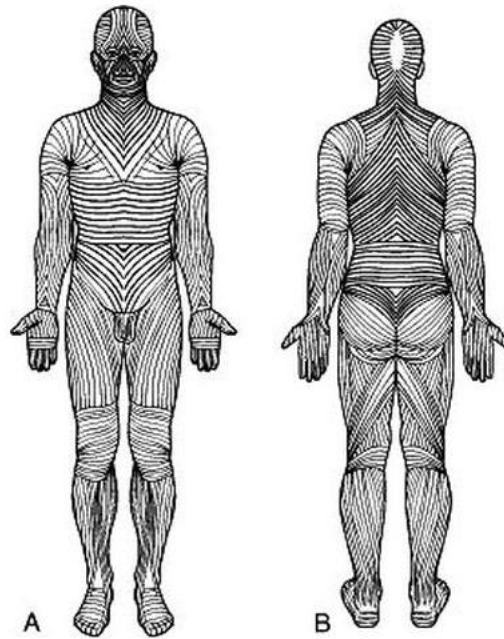
Figure 2.2   Langer lines of a human body (Schierling, 2018)

Figure 2.3 presents a schematic diagram of the Langer lines of a skin sample in which the red lines represent the Langer lines. The extension ability of skin caused by a mechanical load was demonstrated by Langer in which higher extensibility was found on skin samples harvested perpendicular rather than parallel to the Langer lines. Little attention was paid to the effect of the Langer lines in Y-direction of the skin in Figure 2.3 due to the difficulty in investigating the mechanical properties in Y-direction. In fact, not just the anisotropic aspect of skin in Y-direction was not well researched but also the general mechanical properties of skin in Y-direction. This was compounded by the technical difficulty in harvesting and preparing a valid skin sample in Y-direction. The thickness of a whole skin was found to be 521 to 2,350µm as shown in Table 2.1 in Section 2.3.4 and the skin sample was too thin to be clamped for examining the mechanical properties in Y-direction. However, it is reasonable to assume that the extensibility of a skin sample harvested in Y-direction is higher than in Z-direction because, theoretically, the Y-direction was also perpendicular to the Langer lines as

the skin is a 3-dimensional material or structure.
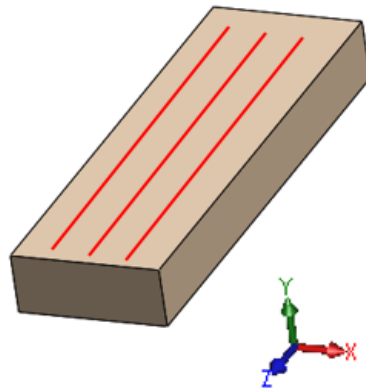
Figure 2.3　　　Schematic diagram of the Langer lines

2.5.2.　Non-linearity of skin

"Linear property" of a material means the relationship of an extension of the material is linear to the magnitudes of the applied loading. However, human skin is far from a linear material (Millington & Wilkinson, 2009). The extensibility of skin changes significantly with the magnitude of the applied mechanical load. Figure 2.4 demonstrates the behaviour of skin under different magnitudes of applied load. The X axis and Y axis in Figure 2.4 represents the strain and stress respectively. The stress and strain are defined as the magnitude of load divided by the cross-sectional area and the magnitude of deformation divided by the original length respectively. As opposed to a linear graph, the curve in Figure 2.4 is non-linear. The skin showed three distinctive phases during the loading progress labelled as I, II and III in Figure 2.4.

In Phase I, the skin extends significantly with relatively low magnitude of applied stress. In Phase II, the skin starts to be stiffened and less amount of strain is caused by relatively high magnitudes of applied stress. By the end of Phase II, most of the fibres are found to be orientated toward the direction of applied load and straightened. In

Phase III, the extensibility of the skin is mainly contributed by the stiffness of the fibres, thus, only little strain was found with high magnitude of stress (Millington & Wilkinson, 2009).
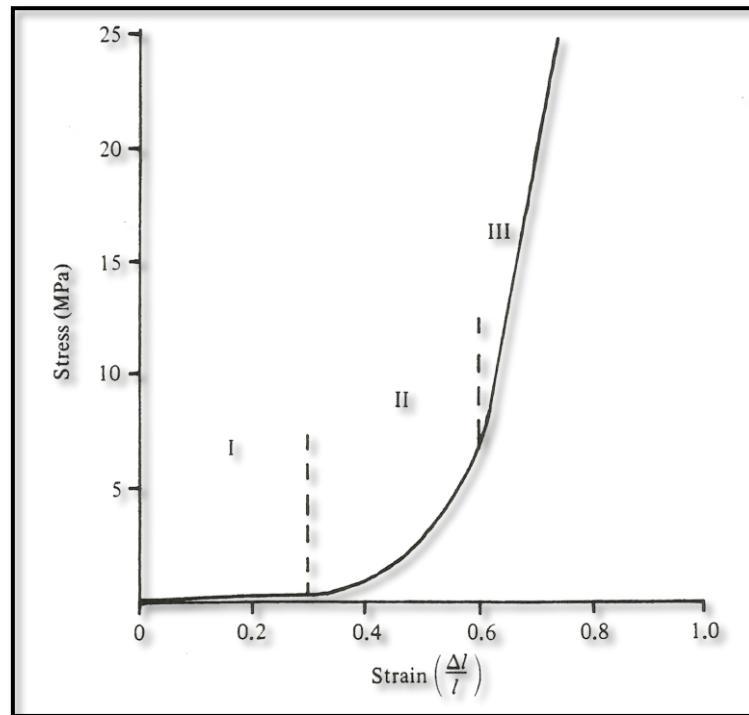
Figure 2.4   Stress-strain curve of a whole skin (Millington & Wilkinson, 2009)

2.5.3.   Viscoelasticity of skin

The viscoelasticity consists of two distinctive phenomena: creep and stress relaxation. Creep and stress relaxation are defined as "The continuous deformation of a material under a constant stress that is well below its yield point" by the Dictionary of Physics ("creep," 2015) and "The reduction in stress with time when the strain is kept constant in a time-dependent material" by the Dictionary of Mechanical Engineering ("stress relaxation," 2013) respectively. One of the examples of stress relaxation in physiological condition is the urinary bladder. The biological function of the urinary bladder highlights the importance of the stress relaxation function. The stress/

pressure only increases with a small amount when the urine flows in urinary bladder ensuring the urine is not back flowed to the kidney due to the high pressure from the bladder (Klabunde, 2007). In contrast, the degree of creep is a measurement of the increase in strain at a constant magnitude of stress with time. Skin demonstrates creep property shown by different research. Agache et al. in 2000 discovered that the creep phenomenon were divided into 3 phases, stage I, stage II and stage III corresponding to the purely elastic deformation, viscoelastic phases and constant creep phase respectively shown in Figure 2.5 (Agache, 2000). However, Khatyr et al. identified that the model developed by Agache could not always represent the reality due to the fact that the creep behaviour suggested by Agache would tend to infinity with time as shown in Figure 2.5 (Khatyr, Imberdis, Vescovo, Varchon, & Lagarde, 2004). In fact, it was very difficult to monitor the creep or stress relaxation responses because the key responses occurred immediately after the initial stretching as these responses were usually in exponential decay (Millington & Wilkinson, 2009). Hence the accuracy in the acquired figures or data in the viscoelasticity of skin was not certain.
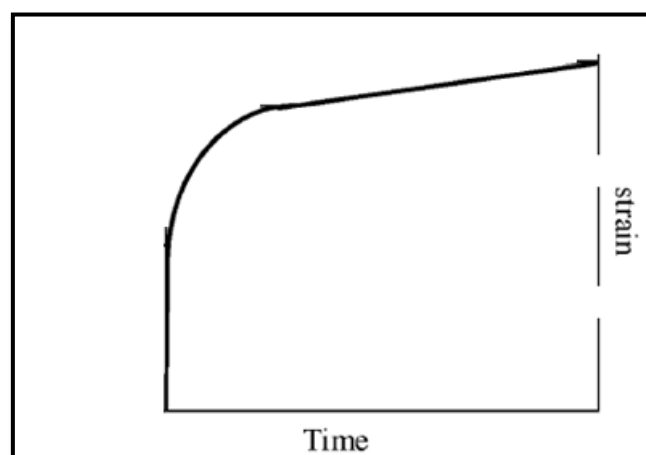
Figure 2.5   Creep phenomenon of skin (Agache, 2000).

2.5.4. Ageing effect of skin

Ageing phenomenon of skin relates to the field of skin integrity and the ageing effects. Ageing effects of skin was investigated on both skin sample of human *in vitro*, *in vivo* and on skin samples of rat over the years. Vogel discovered that the parameters of ultimate load and tensile strength of rats' skin increased with age, reached the maximum at the age of 12 months and decreased after the age of 24 months (Vogel, 1976). For human experiments, skin samples were harder to be harvested and therefore *in vivo* studies were conducted. Graham's study by using the suction cup method demonstrated that the elastic modulus of the participants increased with age and higher averaged values were found in female subjects than male subjects. (Grahame, 1970). Diridollou found an increase of thickness of skin from 0 to 20 years old for human participants and a decrease in thickness after the age of 60, however, the decrease trend was not significant for men. In the same study conducted by Diridollou, Young's modulus of skin was found to be increased with age from 20 to 90 years old (Diridollou et al., 2001). In general, skin is stiffer, thinner, less tense and less flexible as a result of ageing (Pawlaczyk, Lelonkiewicz, & Wieczorowski, 2013). Similar to the values of the mechanical properties and thicknesses of skin presented in Sections 2.3.4 and 2.4.2, it was very difficult to have an exact value to represent the effect of ageing on skin as the characteristics of skin varies significantly.

2.6. Vascularisation of Skin

The vascularisation of skin is a transportation system for providing nutrients, removing metabolic wastes at the cutaneous layers and also a regulating system of temperature for the human body. The vascularisation is relating to the formation of pressure ulcer on skin especially to the aetiology of ischemia. Ischemia resulting from an obstruction to the cutaneous blood vessels is commonly found related to the formation of the

Category I and II pressure ulcers caused by medical devices. This section covers different aspects of the vascularisation of the cutaneous layers including the locations, dimensions and orientation.

2.6.1. General vascularisation of cutaneous layers

Four cutaneous layers which are essential to the development of a computational model in relating to the formation of pressure ulcer are the stratum corneum, epidermis, dermis and hypodermis. The stratum corneum shown in the Section 2.3 is part of the epidermis layer with distinctive mechanical properties due to the formation of this unique layer. For the whole epidermis layer including the layer of stratum corneum, it is an avascular layer. The avascular nature of the epidermis layer means that nutrient is supplied to the epidermis layers by diffusion from the underneath dermis layer (Kaufmann, 2018). The dermis layer is vascularised and plexus of blood vessels is parallel to the body surface and at the superficial positions of the dermis layer. Another horizontal plexus of blood vessels is located at the dermal-hypodermal junction. These horizontal plexuses which are in the scale of arterioles are joined up by ascending arterioles as shown in Figure 2.6. Capillaries networks are from the lower plexus of arterioles to surround the coiled seat glands and hair follicles. (Démarchez, 2011; Millington & Wilkinson, 2009). The hypodermis layer of skin is highly vascularised and the blood supplied from the lower plexus of arterioles from the dermis layer (Millington & Wilkinson, 2009; Saladin, 2007).
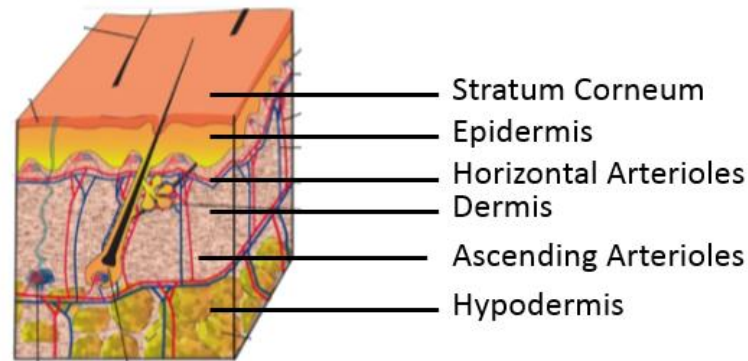
Figure 2.6   Cutaneous vasculature (Démarchez, 2011)

2.6.2.   Dimensions of the cutaneous blood vessels

Different types of blood vessels are present in the human body which are ranging from arteries to capillaries. Blood vessels with different diameters located at different anatomical locations allow various flow rates of blood. The diameters of different types of blood vessels are shown in Figure 2.7 (Kaufmann, 2018). Figure 2.7 shows the relevant blood vessels size at the cutaneous layers and the diameters of the terminals of the arterioles and capillaries are small.
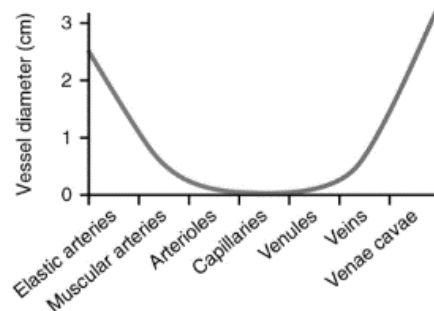
Figure 2.7   Vessel diameters of different vessel types (Kaufmann, 2018)

Although the diameters of the arterioles and capillaries were always provided with different ranges from study to study, Millington et al's brief idea of the diameters of the cutaneous arterioles and capillaries were 17 to 26µm and 4 to 6µm respectively (Millington & Wilkinson, 2009). For the case of the transition from arterioles and capillaries, the diameters values of the terminal of the arterioles and capillaries were

42

15µm and 10 to 12µm respectively (Yen & Braverman, 1976).

2.6.3. Computational modelling of blood vessel

Angiogenesis is defined as "the formation of new blood vessels, which occurs during wound healing and is promoted by growth factors" by Concise Medical Dictionary (2015) and the computational models of angiogenesis are mainly aimed to demonstrate or replicate the experimental angiogenesis patterns. These computational models built up the understanding of angiogenesis for gene therapy or cancer treatment. Szczerba, developed a computational model which mimicked the pattern of *in vitro* angiogenesis experiment as shown in Figure 2.8 (Szczerba & Székely, 2005). It is a complicated field because of the involvement of multidisciplinary factors for instance with tension and compression for physical forces and shear stress for flow quantity. The computational models in angiogenesis are far too complicated to be implemented in the computational modelling in prevention of pressure ulcers. A simplified configuration is introduced in Chapter 6.
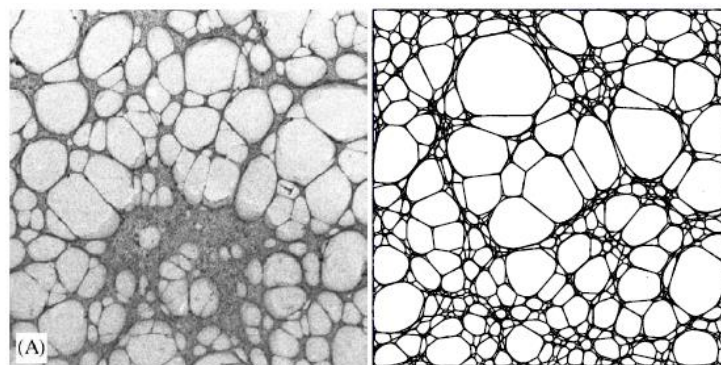
Figure 2.8   Left: pattern found in *In vitro* angiogenesis experiment, Right: pattern mimicked by the developed computational model (Szczerba & Székely, 2005)

2.7. Integrity of Skin

Although skin is subjected to various external physical and chemical stimuli, the

structure of skin enables it to maintain its health. The collagen structure of skin allows it to deform and recoil extensively for the purpose of body movement. However, the public generally neglects the importance of maintaining a healthy balance for skin leading to the failures in the integrity of skin consequently. Different types of failures of skin include acne, infection, skin cancer, pressure ulcers, friction blister, etc. The failure of skin is affected by different factors. For instance, acne is affected by hair follicles blockages (NHS, 2016a). Skin cancer (Melanoma) is caused by the abnormal development of skin cells. The ultraviolet light is one of the most important contributing factors which causes the melanoma (NHS, 2017). Some of these failures of skin are affected by factors which are irrelevant from the aspect of the mechanical engineering. Therefore, this section focuses on the failures of skin which are directly contributed by mechanical loadings, for instance, friction, pressure and shear.

2.7.1. Friction blister

The aetiology of the friction blister was investigated and a range of experiments were undertaken to recreate and understand the formation of friction blisters, typically caused by a rubbing technique (Akers & Akers, 1985; Cortese Jr, Griffin, Layton, & Hutsell, 1969) which requires a mechanical probe to continuously apply linear or circular force across the skin surface. As a result, the stratum corneum firstly had slight exfoliation followed by reddened area appeared around the rubbing area (Naylor, 1955; Sulzberger, Cortese, Fishman, & Wiley, 1966). The participants in the experiments suddenly had stinging or burning feelings with a pale narrow area formed around the rubbing area. With the continuation of the rubbing, the pale area subsequently enlarged to the entire rubbing area and be elevated from the underlying skin and the cavities were filled with fluid (Knapik, Reynolds, Duplantis, & Jones, 1995).

The main contributing factors causing the formation of friction blister is the magnitude of the applied force, the number of cycles for experiments and duration for actual friction blister incidents. For a higher magnitudes of force applied, lower numbers of cycles of rubbing are capable of forming friction blisters (Chimata & Schwartz, 2015; Comaish, 1973). Thus, the magnitude of applied force is inversely related to the number of cycles and presumably the duration required for actual incidents of friction blisters for non-experimental environments.

Friction blister is a common failure of skin in the field of athletics and military. The marathon is one of the athletic activities that friction blisters are commonly found. Mailler published a review paper on more than 15 marathons from 1973 to 1995. It showed as high as 26% of participants in one marathon were found to have blisters related injuries on skin (Mailler & Adams, 2004). A study conducted by Bush et al. revealed that 120 blisters were presented in 2,130 recruits for military training which was equivalent to 2.05 blisters per 100 recruit-months. It is the most common dermatological injury and contributed 10.7% to the total clinical diagnoses. The recruits with blisters resulted in 159 clinic visits, 103 days of assigned light duty and 177 lost days of training. The overall costs relating to the friction blisters was at least USD29,529 and further calculation revealed the approximate expense of USD690,000 annually regarding the blisters of the recruits. (Bush, Brodine, & Shaffer, 2000).

In recent years, due to the advancement of the computing technology, finite element computational models were developed to provide a better understanding of the causes of friction blisters. A computational model was developed by Xing et. al. to investigate the performance of a friction blister under different loading frequencies. The natural frequencies of the friction blister model were calculated and compared

with the loading frequencies by human gait (for both walking and running). It concluded that the frequencies of the human gaiting cycle were far lower than the natural frequencies of the friction blister. Therefore, no resonance could be caused by gaiting (Xing, Pan, Zhong, & Maibach, 2007). The computational model developed by Xing et. al. allowed the investigation on the performance of friction blister in such a way that *in vivo* examination is infeasible. The finite element model demonstrated the performance of a friction blister with the accurate input of the mechanical properties of cutaneous layers.

2.7.2. Pressure ulcer

Pressure ulceration is a global issue and occurs in all geographic locations, regardless of race, gender or age group. Two advisory panels including European Pressure Ulcer Advisory Panel (EPUAP) and National Pressure Ulcer Advisory Panel (NPUAP) provide guidance on preventive interventions and precautions. The severity of pressure ulcers vary from slightly discoloured skin to serious full thickness tissue loss including the deeper layers of the human body, i.e. muscles and bones. These severities are determined by the depth of the ulcer on skin and identified in 4 categories; category I refers to the perfectly intact skin but just discoloured and category IV refers to the skin with open wounds and exposed bones and extra categories including deep tissue injury refers to the injury at the deep tissue with intact superficial layers and unstageable refers to the ulcers which cannot be evaluated due to the obstruction on estimating the wound depths. The presences of pressure ulcers lower the quality of lives of patients, not only limit their physical mobility but also the mental health. Development of a pressure ulcer, particular category III and IV, can lead to sepsis, osteo myelitis, necrotizing fasciitis and gas gangrene and in the worst case mortality. The mortality rates as high as 60% for the older people with pressure ulcers within 1 year

after hospital discharge (Richard M. Allman, Goode, Patrick, Burst, & Bartolucci, 1995; Thomas, Goode, Tarquine, & Allman, 1996). Even though the presence of the pressure ulcer did not directly contribute to the deaths, it contributed to the malfunctions to other parts of the human body. Despite all the research and precautions suggested by the advisory panels, the prevalence rate of the pressure ulcers was still high across the globe. 24,674 patients developed new pressure ulcers between April 2015 and March 2016 in England according to the data from the NHS Safety Thermometer. The treatment costs of the pressure ulcers contributed £3.8 million every day to the total expenditure of the National Health Service (NHS) (NHS, 2016b). Ischemia and excessive stress caused by the application of mechanical loads including pressure, friction and shear were the aetiologies of the formation of the pressure ulcers. Two loading thresholds are related to the aetiology of pressure ulcer in which mechanical loading exceeding the lower threshold requires longer period of time to cause a pressure ulcer comparing to loading could result in a pressure ulcer in a shorter period of time if the magnitude exceeds the higher thresholds. However, the definite magnitudes of the thresholds and loading periods are patient dependent. The anatomical locations for pressure ulcers varies depends on the aetiologies, for instance, pressure ulcer caused by excessive stress is located at load bearing locations i.e. sacrum and heels while pressure ulcer caused by ischemia could be resulting from the attached medical device and located at fingers and neck. Different computational models were developed and experiments were conducted over the years to have a better understanding on the formations of pressure ulcers especially relating to the aetiology of excessive stress and deformation of deeper tissue. A computational model was developed with the presence of magnetic resonance imaging (MRI) by Makhsous et al. The geometry of the finite element model was developed with the captured imagining by the MRI. It demonstrated the compressive pressure was 55 to 80kPa for

skin, fat and muscle (Makhsous et al., 2007). The computational model allowed the investigation of the stress and deformation in deep tissue which was infeasible to be examined by *in vivo* experiment. The study demonstrated the necessity of developing computational models to understand the behaviours of *in vivo* conditions. The development of computational models facilitate the understanding of in vivo conditions and the models can also be predictive indicators for the possibility of the formation of pressure ulcers. However, computational model on ischemia condition cannot be found which is also the aim of the study to investigate and provide a related tool in such area.

2.8. Conclusions

The literature was reviewed from a mechanical engineering perspective which highlighted the related and essential characteristics of skin in relating to the computational modelling of the cutaneous layers and the formation of pressure ulcer. Although the mechanical properties of skin vary with different factors, the ranges of values of the mechanical properties and thicknesses of the cutaneous layers were investigated and acquired from the literature. The stratum corneum layer was essential to be treated as a separated layer in computational modelling as the mechanical properties of such layer was found to be distinctive as compared to viable epidermis. The set of skin mechanical properties provided by Lévêque is deemed to be most relevant and adopted in the current study for computational modelling.

The effect of the Langer lines contributed to the anisotropic mechanical properties of skin, however, no research evidence showed the direct effect of the Langer lines to the mechanical properties of skin in depth direction (perpendicular to the skin surface). In fact, limited attempts were made to investigate the mechanical properties of skin in

depth direction for the individual layers of skin. It is the fact that skin is relatively thin and skin samples in depth direction is impossible to be clamped on the tensile test machine. However, the two-dimensional effect of the Langer lines is clear that the mechanical properties of skin parallel to the Langer lines are higher or stiffer than perpendicular to Langer lines because of the orientation of the fibres. This is a common phenomenon on fibrous materials.

The stress-strain curve of skin presented in Figure 2.4 demonstrated the non-linearity of skin. However, Phase I and III of the skin were fairly linear if the curve was treated as three individual Phases. The Phase II of the curve was a transitional period from "high strain caused by low stress" to "low strain caused by high stress".

The vascularisation of skin is a complicated subject and research had shown its vascular structure of the cutaneous layers. The epidermis is an avascular layer and two main arterioles plexuses are located at the epidermis-dermis junction and the deep layers of the dermis layers. The dimension of blood vessels in human body is within a wide range of diameters from 2.5 centimetre (artery) to 4 micrometre (capillaries). It was found that the cutaneous blood vessels were relatively small with a range from 4 to 26 micrometre and the translational size of arterioles to capillaries is 15 micrometre.

The importance of maintaining an intact skin was demonstrated. Loss of skin integrity could lead to the occurrences of friction blister commonly found in the field of athletic and military and pressure ulcers on the hospitalised or immobilised patients. The cutaneous injuries or loss of skin integrity are regarded as minor and unimportant by the public. Research had shown that these injuries not only just lower the life quality of patients but also become financial burdens to the governments across the globe. In

some of the serious cases, loss of skin integrity could become fatal incidents.

An increasing prevalence and trend of financial expenditure of the pressure ulcers is definitely a global issue. Only a few research in recent years had been conducted on the medical devices related superficial pressure ulcers which are often misapprehended as relatively minor or not as serious as deep tissue injury. Hence, it is the aim of this project to develop an effective tool to demonstrate the effect of mechanical loading on the formation of superficial pressure ulcer. This tool can be utilised by the medical device developers to evaluate the effect of their products on the cutaneous layers in relating to the formation of pressure ulcers.

Chapter 3   Pressure Ulceration

3.1.   Introduction

Pressure ulceration is a common cause of loss of integrity of skin across the globe. The chapter focuses on an illustration of the severity of pressure ulcers, the implications of the occurrences of pressure ulcers on suffering patients and healthcare providers. The risk factors associated with the formation mechanism of pressure ulcers are highlighted and the preventive methods are discussed. The two important aetiologies of pressure ulcers "ischemia" and "excessive stress" are discussed in detail. The aetiologies and existing computational models in relating to the formation of pressure ulcers are broadly overviewed which are the key elements in the existing research project.

3.2.   Background of the Pressure Ulcers

The terminologies for describing pressure ulcers varies over the centuries with the investigation on the aetiologies of the pressure ulcers. It was originally named as "decubitus" and described as dead tissue by Wohlleben in 1777. Despite the recognition of such failure of skin centuries ago, the aetiology research did not start until 1942 by Groth (EPUAP, 2014). The terminology of pressure ulcers evolved from "decubitus" to "decubitus ulcer" and "ischemic ulcers" with the progress of the aetiologies research over the years (Kosiak, 1959; Reichel, 1958). A conference in relating to the aetiologies of the pressure ulcers was held in Glasgow in 1975 with a publication named as "Bedsore Biomechanics" which associated the pressure ulcers with beds despite the understanding by that time that pressure ulcers could occur when skin was in contact with any kind of support surfaces. "Sore" was just a description of the patients' pain feelings caused by the pressure ulcers. The

terminology of "Pressure Sore" was commonly used in the 1980s to minimise the bed-related perception. "Pressure Ulcer" started to be used frequently from early 1990s. The term "Pressure Ulcer" highlighted some pressure ulcers in which superficial layers of skin are not intact and the cavities of wounds are exposed due to the definition of ulcer "A break in an epithelial surface/ a break in the skin extending to all its layers" (Concise_Meidcal_Dictionary, 2015). However, some of the pressure ulcers are not necessarily with visibly opened wound cavities. These pressure ulcers are in the form of internal injuries with intact superficial layers of skin which are labelled as "Deep Tissue Injury" (DTI) in present day (EPUAP, 2014). All the terminologies included in this section are still commonly used by the public, clinicians and patients. Although a new terminology of "Pressure Injury" is recently adopted in some of the geographic regions including South-East Asia, Australia and New Zealand, the terminology of "pressure ulcer" is still more commonly used in Europe and North America (EPUAP, 2014). Some of the clinicians also expressed their concerns regarding the new terminology i.e. "Pressure Injury". Pressure injury includes the injuries or traumas contributed by the high-pressure impact which is fundamentally caused with different aetiologies. The terminology of "pressure ulcer" was recommended to use by the National Health Service (NHS) of the United Kingdom because this terminology is consistent with the European Pressure Ulcer Advisory Panel's (EPUAP) definitions and the common usage across the UK (NHS_Improvement, 2018). Hence, the terminology of "Pressure Ulcer" is adopted in this thesis.

3.3. Categories of Pressure Ulcers

The most common pressure ulcer grading system are those developed by the European Pressure Ulcer Advisory Panel (EPUAP) and National Pressure Ulcer Advisory Panel (NPUAP) (EPUAP&NPUAP, 2009). The terminologies of "Stage" and "Category"

in the grading of pressure ulcers have been used interchangeably in numerous research papers. EPUAP and NPUAP describe the category of pressure ulceration as

3.3.1. Category I: nonblanchable erythema

Category I pressure ulcer is the mildest and the layers of skin are still intact as shown in Figure 3.1. The skin can appear discoloured and may be warmer, cooler, firmer, softer comparing to the adjacent skin surfaces. Pain can be result from the pressure ulcers for the patients. The appearance of the Category I pressure ulcer is red colour in Caucasians but purple or blue for people with darker skin tones.
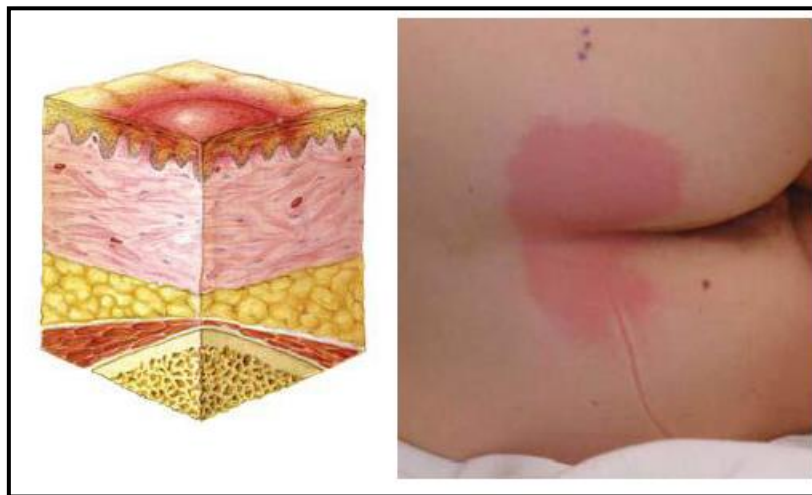
Figure 3.1   Category I pressure ulcer (EPUAP, 2014)

Left: Schematic diagram of only discolouration of skin
Right: Red mark on patient with Category I pressure ulcer

3.3.2. Category II: partial thickness skin loss

Category II pressure ulcer is in a form of open wound. Superficial layers and deeper layer of dermis could be damaged as shown in Figure 3.2. The wound of the pressure ulcer looks similar to a slough or a blister but not bruising. The occurrence of bruising is an indicator of possible deep tissue injury.

Figure 3.2   Category II pressure ulcer (EPUAP, 2014)

Left: Schematic diagram of only open wound

Right: Open wound on patient with Category II pressure ulcer

3.3.3.   Category III: full thickness skin loss

Category III pressure ulcer is a damage of full thickness of skin. The subcutaneous fat may also be visible without the exposure of tendon, muscle and bone. The depth of the pressure ulcer fallen in this category varies on different anatomical locations. The depths of the pressure ulcers occurring at the nose and ear are shallower than those at other anatomical locations with more adiposity. The appearance of this Category III pressure ulcer looks like a cavity as shown in Figure 3.3.
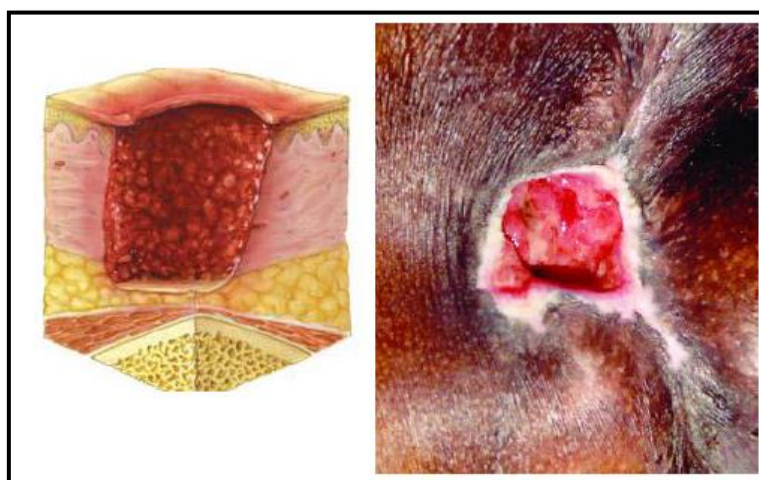
Figure 3.3   Category III pressure ulcer (EPUAP, 2014)

Left: Schematic diagram of only open wound affecting hypodermis layer

Right: Open wound with the exposure of hypodermis

3.3.4. Category IV: full thickness tissue loss

As described by the category title "Full thickness Tissue Loss", not only the layers of skin but also other supporting tissues including muscles, tendons and bones are affected by the Category IV pressure ulcer as shown in Figure 3.4. For instance, the bone as a supporting structure may also be exposed. The depth of the Category IV pressure ulcer also depends on the anatomical location in which deeper wound cavities for the pressure ulcers located at the higher adiposity locations. Undermining and tunnelling are likely to occur for Category IV pressure ulcer. Patients with Category IV pressure ulcer are susceptible for fatal infection.
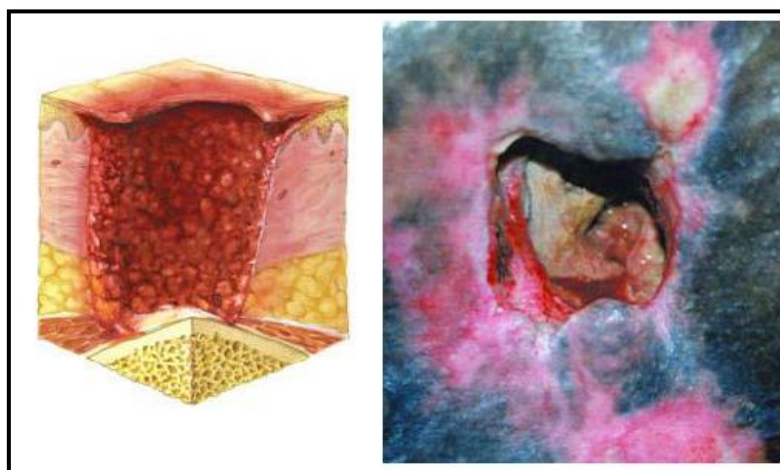
Figure 3.4   Category IV pressure ulcer (EPUAP, 2014)

Left: Schematic diagram of wound affecting all tissues

Right: Open wound on patient with Category IV pressure ulcer with the exposure of bone

3.3.5. Unstageable

Unstageable is an extra category which is not within the four classic categories of the pressure ulcers. However, due to the high prevalence of the unstageable pressure

ulcers, it is currently adopted as one of the categories for the pressure ulcer grading system. The severity of the pressure ulcer is usually categorised by the depth of the wound and the types of the affected tissues. A pressure ulcer falls to a higher level of category when the wound is deeper and/ or deeper layers of tissue are affected. However, some wound cavities of the pressure ulcers are covered by slough or eschar whose appearance could be in different colours in yellow, grey, green or brown. The slough obscures the actual depth of wound and the determination of the types of the affected tissues as shown in Figure 3.5. Hence, this kind of pressure ulcer is categorised with "Unstageable".
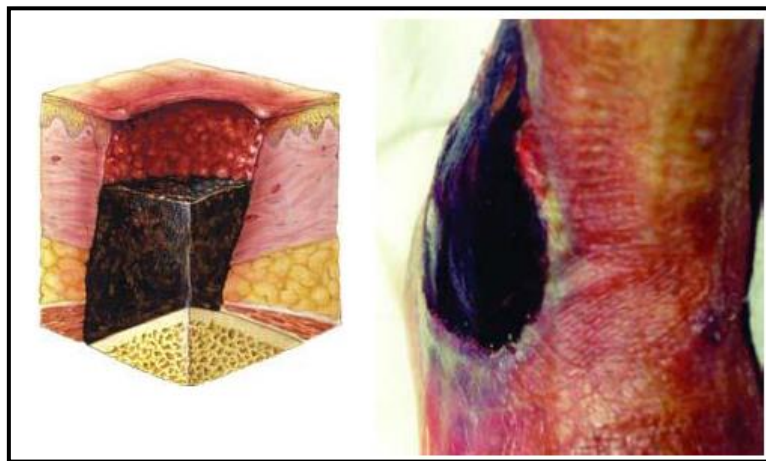
Figure 3.5   Unstageable pressure ulcer (EPUAP, 2014)

Left: Schematic diagram of unstageable pressure ulcer
Right: Wound on patient with undetermined depth

3.3.6.   Deep tissue injury

Deep tissue injury (DTI) is a specific type of pressure ulcers in which the superficial layers of skin is intact but the deeper layers of tissue is damaged. The DTI pressure ulcer may be difficult to be recognised for the people with dark skin tones. The skin may be intact with an appearance of discoloured, purple, maroon colour, or blood-filled blister because of the damage contributed by pressure or shear at deeper layers

as shown in Figure 3.6. The deep tissue injury may occur at the tissue that is painful, firm, mushy, boggy, warmer or cooler as compared with surrounding skin surfaces. A DTI pressure ulcer could quickly turn into a Category III or IV pressure ulcer when the superficial layers of skin are broken and the deeper layers are exposed.
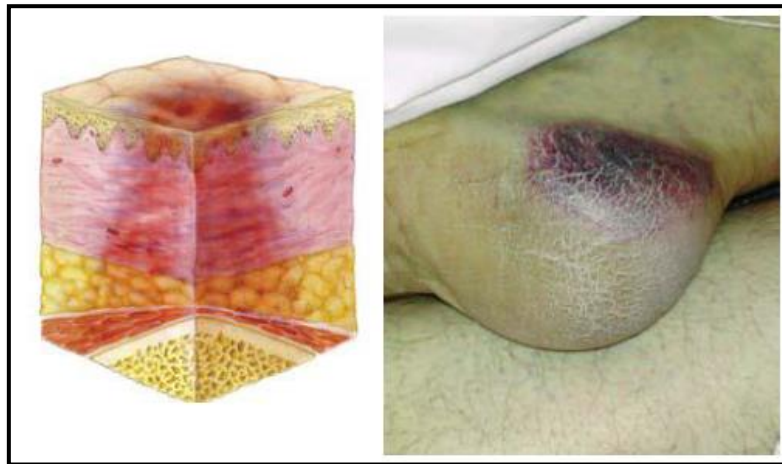
Figure 3.6   Deep tissue injury (EPUAP, 2014)

Left: Schematic diagram of deep tissue injury
Right: Discoloured skin indicating deep tissue injury on patient

3.4.   Prevalence of Pressure Ulcers

According to the statistics from NHS Safety Thermometer, the pressure ulcer prevalence rate for all categories was approximately 4.36% across all settings including actual hospital ward, community hospital ward, mental health community, nursing home and residential care home from July 2017 to July 2018 in the United Kingdom (Safety_Thermometer, 2018). The prevalence rate of hospital-acquired pressure ulcer in the United States of America between 2006 and 2007 was 4.5% (Lyder et al., 2012). According to the Agency for Healthcare Research and Quality of the U.S. department of Health & Human Services that pressure ulcers affected 2.5 million patients every year (Agency_for_Healthcare_Research_and_Quality, 2014). The Local Health Districts and Speciality Health Networks conducted a study in Australia in 2016 that 5.3% of the

inpatients among 10,255 patients involved in the survey were found to have pressure ulcers (Clinical_Excellence_Commission, 2016). A study conducted by Woodbury found that the prevalence rate of pressure ulcers in all healthcare settings in Canada was as high as 25.2% to 26.8% between the year of 1990 and 2003 (Woodbury & Houghton, 2004). Over 2.2% and 9.6% of the prevalence rate of pressure ulcers in Japan was found in general acute hospitals in 2006 by Sugama and in long-term care hospital in 2013 by Igarashi et.al. respectively (Igarashi et al., 2012; Sugama, 2008).

3.5. Financial Implications of Pressure Ulcers

Despite the efforts on understanding the formation of pressure ulcers and development of the risk assessment tools for pressure ulcer formations and preventive measures recommendations over the years, the prevalence of pressure ulcers is still high among various groups of patients and causes a financial burden to the governments across the globe. Pressure ulcer is deemed to be one of the most expensive type of wound to be treated (Graves & Zheng, 2014). The increasing trend of the financial resources spent relating to the pressure ulcers was significant over the years. Financial spending on pressure ulcer related issues was a very good indicator for the severity of the pressure ulcers. The public always underestimates the impact to both of the healthcare providers and the patients with the formations of the pressure ulcers. The statistical figures in this section highlight three main points:

- Pressure ulcer is a globe challenge;
- The influencing magnitude of the pressure ulcers to patients and health care providers; and
- An increasing financial input for treating pressure ulcers.

A number of pressure ulcer advisory panels were setup to address the issue and some

countries are associated with them, for instance, the United Kingdom, the United State of America and Japan, i.e. European Pressure Ulcer Advisory Panel (EPUAP) in Europe, National Pressure Ulcer Advisory Panel (NPUAP) in the United State of America and Pan Pacific Pressure Injury Alliance (PPPIA) in the South-East Asia. These three advisory panels jointly developed and issued clinical guidelines, for instance, the "Prevention and Treatment of Pressure Ulcers: Clinical Practice Guideline" in which the background, prevention, interventions, treatment and statistical data were included (EPUAP, 2014). Despite all the efforts, pressure ulcers are still posing a huge financial burden to the governments across the globe. GBP3.8 million was spent daily by the National Health Service in relating to pressure ulcers in the United Kingdom(UK) (NHS, 2016b) and total annual cost was GBP1.4 to 2.1 billion which was approximately 4.1% of the total NHS expenditures in 2000 (Bennett, Dealey, & Posnett, 2004). Pressure ulcers cost USD9.1 to 11.6 billion annually in the United State of America (Agency_for_Healthcare_Research_and_Quality, 2014). The estimated annual cost across all states in the Australia was AUD983 million which was 1.9% of all public hospital expenditure and 0.6% of the public recurrent health expenditure (Nguyen, Chaboyer, & Whitty, 2015). These significant expenditures indicated that pressure ulcer is definitely a global issue which requires more efforts to prevent it from occurrence. An increasing trend of the cost associated with pressure ulcers was noticed from the statistics over the years. The treatment cost of each pressure ulcer was increased from GBP1,064 to 10,551 to GBP1,214 to 14,108 from year of 2004 to 2012(Bennett et al., 2004; C. Dealey, Posnett, & Walker, 2012). It was estimated that the treatment of pressure ulcers cost the NHS GBP60 million annually in 1973 while the cost associated with pressure ulcers is GBP3.85 million every day in recent years which is approximately GBP1.41 billion annually (NHS, 2016b; Torrance, 1983).

The costs for treating pressure ulcers are not only limited to wound dressing but also those intangible services forgotten or neglected by the majorities of the public which include the visits by general practitioners, practice nurses, community nurses, specialist nurses and ambulance services, diagnostic tests, devices and the prescriptions for drugs (Guest et al., 2016). The prolonged hospital stay was also one of the key expenditures associated with the pressure ulcers. Studies showed that the average hospital stays were prolonged by 4 days approximately due to the formations of the pressure ulcers. (R. M. Allman, Goode, Burst, Bartolucci, & Thomas, 1999; Graves, Birrell, & Whitby, 2005). The cost of the treatments depends on the category of pressure ulcer. The expected cost associated with Category I to Category IV pressure ulcer was GBP1,214 to 14,108 per patient (C. Dealey et al., 2012). The cost of the nursing time associated with the treatments contributed to 90% to 96% of the total costs for treating different categorised pressure ulcers (NICE, 2014). From the perspectives of the management boards of the healthcare providers or clinicians in practice, the incidences of pressure ulcers should be minimised because lawsuits were also involved. It was shown in the website of the Agency for Healthcare Research Quality that more than 17,000 lawsuits were associated with pressure ulcers annually in the United Statement of America. That was the second most common claim after wrongful death (Agency_for_Healthcare_Research_and_Quality, 2014). The jury awarded an 86-year-old woman USD16.7 million in punitive damages and USD2.5 million in compensatory damages regarding the disregarded procedures for preventing pressure ulcers in 2015. A jury awarded USD5.4 million to a man who developed a Category IV pressure ulcer on his hip four days after the admission against the defendant hospital in New York (Genesio, 2016).

3.6. Implications of Pressure Ulcers to Patients

The occurrences of pressure ulcers or other types of loss of skin integrity are underestimated (Health_Service_Executive, 2017). The general public have the perceptions of "putting a bandage on the wound and it would be healed". In fact, the occurrences of pressure ulcers are not just only financial burdens to the governments around the globe as discussed in Section 3.5 but also serious physical and psychological impacts and limitations to the suffering patients. Needless to say, pressure ulcers can also be fatal when it turns into blood poisoning, bone and joint infection, necrotizing fasciitis or gas gangrene especially for the highly categorised pressure ulcers.

3.6.1. Health-related quality of life

The Health-related quality of life (HRQoL) survey is one of the methods for quantifying the implications on the patients suffering from pressure ulcers. This HRQoL survey takes physical, mental, emotional and social functioning factors into account including "physical functioning", "role limitations (physical)". Two studies on HRQoL survey conducted by Franks and Essex in 2002 and 2009 respectively are presented in this section to highlight the implications of pressure ulcers to patients as shown in Table 3.1 (Essex, Clark, Sims, Warriner, & Cullum, 2009; Franks, Winterberg, & Moffatt, 2002). The attributes listed in Table 3.1 were significantly affected with the presences of the pressure ulcers. Table 3.1 presented the difference in the values given by the patients with and without pressure ulcers (values given by patients without PU minus values given by patients with PU). "Physical functioning" was found to be one of the most outstanding attributes among the many. The score for patients suffering from pressure ulcer was lower than those without pressure ulcer. This indicated that the physical movement of patients was limited because of the presence of the pressure ulcers. The "Role Limitations (Physical)" was a measurement of limitation of patient's role due to

physical problems as shown in both of the studies. Some of the attributes in Table 3.1 were conclusive but insignificant in individual studies, for instance, the "Social Functioning", "Mental Health", "Vitality", and "General health Perception". However, all of these attributes in Table 3.1 showed that the general health-related quality of life of patients were lowered by the presences of pressure ulcers.

Table 3.1 Data of health-related quality of life surveys

Attributes	Study conducted by Franks et. al. (2002)	Study conducted by Essex et. al. (2009)
Physical Functioning	37.6	23.52
Social Functioning	33.9	0.79
Role Limitations (Physical)	11.8	21.5
Mental Health	0.7	2.94
Vitality	3.0	11.48
General Health Perception	3.8	10.4

3.6.2.　Patients' perspectives of pressure ulcers

Aside from the evaluation of the implications of pressure ulcers to the patients by the quantitative research shown in Section 3.6.1, qualitative research also played an important part which could reflect the feelings of patients and their perspectives on the occurrences of pressure ulcers. Interviews to investigate the quality of life of the thirty patients with different severities of pressure ulcers from Category I to Category IV in a study were conducted by Gorecki et. al. in the United Kingdom (Gorecki, Nixon, Madill, Firth, & Brown, 2011). The participants of the study were aged between 22 to 94 years old and mixed genders which aimed to represent a wider range of populations.

The participants expressed the feeling of restricted and incapability in participating in the social and leisure activities. The participants with the prolonged hospitalisation for the treatment of pressure ulcers also caused the isolation perceptions, claustrophobic, disconnected and lacking mental stimulation. One of the interviewees of the study had the following comment.

"I haven't seen anybody, I haven't been out of this room (in hospital) in God knows how many months….. my brain is really just dying in here not having any stimulation"

The study also discovered that participants' negative perceptions of the hospital were risen because of the formation of pressure ulcers. Participants had negative feelings on hospitals where the pressure ulcers on patients originally developed and deteriorated. The participants had the perceptions that the hospital care would primarily focus on the acute conditions while and the pressure ulcers as a secondary condition were inadequately addressed. Some participants even believed that they would have better and more individualised care at home while only severe pressure ulcers should be treated in hospital setting as the community clinicians were lack of resources to manage complex wounds.

In terms of treatments by clinicians, the participants of the study worried about the inconsistency of the treatment techniques among hospitals and individual nurses. In some occasions, nurses just placed a wound dressing on a pressure ulcer that deemed to be a completed treatment because of the heavy workload in clinical practice. The daily routines of the participants were disrupted because of the treatment for the pressure ulcers. Another interviewee of the study conducted by Gorecki et. al. also commented:

"Daily dressing is disruptive, you never know when they (community nurses) are

Discomfort feeling on support surface was another issue for the patients, for instance, the uncomfortable pressure relieving mattresses and cushions. The participants of the study described those pressure-relieving equipment as "uncomfortable", "too hot", "noisy" and "vibrate". Most importantly, pain was a common sensation of the patients suffering from pressure ulcers. Interviewers of the study expressed the view that the pain was usually unrecognised or ignored by the clinicians and analgesia was ineffective for pain release in some situations.

3.6.3. Mortality associated with pressure ulcers

Pressure ulcer is not just a skin breakdown and its implications are not limited to pain/ sores or capability in socialising but also fatal. A study conducted by Bauer et. al. showed that the mortality rate of the in-patients with a pressure ulcer was 2.8 times higher than in-patients without a pressure ulcer (Bauer, Rock, Nazzal, Jones, & Qu, 2016). A mortality rate of fivefold increase in the elderly patients with pressure ulcers was demonstrated by Grey et. al. (Grey, Harding, & Enoch, 2006). Redelings also found that 114,380 persons equivalent to 3.79 per 100,000 population were reported dead with the cause of pressure ulcers in the United States of America between the year of 1990 and 2001 (Redelings, Lee, & Sorvillo, 2005).

3.7. Risk Factors of the Formation of Pressure Ulcers

Risk factors for the formation of pressure ulcers can be categorised as intrinsic and/or extrinsic (Carol Dealey, 1997; Ousey, 2005). Figure 3.7 presents examples of intrinsic and extrinsic factors that may contribute to pressure ulcer formation. The arrow after each of the risk factor indicates the nature of the factor, upward and downward

pointing arrows represent an increase and decrease of the likelihood of the formation of pressure ulcers. For instance, the higher mobility of the patients, the less risk of pressure ulcer development.
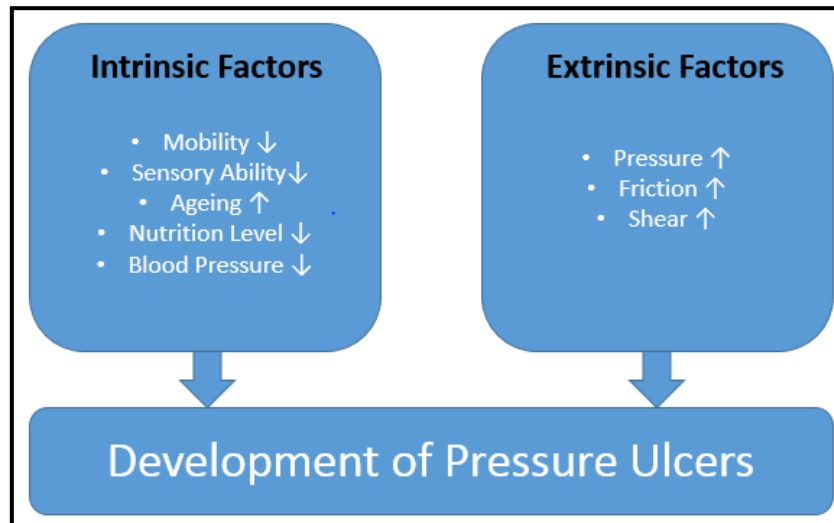
Figure 3.7   Risk factors of the formation of pressure ulcers

3.7.1. Extrinsic factors of pressure ulcer

Pressure

Extrinsic factors include pressure, friction and shear. Pressure is defined as "Force" over an "Area," Equation 3.1 demonstrates the magnitude of pressure, a higher magnitude of pressure would be caused when the applied force is increased and/or the loaded area is decreased.

$$Pressure = \frac{Force}{Area}$$
     Equation 3.1 Equation of pressure

In fact, skin is an organ which can healthily withstand a relatively high magnitude of

pressure. Ahmed Gabr set a new world record on scuba diving at 332.35 metre under the sea level in 2014 (Guinness_World_record, 2018). The equivalent applied pressure on the diver was 3440.86kPa. However, in relating to pressure ulcer development, as little as 5.99 kPa has been identified (Dinsdale, 1974). The loading direction is the critical factor of the capability in withstanding the pressure by skin. In the case of scuba diving, the hydrostatic pressure coming from all directions equally imposed on skin but the applied pressure for causing a pressure ulcer is localised and created localised stress to the tissue. Therefore, a relatively low magnitude of pressure could result in forming a pressure ulcer. An applied pressure on skin with the magnitude higher than the capillary pressure slows the blood flow down resulting in insufficient supply of oxygen and nutrients as well as deficient removal of the metabolic waste (Defloor, 1999; Ousey, 2005).

Friction

Friction as another common mechanical load found at the interface between patients and support surfaces is also an extrinsic factor for the formation of pressure ulcers. The most significant study regarding pressure ulcer formation and the application of friction was conducted by Dinsdale in 1974. Friction and pressure were applied on the posterior superior iliac spines of female pigs while only pressure was applied on the other side. Repeated pressure and friction were applied to one side of the pigs in every 15 minutes for 1.5 hour every day for the first week and pressure alone was applied on the opposite side for the following week. In this study, it was proved that application of friction reduced the magnitude of applied pressure required for the development of pressure ulcers. Only 45mmHg of pressure was sufficient to form a pressure ulcer with the application of friction while 290mmHg of pressure was required to form a pressure ulcer without the presence of friction (Dinsdale, 1974). Equation 3.2 is the

equation for calculating the magnitude of friction where "μ" and "N" were the coefficient of friction for two surfaces in contact and perpendicular force maintaining the surfaces to be in contact respectively. For the prevention of pressure ulcers, clinicians attempt to minimise the magnitude of friction as it reduced the pressure required for the formation of pressure ulcers.

$$Friction = \mu N$$ Equation 3.2 Equation of friction

Shear

Shearing force was recognised as the third extrinsic factor for the formation of pressure ulcers. The definition of shearing force often leads to clinicians' confusions due to the difficulties in differentiating with friction. According to the dictionary of mechanical engineering, shear is "*A form of deformation of a fluid or solid in which adjacent planes in a material are displaced in opposite directions*" (Dictionary_of_Mechanical_Engineering, 2013). In clinical setting, shear occurred when friction resisted the motion of the superficial layers of skin of patients from sliding down caused by the gravity while the deeper tissues under the skin would slide down. The distortion of the tissue resulted in excessive stress at the deep tissue and cells started to be damaged which is discussed in detail in Section 3.8.3. A study conducted by Manorama demonstrated that the presence of shear reduced the blood perfusion in addition to the reduction initially caused by the normal load (pressure) (Manorama, Baek, Vorro, Sikorskii, & Bush, 2010). This study conducted by Manorama indicated that shearing force played an important role in the formation of pressure ulcers.

3.7.2. Intrinsic factors of pressure ulcer

There are a range of intrinsic factors associated with the development of pressure ulcers. Significant factors are included in this section and presented in Figure 3.7.

Immobility

Impaired mobility has been highlighted as one of the risk factors that can increase the risk of pressure ulcer development (David, 1983; Carol Dealey, 1994). The reduction on the mobility of a patient or a completely immobilised patient is unable to reposition the body. The reposition to relive the pressure at the body is a curial preventive method for the formation of pressure ulcers. It is unrealistic and unfeasible to rely on the clinicians for repositioning patients' bodies due to the heavy workload. It is therefore the immobilised patients are at a higher risk of forming pressure ulcers. Study conducted by Versluysen indicated that 66% of pressure ulcer incidences included in that study were found in patients who suffered a fractured neck of femur in other words reduction on the mobility (Versluysen, 1986).

Sensory Loss

The sensory ability of a patient is the awareness of the needs of repositioning and reliving the pressure due to the uncomforted feeling or even pain at localised area of the body. Typical loss of sensation ability includes patients with spinal cord injury, neurological disease or loss of consciousness. In some occasions, the loss of sensory ability was deemed to a more crucial factors than immobility (Gebhardt, 1995). The immobilised patients could request repositioning or pressure relived interventions even if they were incapable of reposition themselves. However, the patients with loss of sensory ability could not recognise the needs of repositioning, thus, it was deemed to be more crucial factor than immobility.

Ageing

The properties of skin change with ageing. The skin is stiffer, less elastic, thinner, less tense and less flexible as discussed in Section 2.5.4. These changes in skin properties increase the risk of forming pressure ulcers for the aged patients. Statistics from studies showed that the population of having pressure ulcers were mostly in elderly patients, for instance, 85% of patients with pressure ulcers were over 65 years of old in a study conducted by David et. al., and 46.4% to 62.9% of patients were over 65 years old in two prevalence surveys conducted by Dealey in a teaching hospital (David, 1983; Carol Dealey, 1994). It showed that aged population was more susceptible to the formation of pressure ulcers than other age groups.

Nutrition Level

Research showed that the adequate level of nutrition is vital to both the prevention and healing of pressure ulcers. The study conducted by Pinchcofsky-Devin demonstrated that all the 17 severely malnourished patients were all suffering pressure ulcers while the other 215 patients were not affected including those with moderate malnutrition (Pinchcofsky-Devin & Kaminski, 1986). Berlowitz indicated that impaired nutritional intake was significantly related to the patients with the presence of pressure ulcers and the development of new pressure ulcers (Berlowitz & Wilking, 1989).

Blood Pressure

Blood pressure which is one of the key indicators of health status of human beings. Low blood pressure also plays a role in the formation of pressure ulcers. Systolic blood pressure drives the blood to flow and a reduction in systolic blood pressure, the flow

of the blood decreases. Schubert discovered that the systolic blood pressure of the patients with pressure ulcers were significantly lower than those in the control group (Schubert, 1991). This phenomenon was related to the reactive hyperaemia response which is discussed in Section 3.8.2.

3.8. Formation Mechanisms of Pressure Ulcers

In order to prevent of pressure ulcer formation, it is essential to understand the causative mechanisms of pressure ulcers. Two primarily distinctive mechanisms for the formation of pressure ulcers are "Ischemia" and "Excessive Stress". Both of these mechanisms lead to the occurrences of pressure ulcers in different categories. Superficial pressure ulcer are usually resulting in ischemia while excessive stress usually causes Category III or IV and/or deep tissue injury of pressure ulcers.

3.8.1. Duration and magnitude of load

There are two key parameters that are responsible for determining the formation mechanism of a pressure ulcer which are the duration and magnitude of the applied loads. The initial research of the relationship between the duration and magnitude of load dated back to 1961 when Kosiak applied the localised pressure on albino rats. The main finding of the experiment was that a critical time interval was identified in which pathologic change occurred (Kosiak, 1961). However, the graphic representation of the critical time interval or labelled as the threshold of acceptable magnitudes of load was unavailable until 1976 when Reswick conducted over 980 observations on the damage on the superficial layers of skin on humans as shown in Figure 3.8 (Reswick & Rogers, 1976). It showed that the acceptable magnitude of pressure was depending on the duration of the application of load on humans.
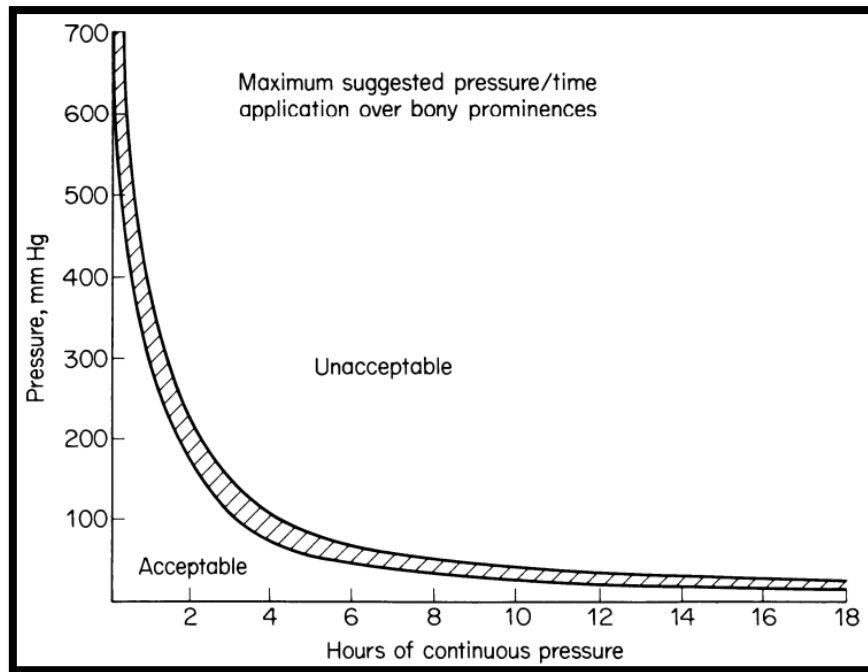
Figure 3.8   Acceptable magnitude of pressure vs duration of load application

(Reswick & Rogers, 1976)

The curve presented in Figure 3.8 indicated that an infinite magnitude of force was required to form a pressure ulcer in a very short period of time while an extensive amount of time was required to form a pressure ulcer with extremely low or no pressure. Linder-Ganz developed a more realistic approach that there was a threshold of pressure required to form a pressure ulcer at very short and very long duration of load application as showed in Figure 3.9. The filled and hollow data points in Figure 3.9 represented the required time of cell death and no damage respectively in studies including the study by Kosiak in 1961. The region above solid line represented death of cells while the region below the dotted line was no damage to the cells. The area in between the lines was deemed to be uncertain. It was essential to note that the individual tolerance to the mechanical load was different, therefore, Figure 3.9 should be deemed to be a reference rather than for quantitative evaluation.
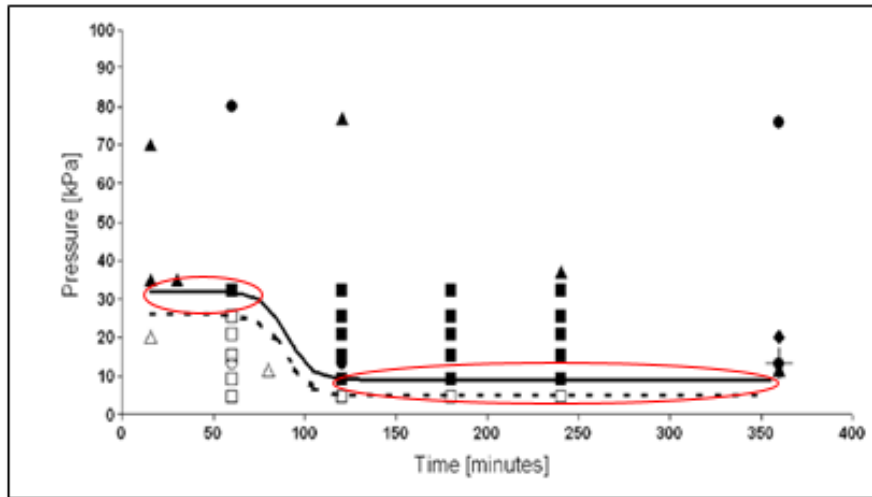
Figure 3.9   Revised pressure-time cell death threshold

The shapes of the data points represent different participants of the study

(Linder-Ganz, Engelberg, Scheinowitz, & Gefen, 2006)

Although the definite acceptable magnitude of pressure for individuals was not demonstrated by Figure 3.9. It was clear that there were two thresholds in the magnitude of the applied pressure. The first threshold or labelled as "higher threshold" which appeared at the beginning of load application (and circled in red on the left) up to about 60 minutes in Figure 3.9. Formation of pressure ulcer in such period started when the magnitude of the applied load was higher than the first threshold in a relatively short period of time. The second threshold or labelled as "lower threshold" was the magnitude of pressure required for a formation of pressure ulcer in a relatively long period of time which was indicated from about 120 minutes onwards(and circled in red on the right) in Figure 3.9. It was a transitional period in between 60 minutes up to 120 minutes in which the threshold value changed significantly with duration. Similar transitional periods were found in another study (Gefen, van Nierop, Bader, & Oomens, 2008).

From the scientific aspect of a single cell level in the study conducted by Gefen et. al., the cell behaviour or response to the applied load was similar to the trend presented in Figure 3.9. The responses of the cells depended on the magnitudes of loads which were classified as low loads, high loads and intermediate loads. Cell survived and sometimes could have self-repair under the application of low loads. High loads on the other hand caused the cells failure catastrophically by deforming the cells and disrupting the structural integrity of the cells. Intermediate loads similar to the second threshold (lower threshold) in Figure 3.9 for a prolonged period of application could lead to cell death gradually (Gefen & Weihs, 2016).

For the formation mechanism of pressure ulcer, ischemia happens at the lower threshold of the curve shown in Figure 3.9. Any magnitude of applied pressure higher than the second threshold (lower threshold) is sufficient to cause a pressure ulcer with the aetiology of ischemia while magnitude of applied pressure is required to be higher than the first threshold (higher threshold) for causing pressure ulcer with the aetiology of excessive stress.

3.8.2. Ischemia

Ischemia is "an inadequate flow of blood to a part of the body, caused by constriction or blockage of the blood vessels supplying it" (Concise_Medical_Dictionary, 2015). In the formation of pressure ulcers, ischemia happens when prolonged pressure loading is applied on skin resulting in occlusion of the cutaneous blood vessels. Consequently, the blood flow in the occluded cutaneous blood vessels is restricted and the transportation of the oxygen and nutrient supply and removal of the metabolic wastes are impaired. The lack of nutrient and oxygen and accumulation of metabolic wastes leading to a change in pH value resulting in cells damage (EPUAP, 2014). The duration

for the formation of pressure ulcers caused by ischemia usually requires a prolonged period of time of the loading applications which associated with the second threshold (lower threshold) in Figure 3.9 and the intermediate loads applied in the single cells by Gefen et. al. in the responses of single cells presented in Section 3.8.1.

The phenomenon of ischemia is a lack of blood supply which leads to hypoxia "A deficiency of oxygen in body tissue" (Dictionary_of_Biology, 2016). After the relief of applied pressure which caused ischemia and hypoxia, the reactive hyperaemia, "the presence of excess blood in the vessel supplying a part of body" (Concise_Meidcal_Dictionary, 2010) occurs (Rendell & Wells, 1998). The reaction of hyperaemia is to supply more oxygen and nutrient, and remove the accumulated metabolic wastes from the location used to be hypoxia. The patients with lower systolic blood pressure had less hyperaemia effect which, consequently, leads to higher risk of pressure ulcer formations.

Landis's study generally accepted that the capillary blood pressure was between 12 to 32 mmHg from venous to arteriole (Landis, 1930). The Landis's experiment was in direct contact with the cutaneous capillary loops by removing the dried epidermis. However, Bridel argued that the concept of setting 32 mmHg of applied pressure as a threshold was inappropriate due to the fact that the response of the cutaneous capillary network (deformation or degree of collapse) was determined by the collagen content of the dermis (Bridel, 1993). From a mechanical engineering perspective, this argument by Bridel was logical and realistic because the cutaneous capillary is embedded in the cutaneous layers. The magnitude of deformation in the response of the capillary would be significantly affected by the mechanical property i.e. stiffness of the primary material, skin. Ischemia had been investigated since very early years,

however, more research efforts focused on the aetiology of excessive stress as it caused severe Category III and IV pressure ulcers in recent years.

3.8.3. Excessive stress

In contrast, pressure ulcers caused by excessive stress were investigated more heavily with a presence of the advancement in technology. The pressure ulcers formed with this aetiology usually associated with a higher magnitude of applied pressure which exceeded the first threshold (higher threshold) presented qualitatively in Figure 3.9 or the high load associated to the single cells experiment conducted by Gefen et. al. presented in Section 3.8.1. The higher magnitude of applied pressure on skin could result in a development of pressure ulcer in a relatively short period of time. Pressure ulcers caused by excessive stress occur at the deeper layers of tissues, i.e. muscle-bone interface. Within this aetiology, interface pressure between a patient and a support surface is not a good indicator of the likelihood of the formation of pressure ulcer. The interface pressure could remain approximately the same while the internal tissue is experiencing 1.5-fold or higher stress and distortion (Elsner & Gefen, 2008). Muscle was stressed the most among all the soft tissues by the high magnitude of applied load by the weight of the patient which was located immediately below the ischial tuberosity (Makhsous et al., 2007). This explained the pressure ulcers caused by magnitude of applied loads exceeding the first threshold (higher threshold) were commonly fallen in Category III or IV.

The pressure ulcers caused by excessive stress are resulting from the application of shear, friction and/or pressure as the application of pressure not just only causes compression to the cutaneous layers, deeper tissue i.e. muscle and fat, but also causes uneven distortion and stress as demonstrated in Figure 3.10 (Wounds_International, 2010). The surface pressure was evenly disturbed however, different types of stress

imposed on the deeper tissue due to the geometry of bone.

This excessive stress caused pressure ulcer appears in deep tissue in a relatively short period of time. This injury initially is recognised as deep tissue injury and it turns into a Category III or IV pressure ulcer when the superficial layers of the skin are broken.
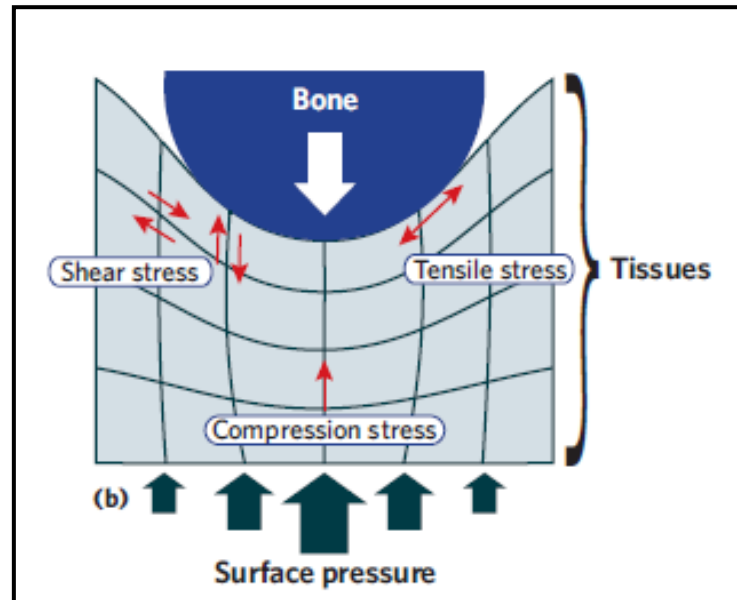
Figure 3.10   Uneven distortion of tissue caused by even loading (Menon et al., 2012)

3.9.   Medical Device Related Pressure Ulcers

Aside from the pressure ulcers commonly caused by the body weight of patients, medical device related pressure ulcers are the result of the direction contacts between medical devices and patients' skin. The effect of medical devices on causing pressure ulcers become more significant especially the ischemia and excessive stress are more aware by the clinicians in recent years. A study conducted by Black found that over one-third of the patients who suffered hospital- acquired pressure ulcers were medical device related (39 out of the total number of 113 incidents). The patients who were with medical devices were found to be 2.4 times more likely to develop a pressure

ulcer than those who were without medical devices. This highlighted the effects of medical devices on the formation of pressure ulcers. The pressure ulcers related to the medical devices were mostly found to be in Category I and II while only a small percentage was in Category III and none in Category IV (J. M. Black et al., 2010) as shown in Figure 3.11. The remaining 24% was contributed by Unstageable. From the Categories of the majority of the medical device related pressure ulcers, it is reasonable to assume that the medical device related pressure ulcers were caused by ischemia rather than excessive stress. The superficial layers of skin were found to be damaged the most. In contrast, deeper tissue for instance muscle was damaged resulting in Category IV pressure ulcers was 0% and only 6% of deep tissue injury.
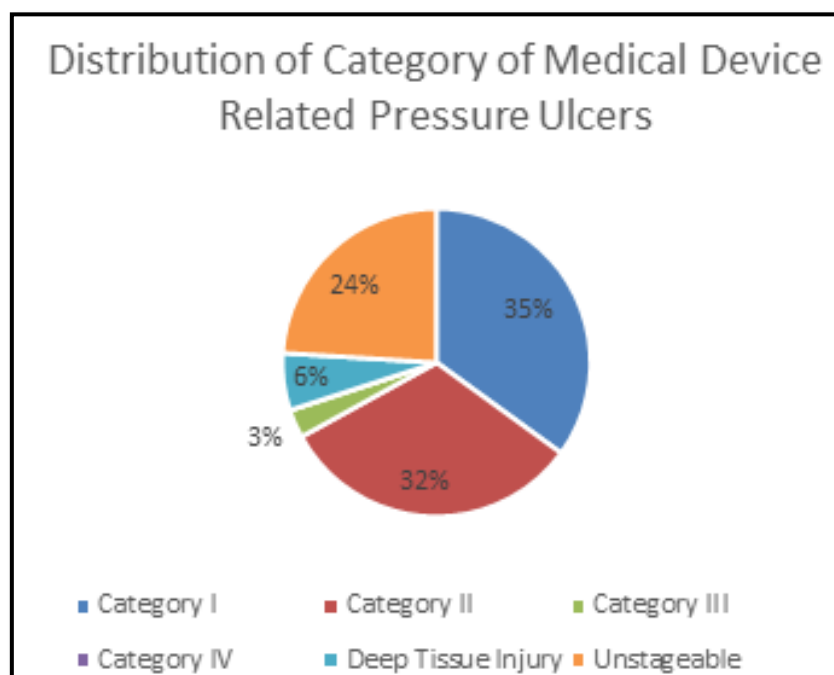
Figure 3.11   Distribution of the category of medical device related pressure ulcers

(J. M. Black et al., 2010)

Any type of medical devices could cause medical device related pressure ulcers regardless of the materials, shape and functionalities. Hence, a wide range of medical devices was reported to associate with pressure ulcer formations including

endotracheal or nasotracheal tubes, nasal cannulas, cervical collars, stockings or compression devices, immobilisers, splints, braces, wraps and drains (J. Black et al., 2015). The shapes of the medical device related pressure ulcers were often found to be in the patterns or shapes of the causing devices. In some occasions, the medical devices with improper fixation method could increase the possibility of pressure ulcer formation by acting like a tourniquet (J. M. Black et al., 2010).

3.10. Common Anatomical Locations for Pressure Ulcers

A significant difference was found on the common anatomical locations of the pressure ulcers between those related and unrelated to medical devices.

3.10.1. Anatomical locations of general pressure ulcers

For the pressure ulcers which are unrelated to medical devices are often caused by the weight of the patients themselves. Figure 3.12 and Figure 3.13 showed the potential supporting anatomical locations of patients in supine and sitting positions respectively. The weight of the patients is mainly supported by the area in black. Some of the anatomical locations are bony prominences which increase the risk of the formation of pressure ulcers including sacrum, heels and elbows. These areas are more susceptible to the formation of pressure ulcers because as demonstrated in Figure 3.10 that stress was imposed at the deep tissue around the bone. In fact, any area of the body can develop pressure ulcers under the situation conditions for the formation of pressure ulcers. However, study conducted by Petersen discovered that some of the anatomical regions were statistically more prevalence in pressure ulcers than others, for instance, 96% of pressure ulcers were found below the level of umbilicus in which 67% around the hip, 29% on the lower limbs (N.C. Petersen & Bittmann, 1971).
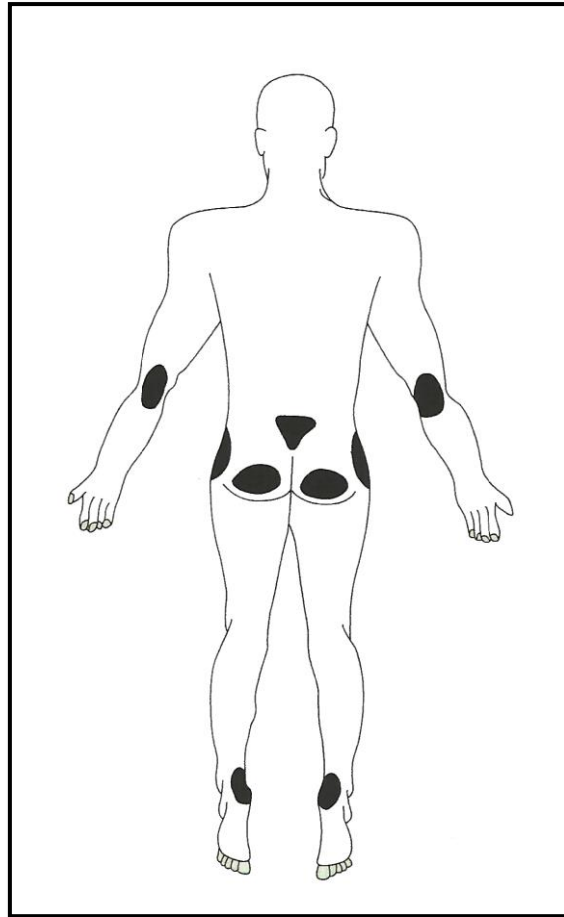
Figure 3.12   Potential anatomical locations for supporting in supine position

(Ousey, 2005)
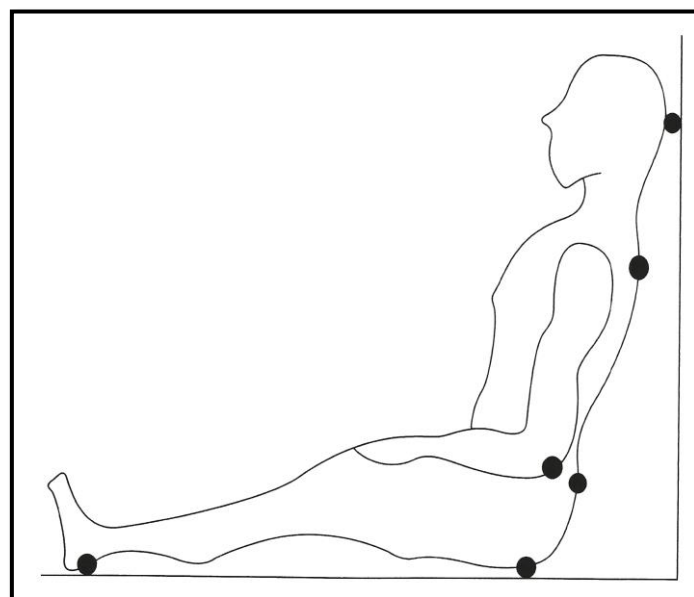
Figure 3.13   Potential anatomical locations for supporting in sitting position

(Ousey, 2005)

3.10.2. Anatomical locations of medical device related pressure ulcers

However, it is a complete different situation when it comes to the medical device related pressure ulcers. The common anatomical locations of occurrence of pressure ulcers depend on the applications and locations of the medical devices. The anatomical locations are no longer limited to the common load bearing areas of the human body for instance the areas presented in Figure 3.12. The anatomical locations associated with medical device related pressure ulcers included lips, tongue, nose, ears, chin, fingers, forehead, neck, ankles, arms, ribs depending on the type of medical devices applied (J. Black et al., 2015).

3.11. Prevention of Pressure Ulcers

Different policies, risk assessment tools and pressure relieving devices were developed over the years to prevent the formation of pressure ulcers. Xakellis et al, deemed that the prevention of the occurrences of pressure ulcer was more cost-effective than treatment (Xakellis & Frantz, 1996).

3.11.1. Risk assessment tools

Risk assessment is the core of the preventive measures for pressure ulcers. It is a key method utilised by the clinicians to identify the patients who are at risk of developing pressure ulcers or even evaluate the likelihood of the formation of pressure ulcers. However, it is rather a very complicated process that many factors have to be taken into account including all the factors detailed in Section 3.7. Over the years, different scoring systems were developed to calculate the risk and the first attempt dated back to 1962 by Norton. The first scoring system developed by Norton targeted the elderly patients and ,over the decades, other scoring systems for assessing patients at acute

care, general medical ward, nursing home, orthopaedic and community were developed. These scoring systems considered patients' physical and mental health, mobility, nutritional level, fluid consumption, body mass index (BMI), age, gender, medication, sensory perception (Bergstrom, Braden, Laguzza, & Holman, 1987; Lowthian, 1987; Milward, Poole, & Skitt, 1993; Norton, 1962, 1975; Pritchard, 1986; Waterlow, 1985).

3.11.2. Pressure reliving devices

Different types of pressure reliving devices were available in the market, more precisely, over 200 in the year of 2005 (Ousey, 2005) and many more in the present. They were designed by commercial companies with different purposes and rationales and tested for various postures to patients. Although the international standards of pressure reliving devices in terms of terminology, category or testing method from the International Organization for Standardization (ISO) or British Standard Institution (BSI) were unavailable, Ousey in 2005 distinguished the pressure reliving devices into three groups including static, dynamic and turning. Static redistributing devices were designed to allow larger contact area of the body resulting in lowering the magnitude of interface pressure. Dynamic redistributing devices were designed to alternate the load bearing anatomical locations of the body in contact with the support surfaces usually by the means of inflating and deflating the air cells inside the devices. The turning type of redistributing devices altered the centre of gravity of the patients and repositioned the support system systematically which were usually found in specific wards (Ousey, 2005).

3.12. Computational Modelling of Skin in Relating to Pressure Ulcers

Different types of computational models were developed over the years to understand the behaviour of skin under pressure or other mechanical loads, for instance computational model regarding friction blister (Xing et al., 2007) and folding behaviour of skin (Lévêque & Audoly, 2013). The computational models related to the formation of pressure ulcers were elaborated in this section.

3.12.1. Aetiology and indicative computational model of pressure ulcers

The needs of understanding the effect of external mechanical load on the internal loading regime was demonstrated by Makhsous et.al. in 2007 and a three-dimensional finite element computational model was developed with the aid of Magnetic Resonance Imagining (MRI) technology. The MRI images provided the structure of buttock-thigh of a healthy male volunteer aged 24. The finite element model was reconstructed by this acquired structure from the MRI. Two loading conditions were captured by the MRI which were with and without sitting pressure. The volunteer was supported by custom-made apparatus made of plastic foam in which the "without pressure stage" had no pressure against the buttock-thigh. However, pressure was applied to the buttock-thigh by the supporting apparatus at the "with pressure" imagining to acquire the deformation of the internal tissue of the volunteer. The finite element model was developed to evaluate the internal pressure and stress distribution in the anatomical location of the buttock and thigh. The model was validated by comparing the deformation of the FE model and the MRI imagines. The results acquired by the FE simulation of pressure applied on surfaces on the buttock-thigh were showed in Figure 3.14. The model on the left indicated the locations of the highest magnitude of the internal pressure while the locations of highest magnitudes

of stress were indicated in the right model. The highest magnitude of pressure and stress were found at the fat and muscle layers at the location immediately beneath the ischial tuberosity (Makhsous et al., 2007).
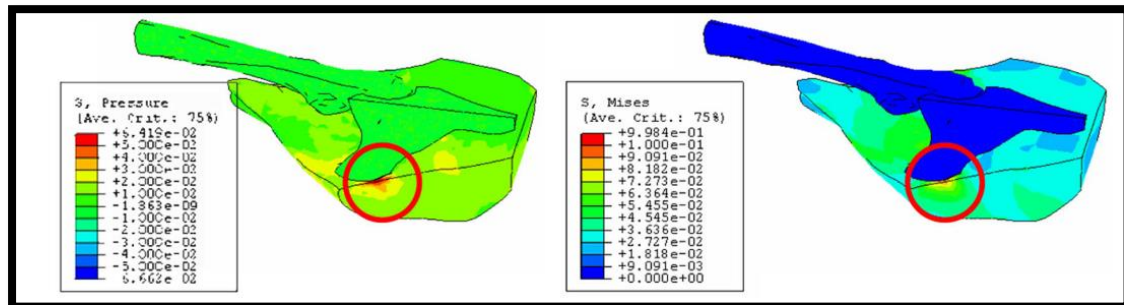
Figure 3.14   FE model of internal loading conditions, anatomical location of buttock thigh. Red circles indicate the peak stress location, i.e. muscle-bone interface. (Makhsous et al., 2007)

A similar computational model was developed by Gefen in 2010 to understand the aetiology of the pressure ulcers locating at the heels. This computational model not just only served to be a demonstrator of the internal loading conditions but also to be an indicator of the risk of the formation of pressure ulcers. Gefen's computational model was developed with the simplified structure of a heel. Despite the fact that the heel consisted of many bones and tendons, the calcaneus of the heel was usually the load bearing anatomical location. The geometry of the lower calcaneus which was in contact with the support surface was simplified as a sphere. The stiffness of bone was much higher than the cutaneous layers, thus, the calcaneus was assumed to be completely rigid. Hence, the model in this study was a rigid sphere with the overlaying layers representing the skin at the heel. Different internal conditions based on the changeable parameters including, foot weight (applied pressure) and the elastic modulus and Poisson's ratio of the soft tissue were demonstrated and presented in a graphics showed in Figure 3.15 (Gefen, 2010). The higher magnitudes of the internal

pressure indicated higher possibility of the formation of pressure ulcer.
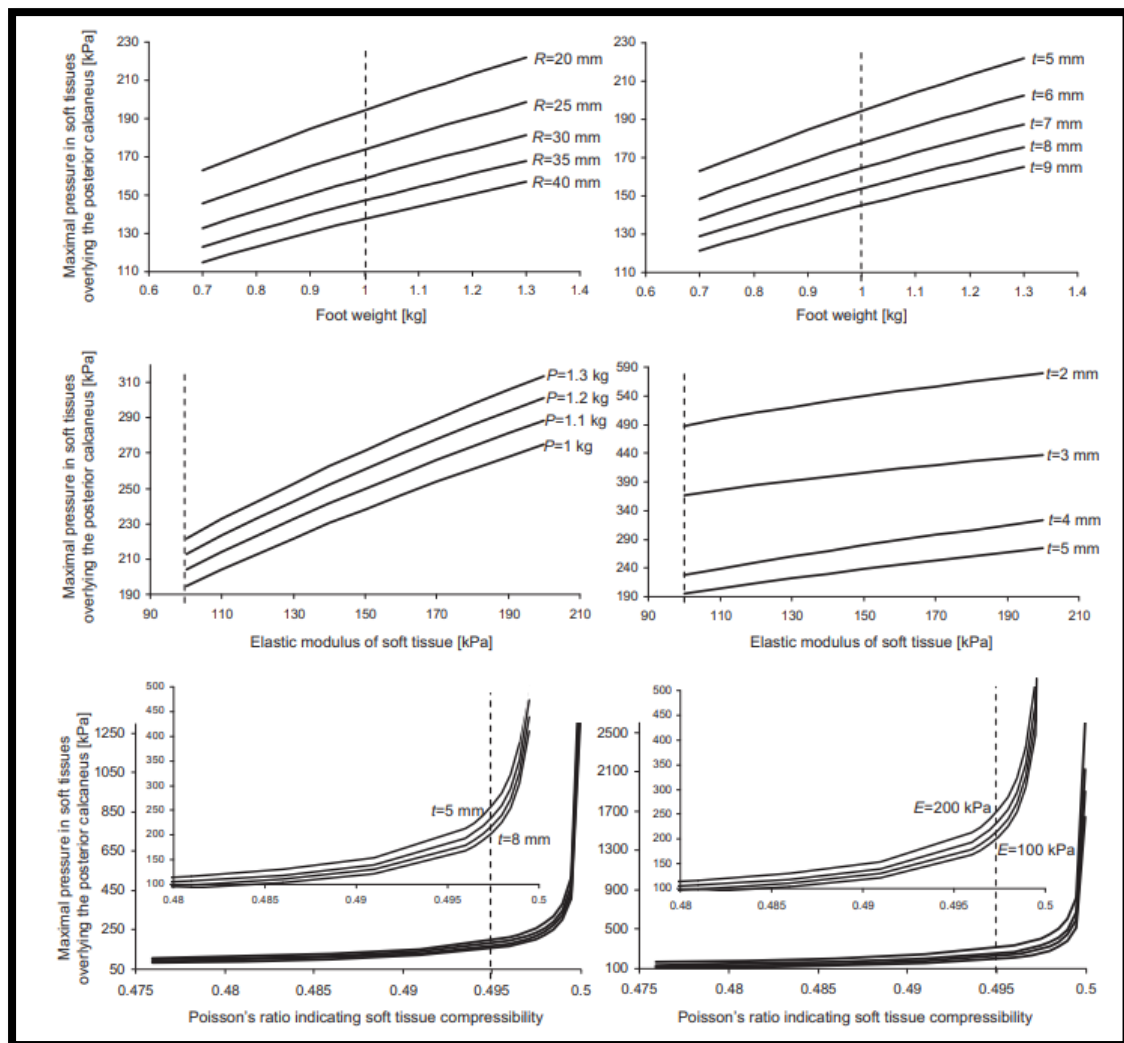
Figure 3.15   Indicative information by the computational model of heel (Gefen, 2010)

3.12.2. Device related computational model of pressure ulcers

A two-dimensional computational model was developed by Levy et. al to evaluate the effectiveness of one type of air-cell-based cushions to the patients suffering spinal cord injury (SCI) and tissue scarring. The geometric features of the computational model were designed against the images acquired by the magnetic resonance imagining (MRI) on a SCI male patient one year after the injury. The results from the

computational simulation with tissue scarring showed lower peak stress value in the soft tissue of the buttocks comparing to the non-scarred simulations when seated on the air-cell-based cushion as shown in Figure 3.16. Figure 3.16 (a) was the internal stress distribution for non-scarring while (b to d) were the internal stress distribution for different severity of scarring (Levy, Kopplin, Gefen, & Bs, 2014).
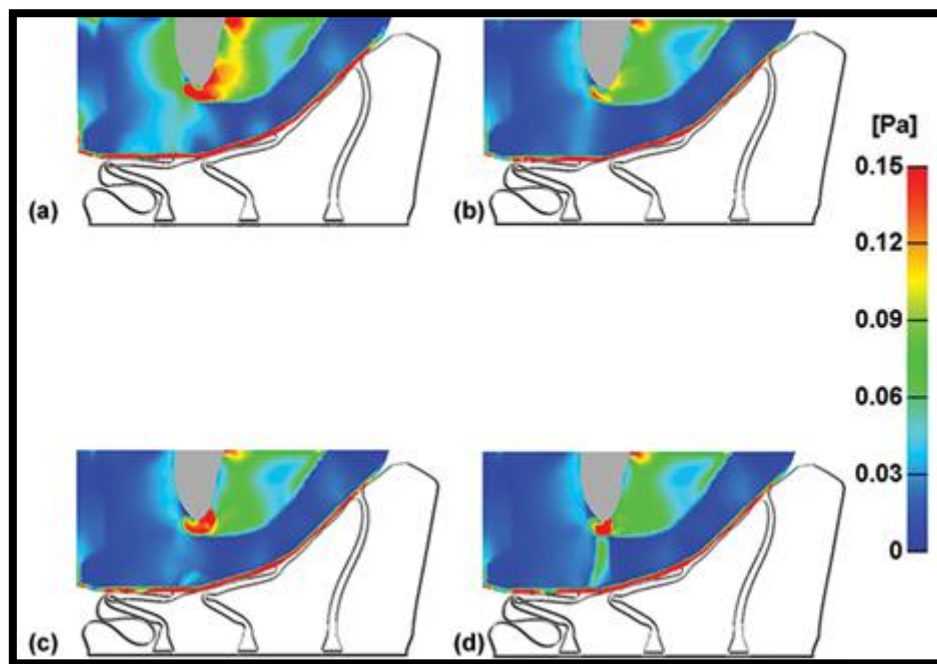
Figure 3.16   Internal stress distribution on air-cell-based cushion (Levy et al., 2014)

The computational models facilitated the understanding of the aetiologies of pressure ulcers by demonstrating the internal conditions typically under different mechanical loads. For instance, the two computational models described in Section 3.12.1 depicted the internal stress and pressure distribution. It allowed the researchers and clinicians to understand that internal stress was usually higher than the applied stress at the muscle and fat layers due to the irregular shape of the bones. The model developed by Gefen could also be an indicative tool for the likelihood of the formation of pressure ulcers at heels. However, the developed computational models were

focused on the aetiology of excessive stress which was the cause of Category III and IV pressure ulcers. There is also a need in developing a computational model in a similar manner to indicate the likelihood of the formation of pressure ulcers in superficial layers of skin typically in Category I and II. Such a tool could be utilised by the clinicians to evaluate the effect of medical devices on patients and also medical devices developers to understand the effect of the medical devices on the skin in relating to pressure ulcers at the developing stage.

3.13. Conclusions

Pressure ulcer is a serious loss of skin integrity and the severity could range from slightly discoloured skin to serious full thickness damage to tissues or even fatality. The treatment and prevention of pressure ulcers were found to be financial burdens to the healthcare providers across the globe. The treatment cost depends on the Category of the pressure ulcers.

Pressure ulcer not just causes huge financial resources to the healthcare providers but also lower the patients' quality of life. These effects were not limited to the physical aspect of patients i.e. mobility but also emotion instability. Patients felt being isolated for prolonged hospitalisation due to the treatment of pressure ulcers (Gorecki et al., 2011).

The aetiologies of pressure ulcers were highlighted which were ischemia and excessive stress. The pressure ulcers caused by ischemia are usually in Category I and II affecting the superficial layers of skin while the pressure ulcers caused by excessive stress are usually in Category III and IV affecting the deeper tissue. For ischemia, the prolonged load caused the obstruction to the cutaneous blood vessels which limited the delivery of oxygen and nutrient to the cutaneous tissue and the removal of the metabolic waste

resulting in the change in pH value and cells deaths eventually. Excessive stress at the deep tissue caused by the mechanical loads was the primary reason for the cell deaths for the pressure ulcers found in Category III and IV. The internal stress and pressure were found to be much higher comparing to the applied pressure at the surface.

Medical device related pressure ulcers were a specific type of pressure ulcers which were caused by the medical devices. These pressure ulcers were usually caused by the aetiology of ischemia and there was no limitation to the anatomical locations. This type of pressure ulcers could occur at any anatomical locations including lips and nasal bridge.

Existing computational models were developed over the decades to understand and demonstrate the formation of pressure ulcers. These models could depict the internal stress and pressure distribution which would not be possible without the aid of the computational simulations. However, these models were limited to simulate the situations of excessive stress. There is no related model in the ischemia aetiology. Hence, this PhD study aims to develop a computational model in order to be an indicator for the clinicians and an assessing tool for the process of medical devices development in relating to the formation of pressure ulcers.

Chapter 4 Methodology of the Designed Evaluation System

4.1. Introduction

Understanding the aetiology of pressure ulcers is essential for maintaining skin integrity as many pressure ulcers are related to the application of mechanical loads including pressure, friction and shear. An engineering approach has been adopted in the study. A typical engineering technique named Finite Element Method (FEM) has been used by various researchers to illustrate the *in vivo* conditions of a human body under different loading conditions (Gefen, 2010; Makhsous et al., 2007). In this chapter, details of FEM are discussed as it is adopted to develop a tool for approximating the effects of mechanical loads on the cutaneous blood vessels in relating to the formation of superficial pressure ulcers.

As the input data of a FEM computational model has to be clinically relevant, this chapter also explores methods of acquiring the input data which is pressure mapping. The computational model will be correlated to a set of acquired physiological data by using Laser Doppler Velocimetry and the related information will also be discussed in this Chapter.

4.2. Finite Element Method

The finite element method (FEM) is a numerical method used to simulate conditions for instance, stress distribution, deformation magnitude, heat transfer and fluid dynamics under the influences of different parameters. FEM provides results which could be utilised as an indicator of the efficiency of an object or the approximated deformation caused by different loadings.

4.2.1. Development of finite element method

Finite element method or sometimes named as finite element analysis (FEA) was originally developed in 1950s in the field of aerospace mainly by Boeing and Bell Aerospace in the United States of America and Rolls Royce in the United Kingdom. The first journal paper on the idea of FEM was published by Turner et.al. in 1956 in which the term "finite element" was not presented (Turner, Clough, Martin, & Topp, 1956). For many years, FEM was developed as an approximated method without mathematical proof. Mathematicians in late 1960s demonstrated that the finite element solutions converge to the correct solution of the partial differential equation when the elements are sufficiently small. The first FEM software was developed in early 1960s which was a freeware but limited to two-dimensional stress analysis. A general purpose three-dimensional FEM programme was developed in 1965 funded by the National Aeronautics and Space Administration (NASA) and this programme was named NASTRAN. From that time onwards, different FEM programs were developed for various purposes and some of the common programmes are Ansys and Abaqus (Fish & Belytschko, 2007).

4.2.2. Flow of the finite element method simulation

"The basic idea of FEM is to discretise the domain of interest in order to obtain an approximate solution of the partial differential equations by a linear combination of basic functions defined within each subdomain. Then the assembly of subdomains puts the finite elements back into their original positions, resulting in a discrete set of equations which are analogous to the original mathematical problem" (Rovitto, 2016). The FEM simulation mainly consists of five stages which are presented in Figure 4.1.
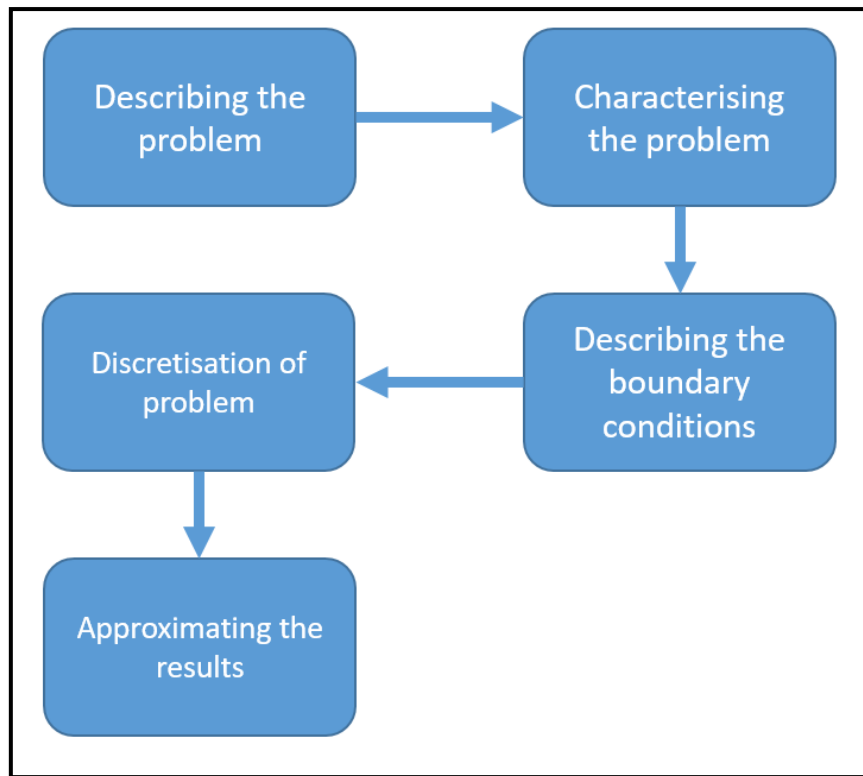
Figure 4.1   Five stages of a FEM simulation

The finite element method simulation is initiated by defining the domain to be modelled. All the later stages are based on the definition of the domain which has to be sufficiently close to reality to produce results of the desired accuracy. The second stage is to characterise the problem by inputting the basic information for instance Young's modulus and Possion's ratio. After modelling the domain, the boundary conditions of the problem have to be determined. This is a process of interpreting the conditions faced in reality to the FEM system. In order to approximate the response of the domain to the boundary conditions, the key principle of the finite element method is to discretize the domain into small finite elements. It is known that the finite element method is a series of approximations which is accurate when the approximating target is small and smooth. The final stage of the FEM simulation is the actual approximation of the change in the defined domain by solving a set of partial differential equations.

The approximation for the first element is followed by determining the influence of the change in the first element to the adjacent elements as these elements are in contact with other elements. The integrating results of each elements result in the approximation of the global domain.

4.2.3. Mechanical deformation simulated by FEM

As mentioned before, the FEM can be utilised in different fields and it is commonly adopted for demonstrating the deformation of a structure in the field of civil and mechanical engineering. This type of stress or deformation simulation by the finite element method is often named finite element analysis (FEA). This section focuses on the implementation of the FEM to the deformation simulation by FEA.

The defined problem or the domain described in Section 4.2.2 is usually in form of an object which is commonly developed by computer aided design (CAD) programmes. The geometry of the model is usually similar to the object in the reality unless it is symmetrical. In such case, the object would be presented in partial when the expected response is also symmetrical which save the computing resources for the simulation. The material properties, for instance, Young's Modulus needs to be input to the FEA system at the characterising stage. This enables the system to understand the behaviour of material under different magnitudes of loads. The material properties could be linear, nonlinear, viscoelastic, anisotropic depending on the type of simulation and assumptions made. The descriptions of the conditions are labelled as application of boundary conditions which could be in the form of, loads, immobilising the model in a certain direction or even in any direction or symmetry condition in deformation analysis. The face, edge or point where the application of boundary conditions is at and the choices of boundary conditions are the descriptions of the

confinement or the restrictions of the problem in reality to the FEA system. The discretisation of the model is required before the actual computational simulation which are labelled as meshing. The meshing process is usually conducted automatically by the FEA however it is necessary to pay attention to the relatively small or curved features of the model as well as the locations where stress gradients are expected to be high. The automatic meshing process may not result in an appropriate meshes over the whole model and manual meshing is required. Hence, the size of the mesh had significant influence on the accuracy of the simulation. After solving the partial differential equations, the FEA provides the results of the problem which can be in term of coloured visual representations or numerical data of the deformation. These results can be utilised to be indicators, for instance, factor of safety.

4.2.4. Finite element analysis and the current study

In this study, FEA is the main tool for evaluating the behaviour of skin under the influences of mechanical loadings. Skin is a combination of tissues with distinctive material properties. As discussed in Chapter 2, skin is a three-layered organ including epidermis, dermis and hypodermis. The cutaneous blood vessels are located in the dermis and hypodermis layers and obstruction of these blood vessels would result in ischemia and the occurrence of superficial pressure ulcers. A FEA simulation of skin is capable of approximating the deformations of the different layers and the change in the cross-sectional area of the cutaneous blood vessels. It is challenging to the design of a FEA simulation and a three-dimensional skin model because of the physical dimension of the cutaneous blood vessels which is discussed in Chapter 6. The aim of the study is to develop a tool for evaluating the effects of mechanical loads on the cutaneous blood vessels. This tool could be utilised by the medical device developers to evaluate the effects of the products on the cutaneous layers and clinicians to

understand the effects of mechanical loads on the skin of patients in relating to the formation of pressure ulcers typically with the aetiology of ischemia. Despite the capability of FEA in approximating the deformation of cutaneous blood vessels, the clinical relevancy of the FEA simulations depends on the characteristics of the model, the influencing factors and the interpretation of the FEA results.

Characteristics of the Model

The study conducted by Lévêque et. al. provided a set of material properties of skin which was also utilised as the characteristics of the computational model presented in that study (Lévêque & Audoly, 2013). Hence, this set of material properties of skin is utilised in the current study to be the characteristics of the FEA model as the set of material properties was proven to be inter-correlated and accurate for computational modelling (Lévêque & Audoly, 2013).

4.2.5. Material law for the FEA model

For computational models developed over the years in the field of pressure ulcer prevention, mainly three different material laws were adopted including, elastic linear, Neo-Hookean and Ogden (Savonnet, Wang, & Duprey, 2018). Elastic linear assumes the material behaves according to Hooke's law where stress and strain of a material can be represented by a linear relationship while Neo-Hookean and Ogden were adopted for materials in which stress-strain relationship is non-linear. For the current study, the magnitudes of pressure were within the range of 20 to 137 mmHg (from the pressure mapping measurement presented in Chapter 5) which is under 0.018 MPa. According to the stress-strain curve of skin, Figure 2.4, the applied load is still well within Phase I which is linear. Hence, an elastic linear material law is used in this study for the simulation.

4.3.   Pressure Mapping

The pressure mapping technique is commonly used in the field of engineering to evaluate the interface pressure between two surfaces in contact. A pressure mapping system is utilised in the current study to serve for two functions: to evaluate the pressure intensity commonly found in clinical setting in order to determine the working pressure range of the computational model; and to be a force measurement tool in conjunction with the laser Doppler for acquiring physiological data. A commercially available pressure mapping system from Tekscan is utilised in the current study. For the purpose of the study, two types of sensors from Tekscan is utilised including a matrix pressure sensor I-Scan 5051 for capturing applied force in physiological data acquisition and a Conformat 5330 for pressure mapping measurement at simulated clinical setting.

4.3.1.   Structure of pressure mapping sensor

According to the technical information from Tekscan, the pressure mapping sensor is made of four layers as shown in Figure 4.2. The top and bottom layers are ultra-thin flexible substrates which provide an enclosed space for the electrons located in between by adhesive and lamination. A layer of dielectric is located in between the two flexible substrates to prevent the electrons from short circuiting. A layer of pressure-sensitive material is also located in between the enclosing layers. This pressure-sensitive layer is the core of the pressure mapping sensor and is located precisely at the intersecting points of the rows and columns of conductive materials. Hence, each of the intersecting point of the rows and columns is a single and independent sensing point which is labelled as "Sensel".
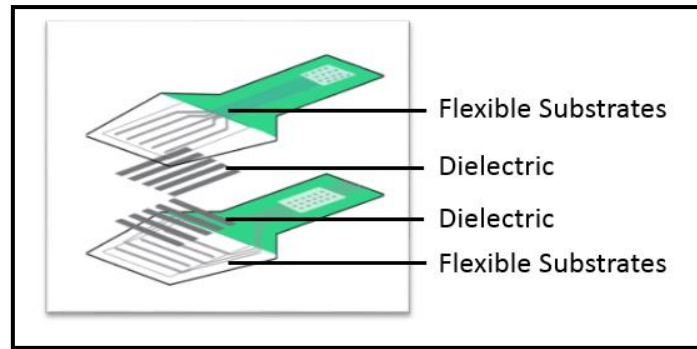
Figure 4.2   Structure of the pressure mapping sensor (Tekscan)

4.3.2. Pressure mapping system

The pressure mapping system consists of three components which are the pressure mapping sensor discussed in Section 4.3.1, a data acquisition electronics and data processing software as shown in Figure 4.3.
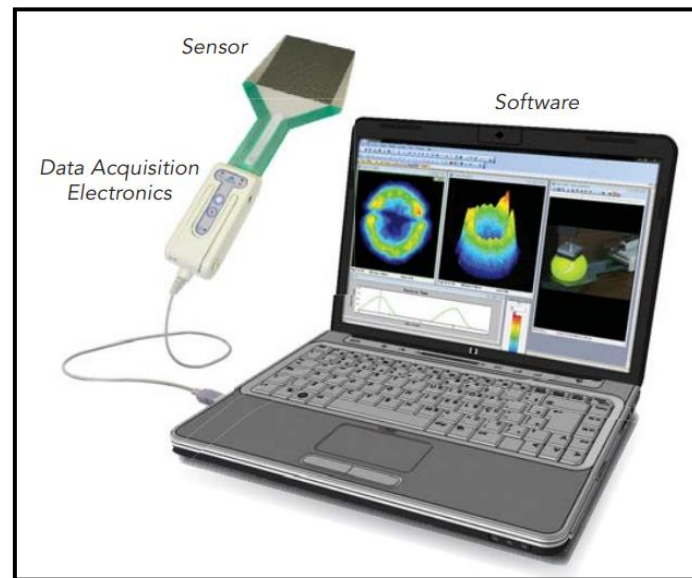
Figure 4.3   Setup of a pressure mapping system (Tekscan)

The intersecting points of the rows and columns of conductive material also named as "Sensels" are viable electrical resistance based on the intensity of captured pressure. The value of the electrical resistance of the "Sensel" is inversely related to the applied pressure as shown blue line in Figure 4.4. The change of the resistance at the "Sensel"

is transmitted by the conductive materials to the data acquisition electronics which is further converted into digital signal and transmitted to and analysed by the Tekscan software installed on a computer. The digital signal is an arbitrary value represented by the red line in Figure 4.4 which relies on the calibration in order to be related to the engineering standard units, for instance, Pascal (Pa) and millimetre of mercury (mmHg). These intensities of pressure captured by the sensor are displayed in form of numerical and graphical data by the software.
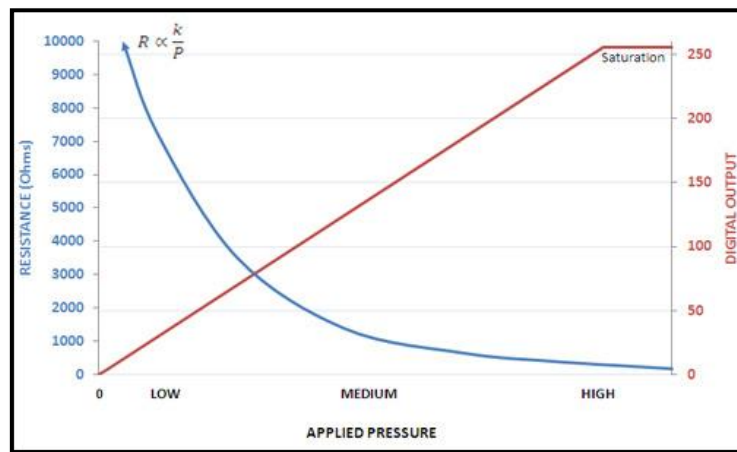
Figure 4.4   Relationship of the electrical resistance of "Sensel" and applied pressure (Tekscan)

4.3.3.   Models of the pressure mapping sensors

Two models of pressure mapping sensors are used in this study, which are sensor I-Scan 5051 and Conformat 5330. The detail of these two sensors are discussed in this section.

I-Scan 5051

I-Scan 5051 is a general purpose pressure mapping sensor and the related parameters are illustrated in Table 4.1 (Tekscan, 2015). It is a flexible and ductile sensor which

could be utilised in measuring the pressure between two solid surfaces.

Table 4.1 Details of I-Scan 5051

Parameters	Values
Number of Sensels	1,936
Height of the Sensing Area	55.9 mm
Width of the Sensing Area	55.9 mm
Overall Length	252.5 mm
Overall Width	81.3 mm
Working Range of Pressure	0 to 48 kPa; 0-360 mmHg

Conformat 5330

Conformat 5330 falls in the category of medical sensors which is mainly utilised to capture the interface pressure between a human body and a support surface typically in seating or supine positions. It is more flexible comparing to I-Scan 5051 because the enclosing layers are made of material similar to normal textile fibres and, most importantly, the "Sensels" are capable of dislocating independently. Hence, the movable "Sensels" can be in the shape of the human anatomy. The details of the Conformat 5330 are illustrated in Table 4.2 (Tekscan, 2016).

Table 4.2 Details of Conformat 5330

Parameters	Values
Number of Sensels	1,024
Height of the Sensing Area	471.4 mm
Width of the Sensing Area	471.4 mm
Overall Length	571.5 mm
Overall Width	627.4 mm
Working Range of Pressure	0 to 34 kPa; 0- 255 mmHg

4.3.4. Roles of pressure mapping in the study

The pressure mapping system utilised in this study contributes mainly to the determination of the working range for the computational model and the evaluation of the applied force in conjunction with the laser Doppler for physiological data acquisition. The acquisition of intensity of pressure commonly found in clinical setting is mainly contributed by the Conformat 5330 because of its flexibility and the large measuring area. Two Conformat 5330 are utilised simultaneously with two data acquisition electronics for capturing the interface pressure at sacrum-mattress and heel-mattress interfaces. The digital signal from the pressure mapping systems are analysed by a Tekscan Software, I-Scan ver. 7.60-30I, in order to provide understandable values of pressure intensities. I-Scan 5051 is utilised to measure the force applied on the probe of the laser Doppler in order to acquire physiological data.

4.4.   Laser Doppler Velocimetry

Laser Doppler Velocimetry (LDV) is a technology for measuring the flow velocity of the particles within a transparent or semi-transparent fluid. The laser Doppler consists of two sets of laser beams which are split from a single beam to ensure the coherence of the two beams. The two beams intersect at the focal point and a set of fringes is generated. Light is reflected and analysed by the laser Doppler velocimetry when a particle is flow through the fringes, hence, to deduce the flowing velocity. A commercially available LDV is utilised in the current study to evaluate the percentage change in blood flow velocity with respect to the magnitudes of the applied mechanical loads.

4.4.1.   Laser Doppler velocimetry of the study

Component PF 5010 – LDPM of the PeriFlux System 5000 from Perimed is utilised as a Laser Doppler Velocimetry in the current study. The LDV captures the change in the microcirculation typically cutaneous blood flow in the current study. The LDV provided by Perimed is total local microcirculatory measurement which captures the microcirculatory for capillaries, arterioles and venules within the measuring zone. The functional details on the Periflux System 5000 and PF 5010 are listed in Table 4.3 (Perimed, 2018). The measuring depth of the LDV depends on tissue properties for instance the structure and density of the microcirculations. i.e. the measuring depth is reduced in blood-rich organs typically kidney (Perimed, 2018). The LDV provides arbitrary measurements in which the changes of the measurements indicate the percentage change in blood flow velocity due to the applied mechanical loads.

Table 4.3 Functional details of Periflux system 5000 and PF 5010

Parameters	Values
Wavelength of Laser	780nm
Measuring Depth	0.5 to 1 millimetre
Measuring units of blood flow velocity	Arbitrary

4.5. Technologies of the Novel Evaluating System

Finite element method, pressure mapping technique and laser Doppler velocimetry are the three key technologies utilised in the current study. Finite element method typically finite element analysis (FEA) is the main tool which approximates and demonstrates the deformation of the cutaneous blood vessels in relating to the formation of superficial pressure ulcers. The pressure mapping technique is utilised to determine the working range of the computational model by investigating the commonly found intensity of pressure at clinical. The pressure mapping system is also utilised in conjunction with the laser Doppler to determine the change in cutaneous blood flow due to the application of different magnitudes of mechanical loads. The relationship of the three technologies is illustrated in Figure 4.5.
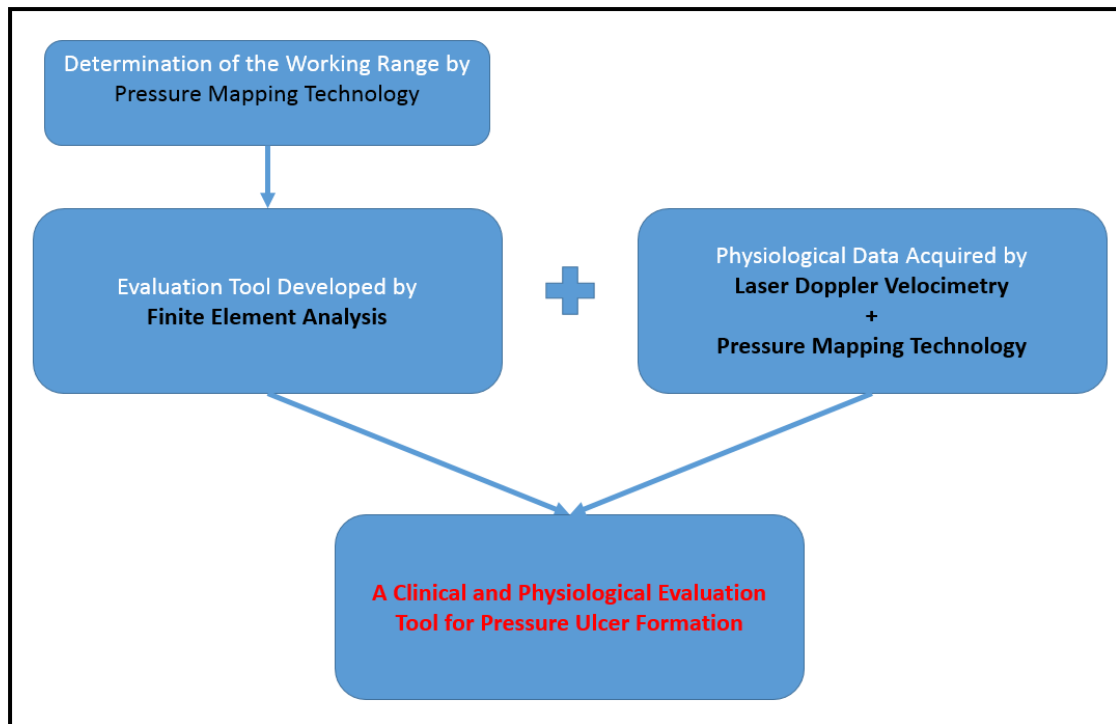
Figure 4.5   Technologies in the novel evaluating system

Chapter 5   Pressure Mapping Measurement

5.1.   Introduction

The clinical relevance of a novel evaluation tool developed in this study is dependent on the input parameters and an understanding and determination of the working range based on the commonly found intensity of interface pressure on skin. The input parameters include dimensions of the cutaneous layers and blood vessels and the material properties of the cutaneous layers based on existing knowledge discussed in Chapter 2 and Chapter 3. The aim of this chapter is to determine the clinically relevant working range of the computational model by acquiring commonly found intensity of interface pressure with pressure mapping equipment. This Chapter presents the design and results of two pressure mapping testing for static and dynamic mattresses. The captured interface pressure by using Conformat 5330 will be presented which determines the working range for the computational model.

5.2.   Methodology of Pressure Measurement

The working range of the computational model is determined by the intensity of interface pressure found in this pressure mapping study. The pressure mapping measurements are conducted by using the Confortmat 5330 for capturing the interface pressure between the volunteers and the mattresses. Two categories of the pressure mapping measurements were conducted in this study; static mattress testing and dynamic mattress testing.

5.2.1.   Static mattress testing

Two static mattresses manufactured from the same company which were made of different grades of foam were used. Four healthy volunteers participated in the static

mattress testing, Body Mass Index (BMI) of the volunteers were from 19.5 to 28 which were within the ranges of healthy weight and slightly overweight (N. H. S. NHS, 2016).

Both of the Confortmat 5330 were connected to the data acquisition electronics and the Tekscan software on a computer as shown in Figure 5.1. The two Confortmat utilised for the measurements were calibrated before conducting the static mattress testing. After four two-kilogram of known mass weight was put on the two Conformat pieces laid on the rigid floor for calibration, the two mattresses were put on a hospital bedding allowing the volunteers to be in clinical relevant postures when the backrest was inclined to 30 and 45 degrees for testing.
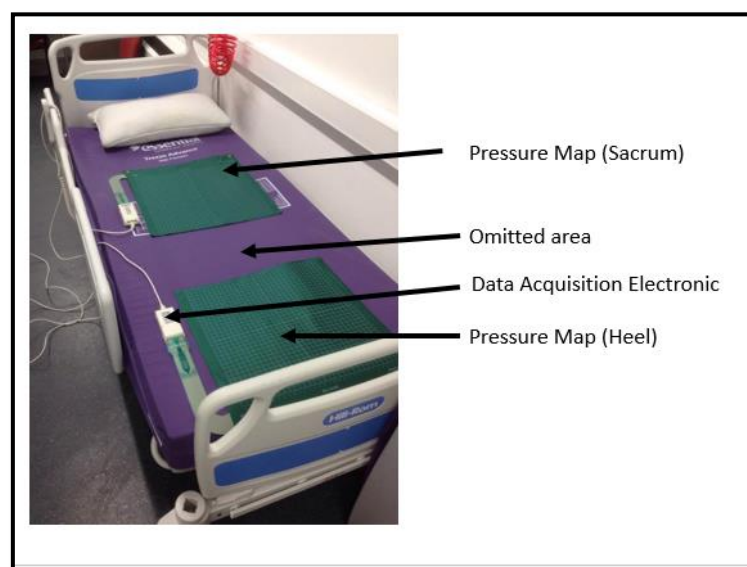
Figure 5.1   Pressure mapping system for static mattress testing

The volunteers were in supine position on the mattresses after emptying the pockets and removing hard objects from the bodies including belts and shoes. The intensities of the interface pressure at the sacrum-mattress and heel-mattress with the backrest inclined at 0, 30 and 45 degree angle were measured for each of the four volunteers.

5.2.2. Dynamic mattress testing

The dynamic mattress testing consisted of five dynamic mattresses in which first four were designed by hospital setting and the fifth one is for community setting by three companies. Due to the physical size of the community mattress, it could not be placed in the hospital bedding and it was tested on the floor only. The dynamic mattresses consisted of a number of air cells which allowed the sections of mattresses to be inflated and deflated independently enabling the relocation of the load bearing location. The same setup procedures mentioned in Section 5.2.1 were conducted for the dynamic mattress testing for the pressure mapping sensor, Confortmat 5330. Three participants with a BMI from 20.6 to 26 took part in the dynamic mattress testing.

Operation of the dynamic mattresses were more complicated as compared to the static mattresses. Each dynamic mattress consisted of an air pump which drove air in and out the air cells of the mattresses and controlled the level of pressure redistribution. The level of pressure redistribution referred to the amount of air flowing into the air cells which could be adjusted to maintain a balance between the intensities of the pressure at patient-mattress interface and stability of the mattress. All mattresses were set at the highest level of pressure redistribution in order to evaluate the best performance which also reflected the realities of clinical practice.

The dynamic mattress testing consisted of three stages including:

- **Air pump off**- Pressure mapping measurement is conducted without air pump.
- **Settling**- The dynamic mattresses are settled with the air pump in order to ensure sufficient air is pumped into the mattresses

- **Operating with air pump**- Pressure mapping measurement is conducted with air pump

First Stage

The first stage of pressure mapping measurement was conducted on the dynamic mattresses without the operation of the air pumps. This is a stage which was only conducted with three of the dynamic mattresses as this is not a suggested functioning condition in clinical practice. However, it does happen in clinical practice.

Second Stage and Final Stage

The second stage of the dynamic mattress testing was to provide a settling period in between 5 to 10 minutes allowing the dynamic mattress to be fully inflated. After the settling period, pressure mapping measurements were conducted with the operation of air pumps. The measurement period was planned in line with the duration of a complete air cells inflating and deflating cycle of the whole mattresses. As these dynamic mattresses were distinctive models from three different companies, the operating cycles were different for each mattress. The operating cycles were approximately 15 to 20 minutes according to the information provided by the companies. Hence, in order to obtain the intensities of the interface pressure, ten pressure mapping measurements were conducted at the sacrum-mattress and heel-mattress interfaces during the 15 to 20 minutes measurement period for each mattress and volunteer. The whole procedure of the dynamic mattress testing was repeated with the backrest at 0 degree and inclined by 30 and 45 degrees.

5.3.   Interface Pressure Measurement for Static Mattress

Pressure ulcer formation is often caused by localised excessive pressure applied on

skin which collapses the cutaneous blood vessels and obstructs the microcirculation. Hence, peak pressure was the key parameter compared to the average interface pressure.

Measured peak interface pressures in millimetres of mercury (mmHg) recorded at heel and sacrum of each volunteer 1 to 4 are presented in Table 5.1 and Table 5.2 respectively. There were a total of 48 measurements, from 4 volunteers, at heel and sacrum on two different mattresses

Table 5.1 Peak interface pressure (mmHg) at heel for static mattress

Mattress	Degree	Volunteer 1	Volunteer 2	Volunteer 3	Volunteer 4
1	0	20	57	39	34
1	30	23	41	21	31
1	45	28	69	37	35
2	0	21	28	23	33
2	30	20	24	24	24
2	45	30	28	39	28

Table 5.2 Peak interface pressure at sacrum (mmHg) for static mattress

Mattress	Degree	Volunteer 1	Volunteer 2	Volunteer 3	Volunteer 4
1	0	32	41	31	27
1	30	27	44	34	38
1	45	37	52	49	34
2	0	27	36	26	22
2	30	26	37	39	37
2	45	28	42	36	35

5.4. Interface Pressure Measurement for Dynamic Mattress

The dynamic mattress testing consisted of five mattresses and three volunteers. The pressure mapping measurements were conducted with the backrest inclined at 0^0, 30^0 and 45^0. Ten measurements were conducted for each dynamic mattresses. An extra measurement was conducted without the operation of the air pumps for three mattresses at all backrest angles (hospital setting ones). In total 762 interface pressure measurements were recorded at the sacrum and heel. Three parameters were presented for the dynamic mattress testing including:

- **Average Peak Pressure (AvPP)** AvPP is the average value of the peak pressure values provided by each set of the 10 measurements during the mattress cycle with the operation of the air pumps.
- **Absolute Peak Pressure (AbPP)** – AbPP is the maximum value of the peak pressure values from each set of the 10 measurements.
- **Peak Pressure Without Air Pump (PPWAP)** – PPWAP is the peak pressure measured when the volunteer in supine position on the dynamic mattresses

without the operation of the air pump.

All the pressure magnitudes presented in this section were in millimetre of mercury.

5.4.1. Average peak pressure of the dynamic mattress testing

Table 5.3 to Table 5.6 present the average peak pressure measured by the pressure mapping system at the sacrum-mattress and heel-mattress interfaces for hospital settings and for community setting with no inclination of backrest

Table 5.3 Average peak pressure (AvPP) for dynamic mattress 1

	Sacrum-Mattress Interface			Heel-Mattress Interface		
Backrest Inclination (degree)	0	30	45	0	30	45
Volunteer 1	41.6	47.8	56.0	47.8	47.8	74.7
Volunteer 2	27.6	44.8	101.3	47.8	88.3	44.5
Volunteer 3	60.4	125.9	103.4	37.4	24.1	31.4

Table 5.4 Average peak pressure (AvPP) for dynamic mattress 2

	Sacrum-Mattress Interface			Heel-Mattress Interface		
Backrest Inclination (degree)	0	30	45	0	30	45
Volunteer 1	66.2	76.7	70	29.5	26	24.5
Volunteer 2	37.0	52.4	63.2	28.7	38.6	26.2
Volunteer 3	40.6	59.4	69.5	25.7	28.3	31.1

Table 5.5 Average peak pressure (AvPP) for dynamic mattress 3

	Sacrum-Mattress Interface			Heel-Mattress Interface		
Backrest Inclination (degree)	0	30	45	0	30	45
Volunteer 1	42.2	46.5	55.4	53.8	83.7	71.3
Volunteer 2	60.6	56.8	63.7	61.0	60.8	61.4
Volunteer 3	51.8	54.7	57.6	40.2	66.3	47.8

Table 5.6 Average peak pressure (AvPP) for dynamic mattress 4

	Sacrum-Mattress Interface			Heel-Mattress Interface		
Backrest Inclination (degree)	0	30	45	0	30	45
Volunteer 1	40.1	41.3	52.3	52.0	55.0	60.3
Volunteer 2	63.5	53.6	53.0	51.7	38.6	56.4
Volunteer 3	37.2	57.3	49.4	37.3	33.5	47.8

Table 5.7 Average peak pressure (AvPP) for dynamic mattress 5

	Sacrum-Mattress Interface	Heel-Mattress Interface
Backrest Inclination (degree)	0	0
Volunteer 1	29.8	29.1
Volunteer 2	51.6	36.2
Volunteer 3	81.4	38.9

5.4.2. Absolute peak pressure of the dynamic mattress testing

Table 5.8 to Table 5.12 present absolute peak pressure measured by the pressure mapping system at the sacrum-mattress and heel-mattress interfaces for hospital settings and for community setting with no inclination of backrest

Table 5.8 Absolute peak pressure (AbPP) for dynamic mattress 1

	Sacrum-Mattress Interface			Heel-Mattress Interface		
Backrest Inclination (degree)	0	30	45	0	30	45
Volunteer 1	45	55	63	51	55	82
Volunteer 2	31	55	116	55	96	57
Volunteer 3	67	137	137	71	35	37

Table 5.9 Absolute peak pressure (AbPP) for dynamic mattress 2

	Sacrum-Mattress Interface			Heel-Mattress Interface		
Backrest Inclination (degree)	0	30	45	0	30	45
Volunteer 1	73	82	79	39	31	35
Volunteer 2	47	67	114	35	55	33
Volunteer 3	51	67	82	31	39	43

Table 5.10 Absolute peak pressure (AbPP) for dynamic mattress 3

	Sacrum-Mattress Interface			Heel-Mattress Interface		
Backrest Inclination (degree)	0	30	45	0	30	45
Volunteer 1	47	57	66	68	129	87
Volunteer 2	69	76	72	74	74	78
Volunteer 3	57	66	66	52	57	65

Table 5.11 Absolute peak pressure (AbPP) for dynamic mattress 4

	Sacrum-Mattress Interface			Heel-Mattress Interface		
Backrest Inclination (degree)	0	30	45	0	30	45
Volunteer 1	44	47	57	78	58	68
Volunteer 2	72	69	57	58	45	78
Volunteer 3	47	59	53	42	39	55

Table 5.12 Absolute peak pressure (AbPP) for dynamic mattress 5

	Sacrum-Mattress Interface	Heel-Mattress Interface
Backrest Inclination	0	0
Volunteer 1	37	45
Volunteer 2	71	47
Volunteer 3	96	61

5.4.3. Peak pressure of dynamic mattress testing without the Operation of air pump

Three mattresses including mattress 1, 2 and 5 were involved in the additional stage for the comparison of the performance of dynamic mattresses with and without the functioning air pumps. Table 5.13 to Table 5.15 present the peak pressure measured without the operation of air pump for each volunteer allowing the dynamic system to function as a static system .

Table 5.13 Peak pressure without air pump (PPWAP) for dynamic mattress 1

	Sacrum-Mattress Interface			Heel-Mattress Interface		
Backrest Inclination (degree)	0	30	45	0	30	45
Volunteer 1	37	67	67	20	55	41
Volunteer 2	49	53	75	45	88	24
Volunteer 3	51	94	122	24	31	26

Table 5.14   Peak pressure without air pump (PPWAP) for dynamic mattress 2

	Sacrum-Mattress Interface			Heel-Mattress Interface		
Backrest Inclination (degree)	0	30	45	0	30	45
Volunteer 1	55	55	59	24	27	37
Volunteer 2	27	41	47	27	27	57
Volunteer 3	31	51	73	26	24	45

Table 5.15   Peak pressure without air pump (PPWAP) for dynamic mattress 5

	Sacrum-Mattress Interface	Heel-Mattress Interface
Backrest Inclination (degree)	0	0
Volunteer 1	24	20
Volunteer 2	106	37
Volunteer 3	75	26

5.5.   Discussions

The measured intensities of the interface pressure for all the pressure mapping measurements are discussed in this section, inter-testing comparisons were also conducted and discussed.

5.5.1.   Clinical relevant intensity of interface pressure

The primary aims of this study were to develop a novel evaluation tool for both clinicians and medical device. Hence, the intensities of the interface pressure were measured with different static and dynamic mattresses which are available in the commercial market. These measured intensities of interface intensities reflect the realities in clinical practices. Figure 5.2 shows the number of occurrences of the intensities of measured peak pressure against the respective range, these occurrences include peak pressure readings from static mattress testing, absolute peak pressure (AbPP) for dynamic mattress testing, peak pressure from the dynamic mattress without air pump. Over 91% of the measured pressure was in the range of 20 to 79 mmHg approximately 8.5% of measurements were out of this range. There were no

intensities of pressure within the range of 0 to 19 mmHg due to the fact that all the intensities presented in this chapter were peak pressure. There was pressure within the range of 0 to 19 mmHg in the pressure mapping measurements, these irrelevant to the study as the pressure ulcer development only occurs at the area of the peak pressure.
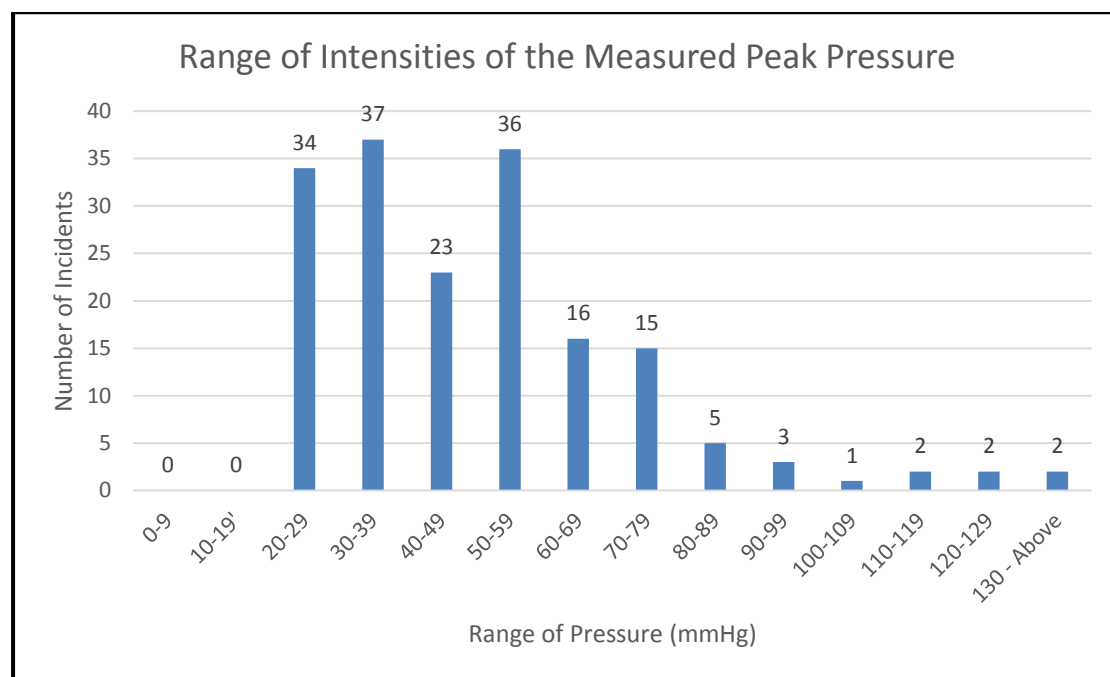
Figure 5.2   Range of intensities of the measured peak pressure

5.5.2.   Relationship of backrest inclination and interface pressure

A total of 768 pressure mapping measurements were conducted on the hospital static and dynamic mattress testing which with the backrest inclined by 0, 30 and 45 degrees. Interface pressures of the static mattress testing, and Average Peak Pressure (AvPP) and Absolute Peak Pressure (AbPP) of the dynamic mattress testing were compared with different backrest inclining angles as shown in Figure 5.3. The comparisons presented in Figure 5.3 include the measurements conducted on both the sacrum and heels. Figure 5.3 shows that the intensities of the interface pressure were higher when

the backrest was inclined. This phenomenon was contributed by the change in postures of the volunteers. The weight of the volunteers were evenly distributed on the mattresses by spreading the load across the whole back when the backrest was not inclined. However, the weights of the upper bodies significantly loaded on the lower end of the elevated section, the sacrum, when the backrest was elevated by 30 and 45 degrees. Indeed heels of the volunteers loaded heavier when the backrest was elevated. This phenomenon was contributed by attempting in stopping the sliding down of the body due to the elevated upper part of the body. The intensities of the interface pressure measured were the highest in the majority of the comparisons when the backrest was inclined by 45 degree. Figure 5.3 demonstrates a significant phenomenon that the elevation of the backrest resulted in a higher interface pressure at both sacrum and heels which could lead to a higher risk of pressure ulcer development. The percentages presented in Figure 5.3 are the percentage of comparison met the following criteria i.e. "pressure at 45 and 30 degree is the highest", "pressure at 45 degree is the highest" and "pressure at 0 degree is the highest".
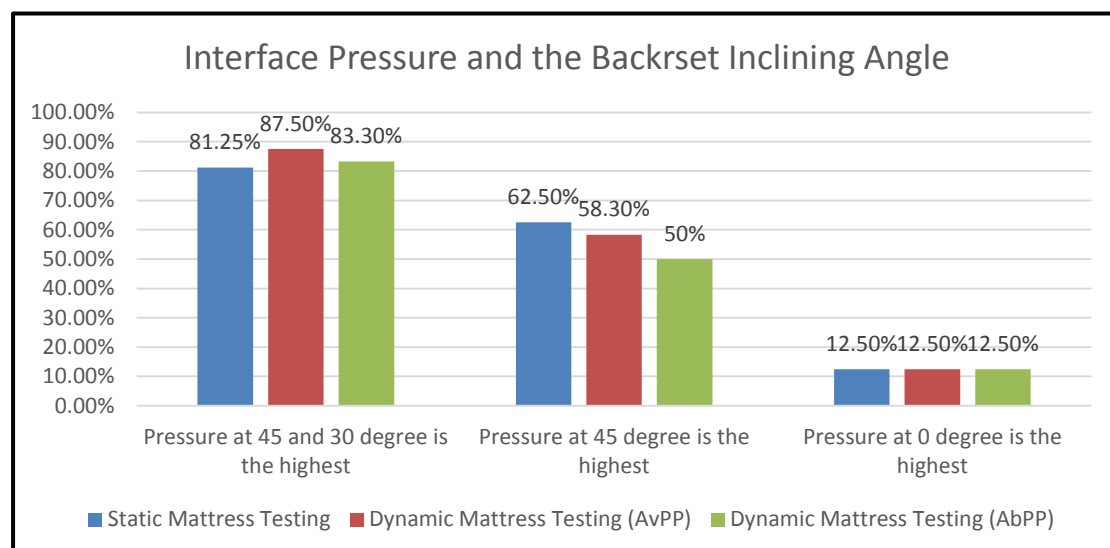
Figure 5.3   Relationship of the interface pressure and the backrest inclining angle

5.5.3. Dynamic mattress without the operation of air pump

The intensities of pressure measured and presented in Section 5.4.3 were the interface pressures between the dynamic mattress and the volunteers without the function of the air pump. The results compare the intensities measured in Section 5.3 from the static mattress testing even though the participants to the pressure mapping measurement were different for static and dynamic mattress testing. The comparisons were conducted with the average values among all the volunteers to be more objective. Table 5.16. highlights 6 comparisons in which the intensities of the interface pressure between the dynamic mattress without air pump were generally higher than intensities of interface pressure measured in static mattress testing. Dynamic mattresses in general consisted of a number of air cells which allowed to be inflated and deflated for the purpose of redistributing the load to different anatomical locations. These air cells were made of plastic and the air cells were deflated after switching off the air pumps. Hence, the volunteers were in contact with plastic when the dynamic mattresses were switched off. In some of the designs, there were foam inside the air cells, and the patients were laying on top of a plastic with a layer of foam underneath. The effect of the foam was uncertain and depended on the stiffness of the plastic material of the air cells. In contrast, the static mattresses consisted of foam even without the capability in re-distributing the loads to different anatomical locations, the static mattresses were capable of lowered the intensities of interface pressure by allowing higher submerging area. The Table 5.16 showed that the volunteers experienced higher intensities of interface pressure comparing to adopting static mattresses when the air pumps of the dynamic mattresses were switched off. Thus, clinicians may consider offering static mattresses to those patients who refuse to be on dynamic mattresses.

Table 5.16   Comparison of the interface pressure from the dynamic mattress without air pump and static mattress

	Sacrum			Heels		
Backrest Inclination (degree)	0	30	45	0	30	45
Dynamic Mattress without Air Pump	Higher	Higher	Higher	Lower	Higher	Higher
Static Mattress	Lower	Lower	Lower	Higher	Lower	Lower

5.5.4.   Standardising pressure mapping procedure of mattress

The procedures for the pressure mapping measurement of both the static and dynamic mattresses have been uniquely designed for this study. There are no commercially available tests that are able to determine, with accuracy, interface pressure between the patient and mattress found in British Standard system and International Organization for Standardization (ISO). The majority of the standard associated with the mattress relate to the ignitability of the mattress, BS EN 597-2015, (British Standards, 2016) and only a few standards relate to the loading aspect of the mattress, BS EN 1957:2012, (British Standards, 2012). The absence of a standard testing procedure guidelines results in mattress testing that is not comparable and prevents clinicians being able to determine efficiency of mattresses. Testing guidelines should not be only limited to the primary function but also to the factors associated to the

efficiency of the products. Hip prosthesis, for instance, testing standards were not limited to the primary loading function of the femoral heads, BS ISO 7206-10:2018, but also to the factors that could determine the efficiency, surface finish BS ISO 7206-2:2011+A1:2016. For the pressure reliving mattresses which are mainly used for hospital and elderly care setting, interface pressure is one of the key factors associating with the efficiency. Hence, there is an urgent need to establish international recognised testing guidelines for both static and dynamic mattresses. With these standardised testing methods, the results of the pressure mapping from different institutes are meaningful and comparable so that the clinicians are capable of understanding the efficiency and performances of the mattresses and allocate suitable mattresses for the patients.

5.6. Conclusions

A comprehensive pressure mapping study was conducted on two static and five dynamic mattresses. The aim of the study was to develop a computational model for both the clinicians and medical device developers and one of the factors to ensure the tool is clinical relevant is the working range. It was determined that the majority of the interface pressure was within the range of 20 to 79 mmHg and the whole range of peak pressure was in between 20 and 137 mmHg within both of the pressure mapping testing.

The elevation of the backrest was discovered to increase the intensities of pressure at both of the interested anatomical locations, sacrum and heel. Interface pressure was found to be the highest in over half of the instances when the backrest was inclined by 45 degree. For the patients who lost of sensations are more susceptible to pressure ulcer formation when they are laying on bed with the inclined backrest, interventions should be applied for instance body turning in more frequent manner.

Higher interface pressure was measured on the dynamic mattresses without the operation of the air pumps comparing to the static mattresses. Clinicians may consider to provide patients with static mattresses when patients are unsatisfied with dynamic mattresses to preventing them from switching off the air pumps.

Standardised guidelines of measuring interface pressure on mattress are essential in the field of pressure ulcer prevention. However, there was a lack of guidelines which were significant when the pressure mapping study was conducted for both the mattresses. There was a lack of pressure mapping guidelines for any kind of static and dynamic mattresses. Different structures of mattresses are available in the commercial market with different working principles, it is crucial to establish guidelines for evaluating the effectiveness of these mattresses as so to provide objective data for the clinicians.

Chapter 6   Quartered Model

6.1.   Introduction

As outlined in the literature survey, there was a gap in the understanding of the deformation of cutaneous blood vessels (CBV) under mechanical loads including pressure, friction and the combination of both. Also, there is a lack of tools for evaluating the effects of medical devices on the blood vessels.

Finite element analysis (FEA) is a conventional method of evaluating and predicting the behaviour and deformation of material under different circumstances in engineering. This method is adopted in this study to demonstrate the deformation of CBV. A group of healthy volunteers was studied to determine the effects of the mechanical loads on their skin. A three-dimensional FEA quartered model is developed which is capable of demonstrating the behaviours of the cutaneous blood vessels with the application of pressure, friction, and the combination of both. The quartered model was also presented in the Journal of Wear (Leung, Fleming, Walton, Barrans, & Ousey, 2017).

6.2.   Background, Aim and Objectives

It is noted that there is a lack of tools to analyse and evaluate the deformation of blood vessels underneath the skin surface caused by different mechanical loads on skin including pressure and friction. Ischemia is a known cause of pressure ulcers (EPUAP, 2014). Prolonged mechanical loadings applied to skin restricts the cutaneous blood flow (EPUAP, 2014). As a result, the lack of oxygen, accumulation of the metabolic wastes and decrease in pH value would ultimately cause cells deaths and the occurrences of pressure ulcers (Harrison & Walker, 1979). A large amount of research

has been conducted to understand the mechanism of pressure ulcers formation, excessive stress, and protocols for pressure ulcer prevention have been established by clinicians. However, little investigation has been carried out on the deformation of CBV in different loading situations. Two types of loadings can cause the formation of pressure ulcer including patients resting on mattresses, caused by self-weight, and also attached medical devices on patients' bodies for monitoring purpose, caused by the fixation force. The effects of the mechanical loads, self-weight and fixation force on the deformation of CBV are essential for the design of medical devices. Aside from the functional aspect of the medical devices, the influence of the devices on the CBV should also be considered especially when the devices are directly in contact with skin. The first step of successfully evaluating the blood vessel deformation caused by mechanical loads is to develop a computational model to demonstrate the loading conditions.

The aim of this chapter is to develop a three-dimensional FEA model which is capable of demonstrating the behaviours of the CBV with the application of pressure, friction and the combination of both.

The study reported in this Chapter has three objectives:

- To acquire pressure mapping measurement of volunteers sitting on foam and rigid support surfaces
- To develop a 3-dimensional finite element analysis model to represent skin
- To study the deformation of CBV under the influence of sitting on foam and rigid surfaces.

6.3. Finite Element Analysis of the Quartered Model of Skin

Finite element analysis is a well-established numerical technique for solving engineering problems. It has a variety of functions for instance evaluating the stress and strain of prosthesis (Colic et al., 2016). For this study, finite element analysis is used to demonstrate the deformation behaviour of the CBV. Abaqus CAE 6.14 is used to develop the model and conduct the simulations. This Chapter presents an initial model which is developed to demonstrate the deformations of blood vessels caused by sitting on foam.

6.3.1. Features of the quartered model

The initial computational model of skin was in the shape of a quartered circle, hence, it is named as quartered model. The quartered model consisted of four layers representing three different skin layers including: epidermis, dermis and hypodermis as shown in Figure 6.1. The extra horizontal layer in the model was stratum corneum which is a sublayer of the epidermis in physiology. This extra layer was created in the model because of the significant differences in its mechanical properties from the remaining epidermis. Each of the layers was modelled with different mechanical properties to accurately predict their behaviours under different mechanical loads. The blood vessels were located at the centre of the quartered model. The quartered model was designed and developed to be excessively large so that the boundary condition of the peripheral surface had minimum effect on the deformation of the blood vessels located at the centre, which will be discussed later in this Chapter. As the model was in the shape of a quartered circle, it was symmetrical in X and Z direction while Y was the vertical depth of skin as shown in Figure 6.2.

Figure 6.1   Horizontal layers of the quartered model
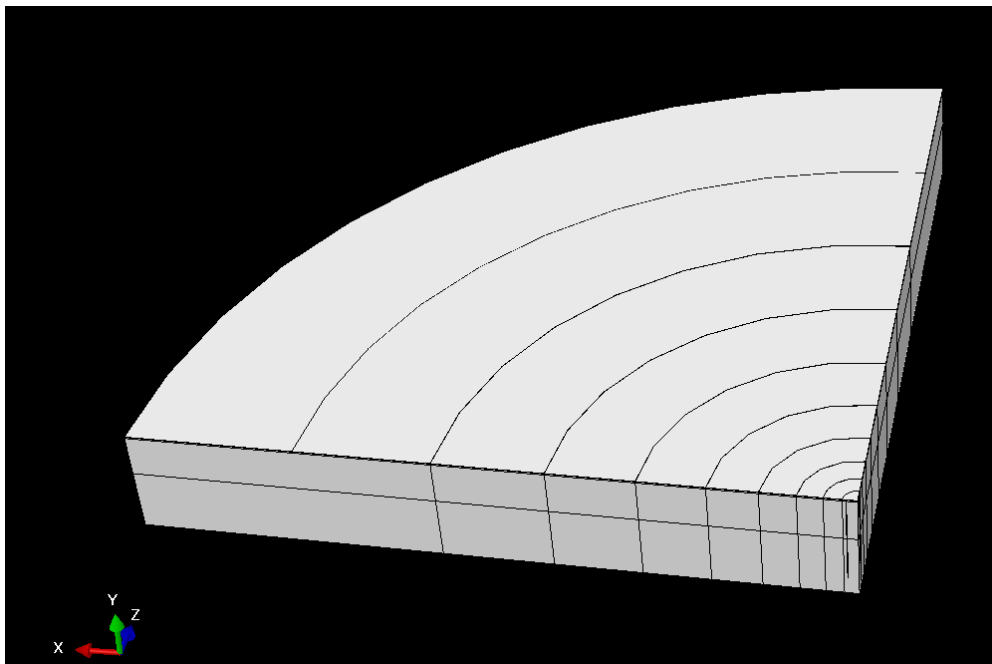
Figure 6.2   Directions of the quartered model

The model had a radius of 20,600 micrometres (20.6 millimetres) and was partitioned into 9 radial sections in total, allowing elements with different mesh sizes could be adopted in each section. The radial sections are named 1 to 9, section 1 at the centre and the section 9 being the outermost, as shown in Figure 6.3.
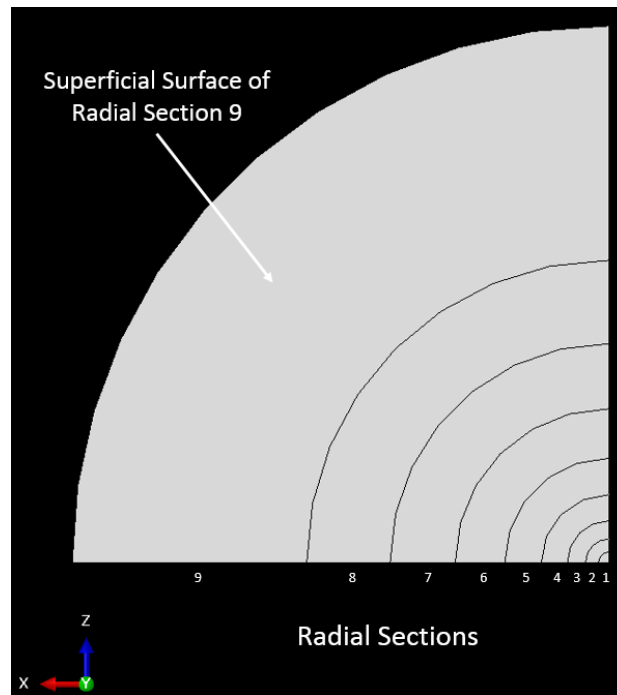
Figure 6.3   Radial section 1 to 9 and partitioning

Abaqus CAE 6.14 is default to SI units and it cannot be changed. The quartered model was developed on the micrometre scale to facilitate the design of the CBV. The input of the mechanical properties and the magnitudes of the loadings, thus, require suitable conversions which will be explained in later section in this Chapter.

6.3.2. Blood vessels

The blood vessels are located at the centre of section 1 in Figure 6.3. The blood vessels configuration in the quartered model was designed according to Michel Démarchez's research who has been an expert in Dermatology and Cosmetics for 30 years. Two vascular plexuses are located at the dermis layer while the superficial and deep vascular plexus are located close to the epidermis-dermis interface and dermis-hypodermis interface respectively. These horizontal vascular plexuses are joined by vertical ascending arterioles (Démarchez, 2011; Millington & Wilkinson, 2009). The blood vessels configuration in the quartered model was designed according to Michel's

discovery in the location of cutaneous blood vessels. Hence, in the quartered model, there were two horizontal circular tubes in the dermis layer close to the epidermis-dermis and dermis-hypodermis interfaces respectively. Both the horizontal and vertical tubes in the quartered model were 15 micrometre in diameter to represent the transitional blood vessels from arterioles and capillaries (Yen & Braverman, 1976). The hypodermis was deemed to be highly vascularised (Millington & Wilkinson, 2009; Saladin, 2007) but exact location of blood vessels is yet to be determined due to the amount of blood vessels, hence an additional seven tubes were created in the hypodermis layer with random spacing. These nine-horizontal vascular tubes were named blood vessel 1 to 9 from the superficial to the bottom. These 9 blood vessels are joined by two vertical ascending arterioles represented by two tubes also with 15 micrometre in diameter as shown in Figure 6.4. Although the CBV plexuses would be in a more complex configuration physiologically, the simplified blood vessels configuration in the computational model do have locational and dimensional relevance. Blood vessels are also spread across the skin and a blood vessel plexus rarely stands alone. However, there is only one set of blood vessel plexuses in this model for simplification in this FEA simulation. This is an initial attempt in developing a computational model or tool to evaluate the effect of mechanical loads on the deformation of cutaneous blood vessels. Even with the simplified vasculature configurations, the effect of mechanical loads can be evaluated. This is a step forward and provides a tool in this underdeveloped area.
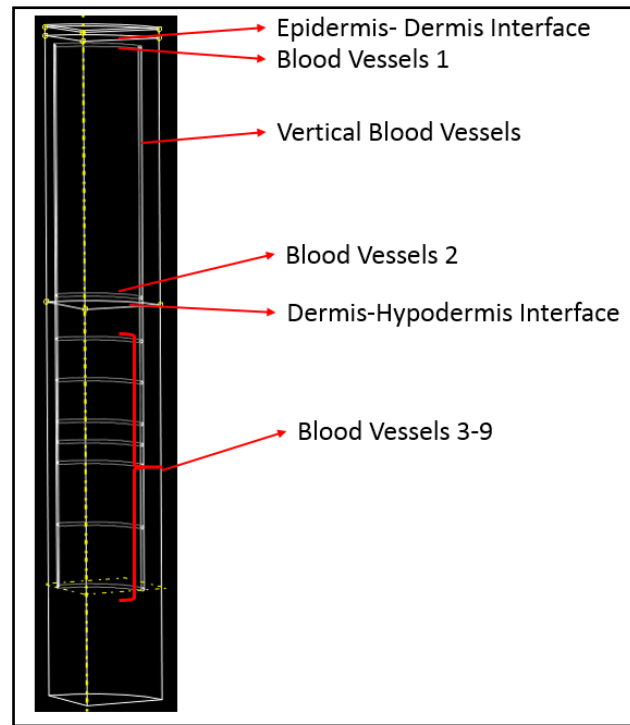
Figure 6.4   Blood vessel configuration in the quartered model

On each of the horizontal blood vessel, there are three sections of interest as shown in Figure 6.5. These sections of interests are labelled A to C from left to right and the number following the letter indicates the vertical location of the blood vessels. "A1" indicated the first section of interest from the left on the first blood vessel from the top. All these sections of interest were established by partitioning the model. As a result of assigning the sections of interest on the blood vessels and partitioning of edges, there were four key nodes at each section of interest enabling the calculation of the change in cross-sectional areas due to the application of mechanical loads on the superficial surfaces.
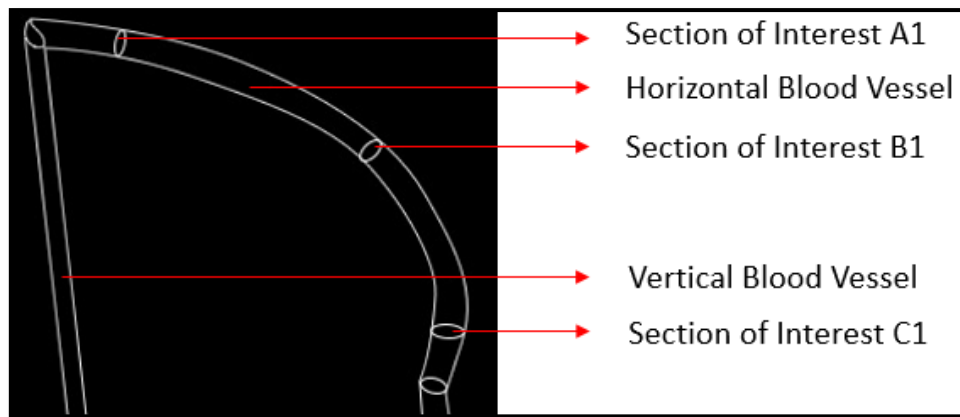
Figure 6.5   Sections of interest on the blood vessels

6.3.3. Mechanical properties and dimensions of skin layers

Research had been conducted on the mechanical properties of skin layers and their respective thicknesses. It was hard to determine the mechanical properties of skin as it is an anisotropic material and its mechanical properties change with factors including: temperature, hydration level, age and nutrition. As this quartered model is an initial step toward a more complete model, it represents a general healthy skin condition. Thus, the most representative skin mechanical properties in the literature will be adopted. Hwang (Hwang, Kim, & Kim, 2016) found that the thicknesses of the epidermis, dermis and hypodermis were 32 to 42 µm, 949 to 1,350 µm and 1,913± 1,066 µm respectively. These results were acquired from different skin regions of 12 cadavers. A computational skin model was developed in 2013 by Lévêque in which the stratum corneum thickness was calculated as 10 to 20 µm (Lévêque & Audoly, 2013). The dermis layer was set to be 1,285 µm which was in line with Hwang's findings in 2016. From the computational model developed by Lévêque, the elastic moduli of the stratum corneum, epidermis and dermis were: 1 to 12 MPa, 0.05 MPa and 0.6 MPa respectively. Liang's in vivo study in 2010 found skin thickness and moduli by using spectral-domain optical coherence tomography (OCT) (Liang & Boppart, 2010). The

128

thicknesses of stratum corneum and epidermis of forearm were 10 μm and 56.8 to 68.2 μm respectively. The palm was found to have an exceptionally thick stratum corneum which was 129.9 μm and an epidermis of 73.8 μm. The Young's moduli of the volar forearm, dorsal forearm and palm were 101.180 kPa, 68.678 kPa and 24.910 kPa respectively. The calculation of Liang's study assumed that the skin density of 1.02 g/cm^2 and a Poisson's ratio of 0.5. By analysing the data found in the literature, the mechanical properties and dimensions of the different cutaneous layers adopted in the quartered model are summarised in Table 6.1. It was noted from Chapter 2 that there was a lack of robust and comprehensive study in the elastic moduli of all the cutaneous layers. However, the set of mechanical properties input for the model developed by Lévêque in 2016 was closely related to the current study hence the set of mechanical properties was adopted.

Table 6.1   Mechanical properties and dimensions of all cutaneous layers in quartered model

Skin Layer	Thickness (μm)	Young's Modulus (MPa)	Young's Modulus in Abaqus (MPa)	Poisson's Ratio of Skin
Stratum corneum	10 μm	1 MPa	1×10^{-6} N/μm^2	0.5
Epidermis	42 μm	0.05 MPa	$5x^{-8}$ N/μm^2	
Dermis	1,285 μm	0.6 MPa	6^{-7} N/μm^2	
Hypodermis	1,913 μm	0.11 MPa	1.1^{-7} N/μm^2	

As mentioned in section 6.3.1, the quartered model was developed with respect to

micrometre. Therefore, the inputs of the Young's Moduli were required to be converted to Newton per square micrometre. The input of Young's modulus of the stratum corneum was 1×10^{-6} calculated as shown below and presented in the fourth column in Table 6.1.

$1 \text{ N/m}^2 = 1\times10^{-12} \text{ N/}\mu\text{m}^2$

$1 \text{ MN/m}^2 = 1\times10^{-6} \text{ N/}\mu\text{m}^2$

6.3.4. Boundary condition

The boundary condition represents the fixation method of the component. It was hard to assign boundary conditions to the model which was representing, demonstrating and behaving like skin as it is soft and deformable. There were three boundary conditions assigned to the quartered model on the peripheral surface, bottom surface and side surfaces as shown in Figure 6.6.
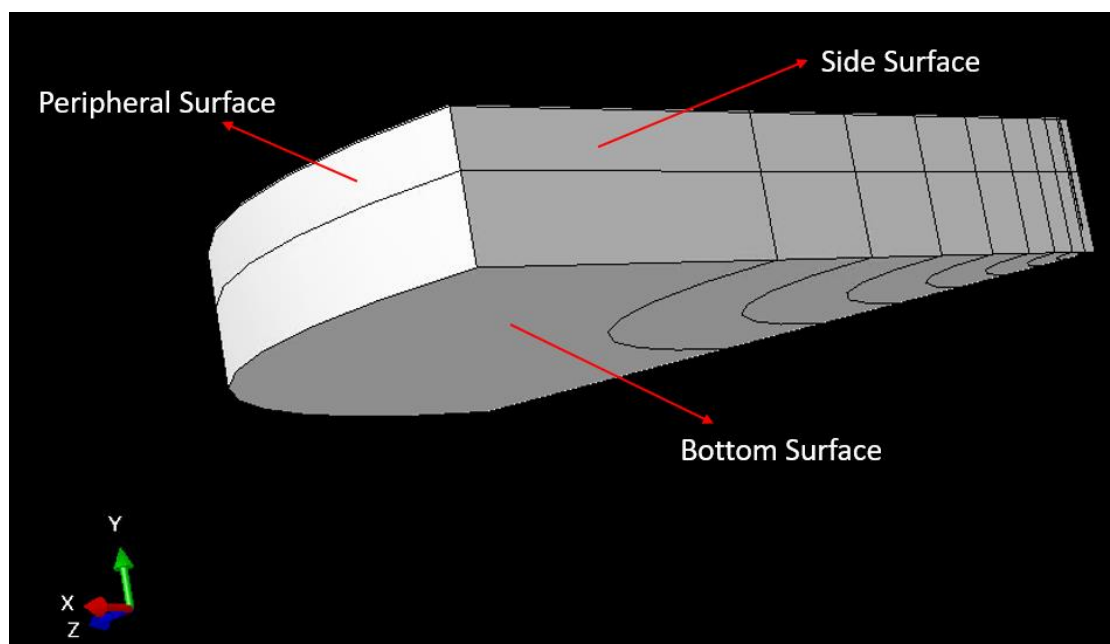
Figure 6.6   Three surfaces of the quartered model

As the quartered model represented skin in a circular shape, the side surfaces were assigned with the symmetric boundary conditions. In Abaqus CAE, the symmetric boundary conditions were labelled as "XSYMM (U1=UR2=UR3=0)" and "ZSYMM (U3-UR1-UR2=0)" respectively on the two side surfaces in which "U", "UR", "1", "2" and "3" represented "translational movement", "rotational movement", "in X direction", "in Y direction" and "in Z direction" respectively. By applying these two mirror boundary conditions, the quartered model would represent the skin in a circular region. Superficial pressure ulcer on bony prominences where little fat and muscle are in between the skin and the bones. Therefore, it was assumed that the bottom is immovable in depth direction and minimum deformation in X and Z direction which is the condition set for the bottom surface. It represented the *in vivo* condition of skin attached to a bone surface and would only be subjected to minimum displacement for the bottom surface. In Abaqus, it was labelled as zero movement for all U1-3 and UR1-3 including all translational and rotational movement. The CBV as described in section 6.3.2 were located at the centre of the model, radial section 1. Any spot on skin *in vivo* is surrounded by skin with similar mechanical properties which, to some degrees, restricts the deformation but it is still deformable. For Abaqus CAE, this complex situation, only some degrees of deformability caused by neighbouring skin, is not easily modelled with the available boundary conditions. Therefore, the peripheral surface of the model was designed to be distant from the centre to minimise the effect of the applied boundary condition of the peripheral surface on the deformation of the CBV located at the centre. As shown in Figure 6.7, a comparison is conducted with "fully" and "un" constrained on the peripheral surface in which "fully" and "un" constrained restricted any translational and rotational movement and no restrictions at all respectively. The blue and red bars represented the cross-sectional area

reductions of the sections of interest of the CBV. The reductions were caused by the application of pressure at the superficial region with a magnitude of 38.6 kPa which was the magnitude of pressure required to form a pressure ulcer without the presence of friction (Dinsdale, 1974). As there was almost no difference between the "fully" and "un" constrained in each respective section of interest, it was proven that as the peripheral surface of the quartered model was distant enough so that the two extreme boundary conditions, "fully" and "un" constrained, would have minimum effect on the deformation of the CBV located at the centre.
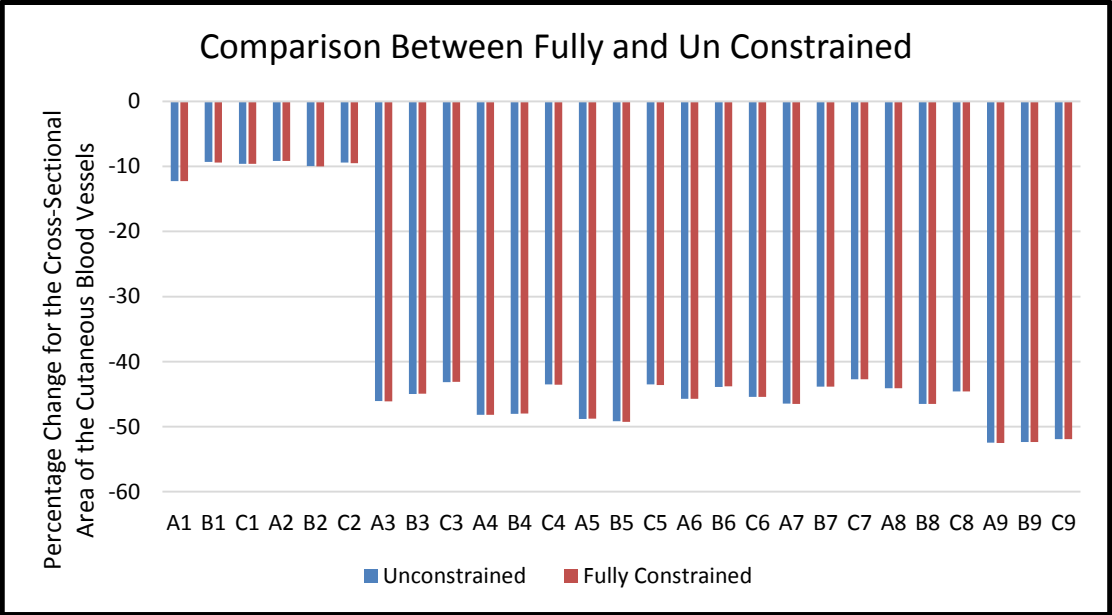
Figure 6.7   Comparison between fully and no constraint at the peripheral surface of the quartered model

6.3.5.   Loading and loading areas

The magnitudes of the loads of the quartered model including pressure and friction which were applied at the superficial region needed to be clinically relevant in order for it to be a useful tool for evaluating the deformation of the CBV. As mentioned in Section 6.3.4, there were nine radial sections. Each of the sections has its own

superficial region and the superficial region of section 9 is indicated in Figure 6.3 for demonstration purposes. The CBV were located in section 1 which was the main focus of the simulations. Even though the deformations of sections 2 to 9 were not relevant for evaluating the changes in the cross-sectional area of the CBV, they were necessary to determine optimal loading area. Hence, it was necessary to perform a simulation test run on the quartered model in order to determine which sectional superficial surfaces should be loaded to provide the most meaningful results of the deformation of the CBV. The loading of the simulation test run was 38.6 kPa (Dinsdale, 1974).

The aim of the quartered model was to demonstrate the deformations of the CBV resulting from being seated on foam. The unit of friction in Abaqus is defaulted to be Newton per square metre, hence, the quartered model was developed with respect to the micrometre. Hence, the units of pressure and friction were both Newton per square micrometre (N/μm^2). The magnitude of the applied friction for the quartered model was calculated with Equation 6.1. The coefficient of friction was 0.79 which was found to be the highest magnitude for the interface between medical textile and human skin in a study conducted by Vilhena in 2016 (Vilhena & Ramalho, 2016).

$$Friction\ (f) = \mu * N$$ Equation 6.1 Equation for frictional force

where f, μ and N were the magnitude of friction, coefficient of friction between medical textile and human skin, and normal force on skin surface respectively

6.3.6.   Meshing

Two types of meshing element were adopted in the current model which were tetrahedral and hexahedral. Tetrahedral elements are made up of triangles and

consisted of four nodes which were adopted in section 1 where the CBV were located. The flexibility of tetrahedral elements enabled the meshing of section 1 to accommodate the complicated geometries of the CBV. Hexahedral elements which have 8 nodes allowed economic and more faithful approximation and are adopted in sections 2 to 9 of the FEA model as demonstrated in Figure 6.8. The core of the model in Figure 6.8 is meshed with tetrahedral elements to accommodate the complicated geometries of the CBV while the rest of the model were meshed with hexahedral elements. The mesh size of the model was also increased gradually with the distances from section 1 because only the deformation of section 1 was directly related to the deformation of the CBV.
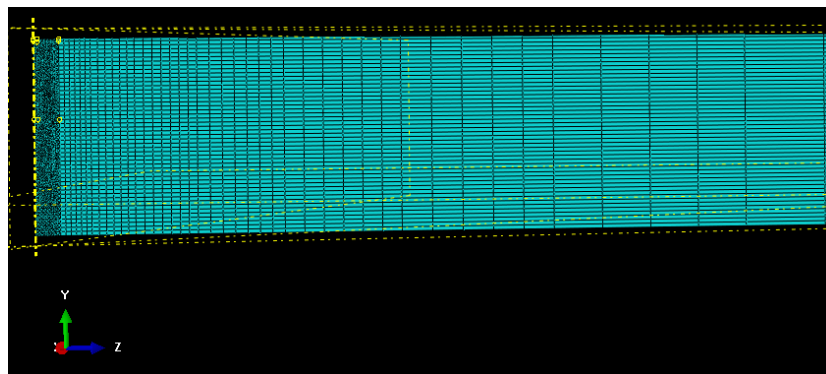
Figure 6.8   Meshing of the quartered model

(Radial section 1 is located at the left hand side of the Figure 6.8)

6.4.   Pressure Mapping

Pressure mapping measurements were conducted with 3 healthy volunteers with body mass indexes (BMI) of 19.9 to 30. The pressure mapping measurements were conducted with "TEKSCAN CONFORMat" which was calibrated before uses. The volunteers were instructed to have the same sitting position on both rigid support and foam support surfaces with their upper bodies vertically upright. Their legs were not supported and hung freely from the seat. The healthy volunteers were also instructed

to sit with minimum movement and the magnitude of the peak contact pressure after settling was captured by the pressure mapping system.

The result of the pressure mapping measurement of the healthy volunteer with the BMI of 19.9 sitting on the foam support is shown in Figure 6.9. The colour of the box in Figure 6.9 represents the intensity of the pressure while the numbers in the cells are the magnitudes of contact pressure in millimetres of mercury (mmHg). The magnitude of the peak contact pressure inside the light green box in Figure 6.9 is 63 mmHg. The valid measured area of the pressure mapping was in the shapes of buttocks and two legs which was the contact area between the healthy volunteer and the foam. The last line of the pickup at the bottom of the Figure 6.9 was not caused by the volunteer but by stretching of the CONFORTMat instead and it is irrelevant.
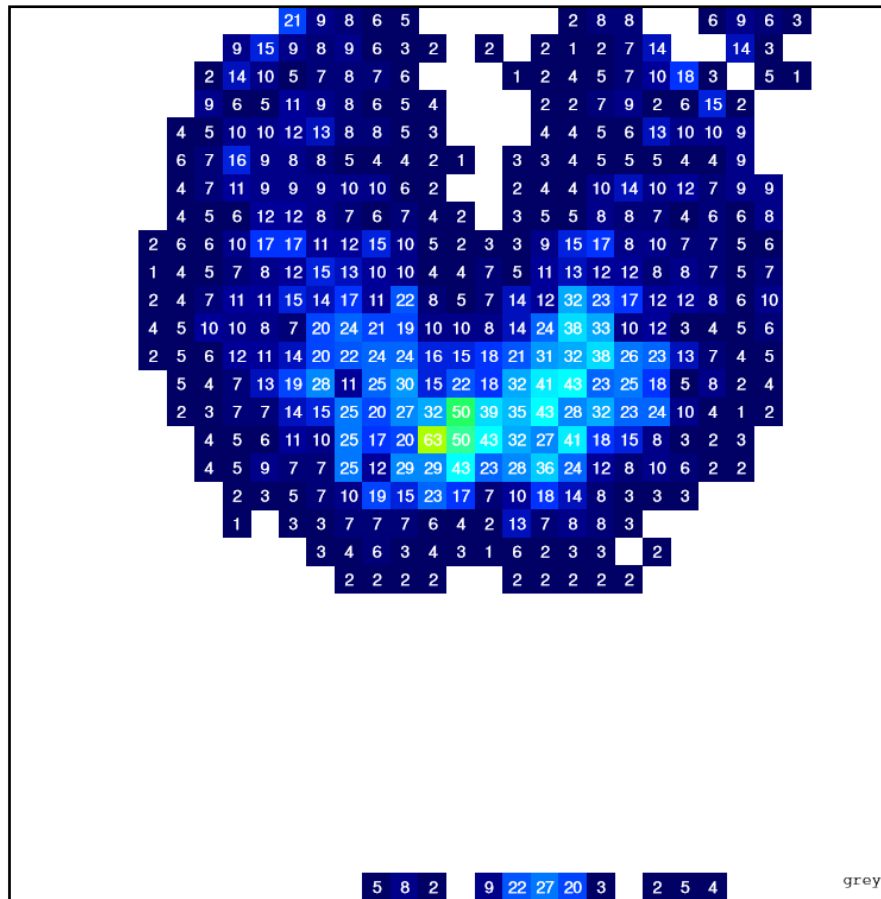
Figure 6.9   Captured image of a healthy volunteer sitting on a rigid support
surface

The six pressure mapping measurements including all three of the healthy volunteers
are summarised in Table 6.2. It shows that the magnitudes of the peak contact
pressure of volunteers sitting on the foam were lower than sitting on the rigid support
surface. The foam was a soft cushion which prevented the bottom of pelvic girdle to
be in direct contact with the support surface. However, the magnitudes of the peak
contact pressure between the rigid support surface and volunteer 1 and 2 were found
to be the same even with significantly different BMI. The highest magnitude of peak
contact pressure was 89 mmHg which was adopted to be the magnitude of the applied
pressure for the quartered model. As mentioned the input of the Abaqus needs to be

136

in Newton per square micrometres, thus, the 89 mmHg of pressure was converted to 1.1865 ×10^{-8} N/μm^2. The peak contact pressure caused by the higher BMI volunteers was found to be lower than the lower BMI volunteer. The fat content was believed to spread the body weight to a bigger contact area.

Table 6.2 Results of the pressure mapping measurement

Volunteers (BMI) / Supporting Surface	Volunteer 1 (19.9)	Volunteer 2 (26)	Volunteer 3 (30)
Foam	63 mmHg	60 mmHg	28 mmHg
Rigid	89 mmHg	89 mmHg	51 mmHg

6.5.   Results of the Simulation Test Runs

The results of the simulation test runs are presented in Figure 6.10. There were twenty-seven sections of interest in the quartered model, three on each of the horizontal blood vessel. The simulation test runs demonstrated two trends of the sections of interest. The sections of interest on the horizontal blood vessels at the dermis layer of the quartered model generally had less reduction in cross-sectional areas than the sections of interest located at the hypodermis layer. The explanation of the significant differences will be discussed in Section 6.9.2. Eight simulation test runs labelled as "T1" to "T8" were conducted. The loading areas of the simulation test runs were incremented as followed:

- T1: Loading on the superficial surface of radial section 1
- T2: Loading on the superficial surfaces of radial section 1 and 2
- T3: Loading on the superficial surfaces of radial section 1 to 3 and so forth
- T8: Loading on the superficial surfaces of radial section 1 to 8

The more superficial regions were loaded, increased convergence of reductions are found as shown in Figure 6.10 especially in T5 to T8 simulation test runs. Figure 6.10 is a convergence graph which shows that the reductions of the cross-sectional areas at the sections of interest converged when more superficial surfaces are loaded. The reduction trend was found to be converged in the T8 simulation, thus, for the rest of the simulations, the pressure and friction were loaded on the superficial surfaces of section 1 to 8. These simulation test runs were an essential optimisation of the loading area and minimised the possibility of affecting the deformation of CBV by applying mechanical loads on different superficial surfaces of the radial sections.
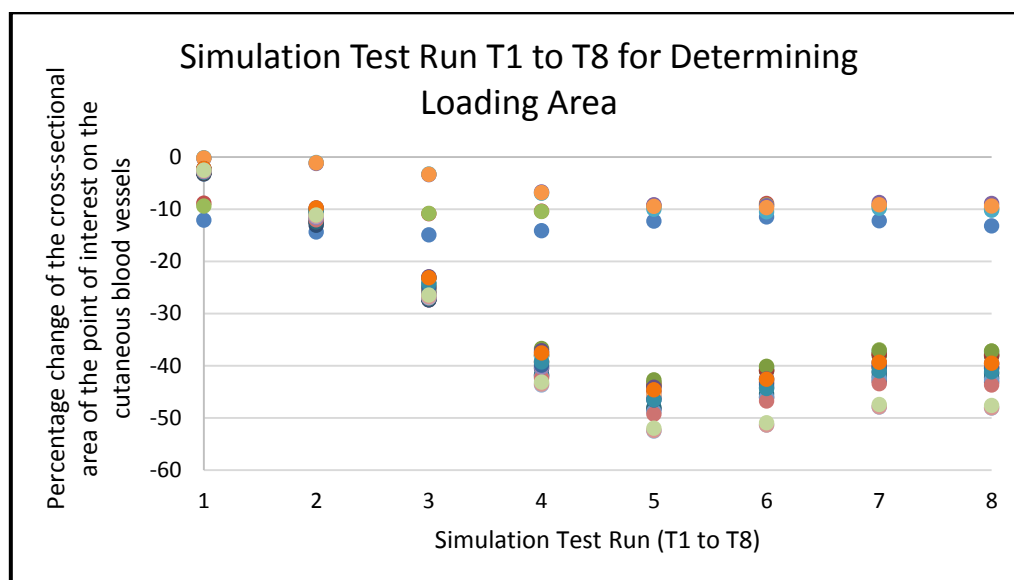
Figure 6.10   Results of the simulation test runs

(The data points are the percentage change in the cross-sectional area of the sections of interest in which the upper and lower converged trend are represent areas at the dermis and hypodermis layers respectively)

6.6.   Calculation of Friction

The magnitude of friction applied on the quartered model was calculated with Equation 6.1. In the situation of a healthy volunteer sitting vertically upright, the

friction would be against it's the force generated during sitting down. Hence, the friction would be directed radially outward and upward assuming the bottom part of the pelvic girdle has a spherical shape. The magnitude of friction would be affected by the average contact pressure surrounding the centre of loading. The magnitude of the average contact pressure was found to be 35 mmHg, 4,666.3 N/m^2, from the pressure mapping measurement. By using Equation 6.1, the calculated friction per unit area was 3,686.3 N/m^2 which was further converted into 3.6863×10^{-9} N/μm^2 for the quartered model.

6.7. Data Processing

The focus of simulations T1 to T8 was the deformation of the cutaneous blood vessels caused by the applied mechanical loads. The FEA package, Abaqus CAE 6.14, did not allow direct measurement of the cross-sectional area of a feature. Hence, the cross-sectional area of the cutaneous blood vessels in the quartered model was calculated from the coordinates of the key nodes at the sections of interest.

6.7.1. Locating key nodes and node numbers

The key nodes referred to those were at the four specific positions at the section of interest on the cutaneous blood vessels which were the top, bottom, left and right most positions. These four key node locations were created on the sectioned vessel edge and a key node would be allocated to the intersection of two section lines at the vessel edge.

There were 141,251 nodes in total for the whole quartered model to facilitate the simulation, however, only 108 nodes were the key to the calculation of the deformation of the cutaneous blood vessels. The data acquisition process began with locating the key nodes.

The coordinates of the key nodes were acquired by probing the nodes in the meshing module of Abaqus. The coordinates of the key nodes were recorded in an Excel spread sheet. The x, y and z coordinates were subsequently combined into one single cell using the "**Concatenate**" function. A data sheet was provided by Abaqus when the simulation was submitted which has all the coordinates of all the nodes of the model. The same method was adopted to combine all the coordinates of all the nodes from the data sheet and compared with the coordinates of the key nodes by the function of "**Vlookup**". The node numbers of the 108 key nodes were thus acquired.

6.7.2. Data acquisition and calculation

The cross-sectional area reductions at the sections of interest on the CBV were the key data from the FEA simulations and the focus of this study. However, the changes in the cross-sectional area, as mentioned, were not directly provided by Abaqus. Hence, changes in the coordinates of the key nodes were the only method of indicating and computing the changes in the cross-sectional area of the cutaneous blood vessels. After the simulations were conducted, the displaced coordinates of the key nodes were acquired with "probe value" function of the visualisation module of Abaqus. The original and displaced coordinates of the key nodes were acquired by inputting the key node numbers. The coordinates of the four key nodes were subsequently analysed and the change in the cross-sectional area at the sections of interest on the CBV were computed as demonstrate in Figure 6.11. Figure 6.11 is the calculation process of the change in the cross-sectional area at the first section of interest from the left of the top horizontal blood vessels also named A1. The full set of spread sheets including pressure only, friction only and pressure with friction simulations of this study are included in Appendix I.

Node Number	Original Coordinates in X (µm)	Original Coordinates in Y (µm)	Original Coordinates in Z (µm)	Final Coordinates in X (µm)	Final Coordinates in Y (µm)	Final Coordinates in Z (µm)	Original Diameter (µm)	Deformed Diameter (µm)	Original Area (µm²)	Deformed Area (µm²)	Percentage Change (%)
86	295.442	3165.500	52.094	296.553	3150.000	52.300	15.000	14.620	176.715	171.397	-3.009
84	295.442	3150.500	52.094	296.554	3130.000	25.293					
85	288.056	3158.000	50.792	289.199	3140.000	51.014	15.000	14.927			
87	302.828	3158.000	53.397	303.902	3140.000	53.589					

Figure 6.11   Computing the change in cross-sectional area of the cutaneous blood vessel

6.8.   Results of the Finite Element Analysis Simulations

Three sets of results were produced by the FEA simulations which were named "pressure only (PO)", "pressure with friction (PF)" and "friction only (FO)" and the loadings of the respective simulations are listed in Table 6.3.

Table 6.3 Loading of the respective simulations for quartered model

Simulations	Loadings to the Superficial Region of Sections 1 to 8
Friction Only (FO)	3.6863×10^{-9} N/µm^2 of frictional force
Pressure with Friction (PF)	1.865×10^{-8} N/µm^2 of pressure and 3.6863×10^{-9} N/µm^2 of frictional force
Pressure Only (PO)	1.865×10^{-8} N/µm^2 of pressure

The percentage changes in the cross-sectional areas at the sections of interest of the cutaneous blood vessels (CBV) are presented in Figure 6.12. The new cross-sectional areas are compared with the original areas. As discussed, A to C indicate the location of the sections of interests on the cutaneous blood vessels from left to right while the numbers indicate the vertical location of the blood vessels from superficial to bottom.

A1 to C2 have an average of 1.79 percent of increase, 1.70 percent of decrease and 3.34 percent of decrease in the cross-sectional area in the simulations of FO, PF and PO respectively. The changes of A3 to C9 are 5.77 percent of increase, 13.02 percent of decrease and 17.07 percent of the decreases in the simulations of FO, PF and PO respectively.
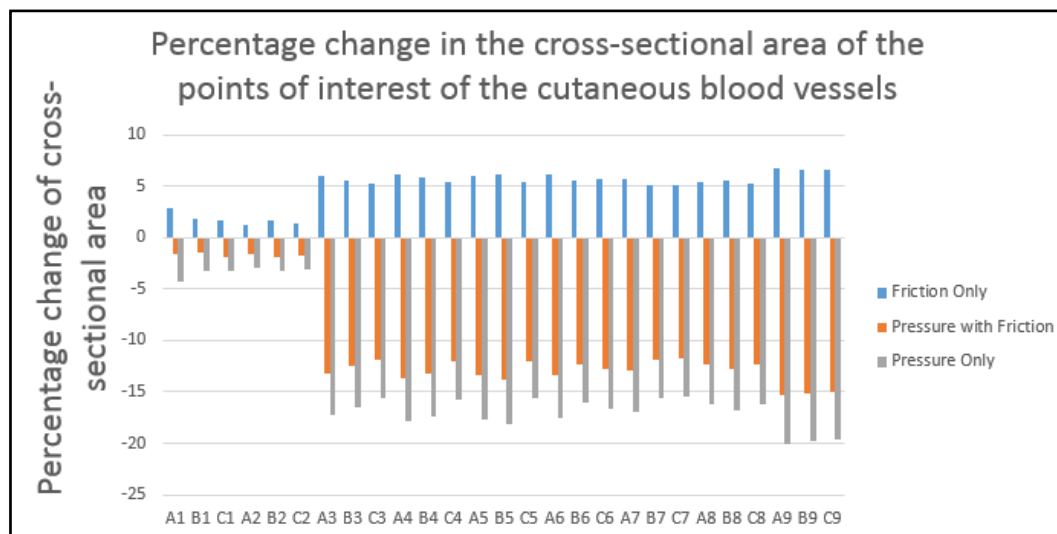
Figure 6.12   Percentage change of the cross-sectional areas at the sections of interest on the cutaneous blood vessels

6.9.   Discussion on the Finite Element Analysis Simulations

There was a significant difference in the percentage change of the cross-sectional areas at "A1 to C2" and "A3 to C9" sections of interest on the CBV. The percentage changes regardless of increase or decrease were lower for "A1 to C2" which were located at dermis layer. This phenomenon was caused by the differences in nodal displacement which will be discussed in detail in section 6.9.2.

6.9.1. "Friction only" simulation

The simulation of "Friction Only" was a case of computationally illustration on the

effects of friction and the simulation also aimed to demonstrate the capability of the quartered model in approximating the deformation of cutaneous layers caused by applied frictional force. The frictional force in FO simulation increased the cross-sectional area of the cutaneous blood vessels, this was contradict to the understanding of friction increase the possibility in the formation of pressure ulcers. The frictional force applied parallel to the superficial surfaces which shear the materials including the blood vessels in radial section 1. However, the method of computing the percentage change in the cross-sectional area by the coordinates of the key nodes did not account for any out of plane effect. Thus, an advancement of computing method is required which should align the key nodes on the same plane and compute the actual cross-sectional area which will be presented in Chapter 7. However, friction is impossible to be applied in reality without pressure. Equation 6.1 showed that the frictional force would be zero with the absence of normal force (pressure). The most relevant simulations would be simulations of PF and PO especially in clinical setting. As mentioned, the purpose of FO simulation is to show the capability of the quartered model and it raised the needs of an advancement in the method of computing the percentage change of the cross-sectional area of the CBV.

The area in red in Figure 6.13 shows the location which has the highest magnitude of deformation in X-direction caused by the applied frictional force. The location of the highest magnitude of deformation in X-direction is further away from the centre, close to the intersection of section 8 and 9, because the frictional force was only loaded at section 1 to 8. The two surfaces pointed by the red arrows in Figure 6.13 are applied with symmetric boundary conditions, therefore, there are equal radial frictional force at the symmetric part as well.
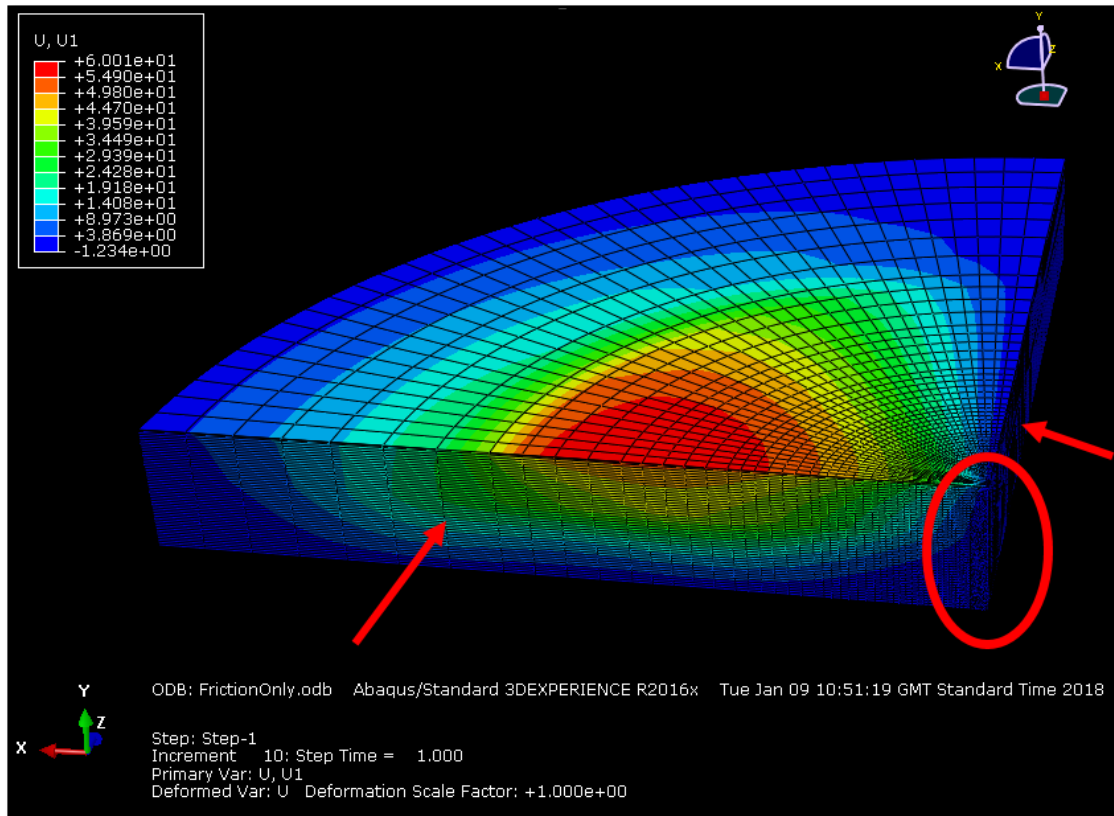
Figure 6.13   Deformation of the quartered model in x-direction for "friction only"

only simulation

6.9.2. "Pressure only" simulation

The cross-sectional areas at the sections of interest on the CBV reduced by approximately 3.34 and 17.07 percent for "A1 to C3" and "A4 to C9" respectively. The pressure applied at the superficial surface of section 1 to 8 caused the compression of the quartered model. The significant difference between the reductions of the cross-sectional areas at the sections of interest at dermis and hypodermis layers was caused by the different magnitudes of the displacements of nodes. The centre line (red colour) of the quartered model is used to demonstrate the displacement of the respective nodes as shown in Figure 6.14. There are sixty-four nodes on the centre line at dermis and hypodermis layers and they are named N1 to N64 from bottom to superficial respectively. The quartered model underwent a compression when a pressure was

applied on the superficial surfaces of section 1 to 8. The nodes on the centre line consequently displaced downward. The nodes closer to the superficial surfaces displaced more than those below them because the displacement of each node was an accumulation of the displacement of all nodes below them. Net displacement of each node on the centre line was calculated by subtracting the displacement experienced by the nodes below it. The results are presented in Figure 6.15. The red and green points in Figure 6.15 represent the net displacement of the nodes, N1 to N64, at hypodermis and dermis layers respectively. The red and green lines are the lines of best fit of the red and green points respectively which show the trends of the points. A significant increase in net nodal displacement was found at the sections of interest at hypodermis layer. This indicates that each node at the hypodermis layer displaced significantly more than the nodes below it, thus, the diameter of the cross-sectional area at the sections of interest at the hypodermis layer were decreased significantly. Even though higher magnitudes of net nodal displacements were found at dermis layers, the relative displacement of two successive nodes were similar. The distance between two nodes, therefore, remained approximately the same. The difference in net displacement for nodes at the dermis and hypodermis layers are also represented by the slopes of the two lines of best-fit in Figure 6.15.
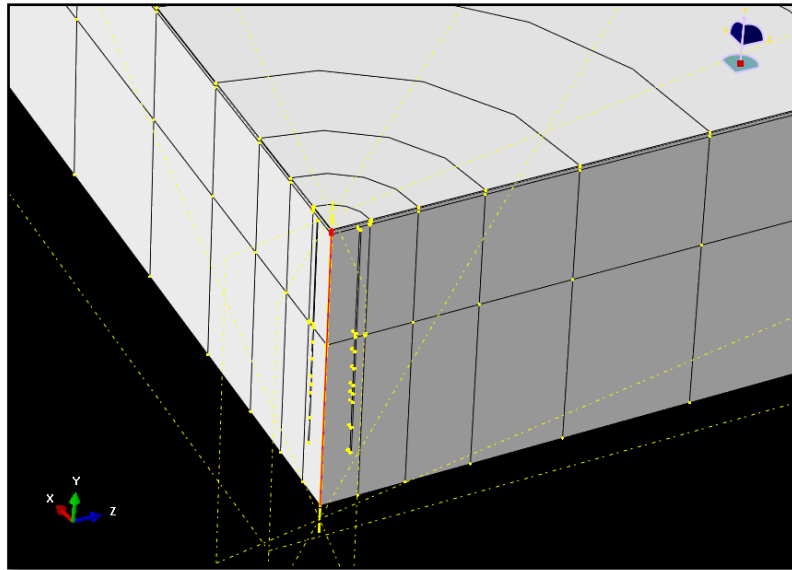
Figure 6.14　　Red centre line of the centre model
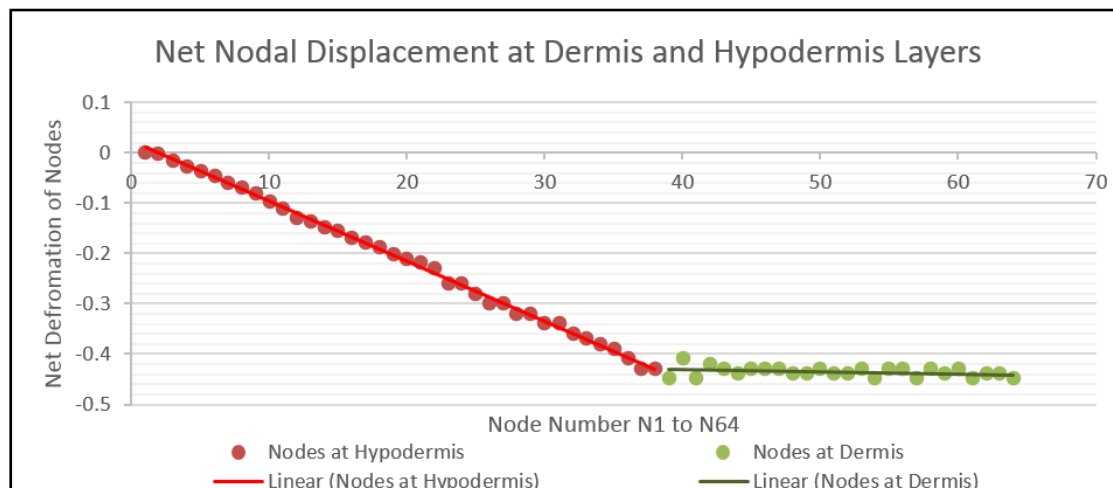
Figure 6.15　　Net nodal deformation at dermis and hypodermis layers

6.9.3. "Pressure and friction" simulation

The magnitudes of the deformation at the sections of interest on the CBV in PF simulation were in between the results of FO and PO simulations. As discussed in section 6.9.1 and 6.9.2, friction opened up the blood vessels because of the computing method which requires advancement while pressure collapsed the blood vessels. The combined effects were demonstrated in PF simulation. The results acquired in PF

146

simulation were the most clinically relevant. The healthy volunteers who participated in the pressure mapping measurement were subjected to both pressure and friction simultaneously with the vertically upright sitting posture. There were approximately 1.70 and 13.02 percent decrease in the cross-sectional areas at the sections of interest on the CBV at the dermis and hypodermis respectively. The PF simulation demonstrated the capability of the developed model, quartered model, in approximating the effect of both applied pressure and friction simultaneously on the percentage change in the cross-sectional area of the CBV. This is an initial attempt and it is novel in terms of its capability in the field of pressure ulcer prevention.

6.10. Conclusions

A three-dimensional FEA, quartered model, was developed to represent skin and demonstrate the effects of mechanical loads on the cutaneous blood vessels.

Pressure mapping measurements were conducted on three healthy volunteers supported by rigid and foam surfaces. The highest peak contact pressure was 89 mmHg.

Loading areas of the quartered model was determined by simulation test run 1 to 8. The trend of convergence was shown in the convergence graph of the simulation test run and is converged at the 8th test run shown in Figure 6.10. Hence, the superficial surfaces of section 1 to 8 were determined to be the adequate loading area for the subsequent FEA simulations.

The changes of the cross-sectional area at the sections of interest on the CBV were unable to be directly acquired from the FEA package. The percentage changes of the

cross-sectional area were computed by analysing the data of original and deformed coordinates of the key nodes.

The significant differences in the magnitudes of the reduction in the cross-sectional areas at the sections of interest at dermis and hypodermis layers were contributed by the difference in net nodal displacement.

Three FEA simulation including "pressure only", "friction only" and "pressure and friction" were conducted. The effects of the applied mechanical loads on the cross-sectional areas of the cutaneous blood vessels are demonstrated in Table 6.4.

Table 6.4 Effects of the applied mechanical loadings on the cross-sectional areas of the cutaneous blood vessels

Mechanical Loading	Effect	Percentage Change of the Cross-sectional Areas on the Cutaneous Blood Vessels (Percent)	
		Dermis Layer	Hypodermis Layer
Pressure	Decrease	3.34	17.07
Friction	Increase	1.79	5.77
Pressure and Friction	Decrease	1.70	13.02

The purpose of FO simulation was to demonstrate the capability of the quartered model in illustrating the effect of applied frictional force on cutaneous blood vessels. An advancement in the method of computing the cross-sectional area of the

cutaneous blood vessels was necessary which will be presented in Chapter 7.

The objectives of this chapter were to:

- To conduct pressure mapping measurement of volunteers sitting on foam and rigid support surfaces;

- To develop a 3-dimensional finite element analysis, quartered model, to represent skin; and

- To study the deformation of cutaneous blood vessels under the influence of sitting on a foam.

The aim was fully satisfied by the development of the quartered model which was capable of representing skin and demonstrating the deformation of CBV by different mechanical loadings including pressure, friction and the combination of both.

Pressure mapping measurements were conducted on three healthy volunteers with different BMI on foam and rigid support surfaces. The highest magnitude of peak contact pressure (89 mmHg) was used to be the reference of the pressure applied to the quartered model.

Sections of interest were introduced to the CBV and the changes in the cross-sectional areas at the sections of interest were demonstrated by the three FEA simulations.

Chapter 7   Advanced FEA Halved Model for

Cutaneous Blood Vessels

7.1.   Introduction

By using the finite element method, the quartered model presented in Chapter 6 demonstrated its capability in approximating the changes in the cross-sectional areas at the sections of interest on cutaneous blood vessels (CBV) in the sitting condition. The quartered model was an initial attempt to develop a novel tool to evaluate the effect of mechanical loads on cutaneous blood vessels. It was capable of simulating conditions where only pressure and/ or radial frictional force is applied. However, some conditions, for instance, single-direction friction could not be simulated. An advancement in developing a computational model based on the quartered model will be presented in this chapter. Also, as discussed in Chapter 6, an advanced method of computing the cross-sectional area of the cutaneous blood vessels will be presented in this chapter for taking the out of plane effects of the key nodes into account. This newer method of computing the cross-sectional area can be adopted in quartered model for simulating aforementioned conditions which could be more economical due to the size and number of mesh of the quartered model. The development of an advanced model, halved model, is presented in this Chapter which aims to simulate more conditions. The advancement in the models is also presented in the Proceeding of the Institution of Mechanical Engineers, Part H: Journal of Engineering in Medicine (Leung, Fleming, Walton, Barrans, & Ousey, 2019).

7.2.   Advancement in Application of Friction

The most significant limitation of the quartered model was the inability of applying a single-direction friction resulting from the application of a symmetric boundary

condition on each side of the model as explained in Section 6.3.4. The applications of a symmetric boundary condition enabled the FEA package to be aware of the presence of other symmetric parts of the model. By definition, however the symmetric boundary conditions were not only applied to the physical geometries but also to the loading conditions. Three loading conditions are presented in Figure 7.1 in which blue coloured sections represent the quartered model and the grey coloured sections are the mirrored parts based on the two applied symmetric boundary conditions. The red arrows in Figure 7.1 (a) and (b) represent the friction applied on the superficial surfaces of the quartered model in two opposite directions. The directions of friction are mirrored by the two applied boundary conditions, hence, the directions of frictions become to and outward from the middle of the model which are not clinically relevant because friction rarely appears on skin in opposite directions. In contrast, friction in Figure 7.1 (c) is applied in radially outward direction which simulates the loading condition of sitting on a support surface. This shows that the quartered model was only capable of simulating limited conditions.

(a)   (b)   (c)
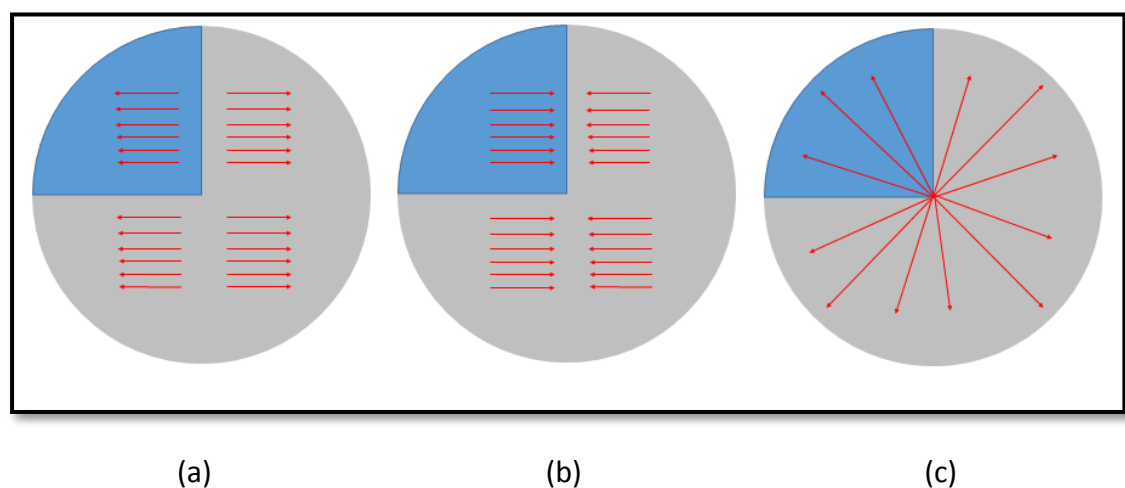
Figure 7.1   Possible friction directions of the quartered model

Developments in the model were required to allow the simulation of more clinically relevant loading conditions especially when friction is in a single direction as well as in

a radial direction. Hence, the new "halved" model is in the shape of a semi-circle. Three loading directions of friction are presented in Figure 7.2 in which green sections are the halved model and the grey section is the mirrored part simulated by applying a symmetric boundary condition in the middle. The friction applied to the halved model can be in a single direction and this same direction of friction is simulated on the mirrored part as shown in Figure 7.2 (a) and (b). This change allowed more clinical relevant loading conditions to be simulated, for instance, patients sitting up on an inclined bed.

(a)   (b)   (c)
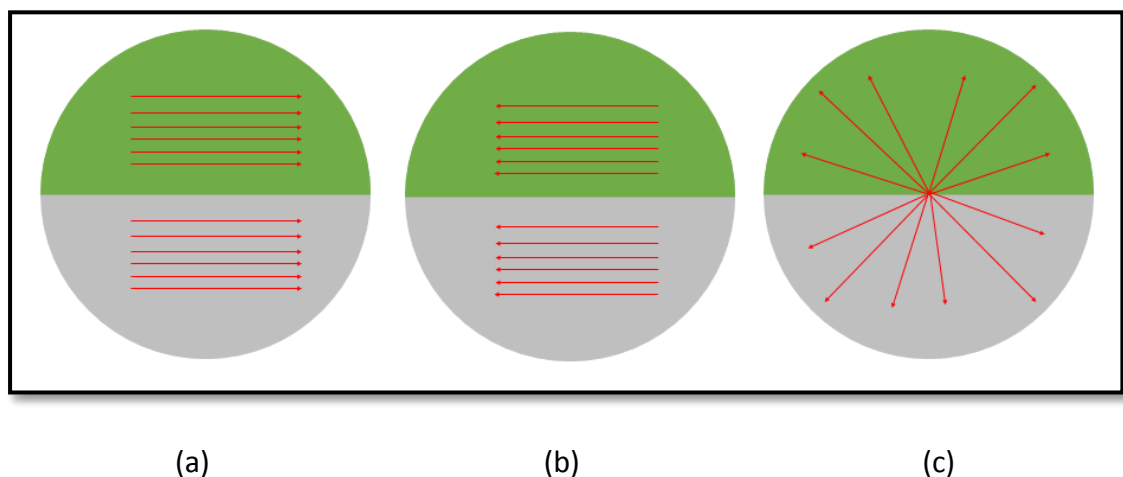
Figure 7.2   Possible friction directions of the halved model

7.3.   Features of the Halved Model

Similar to the quartered model, there are 9 radial sections as shown in Figure 7.3. The sizes of the radial sections are smallest in the centre and are gradually increased radially from the centre. Radial section 1 is the focus of the model where the CBV are located. The halved model consists of four layers which represent: stratum corneum, epidermis, dermis and hypodermis from the outermost to the innermost.
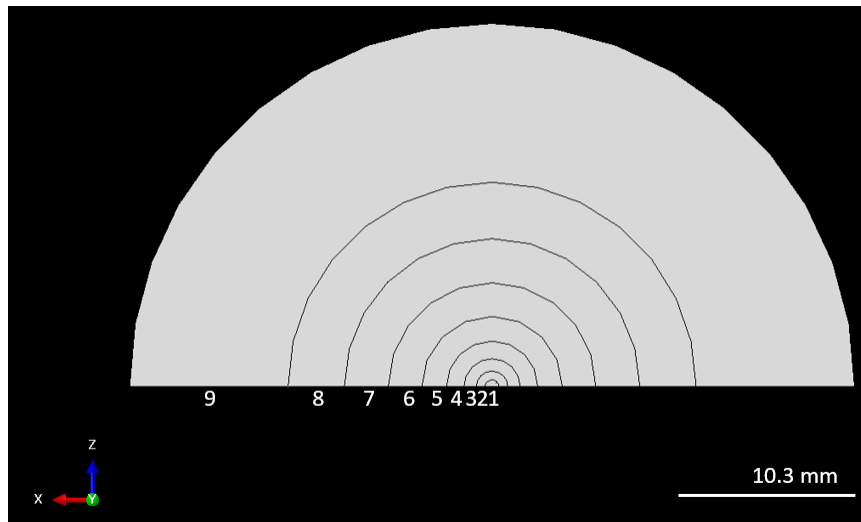
Figure 7.3   Radial sections of the halved model

The number of horizontal blood vessels remains the same as the quartered model and there is an additional vertical blood vessel to connect all the horizontal ones as shown in Figure 7.4. There are six sections of interest in the halved model on each of the horizontal blood vessels labelled as A to F compare to only three in the quartered model. There are in total 54 sections of interest and 529,032 nodes in the halved model in which nodes located at the four specific positions at the sections of interest are regarded as key nodes. There are in total 216 key nodes and by analysing their coordinates, percentage changes in the vessel cross-sectional area are calculated.
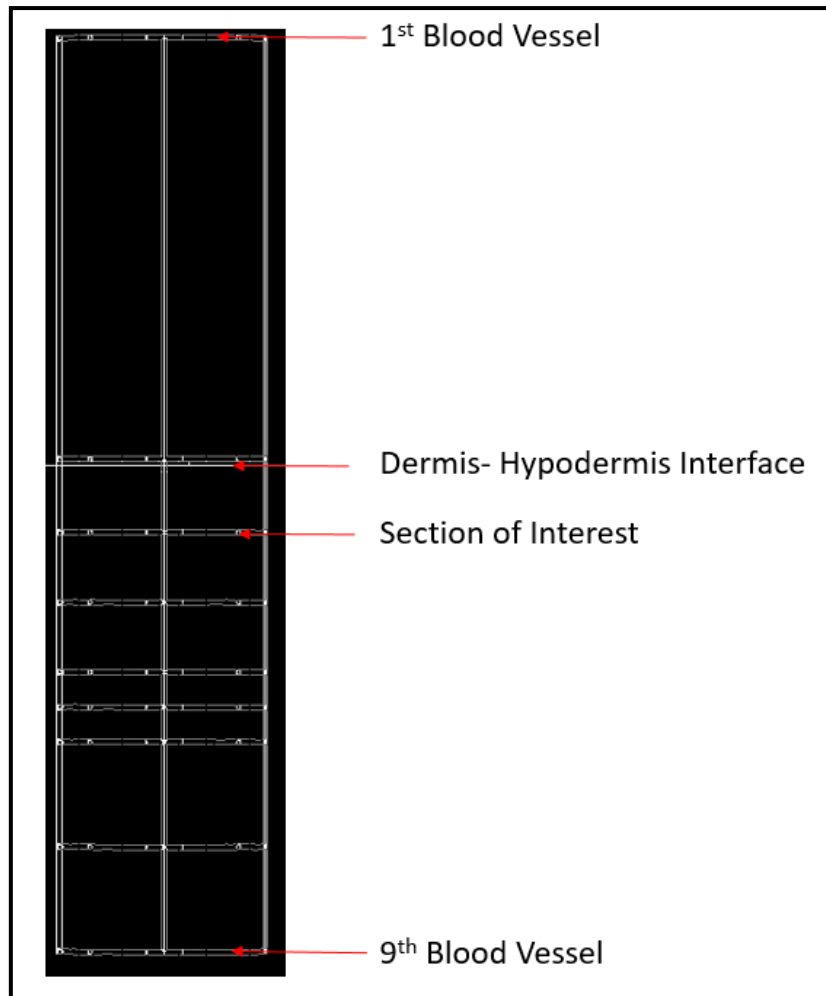
Figure 7.4   Cutaneous blood vessels in the halved model located in radial section

1

7.4.   Boundary Conditions and Loadings of the Halved Model

Two boundary conditions are applied to the halved model in order to simulate the conditions of skin under the influences of mechanical loads. A symmetric boundary condition is applied to the side surface of the model which enables the FEA package to aware of the symmetric part of the model including the physical geometries as well as the loading conditions as shown in Figure 7.5. By definition of the symmetric boundary condition, the translation movement perpendicular and rotational movement parallel to the plane of symmetric are all zero. A fix boundary condition is

applied to the bottom surface of the model similar to the quartered model to simulate the skin on a bony prominence. It was shown in Section 6.3.4 that the boundary condition at the peripheral surface has an insignificant effect on the changes of the cross-sectional areas of the cutaneous blood vessels located at section 1, hence there was no boundary condition applied on the peripheral surface.
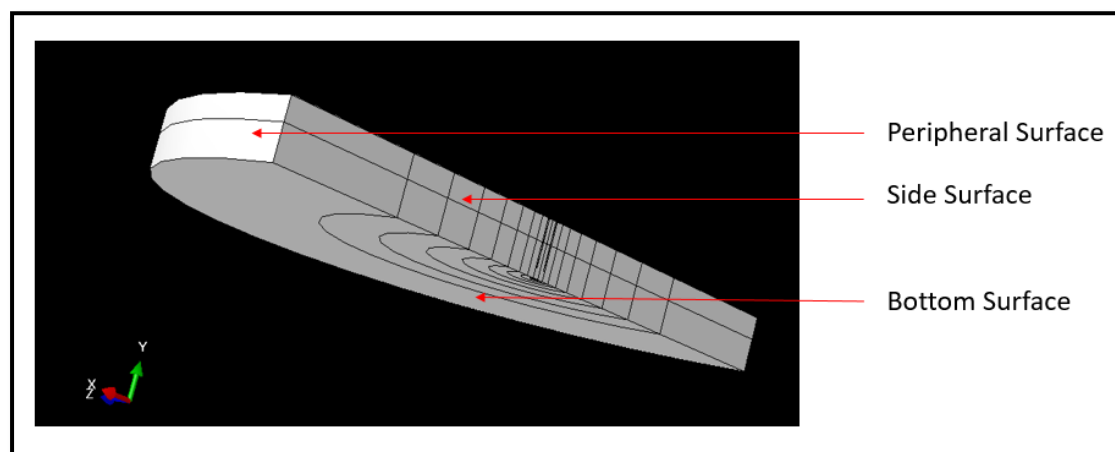
Figure 7.5   Three surfaces of the halved model

Similar to the quartered model a simulation test run was conducted to determine the number of superficial surfaces which should be loaded to minimise the effect of loading area on the changes in the cross-sectional area of the cutaneous blood vessels. Figure 7.6 shows the average percentage changes of the cross-sectional area at the sections of interest on CBVs. There were in total 12 and 42 sections of interest at the dermis and hypodermis layer respectively and the percentage changes in the cross-sectional areas converged in the 8th simulation test run in which the superficial surface of section 1 to 8 were loaded. The change of the cross-sectional areas of the sections of interest at the hypodermis layers increased significantly with the increase in loading area from the first to the sixth simulation test-run. This demonstrates that more area should be loaded to minimise the effect of loading area on the deformation of the

cutaneous blood vessels.
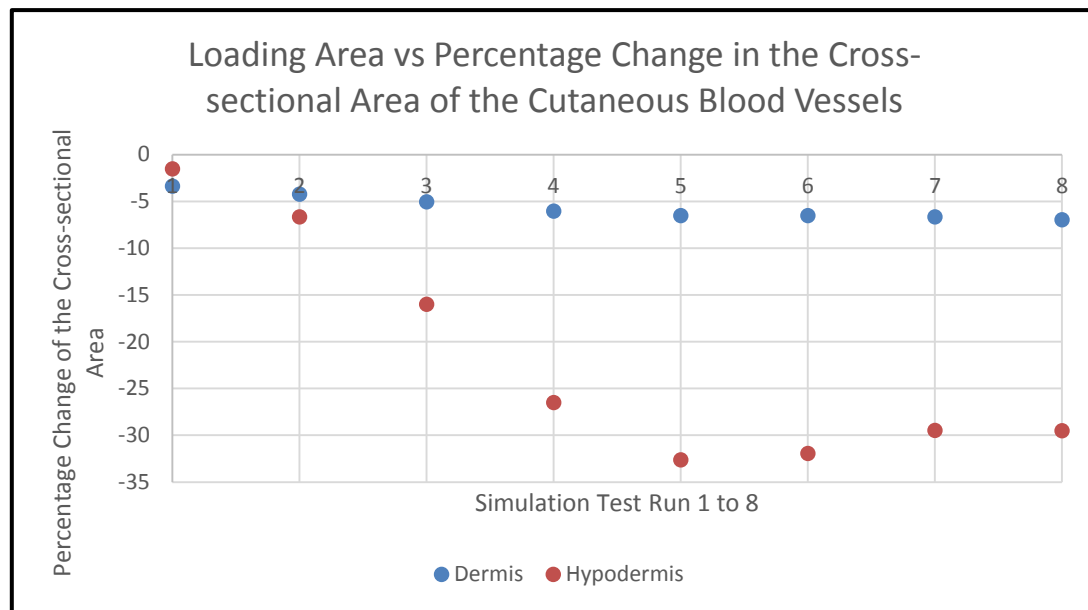
Figure 7.6   Percentage changes in the cross- sectional areas of the cutaneous

blood vessels under the influences of loading area for the halved model

7.5.   Advanced Method to Determine Cross-sectional Area of Cutaneous Blood Vessels

In this section, the advanced method of computing the cross-sectional area at the

sections of interest on the CBV is discussed.

7.5.1.   Deformed shape under the influence of applied pressure

The original cross-sectional areas at the sections of interest on the CBV were calculated

with the formula of the area of a circle because the diameter of the cutaneous blood

vessels was a known value, 15µm for both axis. A two-dimensional simulation was

conducted to demonstrate the deformation of a circular hole under the influence of

an applied pressure on the superficial surface. Figure 7.7 demonstrates that the CBV

is deformed into an elliptical shape when the pressure was applied. The same result

was seen in both of the three-dimensional models, quartered and halved. Hence, the

156

formula of the area of an ellipse is used alongside with the coordinates of the key nodes for computing the change in the cross-sectional area at the sections of interest on the CBV caused by the applied mechanical loads.
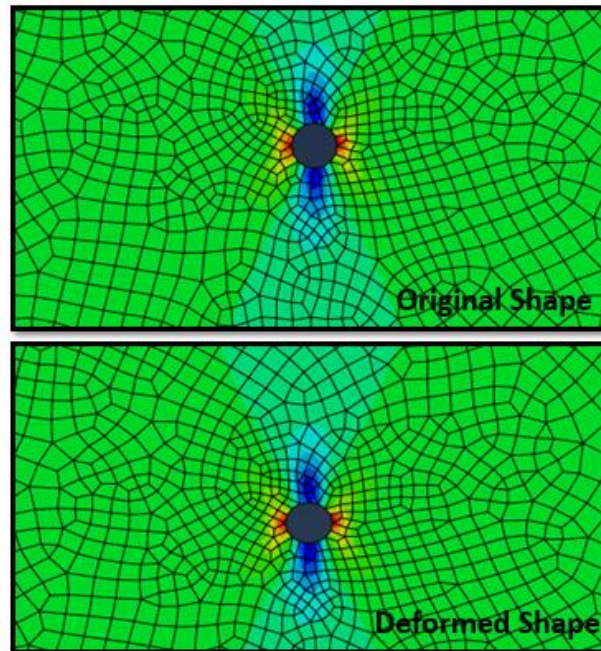
Figure 7.7   Two-dimensional simulation on the deformation of the cutaneous blood vessel under the influence of applied pressure

7.5.2.   Deformed shape under the influence of applied friction

The original method of deducing the cross-sectional area was applicable when the CBV deformed on a plane, i.e. the initial positions of the four key nodes at a section of interest were on a plane and the four nodes were deformed on the same plane under the influence of an applied pressure. However, the displacement of the four nodes was out of the plane when the deformation was caused by friction as the nodes closer to the superficial surface were subjected to more influences of the applied friction than the nodes at the bottom due to the fix boundary condition applied on the bottom surface. The original method of deducing the cross-sectional area of the cutaneous blood vessel presented in Section 7.5.1 was not meaningful with respect to applied

157

friction. The displaced nodes are no longer on the perpendicular plane to the vessel axis as shown in Figure 7.8. The computing of the cross-sectional area of the blood vessels would therefore be faulty increased. The blue, red and green axes in Figure 7.9 are the vessels axis, original perpendicular axis and tilled axis caused by applied friction. The distance between the key nodes represented by the black dotes are increased because they are not on the same axis.
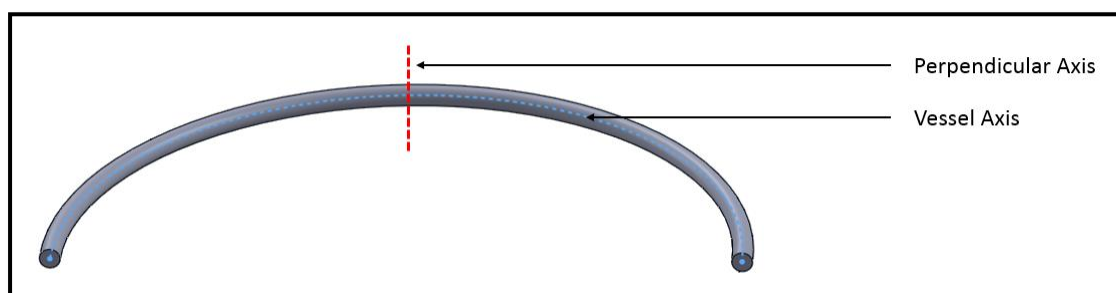
Figure 7.8   Vessel axis and perpendicular axis
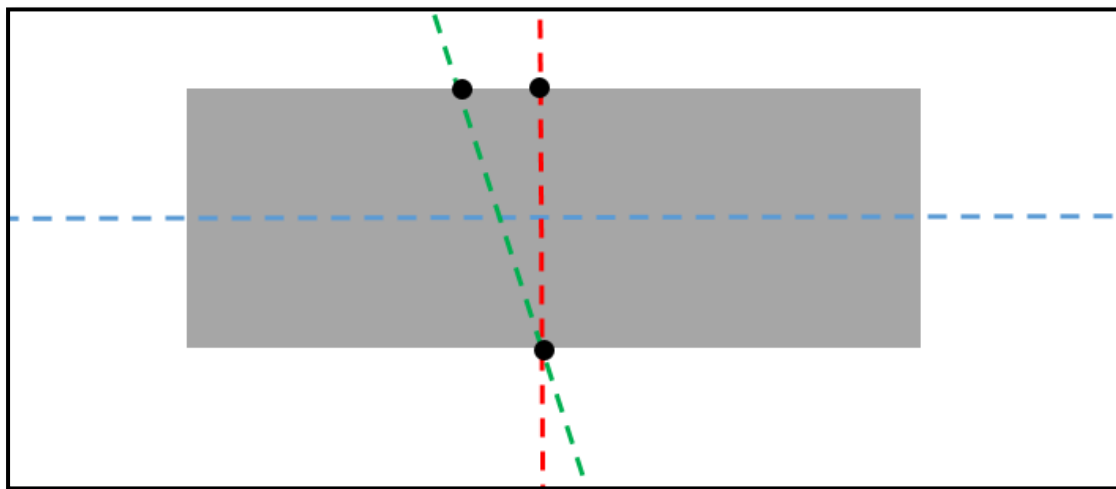
Figure 7.9   Schematic diagram of the cross-section of blood vessel

The advanced method of computing the cross-sectional area of the deformed CBV under the influence of mechanical loads aligns all the key nodes on the same axis prior to analysing the distances between the displaced nodes and calculating the cross-sectional area. The steps of the advanced method were as follows:

158

- Original coordinates of 4 key nodes (A, B, C, D) on a section of interest

  A (x_a, y_a, z_a), B (x_b, y_b, z_b), C (x_c, y_c, z_c), D (x_d, y_d, z_d)

- Distances between the key nodes and the middle axis of the model at their respective depth (y-direction)

  A $\sqrt{x_a{}^2 + z_a{}^2}$, B $\sqrt{x_b{}^2 + z_b{}^2}$, C $\sqrt{x_c{}^2 + z_c{}^2}$, D $\sqrt{x_d{}^2 + z_d{}^2}$

- New 2D coordinates on the same plane of the 4 nodes

  A $(\sqrt{x_a{}^2 + z_a{}^2}$, $y_a)$, B $(\sqrt{x_b{}^2 + z_b{}^2}$, $y_b)$,

  C $(\sqrt{x_a{}^2 + z_a{}^2}$, $y_a)$, D $(\sqrt{x_d{}^2 + z_d{}^2}$, $y_d)$,

- Two diameters on the same plane are therefore calculated

  Diameter AB: $\sqrt{(\sqrt{x_a{}^2 + z_a{}^2} - \sqrt{x_b{}^2 + z_b{}^2})^2 + (y_a - y_b)^2}$

  Diameter CD: $\sqrt{(\sqrt{x_c{}^2 + z_c{}^2} - \sqrt{x_d{}^2 + z_d{}^2})^2 + (y_c - y_d)^2}$

- Deformed Area Computed by the Advanced Method

$$= \frac{\pi}{4} \sqrt{(\sqrt{x_a{}^2 + z_a{}^2} - \sqrt{x_b{}^2 + z_b{}^2})^2 + (y_a - y_b)^2}$$

$$\times \sqrt{(\sqrt{x_c{}^2 + z_c{}^2} - \sqrt{x_d{}^2 + z_d{}^2})^2 + (y_c - y_d)^2}$$

Equation 7.1 Advanced method of computing the cross-sectional area of the cutaneous blood vessels

This advanced method, Equation 7.1, in computing the cross-sectional area of the sections of interest on the CBV projects the key nodes on the same perpendicular

plane. Hence, the actual cross-sectional area could be computed without any false increase by the out of plane effect due to the applied friction. Figure 7.10 is the calculation of the change in the cross-sectional area of the CBV, where column K is inserted for the x-coordinate in the new coordinate system.

Node Number	Original Coordinates in X (µm)	Original Coordinates in Y (µm)	Original Coordinates in Z (µm)	Final Coordinates in X (µm)	Final Coordinates in Y (µm)	Final Coordinates in Z (µm)	Original Diameter (µm)	Equivalent Coordinates in X	Deformed Diameter (µm)	Original Area (µm²)	Deformed Area (µm²)	Percentage Change (%)
168	295.442	3165.500	52.094	296.553	3150.000	52.548	15.000	303.023	14.120	176.713	164.325	-7.010
166	295.442	3150.500	52.094	296.554	3130.000	52.541		303.022				
169	302.828	3158.000	53.397	305.731	3140.000	53.843	15.000	310.436	14.818			
167	188.056	3158.000	50.792	291.141	3140.000	51.255		295.618				

Figure 7.10   Advanced method of computing the changes in cross-sectional areas of the cutaneous blood vessels

The changes in cross-sectional area at the sections of interest on the cutaneous blood vessels calculated by this advanced method were demonstrated by a friction-only simulation with the halved model. As shown in Figure 7.11, the most significant reduction is found at the sections of interest located on the most superficial horizontal blood vessels because it is closest to the superficial surface where the friction is applied. The single-direction friction reduces the cross-sectional area of the sections of interest with different magnitudes on the same horizontal cutaneous blood vessels. It is consistent that sections of interest A and F were affected the least due to the orientations of the sections of interest with respect to the direction of the applied friction.
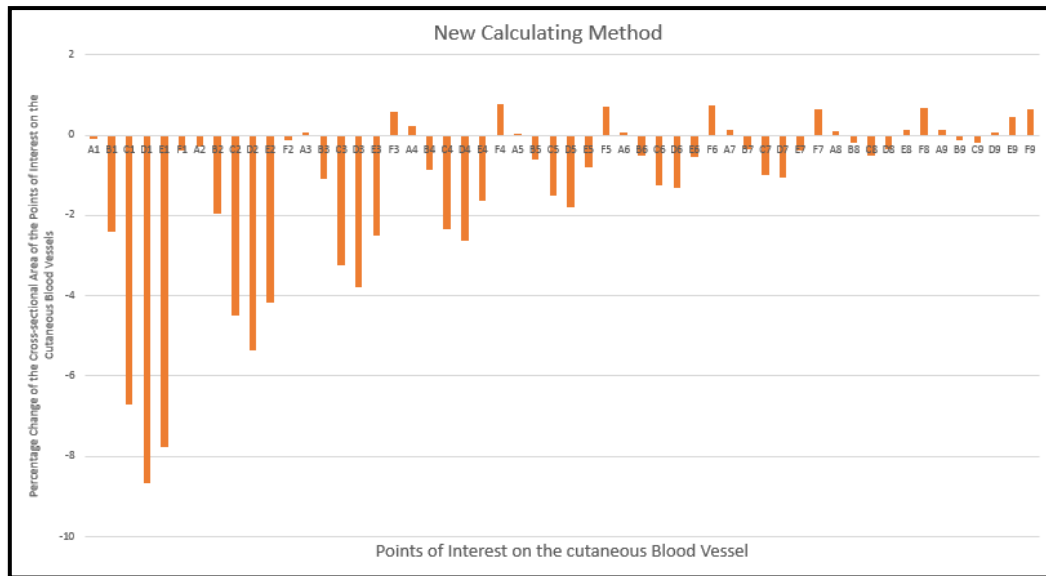
Figure 7.11   Percentage change of the cross-sectional area of the sections of

interest on the cutaneous blood vessels

This advanced method of deducing the cross-sectional area at the sections of interest on the cutaneous blood vessels is adopted in the rest of the study to ensure the cross-sectional area is accurately reported.

7.6.   Convergence Tests for Halved Model

Mesh size is known to affect the approximations of a FEA model and the results of the simulations, hence, there were two convergence tests conducted on the halved model with respect to the deformations of the cutaneous layers and the change of the cross-sectional areas of the cutaneous blood vessels.

7.6.1.   Convergence test on the change of the cross-sectional area of the cutaneous blood vessel

The mesh size of the radial section 1 was amended for the convergence test because the key focus of the study, CBV, were located at this section. A consistent mesh size

was impossible to be adopted for the whole model because it would exceed the capacity of the available computational power and it was not necessary. There were four mesh sizes assigned to the radial section 1 for the convergence test, which were 50, 40, 15 and 10 μm. Figure 7.12 demonstrates the changes of the average cross-sectional areas at the sections of interest on CBV located at the dermis and hypodermis respectively. The results converge at approximately 0.067 of an inverse of mesh size which was equivalent to the mesh size of 15μm.
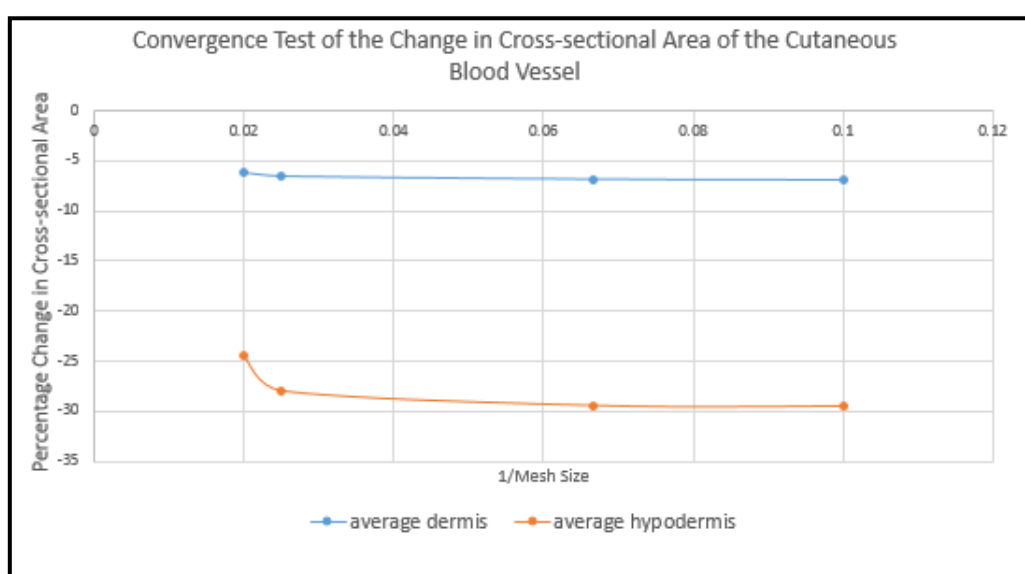
Figure 7.12   Convergence test of the change in cross-sectional area of the cutaneous blood vessel

7.6.2.   Convergence test for middle axis

The middle axis of the halved model in red in Figure 7.13 and is located in the centre of the radial section 1. The CBV are surrounding the middle axis, hence, the deformation of the middle axis affects the deformation of the CBV and consequently the percentage changes of the cross-sectional areas at the sections of interest. A convergence test was performed regarding the deformation of the middle axis with respect to the mesh sizes of the radial section 1 to minimise the effect of the adopted

mesh size on the deformation of the middle axis. Five distinct nodes on the middle axis were pinpointed by the coordinates with respect to the junctions of the cutaneous layers. Table 7.1 shows the five distinct nodes, A to E, from the superficial surface of the radial section 1 above the Stratum Corneum to underneath the hypodermis layer. All the x and z coordinates of the distinct nodes were zero because the nodes were on the middle axis and at the centre of the halved model.

Table 7.1 Positioning of the five distinct nodes on the middle axis

Distinct Nodes	Junction of the Cutaneous Layers	Coordinates (x, y, z)
A	Superficial region on the Stratum Corneum	(0, 3250, 0)
B	Stratum Corneum – Epidermis	(0, 3240, 0)
C	Epidermis-Dermis	(0, 3198, 0)
D	Dermis-Hypodermis	(0, 1913, 0)
E	Bottom of the Hypodermis	(0, 0, 0)
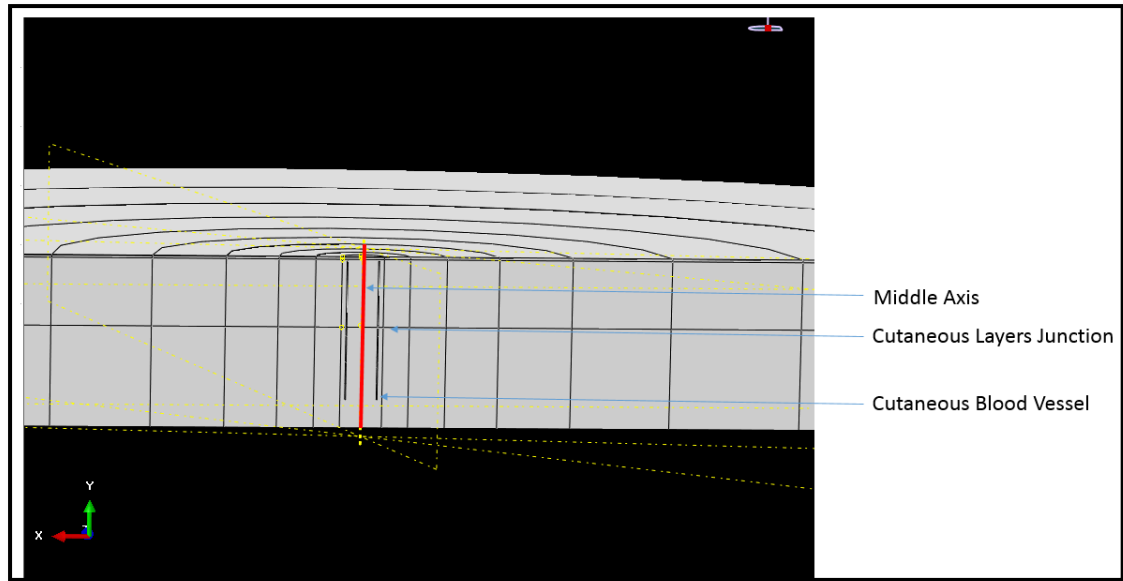
Figure 7.13   Middle axis of the halved model

Similar to the convergence test performed on the percentage change in the cross-sectional area at the sections of interest presented in Section 7.6.1, in this convergence test there are four different mesh sizes applied on radial section 1 including 50, 40, 15 and 10μm. The displacements of the five distinct nodes are captured and analysed for each of the adopted mesh sizes. The displacement of the five distinct nodes are in y-direction which is the depth direction of the halved model and the direction of the applied pressure. For the calculation of the net displacements of the distinct nodes without the influence of the nodes underneath it, the displacement of each node was followed, i.e.

- The net displacement of node A is equal to displacement of node A minus the displacement of node B

- The net displacement of node B is equal to displacement of node B minus the displacement of node C ; and so forth

Figure 7.14 shows the net displacement of the five distinct nodes on the middle axis from the simulations with the four different mesh sizes from 50 to 10µm. The net y-direction displacements of all five nodes converge at the third simulation in which the adopted mesh size is 15µm.
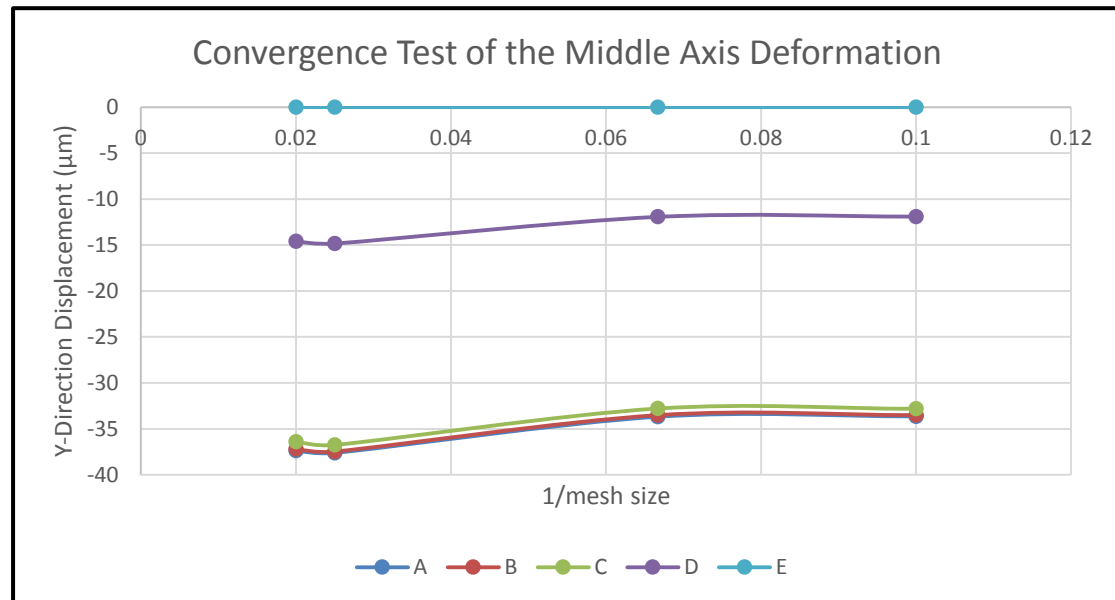
Figure 7.14   Convergence test of the middle axis deformation

In the mesh convergence test of the middle axis, zero displacement at node E confirms the fix boundary condition. The coordinates of the five distinct nodes on the middle axis also demonstrated minimal displacement in x and z direction. All the displacement in x and z direction were less than 1µm and could be neglected as they were approximately 0.003% of the radius of the halved model. The percentage difference in the Y-direction net displacement for the 5 nodes between mesh size of 15 and 10µm were in between 0 and 0.25%.

7.6.3.   Discussion on mesh size convergence tests

Mesh sizes of 50, 40, 15 and 10µm were used for the two convergence tests relating to the percentage change in the cross-sectional area of the sections of interest on the

CBV as well as the net displacement of the nodes on the middle axis. There were only 1.11% and 0.24% differences in the cross-sectional area of the CBV located at the dermis and hypodermis layers respectively when the radial section 1 is meshed with 15 and 10µm elements. The percentage differences between the y-direction displacements of the five distinct nodes on the middle axis are all less than 0.2% between the adopted mesh size of 15 and 10µm which shows that the mesh size of 15µm has minimal effects on the deformation of the middle axis. These two mesh convergence tests showed that the results of halved model would not be significantly influenced by applying meshes smaller than 15µm. Hence, the mesh size of 15µm is adopted for the radial 1 of the halved model.

7.7. Deformation of the Cutaneous Blood Vessels with respect to Applied Pressure

Interface pressure was found not to correlate well with of the formation of pressure ulcers in the literature. This was accurate for the pressure ulcers caused by excessive stress by distortion. Stress experienced in vivo especially at deep tissue, for instance, muscle could be 1.5 times higher than the interface pressure while the interface pressure remained practically unchanged (Elsner & Gefen, 2008). However, for the aetiology of ischemia, the interface pressure plays a significant role in collapsing the blood vessels, obstructing the blood circulation and metabolic wastes removal. This eventually leads to cell deaths and the formation of superficial pressure ulcers.

Computational models related to deep tissue injury have been successfully developed over the years. These models helped with the understanding of the in vivo conditions of the patients in different postures and evaluating the effectiveness of medical devices, for instance, air cushion (Levy et al., 2014). There is still a need for a tool to quantify the effect of mechanical loads on the deformation of the CBV and the

percentage changes in the cross-sectional area. In this section, different magnitudes of pressure are applied to the superficial surfaces of the halved model to establish the relationship between the applied pressure and the percentage changes in the cross-sectional area at the sections of interest on the CBV.

7.7.1. Effects of applied pressure on the cutaneous blood vessels

In this section, five magnitudes of pressure including 0, 23.0, 46.0, 92.0 and 138.0mmHg are applied to the superficial surfaces of the radial section 1 to 8 of the halved model. The two sets of data points coloured in blue and red shown in Figure 7.15 are the average percentage changes of the cross-sectional areas of the CBV at dermis and hypodermis layers respectively and the data points coloured in green are the average percentage change of the cross-sectional areas of all the CBV, a full set of data is provided in Appendix II.
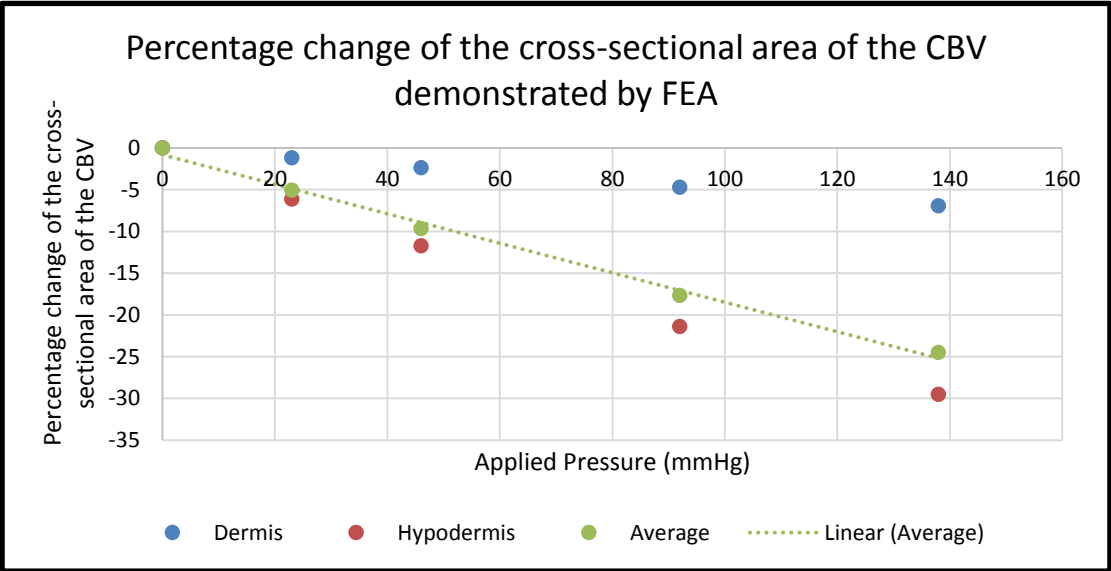
Figure 7.15   Percentage change of the cross-sectional area of the cutaneous blood vessels demonstrated by the halved model

7.7.2. Discussion on the change in the cross-sectional areas of the cutaneous blood vessels

The halved model experienced different magnitudes of deformation with the magnitudes of applied pressure from 0 to 138 mmHg. The range of percentage changes of the cross-sectional area of the CBV at the dermis and hypodermis layers were 0% to -7.0% and 0% to -29.5% respectively. The sections of interest on the CBV at the hypodermis layers experienced higher influence of the applied pressure and demonstrated higher percentage change in the cross-sectional area comparing to the sections of interest at the dermis layer because of the different net displacement experienced by the nodes at the dermis and hypodermis layer. This effect was discussed in detail in Section 6.9.2.

All three sets of data presented in Figure 7.15 are linear which demonstrates that the reduction of the cross-sectional areas of the CBV is linearly related to the applied pressure for the halved model. Skin is known to be non-linear in stress and strain relationship however as shown in Figure 2.4 skin experiences non-linearity at higher magnitude, typically Phase II, of applied stress. For the application of 0 to 138 mmHg of pressure, skin is still experiencing the magnitude of stress within phrase I in Figure 2.4 which can be assumed to be linear.

The average percentage changes of the cross-sectional areas of the CBV located at both dermis and hypodermis layers caused by the applied pressure of 0 to 138 mmHg were 0% to -24.5%. The average values presented in green in Figure 7.15 are closer to the percentage changes of the cross-sectional area of the blood vessels at the hypodermis layer than the dermis layer because the hypodermis layer is highly vascularised and more blood vessels are located at the hypodermis layers. The

168

averaged value of all the cross-sectional areas of the CBV at both dermis and hypodermis was essential for the comparison conducted in the next chapter to correlate the computational data to the clinical data.

The halved model simulations showed that the CBV were not completely collapsed by the applied pressures of magnitude 0 to 138 mmHg. Landis's study in 1930 demonstrated that the capillary pressure was between 12 to 32 mmHg from venous to arteriole (Landis, 1930). The apparatus in Landis's study was in direct contact with the capillary while the halved model was simulating the situation of externally applied pressure. Bridel deemed that the concept of 32 mmHg of applied pressure as a threshold was inappropriate because the responses of the CBV were related to the collagen content at the dermis (Bridel, 1993). The halved model in good agreement to Bridel's idea of changes in the cross-sectional areas of the CBV were contributed by the collagen content as the magnitude of applied pressure than 32mmHg did not collapse the CBV.

The existing methods of acquiring material properties of the cutaneous layers were discussed in detail in Section 2.4 which are mainly the *in vivo* indentation and *in vitro* tensile tests. Neither of these methods provided good representations of the properties or the behaviours of skin *in vivo*. The *in vivo* indentation was incapable of illustrating the behaviour of individual cutaneous layers even though the behaviour of skin as a whole was illustrated clearly and accurately. The *in vitro* tensile test has two limitations including the orientation of the testing and the loss of nutrient supply to the specimens. Regardless the sources of specimens, live donors or cadavers, the excised skin specimens are unable to acquire nutrients or any metabolic needs from its original sources and the behaviours or elastic moduli are no longer the same as *in*

vivo. The computational simulations of skin behaviours would consequently be affected and limited the clinical relevance due to the importance of Young's Modulus to FEA simulations. More importantly, the applied loads for both computational modelling or in clinical practice are mainly in the depth direction of the cutaneous layers. Hence, the elastic moduli would ideally be measured in the same direction. However, the thicknesses of the cutaneous layers are from only 10 to approximately 2,000 micrometres (Chopra et al., 2015) and impossible to attach to any of the clamps for tensile test purposes. The current material properties adopted in the halved model are from the Lévêque which were adopted for the computational modelling on the cutaneous layers as well (Lévêque & Audoly, 2013). This was the closest possible full set of elastic moduli for computational modelling. However, the magnitudes of the percentage changes of the cross-sectional area of the CBV demonstrated by the halved model were expected to be less than the *in vivo* conditions based on the concept of Langer's lines. It was found that the elastic moduli were higher along the Langer's lines than in perpendicular direction (Langer, 1978b).

To minimise the material properties uncertainty of the cutaneous layers and increase the clinical relevance of the halved model, the computational data will be correlated to a set of physiological data, i.e. percentage changes in the cutaneous blood flow velocity, in the next chapter.

A graphical representation was presented which related the magnitude of applied pressure and the change in the cross-sectional areas of the CBV. This could be an indicative parameter for analysing the effect of pressure on the cutaneous blood vessels.

By adopting the finite element method, the halved model was capable of approximating the *in vivo* conditions of the CBV in relating to the formation of

superficial pressure ulcers. However, the magnitudes of the change in the cross-sectional area was still deemed to be not fully physiologically relevant due to the limitation of the skin properties acquisition. The graphical representation could only be indicative and could not be an actual data for clinical use which required a further step to correlate the computational results to a set of physiological data.

7.8. Conclusion

The development of the halved model resolved the limitation of the quartered model in three aspects. Firstly, the halved model was capable of simulating more clinical relevant conditions typically single-direction friction. Secondly, an advanced method was developed to quantify the change in the cross-sectional area of the CBV. Finally, the mesh size of the halved model was analysed and a mesh size of 15μm was adequate. The influences of an externally applied pressure to the changes in the cross-sectional area of the CBV were illustrated graphically in the chapter from the range of 0 to 138.0 mmHg. The computational results from the halved model remained as an indicative parameter and not fully physiologically relevant which required a further correlation with a set of physiological data. Three objectives of this chapter are:

- To develop an advanced model which allows the application of a single-direction friction;

- To develop an advanced method of quantifying the changes in the cross-sectional area at the sections of interest on the cutaneous blood vessels; and

- To systematically evaluate the influence of a range of magnitudes of applied pressure to the change in the cross-sectional area of the cutaneous blood vessel.

The objectives of the chapter has been successfully achieved.

Chapter 8 Clinical Relevance of the Computational Model

8.1. Introduction

The developed computational model, halved model, presented in Chapter 7 demonstrated its capability in evaluating the deformation of cutaneous layers and consequently the change in the cross-sectional area at the sections of interest on the cutaneous blood vessels (CBV). It is a novel tool for understanding the behaviours of CBV under the influences of applied mechanical loads by adopting the finite element method and illustrating the *in vivo* conditions in relating to the formation of superficial pressure ulcers. A graphical representation for the relationship between the change in the cross-sectional area of the CBV and the applied mechanical loads was provided in Chapter 7. In order to be a fully functional and physiologically relevant tool, a correlation between the halved model and a set of physiological data needs to be established which is the aim of this chapter. The concept of correlating the computational results from the halved model with the physiological data is presented in Proceeding of the Institution of Mechanical Engineers, Part H: Journal of Engineering in Medicine (Leung et al., 2019).

8.2. Need for Clinical Relevance

The aim of the halved model was to approximate the changes in the cross-sectional area of the CBV at various cutaneous layers. However, the approximation was subjected to the influences of different factors for instance, the mechanical properties of cutaneous layers and *in vivo* configurations of CBV. The mechanical properties adopted in the halved model was extracted from the study conducted by Lévêque in which the mechanical properties were also adopted to be the input parameters of a

finite element model of skin (Lévêque & Audoly, 2013). However, as mentioned before in Section 2.4, the existing methods of evaluating the mechanical properties of skin were incapable of fully representing the behaviour of cutaneous layers *in vivo* in the direction of interest of the halved model, the depth direction of skin. The CBV within the halved model were end arterioles and blood vessels of other sizes including capillaries were omitted because their inclusion would exceed the computational power. Both of these two factors affect the physiological relevance of the model, however, the halved model could be a clinical relevant tool by correlating the computational results to a set of physiological data in relating to the formation of superficial pressure ulcers.

8.3. Measurement of the Cutaneous Blood Flow

Superficial pressure ulcers are developed when CBV are obstructed or partial restricted which leads to a reduction in blood flow causing a decrease in oxygen and nutrient supply, metabolic waste removal and decrease in pH value. These effects result in cells death and the formations of superficial pressure ulcers. Thus the prerequisite is a reduction of cutaneous blood flow, hence, it is adopted to be the physiological parameter. The set of physiological data was acquired by capturing the percentage change in the blood flow velocity by using Laser Doppler Velocimetry which is a technology for measuring the flow velocity of particles within a transparent or semi-transparent fluid. The change in the blood flow velocity was initiated by applying mechanical loads to the skin surface with the probe of the Laser Doppler. In the current study, a commercially available laser Doppler, PF5010-LDPM, from Perimed was adopted.

8.3.1. Probe of the laser Doppler

The aim of acquiring a set of physiological data was to understand the changes in cutaneous blood flow velocity caused by applied loads which were loaded with the probe of the laser Doppler. Thus, the area of the bottom surface of the probe was essential to the measurement as it was the contact area with the hands of the volunteers.

The area of the bottom surface of the probe affected the magnitude of the applied pressure, hence, a three-dimensional scan of the probe was conducted using an Artec Spider 3D Scanner. The three-dimensional scan of the probe is imported into a 3-dimensional design package for evaluating the area of the bottom surface which is shown in Figure 8.1 (a) and Figure 8.1 (b). The area of the bottom surface of the probe is 162.43 mm^2.

(a) (b)
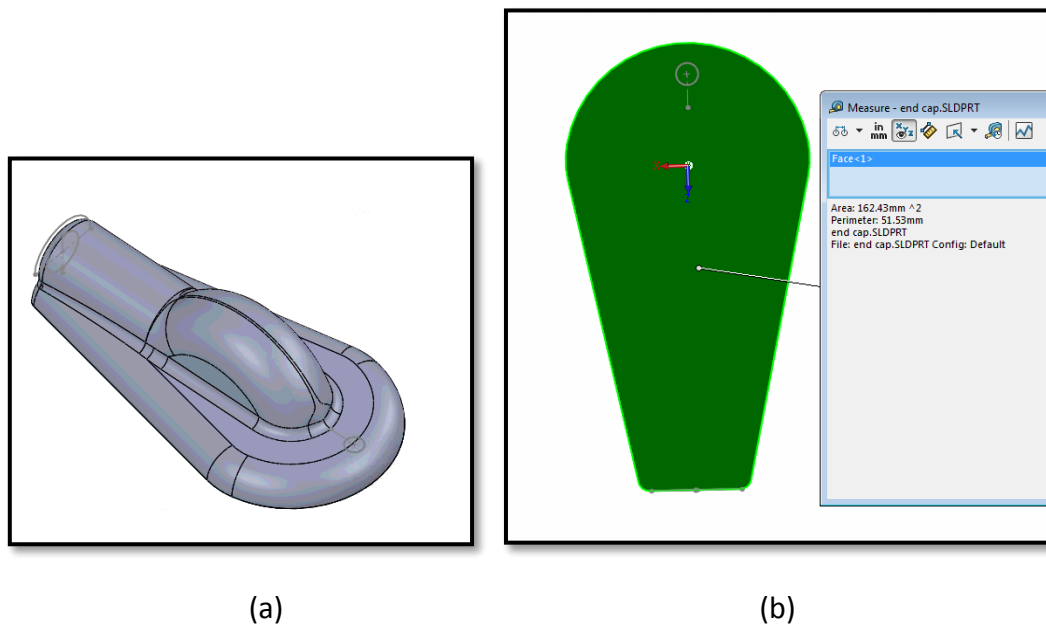
Figure 8.1   3D scanned probe of the laser Doppler velocimetry

8.3.2. Experimental setup for measuring cutaneous blood flow

The measurement of the cutaneous blood flow velocity is conducted at the middle

finger knuckles of the left hands of the three healthy volunteers. It is a bony prominence with a minimal amount of sub-cutaneous fat and it is easily accessible.

The left arm of the healthy volunteer is supported by a table and the left hand is placed in the clamp as shown in Figure 8.2. A rigid supporting wall is attached to the clamp and extended upward and the hand of the volunteer is pressurised against it. A pressure mapping sensor I-Scan 5051 is attached to the extended supporting wall and the force applied to the hand is captured by the pressure mapping system. The probe of the laser Doppler is attached to the middle finger knuckles by using transparent double side tape provided by the laser Doppler company, Perimed.
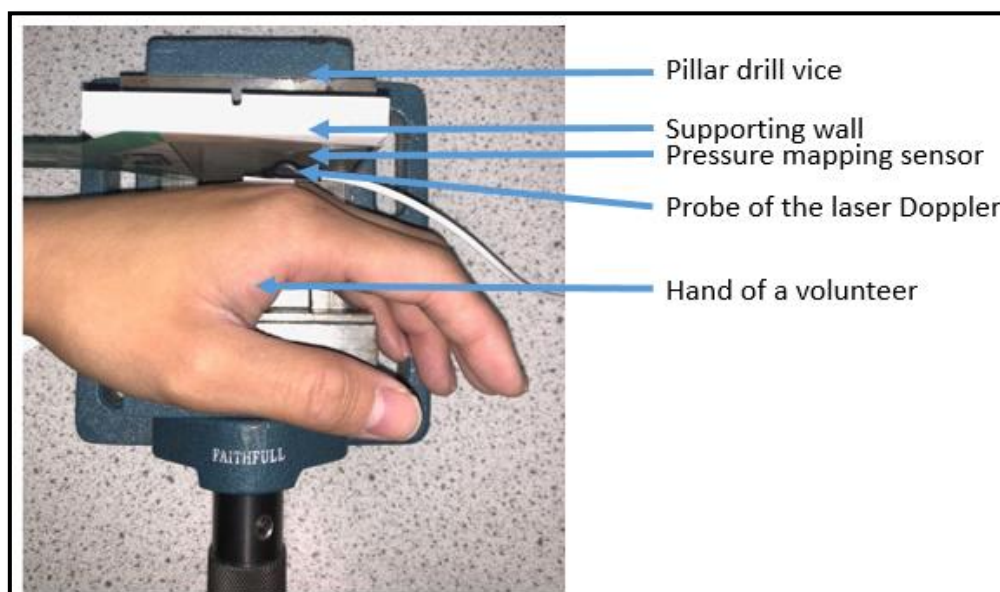
Figure 8.2   Experimental setup of the measurement of the cutaneous blood flow velocity

8.3.3.   Measurement procedures for cutaneous blood flow velocity

Three healthy volunteers aged between 24 and 50 consented to take part in the measurement of their cutaneous blood flow velocity by using a laser Doppler. The laser Doppler was very sensitive to any physical movement and emotional changes of the

participants. Hence, all the participants were instructed to remain calm and minimise any movement and talking throughout the whole measurement period. Laser Doppler velocimetry was incapable of measuring exact velocity of the flowing particles, hence, only the percentage change in the velocity was meaningful to the physiological data. The measurement was commenced by allowing the participant's hand to rest in the clamp with all the equipment in position for 2 minutes which constituted settling period. All the settling and measurement periods in this study lasted for 2 minutes. After the settling period, the cutaneous blood flow velocity was considered to be steady before the commencement of the first measurement period. For the first measurement period there was no force applied to the hand. The reading from the laser Doppler was recorded at 15 seconds interval. This initial set of readings was utilised as the reference data to calculate the percentage change in the blood flow velocity in later measurements. After the first measurement period, the hand of the volunteer was pressurised against the extended supporting wall until the captured reading from the pressure mapping system reached the first intended magnitude shown in Table 8.1. Another settling period was allowed before the commencement of the next measurement period. All the readings were averaged which provided a more meaningful representation of the cutaneous blood flow velocity affected by the applied mechanical loads during the whole measurement period. During the experiment, any slight movement of the hand would affect the magnitudes of the applied load, hence, the applied force to the hand was adjusted throughout the measurement period by the researcher to ensure the magnitude of applied loads was within ±0.1 newton of the intended magnitude. The whole experiment was repeated with the same procedure for the magnitudes of the applied force listed in Table 8.1. The magnitude of the applied force was not increased beyond the magnitude of 115.4 mmHg (2.5 N) because the first volunteer expressed the feeling of discomfort. All the

176

volunteers were instructed to express any discomfort experienced in the hand caused by the applied mechanical loads at any point during the procedure. No discomfort was caused between 0 to 115.4 mmHg for the three participants.

Table 8.1 Magnitudes of pressure for measurement of the cutaneous blood flow velocity

Measurement	Magnitude of Pressure (mmHg)	Applied Force (Newton)
1 (Reference Data)	0	0
2	23.1	0.5
3	46.2	1.0
4	69.3	1.5
5	92.4	2.0
6	115.4	2.5

8.3.4. Measured percentage change of cutaneous blood flow velocity

Nine readings from the laser Doppler were recorded in each of the measurement period and six sets of data in total were acquired for each of the participant. The full set of laser Doppler results for all the participants are listed in Appendix III. The lowest and highest reading from each set of reading were discarded in order to better represent the percentage changes in the blood flow velocity within the measurement period under the influences of the applied mechanical loads and this procedure was conducted by Excel automatically with the equation "(*(the sum of the 9 readings) minus the maximum value –the minimum value) divided by 7*". Table 8.2 shows the percentage changes of the blood flow velocity of each of the participant under the

influences of the applied mechanical loads. The percentage changes presented in Table 8.2 were the mean percentage change with respect to the initial value (measurement 1), hence, there is no percentage change for measurement 1.

Table 8.2 Percentage change of the blood flow velocity of three participants

Measurement	1	2	3	4	5	6
Applied Load (N)	0	0.5	1.0	1.5	2.0	2.5
1st Participant (%)	0	-46.94	-56.30	-74.57	-80.00	-84.97
2nd Participant (%)	0	-64.94	-83.19	-85.19	-93.62	-92.78
3rd Participant (%)	0	-21.63	-40.61	-60.18	-70.74	-89.50

Graphical Representations of the percentage changes of the blood flow velocity under the influence of the applied mechanical loads are presented in Figure 8.3. Blood flow velocity of each of the participants was different and the percentage change in the blood flow velocity was also different because of different physiological factors, for instance, viscosity of the blood and the mechanical properties of skin. Hence, the percentage changes of velocity of the three participants have different magnitudes but with a similar trend.
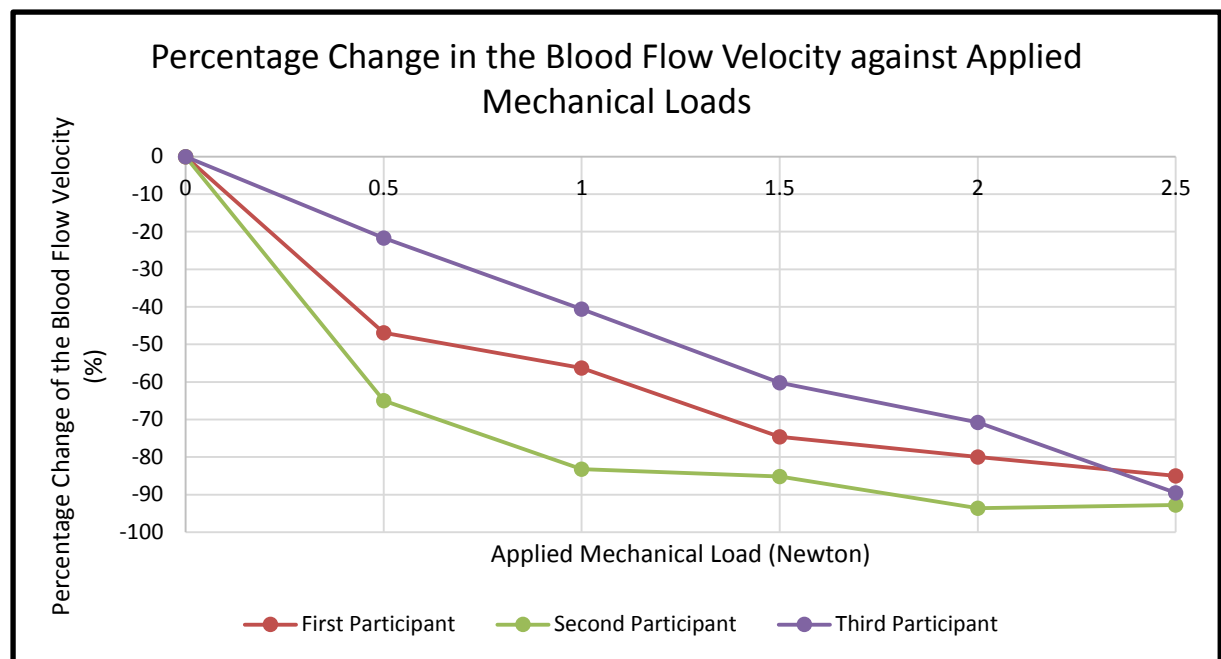
Figure 8.3   Graphical representation of the percentage change of the blood flow

velocity

8.3.5.   Discussion on laser Doppler measurement

A set of average data for all three participants is presented in Figure 8.4 and the upper

and lower limits are the range of the data. A trend line in form of a fourth order

polynomial is fitted to the data. The trend line is a good match with the average data

with the highest trend line fitting error of 2.5% occurring at the third measurement in

which one newton of force was applied to the finger knuckle by the probe of the laser

Doppler. The data labels indicate the equivalent applied pressure in millimetre of

mercury.
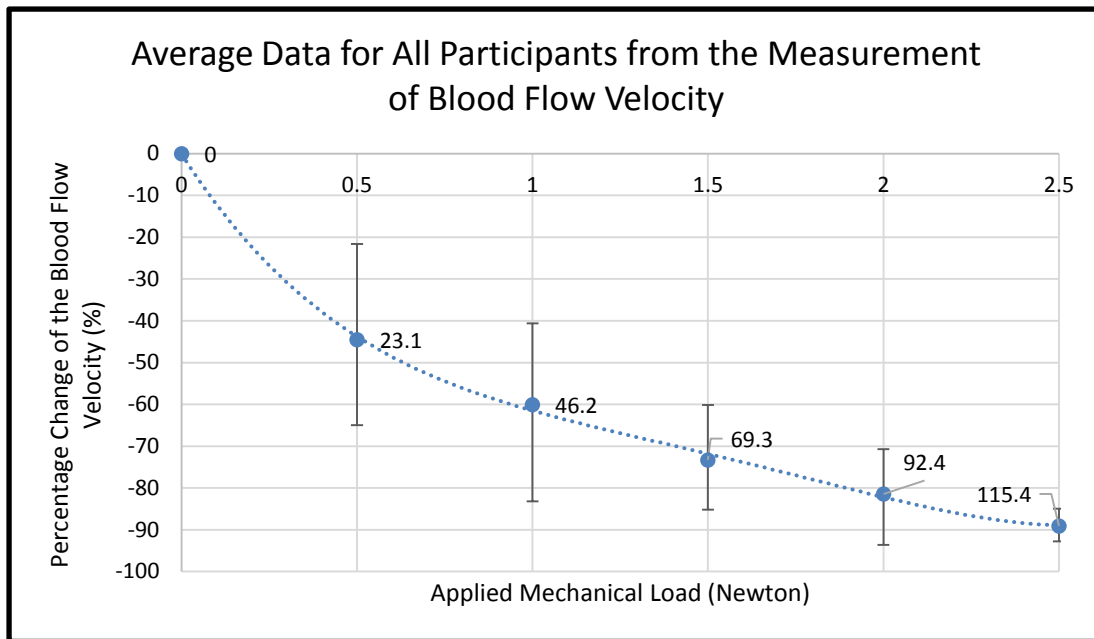
Figure 8.4   Clinical data acquired by laser Doppler velocimetry

The physiological data acquired by using laser Doppler presented in Figure 8.4 is functional at the range of 0 to 2.5 Newton of applied force which is equivalent to 0 to 115.4 mmHg of the applied pressure. Figure 8.4 enables the percentage change of the blood flow velocity to be approximated by referring to the magnitude of the applied force or the equivalent pressure. This data set was the average results of the three volunteers which was a relatively small sampling size but it proved the feasibility in the method of measuring the percentage change of the cutaneous blood flow velocity contributed by applied mechanical loads by using laser Doppler.

The findings of the laser Doppler measurement presented in this study confirmed the argument of using the capillary pressure, 32 mmHg, as a threshold of stopping the blood flow was inappropriate. This is in agreement with the idea from Bridel that the deformation of cutaneous blood vessels (CBV) is influenced by the presence of collagen content at the dermis layer (Bridel, 1993). Although the blood flow velocity

reduced significantly, more than 50%, for the applied pressure exceeding 32 mmHg, the blood flow was not completely stopped.

It highlighted that attentions should also be put on the light medical devices because the blood flow velocity was reduced dramatically by the applied pressure from 0 to 65 mmHg. This explained medical device related pressure ulcers caused by light medical devices, for instance, nasal cannulas and splints (J. Black et al., 2015).

The clinical data acquired by the laser Doppler in this study involved three healthy volunteers aged between 24 and 50. This was a relatively small sampling size for an accurate set of data to represent the general public. However, from the sets of acquired physiological data, it showed the feasibility of correlating the computational model to a set of physiological data to ensure the clinical and physiological relevance. Although the definite change of the cross-sectional area of the CBV *in vivo* was yet to be determined, the set of computational data could be used clinically in conjunction with the established correlation with the data acquired by the laser Doppler measurement. A larger scale of the Doppler measurement should be conducted with more participants to have a more representative set of physiological data which will be discussed in Chapter 11. These participants could also be classified into different groups in terms of ages, races and skin conditions to understand the respective blood flow phenomenon.

The general understanding of the relationship between flow velocity and the cross-sectional area of flowing domain was governed by the Bernoulli Equation. It stated that if the cross-sectional area of the flowing domain is restricted, the flow velocity would increase to remain the constant flow rate provided that the density remains

constant. However, this scenario is different from the cutaneous blood flow condition. The cutaneous blood flow at any point on the cutaneous layers is not a closed system, blood would flow to another area when a particular point of the cutaneous layer is applied with pressure. This situation could be understood as an electrical parallel circuit where a branch was increased with resistance and the current would travel another path with lower resistance. Hence, the fundamental principle of remaining constant flow rate was not applicable at the cutaneous blood flow condition. Human blood is also far from a perfect fluid and different particles are present, for instance, red blood cells and blood platelet. The blood vessels at the cutaneous blood layers are relatively small comparing to the size of the red blood cells unlike other anatomical locations where the blood vessels are relatively large, for instance, coronary artery. Hence, the flow conditions at the CBV is similar to a particle flow rather than perfect fluid flow. Thus, the condition described by the Bernoulli Equation does not hold on the blood flow condition at the cutaneous layers. Therefore, both the physiological data, percentage change in the cutaneous blood flow velocity, and the computational data, cross-sectional area of the cutaneous blood vessels, reduces simultaneously with the applied pressure.

8.4.   Correlating the Halved Model with Physiological Data

The halved model presented in Chapter 7 allows the clinicians or medical device developers to evaluate effect of their products on the change in the cross-sectional area of the CBV. This is an important step for medical device developers to minimise any potential increase in the likelihood of the formation of superficial pressure ulcers. The halved model is also effective for clinicians to understand the influence of mechanical loads on the CBV of patients. Correlating the physiological and simulated data is the final step to enable the computational results from the halved model to be

clinically and physiologically relevant and fully functional.

8.4.1. Computational results and physiological data

Figure 8.5 shows the correlation of the simulated data, Figure 7.15, and physiological data, Figure 8.4. The data labels indicate the applied pressure in millimetre of mercury.
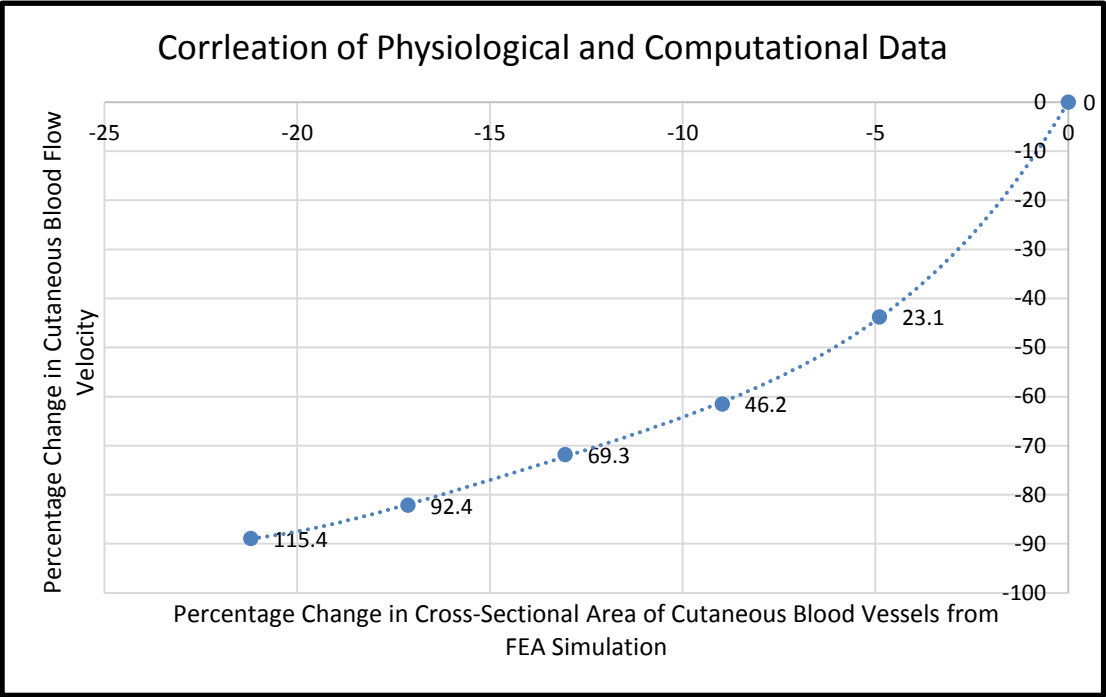
Figure 8.5   Relationship between the computational and clinical Data

A Linear relationship was found between the percentage change in the cross-sectional area at the sections of interest on the cutaneous blood vessels and the applied load. However, the percentage change of the blood flow velocity was non-linear and a fourth order polynomial represented the trend of the reduction. It was important to note that the computational results represented a percentage change of a blood flow cross-sectional area while the acquired physiological data represented a percentage change in blood flow velocity.

The working range of the halved model was 0 to 138.0 mmHg and the acquired physiological data was only in the range of 0 to 115.4 mmHg because further increase

in magnitudes of the applied load would result in feelings of discomfort for the participants. Hence, the working range of the halved model which was deemed to be fully functional and physiological and clinical relevant was 0 to 115.4 mmHg because of the established correlation of the computational results and the acquired physiological data. A pressure range of 20 to 137 mmHg was found within all the pressure mapping testing conducted and presented in Chapter 5. The working range of the halved model with the established relationship with the clinical data covered 78.9 % of the range of pressure found in the Chapter 5.

Figure 8.5 allows the equivalent percentage changes of the cutaneous blood flow velocity to be approximated by extracting the percentage changes of the cross-sectional area of the cutaneous blood vessels (CBV) from the halved model finite element simulation. This could be applied in evaluating the effect of different magnitudes of mechanical loads applied to the skin layers and understanding the effect of various mechanical properties of the cutaneous layers on the formation of superficial pressure ulcers. The benefits brought by the halved model and the correlation with the physiological data include minimising further need for human participation in evaluating the effect of applied pressure on cutaneous blood flow and the effective evaluation on the influence of medical devices on the formation of superficial pressures ulcers.

The correlation between the halved model and the physiological data increases the clinical and physiological relevance and compensates the uncertainties raised by the simplifications of the configurations of the CBV, the insufficient understanding and scientific data in the mechanical properties of cutaneous layers in depth direction and the omitting of blood pressure. Although the physiological data was only acquired by measurements conducted on three volunteers, it demonstrated the feasibility of the method, correlating the computational data to a set of physiological data for increasing

the physiological relevance, and the data showed the trend of changes in the blood flow velocity. The developed computational model with the established correlation is a novel step of relating an external parameter, magnitudes of mechanical loads, with a physiological factor, the percentage change in blood flow velocity. This could also be utilised to understand the effects of the same magnitude of mechanical loads on skin in different conditions, for instance, different races, ages and state of health.

8.5. Effect of oxygen delivery masks on patients

The aim of the physiological data correlated halved model was to evaluate the effects of medical devices on patients. Quantifying of the effects of medical devices on the CBV in relating to the formation of superficial pressure ulcers by analysing physiological data was a novel attempt. The percentage change in the cutaneous blood flow velocity caused by medical device cannot easily be measured because the effects of the medical devices on patients would be completely changed if laser Doppler is placed in between. In this section, the effect of a classic medical device, facial oxygen delivery mask on the patients is demonstrated by the physiological data correlated halved model.

8.5.1. Loading mechanism of the facial oxygen delivery mask

The loading mechanism of the facial oxygen delivery mask was analysed by Brill et. al. in 2018 in which four commercially available non-invasive ventilation (NIV) oxygen delivery masks were evaluated (Brill, Pickersgill, Moghal, Morrell, & Simonds, 2018). In this study, Brill et. al. hypothesised that body positions and NIV mask design had significantly effect on the magnitude of pressure applied on the skin. The overall mean pressure applied on the skin by different NIV masks was between 47.6 and 91.9 mmHg and the mean magnitudes of interface pressure contributed by supine and seated

position were 57.1 and 63.9 mmHg respectively. The physiological effect of these magnitudes of interface pressure was unclear, however, they were a good parameter for the halved model to evaluate the effect of NIV masks on the CBV in relating to the formation of superficial pressure ulcers.

As mentioned before, the halved model was developed in micrometres hence appropriate conversion is required. The applied pressure was converted from millimetres of mercury to Newton per square micrometre as shown in Table 8.3 and the first magnitude is used as an example as follow:

Higher Mean Interface Pressure in mmHg: 91.9

Higher Mean Interface Pressure in N/m^2: 91.9 X 133.322 = 12252.33

Higher Mean Interface Pressure in $N/\mu m^2$: 12252.33 X $1x10^{-12}$ = $1.225x10^{-8}$

Table 8.3 Loading of the halved mode

Loading Condition	Interface Pressure (mmHg)	Applied Load (Newton per square micrometre)
Higher Mean Interface Pressure	91.9	$1.225×10^{-8}$
Lower Mean Interface Pressure	47.6	$6.346×10^{-9}$
Pressure at Supine Position	57.1	$7.613×10^{-9}$
Pressure at Seated Position	63.9	$8.520×10^{-9}$

8.5.2. Blood flow affected by the NIV masks

The effects of the NIV masks on the cutaneous blood vessels (CBV) were demonstrated by four finite element analysis simulations conducted by the halved model. The changes of the cross-sectional area of the CBV were deduced by analysing the displacements of the key nodes at the sections of interest on the CBV. The effects of the NIV masks to the skin are illustrated in Table 8.4 and the approximated equivalent percentage changes of the blood flow velocities are deduced from Figure 8.5.

Table 8.4 Effect of NIV masks on skin demonstrated by halved model and equivalent reduction of blood flow velocity

	Higher Mean Pressure	Lower mean Pressure	Pressure at Seated Position	Pressure at Supine Position
Applied Pressure (mmHg)	91.9	47.6	63.9	57.1
Percentage Change for Cross-sectional Area of the Cutaneous Blood Vessels from the Halved Model	-17.67	-9.96	-12.95	-11.72
Approximated Equivalent Percentage Change for Blood Flow Velocity	-82.42	-64.23	-72.75	-69.57

The four NIV masks had significantly different physiological effects on the patients' skin. The interface pressure of the higher mean pressure was over 1.9 times higher than the lower mean pressure. The computational data from the halved model also

demonstrated that approximately double the percentage changes were found on the cross-sectional area of the cutaneous blood vessels resulting from the higher mean pressure. The approximated equivalent percentage changes of the blood flow velocity was not as significant as the magnitude of the applied pressure or the percentage change of the cross-sectional area. The equivalent percentage changes for the blood flow velocity were -82.42 and -64.23 caused by the higher and lower magnitudes of the mean pressure respectively. The less significant percentage changes of the blood flow velocity were contributed by the fourth order polynomial trend of the blood flow velocity. Although the reduction in the blood flow velocity caused by the higher mean pressure was only approximately 18% further decrease from the lower mean pressure, the blood flow velocity was decreased by 82.42% comparing to the blood flow velocity without any loading. Hence, physiologically, oxygen and nutrient delivery and metabolic waste removal were impaired significantly resulting in a high possibility of the formation of superficial pressure ulcers.

The effect of NIV masks on the patients who were in two distinct positions including seated and supine were demonstrated by the measured interface pressure(s) which was 63.9 and 57.1 mmHg respectively (Brill et al., 2018). These two magnitudes were external parameters which did not indicate the physiological conditions. However, with the simulation conducted with the physiological data correlated halved model, it was approximated that the cutaneous blood flow velocity was reduced by 72.25 and 69.5 percent for seated and supine position respectively.

Evaluating the effect of oxygen delivery masks on the CBV was a good demonstration of the primary function of the physiological data correlated halved model. The effect of the mechanical loads on skin in relating to the formation of superficial pressure ulcers was demonstrated by the change in cutaneous blood flow velocity. The reduction in the blood flow velocity resulted in the impairing the delivery of oxygen

and nutrient, removing metabolic waste from the cells, accumulating of the metabolic waste, decreasing in pH values and cells death (Dictionary_of_Nursing, 2017; EPUAP, 2014). The clinicians or medical device developers can evaluate the physiological effects of medical devices on patients' skin in relating to the formation of superficial pressure ulcers with the understanding of the physiological condition, i.e. percentage change in cutaneous blood flow velocity, rather than just comparing an external parameter, i.e. interface pressure.

8.6.   Effect of Mechanical Loads on Alternate Skin Conditions

The correlated halved model is capable of evaluating the effects of mechanical loads on the CBV as demonstrated in Section 8.5. One of the foundations of the halved model is the input parameters, i.e. the mechanical properties of the cutaneous layers. Each of the cutaneous layers has its respective magnitudes of mechanical property which was acquired from the study conducted by Lévêque (Lévêque & Audoly, 2013). The mechanical properties represented the skin characteristics of the general public but, for some of the patients, their skin properties varied significantly because of disease or ageing. For instance, Sanders found that the elasticity of skin changes with age (Sanders & Sanders, 1973) and Bermudez et. al. found that both the maximum stress and stiffness modulus were decreased for murine and human diabetic skin compare to nondiabetic ones (Bermudez et al., 2011). Although the definite percentage differences in the skin properties of a specific age group or patients are yet to be determined, the developed halved model is capable of evaluating the effects of same magnitude of mechanical loads on different types of patients provided that the skin mechanical properties are known. In this section, the developed halved model will demonstrate the effects of same magnitude of mechanical load on skin in three conditions including typical skin properties and 10 and 20 percent decreases in the

mechanical property in each cutaneous layer. Table 8.5 illustrates the variations of the cutaneous layers mechanical properties in two of the three simulations in which the first simulation represents the typical condition while the second and third simulations represent patients with decreased cutaneous mechanical properties.

Table 8.5 Young's Moduli of cutaneous layers in three simulations

Cutaneous Layers	Simulation 1 (Normal Skin Properties)	Simulation 2 (10% Decrease)	Simulation 3 (20% Decrease)
Stratum Corneum	1 MPa	0.9 MPa	0.8 MPa
Epidermis	0.05 MPa	0.045 MPa	0.04 MPa
Dermis	0.6 MPa	0.54 MPa	0.48 MPa
Hypodermis	0.11 MPa	0.099 MPa	0.088 MPa

8.6.1. Effect of 70 mmHg on skin with alternate skin conditions

The magnitude of 70 mmHg was applied to the superficial surfaces of the halved model in the three simulations and the percentage changes in blood flow velocity are shown in Table 8.6.

Table 8.6 Effect of 70 mmHg on Skin in Three Simulations

	Simulation 1 (Typical Skin Properties)	Simulation 2 (10% Decrease)	Simulation 3 (20% Decrease)
Percentage Change for the Cross-sectional Area of the Cutaneous Blood Vessels from the Halved Model	-13.42	-15.37	-16.97
Approximated Equivalent Percentage Change for Blood Flow Velocity	-73.87	-78.12	-81.17

The simulations approximated the effect of 70 mmHg of pressure on the changes in cutaneous blood flow velocity by providing the percentage changes of the cross-sectional area of the CBV from the halved model with the established correlation with the physiological data. The 10 and 20 percent decrease in mechanical properties of each of the cutaneous layers resulted in approximately 4.25 and 7.3 percent further reduction respectively in the cutaneous blood flow velocity comparing to the simulation conducted with the normal skin properties. It is important to note that these further reduction in the cutaneous blood flow velocity was not consistent for all magnitudes of the applied pressure, for instance, the effect of 30 mmHg of applied

pressure on 10% decrease Young's modulus of skin would not be 4.25 percent. The further reduction in the cutaneous blood flow velocity depends on the acquired physiological data which is in the form of a fourth order polynomial, hence the further reduction would not be the same throughout the working range of the halved model. This is the aim of the halved model with the established correlation, demonstrating the effect of mechanical loads on the cutaneous blood flow velocity. Without the developed computational model and the established correlation with the physiological data, it was very difficult to evaluate the effect of mechanical loads on patients with different skin conditions. By utilising the correlated halved model, the approximated effect of same magnitude of mechanical load on different patients can be analysed. This application also shows that the presence of collagen at dermis layer would result in differences in the percentage change in the cross-sectional area of the CBV.

8.7. Mattresses Testing from External Parameter to Physiological Parameter

Figure 5.2 in Chapter 5 indicated the range of intensities of interface pressure found in the static and dynamic mattresses. It showed the common intensities were 20-29 to 50-59 mmHg which provided a clear understanding on the magnitude of the interface pressure in clinical practice. However, it reminds as an external parameter and it could not represent in vivo condition. Hence, the developed model in this study with the established correlation with the physiological data is used to convert the external parameter to a physiological parameter, percentage change in cutaneous blood flow velocity.

8.7.1. Effect of the commonly found intensities of interface pressure on the cutaneous blood flow velocity

There are four intensities simulated by the halved model which are listed in Table 8.7 alongside with the results on the percentage change in the cross-sectional area of the CBV and equivalent percentage change of the cutaneous blood flow velocity.

Table 8.7 Intensities of loadings for mattresses testing and the simulated results

Intensities of Pressure (mmHg)	Applied Pressure $(N/\mu m^2)$	Change in the Cross-sectional Area (%)	Equivalent Change in Cutaneous Blood Flow Velocity (%)
25	3.333×10^{-9}	-5.46	-44.37
35	4.666×10^{-9}	-7.50	-52.90
45	5.999×10^{-9}	-9.45	-60.29
55	7.333×10^{-9}	-11.34	-66.74

Table 8.7 shows the results from the halved model, percentage change in the cross-sectional area and it gives an indicative idea and general information on the efficiency on the pressure relieving mattresses. The equivalent change in the cutaneous blood flow velocity are also provided which is the result from referring the change in the cross-sectional area to the established correlation. This is the first attempt in the field of pressure ulcer prevention to quantify mattresses by a physiological factor, percentage change in the cutaneous blood flow velocity.

According to Figure 5.2, pressure intensities of 25 to 55 mmHg is relatively low in intensity but commonly found however the established correlation in the study shows

that the cutaneous blood flow velocity has decreased by 44.37 to 66.74 percentage. This may indicate that the delivery of oxygen and nutrient and removal of metabolic waste have been significantly slowed down. The severity of the physiological effect of this change in cutaneous blood flow velocity depends on patients similar to the magnitudes thresholds of pressure for causing pressure ulcers on Figure 3.9. However, it provides a fact on the physiological condition caused by the mattresses.

8.8.   Conclusion

The computational data from the halved model presented in Chapter 7 was correlated to a set of physiological data acquired with a laser Doppler. This procedure ensured the clinical and physiological relevance of the halved model and it allowed an external parameter, for instance interface pressure, to be converted to a physiological factor, i.e. cutaneous blood flow velocity. This is a step closer to evaluate the likelihood of the formation of superficial pressure ulcers. The halved model and the established correlation with the physiological data is a novel tool to understand the formation of superficial pressure ulcers caused by ischemia. The set of physiological data showed that the low magnitude of applied pressure caused more significant relative percentage decrease in the blood flow velocity than high applied pressure. It also confirmed that the capillary pressure should not be deemed to be the threshold of pressure for fully stopping the cutaneous blood flow.

The objectives of the chapter are:

- To acquire a set of physiological data relating to the formation of superficial pressure ulcers

- To relate the computational data to this set of physiological data to increase the clinical and physiological relevancy of the halved model

- To demonstrate the physiological effects, under the influences of various mechanical properties of the cutaneous layers, of attached medical devices and mechanical loads by utilising the fully functional and clinical relevant halved model after the correlation with the physiological data has been established

All of the chapter objectives were accomplished and the clinical and physiological relevance of the computational model was enhanced.

Chapter 9   Discussion

The aim of this study is to develop a tool to evaluate the effects of mechanical loads on the cutaneous blood vessels (CBV) in relation to the formation of superficial pressure ulcers. A computational model was developed in this study with the physiological configurations of cutaneous layers and blood vessels retrieved from existing research.

The insufficient scientific data on the mechanical properties of cutaneous layers were revealed in Section 2.4 which was contributed to by the lack of appropriate methods. The existing measurement of cutaneous mechanical properties are mainly conducted by either *in vivo* suction and torsion tests or *in vitro* tensile test. The *in vivo* tests are capable of measuring cutaneous layers when skin is intact with metabolic supplies, hence, these results are the most representative to physiology. However, these *in vivo* tests only provide the mechanical property of skin as a whole system instead of individual layers. The respective mechanical properties of cutaneous layers are very hard to be determined independently which is essential to the computational modelling. *In vitro* tests are capable of determining some of the cutaneous layers independently, however, it is difficult to physically attach the cutaneous layers in the depth direction to a tensile test machine due to the physical thicknesses, 11.0 to 18.3μm for stratum corneum and 74.9 to 96.5μm for Epidermis (Sandby-Moller et al., 2003). The physical thicknesses of cutaneous layers limits the evaluation of the mechanical properties in the depth direction of skin which is essential to the simulations or approximations of the behaviours of skin under the influence of mechanical loads as most of them are applied to skin perpendicularly. The discovery of Langer's lines plays a role in skin anisotropy, however, limited attempts are found in understanding the effect of Langer's lines on the mechanical properties in the depth

direction. This limits the physiological relevance of the developed computational models.

The vascularisation configuration of the developed models were developed according to research conducted by Démarchez et. al. (Démarchez, 2011). The epidermis and dermis are avascular and vascularised respectively and a horizontal plexus of blood vessels is parallel to the body surface at the superficial level at the dermis layer. The second horizontal plexus of blood vessels is located at the dermal-hypodermal junction of the dermis layer and these two horizontal plexus of blood vessels are joined up by ascending arterioles. The hypodermis layer of skin is highly vascularised and blood is supplied from the lower plexus of arterioles at the dermis layer (Millington & Wilkinson, 2009; Saladin, 2007). The configuration of the cutaneous blood vessels was modelled accordingly in this study. Although the configurations were simplified in the developed models, all the blood vessels were assumed to be 15μm in diameter. This is still physiologically relevant because transitional blood vessels between arterioles and capillaries were found to be 15 μm in diameter (Yen & Braverman, 1976).

More effort from the engineering society to the field of pressure ulcer prevention is required. Currently, a lot of research in the field of pressure ulcer prevention is clinically based which is essential to the understanding of prevalence and clinical implications. However, scientific and engineering input in terms of the understanding of aetiologies and the development of related tools for comprehending the occurrence and prevention of pressure ulcers are required. In the last century, pressure ulcers were deemed to be only contributed by the ischemic conditions to cutaneous tissues (Kosiak, 1961), however, over the last decades, with the involvement of scientific and engineering research, it was demonstrated that ischemia was not the only aetiology of pressure ulcers but also excessive stress at distorted deep tissues (Menon et al., 2012). Computational models were developed to illustrate the aetiology of excessive

stress by approximating the *in vivo* conditions in relation to the formation of Category III and IV pressure ulcers. The models demonstrated that the deep tissues i.e. subcutaneous fat and muscle experience the highest magnitude of stress, hence, deep tissue injuries occur (Makhsous et al., 2007). Upon the breaking of the superficial layers of skin, the deep tissue injury would turn into a Category III or IV pressure ulcer. However, similar computational modelling regarding the aetiology of ischemia which has been acknowledged for a century is not developed due to the difficulties in modelling the cutaneous blood vessels (CBV) which are of a different magnitude of scale compared to the cutaneous layers. Although the pressure ulcers caused by ischemia are usually superficial and fall into Category I and II, this kind of pressure ulcers still affects a significant number of patients. Over one third of the pressure ulcers were medical device related which are usually superficial and caused by ischemia in a prevalence study conducted by Black (J. M. Black et al., 2010). Hence, the developed model in the current study is to serve as a tool to understand the effects of mechanical loads on the cutaneous layers which can be used at the development stage of medical devices for evaluating their effects on the cutaneous layers in relating to the formation of superficial pressure ulcers.

A pressure mapping measurement was conducted to investigate the magnitudes of pressure experienced by the patients in clinical setting which was a reference data to the developed model in this study. Although the pressure mapping measurement did not involve any attachment of medical devices, the measurement was designed at a condition where higher magnitudes of pressure were exerted, i.e. at the patient-mattress interfaces. The peak pressure which was the magnitude of interest was in between 20 and 137mmHg in all the two pressure mapping measurements including static and dynamic mattresses. Measurements were conducted at two anatomical locations including heels and sacrum which are reported to be common locations for

the formation of pressure ulcers (Ousey, 2005). The range of magnitudes found in the pressure mapping measurements was used as the ideal working range of the developed models in this study.

The first developed model named as "Quartered Model" which was published in the Journal of Wear in 2017 (Leung et al., 2017) was a novel model and the first attempt to demonstrate the *in vivo* conditions of cutaneous layers and blood vessels in relation to the formation of superficial pressure ulcers. The quartered model was capable of demonstrating the effects of mechanical loads on the cutaneous layers and more importantly the change of the cross-sectional area of the cutaneous blood vessels. The model was used in approximating the change of the cross-sectional area of the CBV when a person was sitting on a foam surface. The simulations of the quartered model demonstrated that the combined effect of the friction and pressure caused a decrease in the cross-sectional areas of the cutaneous blood vessels at the dermis and hypodermis layers by 1.7% and 13.02% respectively due to the different mechanical properties input for the cutaneous layers. The simulation indicated that more attention should be put on the pressure ulcers formation due to a seating position because of the significant reduction in the cross-sectional area of the CBV as demonstrated by the quartered model. However, the quartered model was incapable of simulating single-direction friction as the model was applied with two mirror boundary conditions. Hence, the model was further enhanced which was named as "Halved Model".

The halved model was in the shape of a semi-circle and only one mirror boundary condition was applied hence friction in a single direction could be applied. The CBV were located at the epidermal-dermal junction and dermal-hypodermal junction and randomly spaced in the hypodermis layer. In order to ensure physiological relevance for the halved model, the configuration of the blood vessels was designed with

199

reference to the research conducted by Démarchez et. al. There were sections of interest on the CBV in which four key nodes were used to determine the changes in the cross-sectional area by analysing the three-dimensional coordinates. A newer method of analysing the coordinates of the key nodes at the sections of interest was established which showed that the change of the cross-sectional area of the CBV depended on the depth of the blood vessels' locations especially contributed by friction. The superficial blood vessels were affected more significantly by applied friction comparing to those located at the deeper layer. The halved model was also used to generate a set of magnitudes of load against the percentage change of the cross-sectional area of the CBV which was never be established before experimentally or by computational simulations. The cross-sectional area of the CBV decreased linearly for 1.2% to 7.0% and 6.1% to 29.5% for the cutaneous blood vessels located at dermis and hypodermis respectively with the increasing magnitudes of the applied load from 23 to 138mmHg. As mentioned before, more significant change of the cross-sectional area was found at the CBV at the hypodermis layers than those at the dermis layer which was investigated in Section 6.9.2. The trend of percentage change of the CBV caused by the range of magnitudes of the applied pressure was deemed to be affected by the limitations mentioned earlier including the simplification of the configurations of the CBV and the limited knowledge in the mechanical properties of skin in depth direction. Hence, the set of data generated by the halved model was required to be related to a set of physiological data to ensure its clinical and physiological relevancy.

The set of physiological data was acquired by using laser Doppler on the back of middle finger knuckles of three healthy volunteers which had minimum subcutaneous fat and muscle tissues similar to the computational model in which only four layers were involved including stratum corneum, epidermis, dermis and hypodermis. The acquired

physiological data demonstrated the percentage change of the blood flow velocity influenced by a range of applied pressure from 0 to 115.4mmHg. The three sets of measured data from the volunteers were different in magnitudes but with a similar decreasing trend. The averaged results of the measured data of the three volunteers was in the form of a fourth order polynomial. A more significant decrease was found at the lower magnitudes of applied loads from 0 to 65mmHg which highlighted the importance of attention to the light weight medical device on the patients' bodies, for instance, nasal cannulas and splints. The physiological data acquired by the laser Doppler demonstrated that the cutaneous blood flow was not stopped when the applied pressure reached 32mmHg even the blood flow velocity was reduced by more than fifty percent. This finding agreed with Bridel's argument of 32mmHg of pressure should not be the threshold of stopping the cutaneous blood flow (Bridel, 1993). The idea of deeming the capillary pressure to be the threshold of collapsing the cutaneous blood vessels resulting in stopping the blood flow was from Landis in which attempts were made by directly and physically pressuring on the cutaneous capillary to determine the pressure for stopping the blood flow (Landis, 1930). The removal of epidermis resulting in direct contact with the capillary acquired an essential information on capillary pressure, however, Bridel deemed that the presence of collagen content at the dermis layer also affected the magnitudes of applied pressure which the skin can withstand without stopping the cutaneous blood flow. This was proven by the physiological data acquired in this study that the blood flow velocity was reduced by more than fifty percent but not completely stopped. The computational data from the halved model showed that the cross-sectional area of the blood vessels reduced when mechanical loads were applied while the acquired physiological data also demonstrated reduction in blood flow velocity with the applied mechanical load. The simultaneous reductions in the cross-sectional area of the flowing domain and the

flow velocity were deemed to be contributed by the effect of particle flow and non-Newtonian fluid mechanics. The red blood cells and blood plasma contribute to 45 and 55 percent of the whole blood volume according to the American Society of Haematology (American_Society_of_Hematology). The large portion of the red blood cells affects the rheological characteristics of human blood which is also demonstrated by the blood flow simulations conducted by Nagayama et. al. in which it showed that red blood cells had to line up in a specific pattern and squeezed through capillaries and narrow blood vessels (Nagayama & Honda, 2012). This also explains the phenomena of reductions in blood flow velocity and cross-sectional area of the CBV simultaneously found in the physiological data and the computational data from the halved model. Furthermore, the plasma contributes to 55 percent of the whole blood volume and plasma is proven to be a non-Newtonian fluid and its viscoelastic properties has significant effects on blood flow (Brust et al., 2013). Bernoulli's Equation describes flows in the condition of constant flow rate at any cross-section of the flowing domain. However, it is not applicable in the cutaneous blood flow because the blood can flow elsewhere when pressure is applied to a specific location of skin and resistance of flow is increased. The cutaneous blood flow velocity was therefore reduced while the cross-sectional area of the blood vessels were reduced in the measurement. The physiological data was acquired with three healthy volunteers which was a relatively small sampling size however the method of acquiring such physiological data was proven to be successful and enlarging the sampling size would be the next stage of the project to acquire similar physiological data with more participants from different races and ages to investigate the differences in cutaneous blood flow velocity.

It was very difficult to compare the two parameters directly as one of those was a cross-sectional area while another one was a velocity. Hence a graphical correlation between the two parameters also known as the computational data and physiological

data, the percentage changes of the cross-sectional area of the CBV and the cutaneous blood flow velocity respectively, was established. The correlation serves as a tool to approximate the percentage change of the cutaneous blood flow velocity when a specific percentage change of the cross-sectional area of the CBV is provided by the halved model. Figure 9.1 indicates the accomplishment of the projects in which two finite element models had been developed which aimed to approximate the in vivo conditions of the cutaneous layers and cutaneous blood vessels under different magnitudes of pressure. The gap or bridge between the engineering achievement and the clinical and medical device designers' requirements were filled by the establishment of the correlation between the physiological and computational data. With the aid of the developed halved model and established correlation, the effect of a medical device and mechanical load can be approximated once the physiological data was acquired with larger sampling size to represent the typical general public.

Clinical & Medial Device Designers' aspects

-The necessity to have a tool to quantify the effect of mechanical loads to the cutaneous blood vessels in relation to the formation of superficial pressure ulcers

Establishment of the correlation between the computational and physiological data

Engineering aspect

-Finite element model to approximate the *in vivo* conditions of human cutaneous layers
-Development of quartered and halved models

Figure 9.1   Accomplishment of the project

The halved model and the established correlation was used in three applications in the current study including the evaluation on the effect of medical devices, the effect of same magnitude loads on different skin conditions and converting an external parameter from mattress testing to a physiological parameter. A comprehensive pressure mapping measurement was conducted in 2018 for non-invasive ventilation oxygen delivery masks by Brill et.al in which four different magnitudes from 47.6 to 91.9mmHg of interface pressure was found for general positions and in two different specific postures for the patients(Brill et al., 2018). This set of numerical data was a very good indicator for clinical reference and also a useful reference value for further medical device development. However, it had no meaning on the physiological effect, clinicians or medical device developers were unable to relate the interface pressure with the actual physiological effect. The application of the halved model and the established correlation converted the interface pressure from Brill's measurement to actual clinical physiological data, i.e. the approximated percentage reduction of cutaneous blood flow velocity was 64.23% to 82.42% for the interface pressure of 47.6 to 91.9 mmHg. This was a novel method of understanding the effect of a mechanical load on the cutaneous blood flow which facilitated the evaluation on the effect of different magnitudes of mechanical loads to the cutaneous layers in relation to the formation of superficial pressure ulcer formation caused by ischemia. 70mmHg of pressure was applied to the halved model with different mechanical properties which is the second application of the halved model in this study. Patients are often with significant different mechanical properties of skin due to different conditions, for instance, diabetic skin was found to be less stiff than nondiabetic skin (Bermudez et al., 2011). Hence, it is necessary to develop a tool to evaluate the effect of mechanical

205

loads on skin with different conditions. Upon acquiring the respective mechanical properties of the skin condition, the halved model is capable of demonstrating the respective percentage change of the cross-sectional area of the CBV as demonstrated by the second application. An arbitrary pressure within the working range of the halved model, 70mmHg, was applied and demonstrated the effects of same mechanical loads on the cutaneous layers with ten and twenty percentage decrease in each of the cutaneous layer. It was found that there were 73.87, 78.12 and 81.17 percent reduction for skin with normal, and 10% and 20% decrease in the mechanical properties respectively. It was important to note that the differences in the percentage reduction were not constant through the working range as the physiological data was in the trend of a fourth order polynomial and non-linear. The final application aimed to convert the interface pressure measured in Chapter 5 to a physiological parameter, percentage change in the cutaneous blood flow velocity. It indicated that the commonly found magnitude of interface pressure, 25-55 mmHg, were associated with 44.37% to 66.74% of decrease in the cutaneous blood flow velocity. It was the first time of evaluating the effectiveness of pressure redistributing mattresses by using a physiological parameter in the field of pressure ulcer prevention.

The halved model was developed with the similar aim as other computational models developed over the years in the field of pressure ulcer prevention which is to demonstrate or simulate the *in vivo* conditions of patients to understand the formation of pressure ulcers; or to evaluate the effect of medical devices relating to the formations of pressure ulcers. Makhsous et. al. developed a model which highlighted the *in vivo* conditions of deep tissue and the *in vivo* location of maximum stress (Makhsous et al., 2007) while the halved model highlights the change in the cross-sectional area of the CBV which filled the gap of lacking of evaluation tool in the formation of superficial pressure ulcers. The halved model can also be used as an

indicative tool with similar function as the data provided by Gefen (Gefen, 2010). By alternating the skin properties, the halved model can be an indicative tool to demonstrate the effect of a mechanical load on a range of skin conditions.

Chapter 10 Conclusions

The aim of this study was to develop a computational tool to evaluate the effect of mechanical loads on the cutaneous blood vessels (CBV) in relation to the formation of superficial pressure ulcers. The following objectives were set out in order to achieve the aim:

- To gain better understanding of pressure ulcer prevention and the current engineering input to the field;

- To acquire the necessary properties of skin for computational modelling;

- To find the common magnitudes of pressure experienced in clinical settings;

- To develop a computational models of skin and CBV;

- To investigate the percentage changes of the cross-sectional area of the CBV under a range of magnitudes of pressure; and

- To establish the correlation between the computational model and the physiological data.

A number of sub-studies were developed and completed to achieve the aim and objectives for the study, the following conclusions can be drawn from those sub-studies:

- Significant engineering input was found in preventing pressure ulcers caused by excessive stress but limited in those caused by ischemia;

- A set of mechanical properties from previous research of skin was acquired, it highlighted the limitations of properties in the depth direction and this requires further investigation;

- A pressure mapping study was conducted on static and dynamic mattresses to investigate the magnitudes of pressure experienced in clinical setting;

- From this study the needs for standardisation of pressure mapping

measurement for mattresses was evident;

- A computational model, "Quartered Model", was developed to simulate the effect of body weight on the centre of buttocks with the aid of pressure mapping analysis;

- The combined effect of pressure and friction was found to decrease the cross-sectional area of the CBV which would have an   effect on the cutaneous blood flow;

- An advancement of the computational model, "Halved Model", was completed by increasing the sections of interest and developing new methods of computing the cross-sectional area of the CBV;

- A set of computational data was acquired by a series of simulations by the halved model to demonstrate the change in the cross-sectional area of the CBV under the influences of a range of magnitudes of the applied mechanical loads;

- A set of physiological data, i.e. cutaneous blood flow velocity, was acquired by using Laser Doppler which demonstrated the effects on the velocities by a range of magnitudes of the applied mechanical loads;

- A correlation was established between the computational data and the physiological data to increase clinical and physiological relevance of the halved model. Approximated equivalent percentage change of the cutaneous blood flow velocity could be acquired from the computational data;

- The effect of the pressure applied on skin by the oxygen delivery masks was input to the halved model to establish a   correlation demonstrating the physiological effect of the oxygen delivery masks on patients;

- Alternate skin conditions demonstrating changes in skin health was applied to the halved model to demonstrate the possible implications of skin condition on pressure ulcer development.

- The magnitude of pressure was converted to a physiological parameter by the correlated computational model which is the first attempt in the field of pressure ulcer prevention.

The above conclusions summarised the study and demonstrated that the development of the halved model and the established correlation between the halved model with the physiological data is an useful tool to demonstrate the effect of mechanical loads on skin in relating to the formation of superficial pressure ulcers. This computational tool was novel and the first of its kind tool in the field of pressure ulcers caused by ischemia. By using this developed tool, it reduces the involvement of live participants in the testing of medical devices regarding to the formation of superficial pressure ulcers.

Chapter 11 Further Studies

The properties of skin and the aetiologies of pressure ulcers were investigated through the literature review and this research study. The study demonstrated that the development of Finite Element Analysis (FEA) Halved Model and the established correlation between the FEA Halved Model with the physiological data is a useful tool to demonstrate the effect of mechanical loads on skin in relating to the formation of superficial pressure ulcers. In order to enhance the clinical applications of the computational model and tool, the following areas require further investigated.

Further studies should consist of two objectives including increasing the physiological relevance of the computational model and improving the accuracy of the acquired physiological data. Layer independent mechanical properties of skin in depth direction is still unclear despite the quantity of research conducted in examining and measurement the behaviours of skin under different applied loadings. Further study should be conducted for acquiring layer independent mechanical properties in depth direction as it is an essential parameter for computational models as all the loads are perpendicular to the skin surface. This could be achieved by utilising Atomic Force Microscopy (AFM) in which the direction of measurement is determined by the direction of the excised samples. The mechanical properties in depth direction could consequently be measured with specific excising techniques. Other skin characteristics including viscoelasticity and anisotropy should also be further investigated in the AFM study as well. A comprehensive properties study on skin allows not only better understanding physiologically but also enhances the relevance of the computational model and better represents the skin *in vivo*.

The physiological data measurement in the current study was conclusive and found to be a robust method to analyse the cutaneous blood flow velocity under the influences of applied mechanical loads. This approach should be adopted in further study with larger number of participants. The increase the sampling size is useful in acquiring a more representative trend of the general public but also beneficial to the understanding on the effect of aging, gender, races on the cutaneous blood flow velocity and the differences in the responses to the applied mechanical loads. The same measurement should also be conducted on more anatomical locations to investigate the related effects. Specific loading equipment should be designed to ensure robust loading mechanism and accuracy of the acquired data.

Reference

Agache. (2000). *Physiologie de la peau et exploitations fonctionnelles cutanees*.

Agache, P. G., Monneur, C., Leveque, J. L., & De Rigal, J. (1980). Mechanical properties and Young's modulus of human skin in vivo. *Archives of Dermatological Research, 269*(3), 221-232. doi:10.1007/BF00406415

Agency_for_Healthcare_Research_and_Quality, U. S. D. o. H. H. S. (2014, October 2014). Preventing Pressure Ulcers in Hospitals, are we ready for this change? Retrieved from https://www.ahrq.gov/professionals/systems/hospital/pressureulcertoolkit/putool1.html

Akers, W. A., & Akers, C. W. A. (1985). Measurements of friction injuries in man. *American Journal of Industrial Medicine, 8*(4-5), 473-481. doi:10.1002/ajim.4700080429

Akkus, O. (2012). Evaluation of Skin and Subcutaneous Adipose Tissue Thickness for Optimal Insulin Injection. *Journal of Diabetes & Metabolism, 3*(8). doi:10.4172/2155-6156.1000216

Allman, R. M., Goode, P. S., Burst, N., Bartolucci, A. A., & Thomas, D. R. (1999). Pressure ulcers, hospital complications, and disease severity: impact on hospital costs and length of stay. *Advances in wound care : the journal for prevention and healing, 12*(1), 22-30.

Allman, R. M., Goode, P. S., Patrick, M. M., Burst, N., & Bartolucci, A. A. (1995). Pressure Ulcer Risk Factors Among Hospitalized Patients With Activity Limitation. *JAMA, 273*(11), 865-870. doi:10.1001/jama.1995.03520350047027

American_Society_of_Hematology. Blood Basics. Retrieved from https://www.hematology.org/Patients/Basics/

Bauer, K., Rock, K., Nazzal, M., Jones, O., & Qu, W. (2016). Pressure Ulcers in the United States' Inpatient Population from 2008 to 2012: Results of a Retrospective Nationwide Study. *Ostomy Wound Management, 62*(11), 30-38.

Bennett, G., Dealey, C., & Posnett, J. (2004). The cost of pressure ulcers in the UK. *Age and Ageing, 33*(3), 230-235. doi:10.1093/ageing/afh086

Bergstrom, N., Braden, B. J., Laguzza, A., & Holman, V. (1987). The Braden Scale for Predicting Pressure Sore Risk. *Nursing Research, 36*(4), 205-210. doi:10.1097/00006199-198707000-00002

Berlowitz, D. R., & Wilking, S. V. B. (1989). Risk factors for pressure sores. A comparison of cross-sectional and cohort-derived data. *Journal of the American Geriatrics Society, 37*(11), 1043-1050. doi:10.1111/j.1532-5415.1989.tb06918.x

Bermudez, D. M., Herdrich, B. J., Xu, J., Lind, R., Beason, D. P., Mitchell, M. E., . . . Liechty, K. W. (2011). Impaired Biomechanical Properties of Diabetic Skin. *American Journal of Pathology, The, 178*(5), 2215-2223. doi:10.1016/j.ajpath.2011.01.015

Black, J., Alves, P., Brindle, C. T., Dealey, C., Santamaria, N., Call, E., & Clark, M. (2015). Use of wound dressings to enhance prevention of pressure ulcers caused by medical devices. *International Wound Journal, 12*(3), 322-327. doi:10.1111/iwj.12111

Black, J. M., Cuddigan, J. E., Walko, M. A., Didier, L. A., Lander, M. J., & Kelpe, M. R. (2010). Medical device related pressure ulcers in hospitalized patients. *International Wound Journal, 7*(5), 358-365. doi:10.1111/j.1742-481X.2010.00699.x

Bridel, J. (1993). The aetiology of pressure sores. *Journal of Wound Care, 2*(4), 230-238. doi:10.12968/jowc.1993.2.4.230

Brill, A.-K., Pickersgill, R., Moghal, M., Morrell, M. J., & Simonds, A. K. (2018). Mask pressure effects on the nasal bridge during short-term noninvasive ventilation. *ERJ open research, 4*(2), 168. doi:10.1183/23120541.00168-2017

British Standards, I. (2012). BS EN 1957:2012: Furniture. Beds and mattresses. Test methods for the determination of functional characteristics and assessment criteria. In: British Standards Institute.

British Standards, I. (2016). Furniture - Assessment of the ignitability of mattresses and upholstered bed bases - Part 1: Ignition source smouldering cigarette. In.

Brust, M., Schaefer, C., Doerr, R., Pan, L., Garcia, M., Arratia, P. E., & Wagner, C. (2013). Rheology of human blood plasma: Viscoelastic versus Newtonian behavior. *Physical Review Letters, 110*(7), 078305. doi:10.1103/PhysRevLett.110.078305

Bush, R. A., Brodine, S. K., & Shaffer, R. A. (2000). The association of blisters with musculoskeletal injuries in male marine recruits. *Journal of the American Podiatric Medical Association, 90*(4), 194-198.

Chimata, G. P., & Schwartz, C. J. (2015). Investigation of the effect of the normal load on the incidence of friction blisters in a skin-simulant model. *Proceedings of the Institution of Mechanical Engineers, Part J: Journal of Engineering Tribology, 229*(3), 266-272. doi:10.1177/1350650114535569

Chopra, K., Calva, D., Sosin, M., Tadisina, K. K., Banda, A., De La Cruz, C., . . . Christy, M. R. (2015). A Comprehensive Examination of Topographic Thickness of Skin in the Human Face. *Aesthetic Surgery Journal, 35*(8), 1007-1013. doi:10.1093/asj/sjv079

Clinical_Excellence_Commission. (2016). *2016 NSW Pressure Injury Point Prevalence Survey Report*. Retrieved from

http://www.cec.health.nsw.gov.au/__data/assets/pdf_file/0006/361995/2016-NSW-Pressure-Injury-Point-Prevalence-Survey-report.pdf

Colic, K., Sedmak, A., Sedmak, S., Grbovic, A., Tatic, U., & Djordjevic, B. (2016). Finite Element Modeling of Hip Implant Static Loading. *Procedia Engineering, 149*, 257-262. doi:10.1016/j.proeng.2016.06.664

Comaish, J. S. (1973). EPIDERMAL FATIGUE AS A CAUSE OF FRICTION BLISTERS. *The Lancet, 301*(7794), 81-83. doi:10.1016/S0140-6736(73)90472-8

Concise_Medical_Dictionary. (2015). ischaemia. In (9 ed.): Oxford University Press.

Concise_Meidcal_Dictionary. (2010). hyperaemia. In (8 ed.): Oxford University Press.

Concise_Meidcal_Dictionary. (2015). ulcer. In (9 ed.): Oxford University Press.

Cortese Jr, T. A., Griffin, T. B., Layton, L. L., & Hutsell, T. C. (1969). Experimental Friction Blisters in Macaque Monkeys. *The Journal of Investigative Dermatology, 53*(2), 172-177. doi:10.1038/jid.1969.28

Cranston, W. I. (1989). Thermoregulation and the Skin. In *Handbook of Experimental Pharmacology* (Vol. 87): Springer, Berlin, Heidelberg.

creep. (2015). In (7 ed.): Oxford University Press.

David, J. A. (1983). *An investigation of the current methods used in nursing for the care of patients with established pressure sores*.

Dealey, C. (1994). Monitoring the pressure sore problem in a teaching hospital. *Journal of Advanced Nursing, 20*, 652-659.

Dealey, C. (1997). *Managing pressure sore prevention*. Dinton: Quay Books.

Dealey, C., Posnett, J., & Walker, A. (2012). The cost of pressure ulcers in the United Kingdom. *Journal of Wound Care, 21*(6), 261-266. doi:10.12968/jowc.2012.21.6.261

Defloor, T. (1999). The risk of pressure sores: A conceptual scheme. *Journal of Clinical Nursing, 8*(2), 206-216. doi:10.1046/j.1365-2702.1999.00254.x

Démarchez, M. (2011, 15 May 2011). Cutaneous vasculature. Retrieved from http://biologiedelapeau.fr/spip.php?article21

Dictionary_of_Biology. (2016). hypoxia. In (7 ed.): Oxford University Press.

Dictionary_of_Mechanical_Engineering. (2013). shear. In (1 ed.): Oxford University Press.

Dictionary_of_Nursing. (2017). ischaemia. In (7 ed.): Oxford University Press.

Dinsdale, S. M. (1974). Decubitus ulcers: role of pressure and friction in causation. *Archives of physical medicine and rehabilitation, 55*(4), 147-152.

Diridollou, S., Vabre, V., Berson, M., Vaillant, L., Black, D., Lagarde, J. M., . . . Patat, F. (2001). Skin ageing: changes of physical properties of human skin in vivo. *International Journal of Cosmetic Science, 23*(6), 353-362. doi:10.1046/j.0412-5463.2001.00105.x

Dupuytren, G. (1836). *Theoretisch-praktische Vorlesungen über die Verletzungen durch Kriegswaffen*.

Edwards, C., & Marks, R. (1995). Evaluation of biomechanical properties of human skin. *Clinics in Dermatology, 13*(4), 375-380. doi:10.1016/0738-081X(95)00078-T

Elsner, J. J., & Gefen, A. (2008). Is obesity a risk factor for deep tissue injury in patients with spinal cord injury? *Journal of Biomechanics, 41*(16), 3322-3331. doi:10.1016/j.jbiomech.2008.09.036

EPUAP, N., PPPIA. (2014). *Prevention and Treatment of Pressure Ulcers: Clinical Practice Guideline*. Retrieved from Western Australia:

EPUAP&NPUAP, E. P. U. A. P. a. N. P. U. A. P. (2009). *Prevention and treatment of pressure ulcers: quick reference guide*. Retrieved from http://www.epuap.org/guidelines/Final_Quick_Prevention.pdf

Essex, H. N., Clark, M., Sims, J., Warriner, A., & Cullum, N. (2009). Health-related quality of life in hospital inpatients with pressure ulceration: Assessment using generic health-related quality of life measures. *Wound Repair and Regeneration, 17*(6), 797-805. doi:10.1111/j.1524-475X.2009.00544.x

Fish, J., & Belytschko, T. (2007). *A first course in finite elements*. Chichester: John Wiley.

Franks, P. J., Winterberg, H., & Moffatt, C. J. (2002). Health-related quality of life and pressure ulceration assessment in patients treated in the community. *Wound Repair and Regeneration, 10*(3), 133-140. doi:10.1046/j.1524-475X.2002.11002.x

Gallagher, A. J., Ní Annaidh, A., Bruyère, K., & al, e. (2012). Dynamic Tensile Properties of Human Skin. In: International Research Council on the Biomechanics of Injury U6 - institution=44HUD_INST&vid=44HUD_INST%3AServices&%3Fctx_ver=Z39.88-2004&ctx_enc=info%3Aofi%2Fenc%3AUTF-8&rfr_id=info%3Asid%2Fsummon.serialssolutions.com&rft_val_fmt=info%3Aofi%2Ffmt%3Akev%3Amtx%3Ajournal&rft.genre=article&rft.atitle=Dynamic+Tensile+Properties+of+Human+Skin&rft.au=Gallagher%2C+A.+J&rft.au=N%C3%AD+Annaidh%2C+Aisling&rft.au=Bruy%C3%A8re%2C+Karine&rft.au=et+al&rft.date=2012-01-01&rft.pub=International+Research+Council+on+the+Biomechanics+of+Injury&rft.externalDBID=n%2Fa&rft.externalDocID=oai_researchrepository_ucd_ie_10197_4772&paramdict=en-US U7 - Web Resource.

Gebhardt, K. (1995). Tissue viability. What causes pressure sores? *Nursing standard (Royal College of Nursing (Great Britain) : 1987), 9*(31), 48-51.

Geerligs, M., van Breemen, L., Peters, G., Ackermans, P., Baaijens, F., & Oomens, C. (2011). In vitro indentation to determine the mechanical properties of

epidermis. *Journal of Biomechanics, 44*(6), 1176-1181. doi:10.1016/j.jbiomech.2011.01.015

Gefen, A. (2010). The biomechanics of heel ulcers. *Journal of Tissue Viability, 19*(4), 124-131. doi:10.1016/j.jtv.2010.06.003

Gefen, A., van Nierop, B., Bader, D. L., & Oomens, C. W. (2008). Strain-time cell-death threshold for skeletal muscle in a tissue-engineered model system for deep tissue injury. *Journal of Biomechanics, 41*(9), 2003-2012. doi:10.1016/j.jbiomech.2008.03.039

Gefen, A., & Weihs, D. (2016). Cytoskeleton and plasma-membrane damage resulting from exposure to sustained deformations: A review of the mechanobiology of chronic wounds. *Medical engineering & physics, 38*(9), 828-833. doi:10.1016/j.medengphy.2016.05.014

Genesio, J. (2016). Pressure Ulcers Are Easy Pickings For Lawsuits. In (Vol. 42, pp. 35-38). United States.

Gorecki, C., Nixon, J., Madill, A., Firth, J., & Brown, J. M. (2011). What influences the impact of pressure ulcers on health-related quality of life? A qualitative patient-focused exploration of contributory factors. *Journal of Tissue Viability, 21*(1), 3-12. doi:10.1016/j.jtv.2011.11.001

Grahame, R. (1970). A method for measuring human skin elasticity in vivo with observations of the effects of age, sex and pregnancy. *Clinical science, 39*(2), 223-229.

Grant, C. A., Twigg, P. C., & Tobin, D. J. (2012). Static and dynamic nanomechanical properties of human skin tissue using atomic force microscopy: effect of scarring in the upper dermis. *Acta biomaterialia, 8*(11), 4123-4129. doi:10.1016/j.actbio.2012.06.042

Graves, N., Birrell, F., & Whitby, M. (2005). Effect of Pressure Ulcers on Length of Hospital Stay. *Infection Control and Hospital Epidemiology, 26*(3), 293-297. doi:10.1086/502542

Graves, N., & Zheng, H. (2014). *Modelling the direct health care costs of chronic wounds in Australia*. Retrieved from Australia: http://www.awma.com.au/journal/2201_02.pdf

Grey, J. E., Harding, K. G., & Enoch, S. (2006). Pressure ulcers. *BMJ, 332*(7539), 472-475. doi:10.1136/bmj.332.7539.472

Groves, R. (2012). *Quantifying the mechanical properties of skin in vivo and ex vivo to optimise microneedle device design.* (Dissertation/Thesis), ProQuest Dissertations Publishing U6 - institution=44HUD_INST&vid=44HUD_INST%3AServices&%3Fctx_ver=Z39.88-2004&ctx_enc=info%3Aofi%2Fenc%3AUTF-

8&rfr_id=info%3Asid%2Fsummon.serialssolutions.com&rft_val_fmt=info%3A
ofi%2Ffmt%3Akev%3Amtx%3Abook&rft.genre=dissertation&rft.title=Quantif
ying+the+mechanical+properties+of+skin+in+vivo+and+ex+vivo+to+optimise
+microneedle+device+design&rft.DBID=H8S%3BGI4%3BG20%3B0BH%3BEU9
%3B053&rft.PQPubID=51922&rft.au=Groves%2C+Rachel&rft.date=2012-01-
01&rft.pub=ProQuest+Dissertations+Publishing&rft.externalDocID=28025836
71&paramdict=en-US   U7   -   Dissertation,   Retrieved   from
http://hud.summon.serialssolutions.com/2.0.0/link/0/eLvHCXMwpV3rS8JQFL
8kfon6UFT0MLgQ-
k2Z25zzQ0TmK6glnPRR5nZXI91CTfS_73fu3AMNIQI5XnfZw989u-
dxzzmXMU2tKOWNOUGpjSAZIay9kSGk2HRhxZk11THsqiP9b63Gy3Pj6V633tb
beVJqzMe3W7HHE_uXXAfKWqUox1W8z9Sdv15eJy-
TrvcGrSEMYKu0wPCmPzHw8VtYKmqd__IMjoFrKAf3D3yTXBQH0Ab3gIJ_QDd
U661F-aS-
BoUSreKMqomgNGE5ql_kw59SMVbSNmefvgyYXPiLUK5GiGXUhmIbYk4CL-
FsCv0LICyjVC1Ag68kfCTa9dXsF7Vm91EnqiqgSrMH2h40qB3V-
018XdAK1SQ2ujvFKEVeIypRPc56M2RYSNab8ToNpaOXao8mf3yWccmlYisJJlR
N6G2mZtSrJSqXPnF9Z34rgvKgn2N5lXKUtuSsVB6sI3aQvc0x2xPBCXvPgMsBLk_
B5Sm4PPQ4gcvxIUA5wOViGbXnIY_B5RlweQQuj8A9ZTedtvXQK8ePNlzPHjNYZ
WRn67R5wBk7tCnVIZjLlEj3nPG6QBfUeNPTq7qwPRgeNWi1bt0QmiEc-
4IVdl3ycnf3FdtPx6XA8h66xTXL4U38ASWBP4k

Guest, J. F., Ayoub, N., McIlwraith, T., Uchegbu, I., Gerrish, A., Weidlich, D., . . . Vowden, P. (2016). Health economic burden that different wound types impose on the UK's National Health Service: Annual NHS cost of managing different wound types in the UK. *International Wound Journal*. doi:10.1111/iwj.12603

Guinness_World_record. (2018, 2014). Deepest scuba dive (male). Retrieved from http://www.guinnessworldrecords.com/world-records/deepest-scuba-dive-(male)

Harrison, D. K., & Walker, W. F. (1979). Micro-electrode measurement of skin pH in humans during ischaemia, hypoxia and local hypothermia. *The Journal of Physiology, 291*(1), 339-350. doi:10.1113/jphysiol.1979.sp012817

Health_Service_Executive. (2017). Bed sores. Retrieved from https://www.hse.ie/eng/health/az/b/bed-sores/causes-of-pressure-ulcers.html

Hendriks, F. M., Brokken, D., Oomens, C. W. J., & Baaijens, F. P. T. (2004). Influence of hydration and experimental length scale on the mechanical response of human skin in vivo, using optical coherence tomography. *Skin Research and Technology, 10*(4), 231-241. doi:10.1111/j.1600-0846.2004.00077.x

Hwang, K., Kim, H., & Kim, D. J. (2016). Thickness of skin and subcutaneous tissue of the free flap donor sites: A histologic study: Thickness of the Free Flap Donor Sites. *Microsurgery, 36*(1), 54-58. doi:10.1002/micr.30000

Igarashi, A., Yamamoto-Mitani, N., Gushiken, Y., Takai, Y., Tanaka, M., & Okamoto, Y. (2012). Prevalence and incidence of pressure ulcers in Japanese long-term-care hospitals. *Archives of Gerontology and Geriatrics, 56*(1), 220-226. doi:10.1016/j.archger.2012.08.011

ISIIP, U. o. H. (2016). Institute of Skin Integrity and Infection Prevention. Retrieved from http://www.hud.ac.uk/research/researchcentres/isiaip/

Jorgen Serup, G. B. E. J. *Handbook of NON-INVASIVE METHODS and the SKIN*.

Kalra, A., & Lowe, A. (2016). An Overview of Factors Affecting the Skins Youngs Modulus. *Journal of Aging Science, 4*(2). doi:10.4172/2329-8847.1000156

Kaufmann, M. L., Philip Matern, Katie Morrison-Graham, Devon Quick. (2018). *Anatomy & Physiology*: Open Oregon State, Oregon State University.

Kendall, M. A. F., Chong, Y.-F., & Cock, A. (2007). The mechanical properties of the skin epidermis in relation to targeted gene and drug delivery. *Biomaterials, 28*(33), 4968-4977. doi:10.1016/j.biomaterials.2007.08.006

Khatyr, F., Imberdis, C., Vescovo, P., Varchon, D., & Lagarde, J. M. (2004). Model of the viscoelastic behaviour of skin in vivo and study of anisotropy. *Skin Research and Technology, 10*(2), 96-103. doi:10.1111/j.1600-0846.2004.00057.x

Klabunde, R. E. (2007, June 2007). Stress Relaxation. Retrieved from https://www.cvphysiology.com/Blood%20Pressure/BP027

Knapik, J. J., Reynolds, K. L., Duplantis, K. L., & Jones, B. H. (1995). Friction blisters. Pathophysiology, prevention and treatment. *Sports Medicine, 20*(3), 136-147.

Kosiak, M. (1959). Etiology and pathology of ischemic ulcers. *Archives of physical medicine and rehabilitation, 40*(2), 62.

Kosiak, M. (1961). Etiology of decubitus ulcers. *Archives of physical medicine and rehabilitation, 42*, 19-29.

Landis, E. (1930). micro-injection studies of capillary blood pressure in human skin. *Heart: offical journal of the british cardiac society, 15*, 209.

Langer, K. (1978a). On the anatomy and physiology of the skin: I. The cleavability of the cutis. *British Journal of Plastic Surgery, 31*(1), 3-8. doi:10.1016/0007-1226(78)90003-6

Langer, K. (1978b). On the anatomy and physiology of the skin: III. The elasticity of the cutis. *British Journal of Plastic Surgery, 31*(3), 185-199. doi:10.1016/S0007-1226(78)90081-4

Lee, Y., & Hwang, K. (2002). Skin thickness of Korean adults. *Surgical and Radiologic Anatomy, 24*(3), 183-189. doi:10.1007/s00276-002-0034-5

Leung, I. P. H., Fleming, L., Walton, K., Barrans, S., & Ousey, K. (2017). Development of a model to demonstrate the effects of friction and pressure on skin in relation to pressure ulcer formation. *Wear, 376-377*, 266-271. doi:10.1016/j.wear.2016.11.026

Leung, I. P. H., Fleming, L. T., Walton, K., Barrans, S. M., & Ousey, K. (2019). Finite element analysis to model ischemia experienced in the development of device related pressure ulcers. *Proceedings of the Institution of Mechanical Engineers, Part H: Journal of Engineering in Medicine, 233*(7), 745-753. doi:10.1177/0954411919851387

Lévêque, J. L., & Audoly, B. (2013). Influence of Stratum Corneum on the entire skin mechanical properties, as predicted by a computational skin model. *Skin Research and Technology, 19*(1), 42-46. doi:10.1111/j.1600-0846.2012.00664.x

Levy, A., Kopplin, K., Gefen, A., & Bs. (2014). Computer simulations of efficacy of air-cell-based cushions in protecting against reoccurrence of pressure ulcers. *Journal of rehabilitation research and development, 51*(8), 1297-1310. doi:10.1682/JRRD.2014.02.0048

Liang, X., & Boppart, S. A. (2010). Biomechanical Properties of In Vivo Human Skin From Dynamic Optical Coherence Elastography. *IEEE Transactions on Biomedical Engineering, 57*(4), 953-959. doi:10.1109/TBME.2009.2033464

Linder-Ganz, E., Engelberg, S., Scheinowitz, M., & Gefen, A. (2006). Pressure–time cell death threshold for albino rat skeletal muscles as related to pressure sore biomechanics. *Journal of Biomechanics, 39*(14), 2725-2732. doi:10.1016/j.jbiomech.2005.08.010

Lowthian, P. (1987). The practical assessment of pressure sore risk. *Care Sci Pract, 5*(4), 3-7.

Luebberding, S., Krueger, N., & Kerscher, M. (2014). Mechanical properties of human skin in vivo: a comparative evaluation in 300 men and women. *Skin Research and Technology, 20*(2), 127-135. doi:10.1111/srt.12094

Lyder, C. H., Wang, Y., Metersky, M., Curry, M., Kliman, R., Verzier, N. R., & Hunt, D. R. (2012). Hospital-Acquired Pressure Ulcers: Results from the National Medicare Patient Safety Monitoring System Study. *Journal of the American Geriatrics Society, 60*(9), 1603-1608. doi:10.1111/j.1532-5415.2012.04106.x

Mailler, E. A., & Adams, B. B. (2004). The wear and tear of 26.2: Dermatological injuries reported on marathon day. *British Journal of Sports Medicine, 38*(4), 498-501. doi:10.1136/bjsm.2004.011874

Makhsous, M., Lim, D., Hendrix, R., Bankard, J., Rymer, W. Z., & Lin, F. (2007). Finite Element Analysis for Evaluation of Pressure Ulcer on the Buttock: Development

and Validation. *IEEE Transactions on Neural Systems and Rehabilitation Engineering, 15*(4), 517-525. doi:10.1109/TNSRE.2007.906967

Manorama, A. A., Baek, S., Vorro, J., Sikorskii, A., & Bush, T. R. (2010). Blood perfusion and transcutaneous oxygen level characterizations in human skin with changes in normal and shear loads — Implications for pressure ulcer formation. *Clinical Biomechanics, 25*(8), 823-828. doi:10.1016/j.clinbiomech.2010.06.003

Menon, G. K., Cleary, G. W., & Lane, M. E. (2012). The structure and function of the stratum corneum. *International Journal of Pharmaceutics, 435*(1), 3-9. doi:10.1016/j.ijpharm.2012.06.005

Millington, P. F., & Wilkinson, R. (2009). *Skin* (Vol. 9). Cambridge: Cambridge University Press.

Milward, P., Poole, M., & Skitt, T. (1993). Scoring pressure sore risk in the community. *Nursing Standard, 8*(7), 50-55. doi:10.7748/ns.8.7.50.s61

MXP, M. E. P. (2017, Jun 2017). Langer's Lines and Surgical Incisions. Retrieved from https://www.medicalexamprep.co.uk/langers-lines-surgical-incisions/

N.C. Petersen, & Bittmann, S. (1971). THe Epidemiology of Pressure Sores. *Scandinavian Journal of Plastic and Reconvstructive Surgery, 5*, 62-66.

Nagayama, K., & Honda, K. (2012). 3D Particle Simulations of Deformation of Red Blood Cells in Micro-Capillary Vessel. In: InTech U6 - institution=44HUD_INST&vid=44HUD_INST%3AServices&%3Fctx_ver=Z39.88-2004&ctx_enc=info%3Aofi%2Fenc%3AUTF-8&rfr_id=info%3Asid%2Fsummon.serialssolutions.com&rft_val_fmt=info%3Aofi%2Ffmt%3Akev%3Amtx%3Ajournal&rft.genre=article&rft.atitle=3D+Particle+Simulations+of+Deformation+of+Red+Blood+Cells+in+Micro-Capillary+Vessel&rft.au=Nagayama%2C+Katsuya&rft.au=Honda%2C+Keisuke&rft.date=2012-02-24&rft.pub=InTech&rft.externalDBID=n%2Fa&rft.externalDocID=oai%3Adnet%3Aintech_____%3A%3Ac90367479a2dcd39da80f57a5cc4691e&paramdict=en-US U7 - Publication.

Naylor, P. F. D. (1955). EXPERIMENTAL FRICTION BLISTERS. *British Journal of Dermatology, 67*(10), 327-342. doi:10.1111/j.1365-2133.1955.tb12657.x

Nguyen, K.-H., Chaboyer, W., & Whitty, J. A. (2015). Pressure injury in Australian public hospitals: a cost-of-illness study. *Australian health review : a publication of the Australian Hospital Association, 39*(3), 329-336. doi:10.1071/AH14088

NHS. (2016a, April 2016). Causes Acne. Retrieved from https://www.nhs.uk/conditions/acne/causes/

NHS. (2016b). Stop the pressure. Retrieved from http://nhs.stopthepressure.co.uk/

NHS. (2017, January 2017). Overview skin cancer (melanoma). Retrieved from https://www.nhs.uk/conditions/melanoma-skin-cancer/

NHS, N. H. S. (2016). What is the body mass index (BMI)? Retrieved from https://www.nhs.uk/common-health-questions/lifestyle/what-is-the-body-mass-index-bmi/

NHS_Improvement. (2018). *Pressure ulcers: revised definition and measurement Summary and recommendations*. Retrieved from London, UK: https://improvement.nhs.uk/documents/2932/NSTPP_summary__recommendations_20June2018.pdf

NICE, N. I. f. H. a. C. E. (2014). *Costing statement: Pressure ulcers Implementing the NICE guideline on pressure ulcers (CG179)*. Retrieved from https://www.nice.org.uk/guidance/cg179/resources/costing-statement-pdf-248688109

Norton, D. (1962). *An investigation of geriatric nursing problems in hospital*. England;United Kingdom; U6 - institution=44HUD_INST&vid=44HUD_INST%3AServices&%3Fctx_ver=Z39.88-2004&ctx_enc=info%3Aofi%2Fenc%3AUTF-8&rfr_id=info%3Asid%2Fsummon.serialssolutions.com&rft_val_fmt=info%3Aofi%2Ffmt%3Akev%3Amtx%3Abook&rft.genre=book&rft.title=An+investigation+of+geriatric+nursing+problems+in+hospital&rft.au=Norton%2C+Doreen&rft.date=1962&rft.externalDBID=n%2Fa&rft.externalDocID=uc1.b4338970&paramdict=en-US U7 - Book.

Norton, D. (1975). *An investigation of geriatric nursing problems in hospital*. Scotland;United Kingdom;.

Ousey, K. (2005). *Pressure area care*. Oxford: Blackwell.

Panzer, H. J. M. B. (2018). Skin mechanical properties and modeling: A review. *Proc IMechE Part H: J Engineering in Medicine, 232*(4), 323-343.

Pawlaczyk, M., Lelonkiewicz, M., & Wieczorowski, M. (2013). Age-dependent biomechanical properties of the skin. *Postepy Dermatologii i Alergologii, 30*(5), 302-306. doi:10.5114/pdia.2013.38359

Perimed. (2018). Laser Doppler Monitoring. Retrieved from https://www.perimed-instruments.com/laser-doppler-monitoring

Pinchcofsky-Devin, & Kaminski. (1986). Correlation of Pressure Sores and Nutritional Status. *Journal of the American Geriatrics Society, 34*(6), 435-440. doi:10.1111/j.1532-5415.1986.tb03411.x

Pritchard, V. (1986). Pressure sores. Calculating the risk. In (Vol. 82, pp. 59-61). England.

Redelings, M. D., Lee, N. E., & Sorvillo, F. (2005). Pressure ulcers: more lethal than we thought? *Advances in Skin & Wound Care, 18*(7), 367-372. doi:10.1097/00129334-200509000-00010

Reichel, S. M. (1958). SHEARING FORCE AS A FACTOR IN DECUBITUS ULCERS IN PARAPLEGICS. *Journal of the American Medical Association, 166*(7), 762-763. doi:10.1001/jama.1958.62990070004010a

Rendell, M. S., & Wells, J. M. (1998). Ischemic and pressure-induced hyperemia: A comparison. *Archives of physical medicine and rehabilitation, 79*(11), 1451-1455. doi:10.1016/S0003-9993(98)90243-X

Reswick, J. B., & Rogers, J. E. (1976). Experience at Rancho Los Amigos Hospital With Devices and Techniques to Prevent Pressure Sores. In R. M. Kenedi & J. M. Cowden (Eds.), *Bed Sore Biomechanics: Proceedings of a seminar on Tissue Viability and Clinical Applications organised in association with the Department of Biomedical Engineering, the Institute of Orthopaedics (University of London), Royal National Orthopaedic Hospital, Stanmore, London, and held at the University of Strathclyde, Glasgow, in August, 1975* (pp. 301-310). London: Macmillan Education UK.

Rovitto, M. (2016). Electromigration Reliability Issue in Interconnects for Three-Dimensional Integration Technologies. In.

Safety_Thermometer. (2018). *ST Nati Safe Harm Tab Jul 2017 Jul 2018*. Retrieved from

Saladin, K. (2007). *Human Anatomy 2007 Ed 2007 Edition*: Rex Bookstore, Inc.

Sandby-Moller, J., Poulsen, T., & Wulf, H. C. (2003). Epidermal Thickness at Different Body Sites: Relationship to Age, Gender, Pigmentation, Blood Content, Skin Type and Smoking Habits. *Acta Dermato-Venereologica, 83*(6), 410-413. doi:10.1080/00015550310015419

Sanders, R., & Sanders, R. (1973). Torsional elasticity of human skin in vivo. *Pflugers Archiv European Journal of Physiology, 342*(3), 255-260. doi:10.1007/BF00591373

Savonnet, L., Wang, X., & Duprey, S. (2018). Finite element models of the thigh-buttock complex for assessing static sitting discomfort and pressure sore risk: a literature review. *Computer Methods in Biomechanics and Biomedical Engineering, 21*(4), 379-388. doi:10.1080/10255842.2018.1466117

Schierling, R. (2018). FASCIAL ADHESIONS AND LANGER'S LINES OF CLEAVAGE. Retrieved from http://www.doctorschierling.com/blog/fascial-adhesions-and-langers-lines-of-cleavage

Schubert, V. (1991). Hypotension as risk factor for the development of pressure sores in elderly patients. *Age and Ageing, 20*, 255-261.

Sibbald, R. G., Krasner, D. L., & Lutz, J. (2010). SCALE: Skin Changes at Life's End. *Advances in Skin & Wound Care, 23*(5), 225-236. doi:10.1097/01.ASW.0000363537.75328.36

stress relaxation. (2013). In.

Sugama, J. (2008). The prevalence rate, site and severity of pressure ulcers by care settings. *Japanese Journal of Pressure Ulcers, 10*, 153-161.

Sulzberger, M. B., Cortese, T. A., Fishman, L., & Wiley, H. S. (1966). Studies on blisters produced by friction. I. Results of linear rubbing and twisting technics. *Journal of Investigative Dermatology, 47*(5), 456-465 contd.

Szczerba, D., & Székely, G. (2005, 2005). *A computational model of micro-vascular growth*.

Tekscan. *I-Scan Product Selection Guide*. Retrieved from https://www.tekscan.com/sites/default/files/IDL-IScan-SelectionGuide_RevE.pdf

Tekscan. (2015). Pressure Mapping Sensor 5051 (Datasheet).

Tekscan. (2016). *Pressure Mapping Sensor 5330 (Datasheet)*. Retrieved from https://www.tekscan.com/products-solutions/pressure-mapping-sensors/5330?tab=specifications

Thomas, D. R., Goode, P. S., Tarquine, P. H., & Allman, R. M. (1996). Hospital-Acquired Pressure Ulcers and Risk of Death. *Journal of the American Geriatrics Society, 44*(12), 1435-1440. doi:10.1111/j.1532-5415.1996.tb04067.x

Torrance, C. (1983). *Pressure sores: aetiology, treatment and prevention*. London: Croom Helm.

Turner, M. J., Clough, R. W., Martin, H. C., & Topp, L. J. (1956). Stiffness and Deflection Analysis of Complex Structures. *Journal of the Aeronautical Sciences, 23*(9), 805-823. doi:10.2514/8.3664

Versluysen, M. (1986). How elderly patients with femoral fracture develop pressure sores in hospital. *British Medical Journal (Clinical research ed.), 292*(6531), 1311-1313. doi:10.1136/bmj.292.6531.1311

Vilhena, L., & Ramalho, A. (2016). Friction of Human Skin against Different Fabrics for Medical Use. *Lubricants, 4*(1), 6. doi:10.3390/lubricants4010006

Vogel, H. G. (1976). Tensile strength, relaxation and mechanical recovery in rat skin as influenced by maturation and age. *Journal of Medicine, 7*(2), 177-188.

Wang, Y., Marshall, K. L., Baba, Y., Gerling, G. J., & Lumpkin, E. A. (2013). Hyperelastic Material Properties of Mouse Skin under Compression. *PLoS ONE, 8*(6), e67439. doi:10.1371/journal.pone.0067439

Waterlow, J. (1985). Pressure sores: a risk assessment card. In (Vol. 81, pp. 49-55). England.

Woodbury, M. G., & Houghton, P. E. (2004). Prevalence of pressure ulcers in Canadian healthcare settings. *Ostomy/wound management, 50*(10), 22-38.

Wounds_International. (2010). *International review. Pressure ulcer prevention: pressure, shear, friction and microclimate in context. A consensus document.* Retrieved from London:

Xakellis, G. C., & Frantz, R. A. (1996). The cost-effectiveness of interventions for preventing pressure ulcers. *Journal of the American Board of Family Practice, 9*(2), 79-85.

Xing, M., Pan, N., Zhong, W., & Maibach, H. (2007). Skin friction blistering: computer model. *Skin Research and Technology, 13*(3), 310-316. doi:10.1111/j.1600-0846.2007.00230.x

Yen, A., & Braverman, I. (1976). Ultrastructure of the human dermal microcirculation: the horizontal plexus of the papillary dermis. *The Journal of Investigative Dermatology, 66*(3), 131-142.

Appendix I

Results of Pressure Only Simulation

New Node no.	Ori. X	Ori. Y	Ori. Z	Def. X	Def. Y	Def. Z	Ori. Dia.	Def. Dia.	Ori. Area	Def. Area	%Change
86	295.4423	3165.5	52.09445	296.553	3.15E+03	52.3009	15	14.62	176.7146	171.3967	-3.00932
84	295.4423	3150.5	52.09445	296.554	3.13E+03	52.2926					
85	288.0563	3158	50.79209	289.199	3.14E+03	51.0144	15	14.92674			
87	302.8284	3158	53.39682	303.902	3.14E+03	53.5891					
91	212.132	3165.5	212.132	212.925	3.15E+03	212.921	15	14.72001	176.7146	172.7442	-2.24679
89	212.132	3150.5	212.132	212.933	3.13E+03	212.936					
90	206.8287	3158	206.8287	207.637	3.14E+03	207.633	15	14.94189			
88	217.4353	3158	217.4353	218.201	3.14E+03	218.2					
164	52.09445	3165.5	295.4423	52.2795	3.15E+03	296.558	15	14.71001	176.7146	172.6285	-2.31224
162	52.09445	3150.5	295.4423	52.2784	3.13E+03	296.545					
163	50.79209	3158	288.0563	50.9821	3.14E+03	289.189	15	14.94204			
161	53.39682	3158	302.8284	53.5826	3.14E+03	303.903					
94	295.4423	1960.5	52.09445	296.513	1.95E+03	52.279	15	14.72001	176.7146	173.0918	-2.05007
92	295.4423	1945.5	52.09445	296.528	1.94E+03	52.2803					
93	288.0563	1953	50.79209	289.148	1.95E+03	50.9838	15	14.97196			
95	302.8284	1953	53.39682	303.893	1.95E+03	53.5808					

99	212.132	1960.5	212.132	212.914	1.95E+03	212.911	15	14.7	176.7146	172.5829	-2.33808
97	212.132	1945.5	212.132	212.907	1.94E+03	212.915					
98	206.8287	1953	206.8287	207.633	1.95E+03	207.623	15	14.94825			
96	217.4353	1953	217.4353	218.199	1.95E+03	218.197					
160	52.09445	1960.5	295.4423	52.2856	1.95E+03	296.537	15	14.73001	176.7146	172.9325	-2.14022
158	52.09445	1945.5	295.4423	52.2819	1.94E+03	296.519					
159	50.79209	1953	288.0563	50.985	1.95E+03	289.17	15	14.94802			
157	53.39682	1953	302.8284	53.5802	1.95E+03	303.891					
110	295.4423	1750.5	52.09445	296.428	1.74E+03	52.2486	15	13.90003	176.7146	154.1723	-12.7563
108	295.4423	1735.5	52.09445	296.432	1.73E+03	52.2777					
109	288.0563	1743	50.79209	289.456	1.74E+03	51.0079	15	14.12215			
111	302.8284	1743	53.39682	303.357	1.74E+03	53.4908					
115	212.132	1750.5	212.132	212.879	1.74E+03	212.876	15	13.90035	176.7146	155.3679	-12.0798
113	212.132	1735.5	212.132	212.787	1.73E+03	212.841					
114	206.8287	1743	206.8287	207.808	1.74E+03	207.788	15	14.23134			
112	217.4353	1743	217.4353	217.909	1.74E+03	217.813					
172	52.09445	1750.5	295.4423	52.2555	1.74E+03	296.483	15	13.99046	176.7146	156.3546	-11.5214
170	52.09445	1735.5	295.4423	52.2732	1.73E+03	296.371					
171	50.79209	1743	288.0563	50.986	1.74E+03	289.378	15	14.22947			
169	53.39682	1743	302.8284	53.4698	1.74E+03	303.389					
156	295.4423	1550.5	52.09445	296.192	1.55E+03	52.2367	15	13.90055	176.7146	153.463	-13.1577
154	295.4423	1535.5	52.09445	296.315	1.53E+03	52.2505					
153	288.0563	1543	50.79209	289.368	1.54E+03	50.9734	15	14.05665			

155	302.8284	1543	53.39682	303.21	1.54E+03	53.4185				
150	212.132	1550.5	212.132	212.764	1.55E+03	212.74	15	13.86005	176.7146	153.9542	-12.8797
152	212.132	1535.5	212.132	212.727	1.53E+03	212.746				
149	206.8287	1543	206.8287	207.769	1.54E+03	207.733	15	14.14285		
151	217.4353	1543	217.4353	217.776	1.54E+03	217.727				
190	52.09445	1550.5	295.4423	52.2267	1.55E+03	296.297	15	13.95019	176.7146	156.1031	-11.6637
192	52.09445	1535.5	295.4423	52.1965	1.53E+03	296.23				
189	50.79209	1543	288.0563	50.9885	1.54E+03	289.291	15	14.24759		
191	53.39682	1543	302.8284	53.4783	1.54E+03	303.319				
118	295.4423	1350.5	52.09445	296.084	1.35E+03	52.173	15	13.86037	176.7146	153.718	-13.0134
116	295.4423	1335.5	52.09445	296.182	1.33E+03	52.1995				
117	288.0563	1343	50.79209	289.221	1.34E+03	50.9312	15	14.12082		
119	302.8284	1343	53.39682	303.126	1.34E+03	53.3881				
123	212.132	1350.5	212.132	212.615	1.35E+03	212.636	15	13.84001	176.7146	153.0014	-13.4189
121	212.132	1335.5	212.132	212.632	1.33E+03	212.628				
122	206.8287	1343	206.8287	207.673	1.34E+03	207.682	15	14.07567		
120	217.4353	1343	217.4353	217.63	1.34E+03	217.631				
176	52.09445	1350.5	295.4423	52.1772	1.35E+03	296.161	15	13.96042	176.7146	156.4094	-11.4904
174	52.09445	1335.5	295.4423	52.2605	1.33E+03	296.091				
175	50.79209	1343	288.0563	50.9773	1.34E+03	289.142	15	14.26509		
173	53.39682	1343	302.8284	53.4435	1.34E+03	303.192				
142	295.4423	1250.5	52.09445	296.044	1.25E+03	52.1684	15	13.97026	176.7146	153.7467	-12.9972
140	295.4423	1235.5	52.09445	296.115	1.23E+03	52.1214				

141	288.0563	1243	50.79209	289.217	1.24E+03	50.9609	15	14.01237			
143	302.8284	1243	53.39682	303.017	1.24E+03	53.3902					
147	212.132	1250.5	212.132	212.564	1.25E+03	212.528	15	13.97007	176.7146	155.6276	-11.9328
145	212.132	1235.5	212.132	212.555	1.23E+03	212.571					
146	206.8287	1243	206.8287	207.581	1.24E+03	207.598	15	14.18398			
144	217.4353	1243	217.4353	217.614	1.24E+03	217.624					
188	52.09445	1250.5	295.4423	52.1921	1.25E+03	296.063	15	13.97008	176.7146	154.9031	-12.3428
186	52.09445	1235.5	295.4423	52.1536	1.23E+03	296.034					
187	50.79209	1243	288.0563	50.9305	1.24E+03	289.136	15	14.11794			
185	53.39682	1243	302.8284	53.4118	1.24E+03	303.034					
134	295.4423	1150.5	52.09445	295.964	1.15E+03	52.1935	15	13.95032	176.7146	154.6685	-12.4755
132	295.4423	1135.5	52.09445	296.058	1.13E+03	52.191					
133	288.0563	1143	50.79209	289.092	1.14E+03	50.8996	15	14.11653			
135	302.8284	1143	53.39682	302.985	1.14E+03	53.3984					
139	212.132	1150.5	212.132	212.546	1.15E+03	212.541	15	14.00001	176.7146	156.4497	-11.4676
137	212.132	1135.5	212.132	212.562	1.13E+03	212.549					
138	206.8287	1143	206.8287	207.553	1.14E+03	207.553	15	14.22842			
136	217.4353	1143	217.4353	217.615	1.14E+03	217.613					
184	52.09445	1150.5	295.4423	52.1312	1.15E+03	296.071	15	14.1302	176.7146	156.6709	-11.3424
182	52.09445	1135.5	295.4423	52.1283	1.13E+03	295.996					
183	50.79209	1143	288.0563	51.0014	1.14E+03	289.124	15	14.11725			
181	53.39682	1143	302.8284	53.4102	1.14E+03	303.034					
102	295.4423	850.5	52.09445	295.828	848.63	52.134	15	14.05739	176.7146	155.7043	-11.8894

100	295.4423	835.5	52.09445	295.928	834.573	52.163				
101	288.0563	843	50.79209	288.95	841.615	50.9419	15	14.10283		
103	302.8284	843	53.39682	302.833	841.696	53.4209				
107	212.132	850.5	212.132	212.463	848.668	212.451	15	13.98402	176.7146	154.8886	-12.351
105	212.132	835.5	212.132	212.47	834.684	212.473				
106	206.8287	843	206.8287	207.493	841.648	207.467	15	14.10255		
104	217.4353	843	217.4353	217.454	841.641	217.45				
168	52.09445	850.5	295.4423	52.1222	848.632	295.941	15	13.99317	176.7146	155.7541	-11.8612
166	52.09445	835.5	295.4423	52.1553	834.639	295.881				
167	50.79209	843	288.0563	50.8928	841.672	288.93	15	14.17208		
165	53.39682	843	302.8284	53.3733	841.579	302.883				
126	295.4423	550.5	52.09445	295.721	549.279	52.1038	15	13.68329	176.7146	150.5069	-14.8305
124	295.4423	535.5	52.09445	295.792	535.596	52.1573				
125	288.0563	543	50.79209	288.857	542.563	50.9228	15	14.00477		
127	302.8284	543	53.39682	302.653	542.425	53.328				
131	212.132	550.5	212.132	212.443	549.306	212.416	15	13.82911	176.7146	150.8693	-14.6255
129	212.132	535.5	212.132	212.315	535.478	212.296				
130	206.8287	543	206.8287	207.435	542.43	207.462	15	13.89046		
128	217.4353	543	217.4353	217.267	542.394	217.274				
180	52.09445	550.5	295.4423	52.1215	549.338	295.771	15	13.827	176.7146	151.1706	-14.455
178	52.09445	535.5	295.4423	52.1324	535.511	295.771				
179	50.79209	543	288.0563	50.9234	542.316	288.911	15	13.92032		
177	53.39682	543	302.8284	53.339	542.492	302.619				

Results of Friction Only Simulation

New Node no.	Ori. X	Ori. Y	Ori. Z	Def. X	Def. Y	Def. Z	Ori. Dia.	Def. Dia.	Ori. Area	Def. Area	%Change
86	295.4423	3165.5	52.09445	301.39	3.13E+03	53.1686	15	14.60125	176.7146	181.8911	2.929294
84	295.4423	3150.5	52.09445	301.201	3.12E+03	53.142					
85	288.0563	3158	50.79209	293.483	3.13E+03	51.748	15	15.86104			
87	302.8284	3158	53.39682	309.1	3.13E+03	54.5196					
91	212.132	3165.5	212.132	216.422	3.13E+03	216.403	15	14.46164	176.7146	179.9603	1.836675
89	212.132	3150.5	212.132	216.266	3.12E+03	216.251					
90	206.8287	3158	206.8287	210.759	3.13E+03	210.729	15	15.84416			
88	217.4353	3158	217.4353	221.954	3.13E+03	221.941					
164	52.09445	3165.5	295.4423	53.1461	3.13E+03	301.354	15	14.45073	176.7146	179.5927	1.628672
162	52.09445	3150.5	295.4423	53.1525	3.12E+03	301.209					
163	50.79209	3158	288.0563	51.7783	3.13E+03	293.501	15	15.82374			
161	53.39682	3158	302.8284	54.5109	3.13E+03	309.087					
94	295.4423	1960.5	52.09445	297.558	1.95E+03	52.4833	15	14.86007	176.7146	179.0438	1.318047
92	295.4423	1945.5	52.09445	297.512	1.94E+03	52.478					
93	288.0563	1953	50.79209	289.979	1.95E+03	51.1442	15	15.34081			
95	302.8284	1953	53.39682	305.087	1.95E+03	53.8064					
99	212.132	1960.5	212.132	213.641	1.95E+03	213.649	15	14.89003	176.7146	179.5861	1.624915
97	212.132	1945.5	212.132	213.633	1.94E+03	213.62					

98	206.8287	1953	206.8287	208.196	1.95E+03	208.211	15	15.35632			
96	217.4353	1953	217.4353	219.056	1.95E+03	219.068					
160	52.09445	1960.5	295.4423	52.4758	1.95E+03	297.537	15	14.86	176.7146	179.2214	1.418563
158	52.09445	1945.5	295.4423	52.4826	1.94E+03	297.532					
159	50.79209	1953	288.0563	51.154	1.95E+03	289.965	15	15.35611			
157	53.39682	1953	302.8284	53.8081	1.95E+03	305.09					
110	295.4423	1750.5	52.09445	297.015	1.75E+03	52.3895	15	15.26013	176.7146	187.2482	5.960811
108	295.4423	1735.5	52.09445	296.959	1.73E+03	52.3628					
109	288.0563	1743	50.79209	289.299	1.74E+03	51.0342	15	15.62319			
111	302.8284	1743	53.39682	304.687	1.74E+03	53.7326					
115	212.132	1750.5	212.132	213.239	1.75E+03	213.244	15	15.25001	176.7146	186.434	5.500072
113	212.132	1735.5	212.132	213.25	1.73E+03	213.226					
114	206.8287	1743	206.8287	207.734	1.74E+03	207.748	15	15.56557			
112	217.4353	1743	217.4353	218.725	1.74E+03	218.77					
172	52.09445	1750.5	295.4423	52.3857	1.75E+03	296.985	15	15.21001	176.7146	185.9636	5.233868
170	52.09445	1735.5	295.4423	52.3683	1.73E+03	296.996					
171	50.79209	1743	288.0563	51.0459	1.74E+03	289.337	15	15.56713			
169	53.39682	1743	302.8284	53.7413	1.74E+03	304.669					
156	295.4423	1550.5	52.09445	296.591	1.55E+03	52.297	15	15.31038	176.7146	187.4776	6.090628
154	295.4423	1535.5	52.09445	296.484	1.53E+03	52.2828					
153	288.0563	1543	50.79209	288.837	1.54E+03	50.9613	15	15.59098			
155	302.8284	1543	53.39682	304.192	1.54E+03	53.663					
150	212.132	1550.5	212.132	212.912	1.55E+03	212.921	15	15.32004	176.7146	187.0601	5.854342

152	212.132	1535.5	212.132	212.897	1.53E+03	212.89				
149	206.8287	1543	206.8287	207.388	1.54E+03	207.408	15	15.54645		
151	217.4353	1543	217.4353	218.377	1.54E+03	218.405				
190	52.09445	1550.5	295.4423	52.3012	1.55E+03	296.533	15	15.29	176.7146	186.2076	5.371939
192	52.09445	1535.5	295.4423	52.3074	1.53E+03	296.529				
189	50.79209	1543	288.0563	50.9512	1.54E+03	288.867	15	15.50601		
191	53.39682	1543	302.8284	53.6346	1.54E+03	304.139				
118	295.4423	1350.5	52.09445	296.201	1.35E+03	52.2485	15	15.37024	176.7146	187.2424	5.957517
116	295.4423	1335.5	52.09445	296.117	1.33E+03	52.2299				
117	288.0563	1343	50.79209	288.499	1.34E+03	50.9078	15	15.51078		
119	302.8284	1343	53.39682	303.775	1.34E+03	53.5954				
123	212.132	1350.5	212.132	212.664	1.35E+03	212.653	15	15.38005	176.7146	187.6475	6.186788
121	212.132	1335.5	212.132	212.631	1.33E+03	212.635				
122	206.8287	1343	206.8287	207.139	1.34E+03	207.138	15	15.53443		
120	217.4353	1343	217.4353	218.123	1.34E+03	218.123				
176	52.09445	1350.5	295.4423	52.2457	1.35E+03	296.161	15	15.34007	176.7146	186.1784	5.355401
174	52.09445	1335.5	295.4423	52.2008	1.33E+03	296.16				
175	50.79209	1343	288.0563	50.885	1.34E+03	288.527	15	15.45297		
173	53.39682	1343	302.8284	53.5694	1.34E+03	303.745				
142	295.4423	1250.5	52.09445	296.024	1.25E+03	52.2162	15	15.37015	176.7146	187.6332	6.178696
140	295.4423	1235.5	52.09445	295.958	1.24E+03	52.2312				
141	288.0563	1243	50.79209	288.313	1.24E+03	50.858	15	15.54325		
143	302.8284	1243	53.39682	303.62	1.24E+03	53.5574				

147	212.132	1250.5	212.132	212.548	1.25E+03	212.565	15	15.36006	176.7146	186.6275	5.609579
145	212.132	1235.5	212.132	212.532	1.24E+03	212.526					
146	206.8287	1243	206.8287	207.048	1.24E+03	207.04	15	15.4701			
144	217.4353	1243	217.4353	217.985	1.24E+03	217.981					
188	52.09445	1250.5	295.4423	52.2046	1.25E+03	296.009	15	15.35001	176.7146	186.7592	5.684069
186	52.09445	1235.5	295.4423	52.2175	1.24E+03	295.998					
187	50.79209	1243	288.0563	50.871	1.24E+03	288.352	15	15.49114			
185	53.39682	1243	302.8284	53.5484	1.24E+03	303.61					
134	295.4423	1150.5	52.09445	295.886	1.15E+03	52.1725	15	15.38019	176.7146	186.8615	5.741971
132	295.4423	1135.5	52.09445	295.81	1.14E+03	52.1703					
133	288.0563	1143	50.79209	288.211	1.14E+03	50.8553	15	15.46921			
135	302.8284	1143	53.39682	303.449	1.14E+03	53.5192					
139	212.132	1150.5	212.132	212.432	1.15E+03	212.433	15	15.35005	176.7146	185.8324	5.159604
137	212.132	1135.5	212.132	212.401	1.14E+03	212.409					
138	206.8287	1143	206.8287	206.954	1.14E+03	206.952	15	15.41422			
136	217.4353	1143	217.4353	217.851	1.14E+03	217.854					
184	52.09445	1150.5	295.4423	52.1988	1.15E+03	295.832	15	15.3	176.7146	185.7725	5.125747
182	52.09445	1135.5	295.4423	52.1974	1.14E+03	295.841					
183	50.79209	1143	288.0563	50.815	1.14E+03	288.206	15	15.45967			
181	53.39682	1143	302.8284	53.5152	1.14E+03	303.428					
102	295.4423	850.5	52.09445	295.527	851.288	52.1236	15	15.38214	176.7146	186.1829	5.357983
100	295.4423	835.5	52.09445	295.463	835.906	52.1082					
101	288.0563	843	50.79209	287.897	843.597	50.7706	15	15.41108			

103	302.8284	843	53.39682	303.076	843.552	53.4347					
107	212.132	850.5	212.132	212.168	851.269	212.172	15	15.40602	176.7146	186.4757	5.523674
105	212.132	835.5	212.132	212.154	835.863	212.15					
106	206.8287	843	206.8287	206.705	843.581	206.716	15	15.41139			
104	217.4353	843	217.4353	217.607	843.579	217.609					
168	52.09445	850.5	295.4423	52.1296	851.286	295.475	15	15.40501	176.7146	186.1275	5.326634
166	52.09445	835.5	295.4423	52.1141	835.881	295.485					
167	50.79209	843	288.0563	50.7908	843.567	287.904	15	15.38363			
165	53.39682	843	302.8284	53.4557	843.605	303.055					
126	295.4423	550.5	52.09445	295.315	551.234	52.0899	15	15.56107	176.7146	188.6669	6.763614
124	295.4423	535.5	52.09445	295.277	535.673	52.0643					
125	288.0563	543	50.79209	287.698	543.401	50.7356	15	15.43712			
127	302.8284	543	53.39682	302.899	543.457	53.4247					
131	212.132	550.5	212.132	211.992	551.224	212.004	15	15.50217	176.7146	188.4402	6.635357
129	212.132	535.5	212.132	212.046	535.722	212.053					
130	206.8287	543	206.8287	206.561	543.46	206.55	15	15.47716			
128	217.4353	543	217.4353	217.501	543.471	217.498					
180	52.09445	550.5	295.4423	52.0839	551.211	295.295	15	15.50301	176.7146	188.3025	6.557395
178	52.09445	535.5	295.4423	52.0734	535.708	295.285					
179	50.79209	543	288.0563	50.7353	543.512	287.68	15	15.46501			
177	53.39682	543	302.8284	53.4198	543.428	302.91					

Results of Pressure with Friction Simulation

New Node no.	Ori. X	Ori. Y	Ori. Z	Def. X	Def. Y	Def. Z	Ori. Dia.	Def. Dia.	Ori. Area	Def. Area	%Change
86	295.4423	3165.5	52.09445	302.73	3.11E+03	53.4145	15	14.2113	176.7146	176.4529	-0.14809
84	295.4423	3150.5	52.09445	302.541	3.10E+03	53.3802					
85	288.0563	3158	50.79209	294.844	3.11E+03	52.0083	15	15.80903			
87	302.8284	3158	53.39682	310.413	3.11E+03	54.7526					
91	212.132	3165.5	212.132	217.381	3.11E+03	217.355	15	14.16146	176.7146	175.8236	-0.50419
89	212.132	3150.5	212.132	217.232	3.10E+03	217.217					
90	206.8287	3158	206.8287	211.725	3.11E+03	211.688	15	15.80809			
88	217.4353	3158	217.4353	222.892	3.11E+03	222.877					
164	52.09445	3165.5	295.4423	53.371	3.11E+03	302.699	15	14.14092	176.7146	175.3141	-0.7925
162	52.09445	3150.5	295.4423	53.3766	3.10E+03	302.538					
163	50.79209	3158	288.0563	52.0065	3.11E+03	294.852	15	15.78518			
161	53.39682	3158	302.8284	54.7382	3.11E+03	310.399					
94	295.4423	1960.5	52.09445	298.815	1.95E+03	52.7011	15	14.57003	176.7146	175.4611	-0.70931
92	295.4423	1945.5	52.09445	298.784	1.93E+03	52.6971					
93	288.0563	1953	50.79209	291.247	1.94E+03	51.3673	15	15.33312			
95	302.8284	1953	53.39682	306.348	1.94E+03	54.0251					
99	212.132	1960.5	212.132	214.556	1.95E+03	214.561	15	14.58003	176.7146	175.4984	-0.68822
97	212.132	1945.5	212.132	214.541	1.93E+03	214.536					

98	206.8287	1953	206.8287	209.126	1.94E+03	209.131	15	15.32586			
96	217.4353	1953	217.4353	219.961	1.94E+03	219.97					
160	52.09445	1960.5	295.4423	52.7001	1.95E+03	298.818	15	14.58002	176.7146	175.4925	-0.69156
158	52.09445	1945.5	295.4423	52.7036	1.93E+03	298.795					
159	50.79209	1953	288.0563	51.3792	1.94E+03	291.255	15	15.32536			
157	53.39682	1953	302.8284	54.0263	1.94E+03	306.35					
110	295.4423	1750.5	52.09445	298.166	1.74E+03	52.5679	15	14.07008	176.7146	162.3627	-8.12153
108	295.4423	1735.5	52.09445	298.119	1.73E+03	52.5746					
109	288.0563	1743	50.79209	290.894	1.73E+03	51.2764	15	14.69264			
111	302.8284	1743	53.39682	305.36	1.73E+03	53.8455					
115	212.132	1750.5	212.132	214.111	1.74E+03	214.11	15	14.08036	176.7146	163.1737	-7.66257
113	212.132	1735.5	212.132	214.024	1.73E+03	214.058					
114	206.8287	1743	206.8287	208.848	1.73E+03	208.842	15	14.75524			
112	217.4353	1743	217.4353	219.307	1.73E+03	219.25					
172	52.09445	1750.5	295.4423	52.574	1.74E+03	298.2	15	14.12044	176.7146	163.6277	-7.40564
170	52.09445	1735.5	295.4423	52.5718	1.73E+03	298.088					
171	50.79209	1743	288.0563	51.2655	1.73E+03	290.849	15	14.7543			
169	53.39682	1743	302.8284	53.8339	1.73E+03	305.378					
156	295.4423	1550.5	52.09445	297.471	1.54E+03	52.4602	15	14.12003	176.7146	161.7894	-8.44592
154	295.4423	1535.5	52.09445	297.502	1.53E+03	52.4608					
153	288.0563	1543	50.79209	290.323	1.54E+03	51.1652	15	14.58896			
155	302.8284	1543	53.39682	304.69	1.54E+03	53.6999					
150	212.132	1550.5	212.132	213.647	1.54E+03	213.632	15	14.11013	176.7146	162.2018	-8.21257

152	212.132	1535.5	212.132	213.592	1.53E+03	213.608				
149	206.8287	1543	206.8287	208.454	1.54E+03	208.435	15	14.63642		
151	217.4353	1543	217.4353	218.807	1.54E+03	218.781				
190	52.09445	1550.5	295.4423	52.4543	1.54E+03	297.536	15	14.16026	176.7146	163.4633	-7.49872
192	52.09445	1535.5	295.4423	52.4299	1.53E+03	297.453				
189	50.79209	1543	288.0563	51.1734	1.54E+03	290.276	15	14.69802		
191	53.39682	1543	302.8284	53.7345	1.54E+03	304.749				
118	295.4423	1350.5	52.09445	296.957	1.35E+03	52.3429	15	14.15003	176.7146	162.0055	-8.32365
116	295.4423	1335.5	52.09445	296.987	1.33E+03	52.3524				
117	288.0563	1343	50.79209	289.818	1.34E+03	51.0655	15	14.57748		
119	302.8284	1343	53.39682	304.174	1.34E+03	53.5962				
123	212.132	1350.5	212.132	213.235	1.35E+03	213.246	15	14.14003	176.7146	161.6267	-8.53801
121	212.132	1335.5	212.132	213.222	1.33E+03	213.218				
122	206.8287	1343	206.8287	208.095	1.34E+03	208.103	15	14.55368		
120	217.4353	1343	217.4353	218.39	1.34E+03	218.39				
176	52.09445	1350.5	295.4423	52.3459	1.35E+03	297.005	15	14.20027	176.7146	163.5407	-7.45492
174	52.09445	1335.5	295.4423	52.3897	1.33E+03	296.93				
175	50.79209	1343	288.0563	51.0922	1.34E+03	289.77	15	14.66356		
173	53.39682	1343	302.8284	53.6309	1.34E+03	304.212				
142	295.4423	1250.5	52.09445	296.73	1.25E+03	52.3042	15	14.23005	176.7146	161.8866	-8.39093
140	295.4423	1235.5	52.09445	296.747	1.23E+03	52.272				
141	288.0563	1243	50.79209	289.626	1.24E+03	51.049	15	14.48487		
143	302.8284	1243	53.39682	303.891	1.24E+03	53.5629				

147	212.132	1250.5	212.132	213.057	1.25E+03	213.037	15	14.23002	176.7146	163.0668	-7.72308
145	212.132	1235.5	212.132	213.033	1.23E+03	213.041					
146	206.8287	1243	206.8287	207.908	1.24E+03	207.917	15	14.5905			
144	217.4353	1243	217.4353	218.226	1.24E+03	218.233					
188	52.09445	1250.5	295.4423	52.3176	1.25E+03	296.743	15	14.2401	176.7146	162.7119	-7.9239
186	52.09445	1235.5	295.4423	52.2897	1.23E+03	296.697					
187	50.79209	1243	288.0563	51.03	1.24E+03	289.577	15	14.54844			
185	53.39682	1243	302.8284	53.5751	1.24E+03	303.901					
134	295.4423	1150.5	52.09445	296.504	1.15E+03	52.2869	15	14.25003	176.7146	162.5177	-8.0338
132	295.4423	1135.5	52.09445	296.531	1.13E+03	52.2798					
133	288.0563	1143	50.79209	289.386	1.14E+03	50.9813	15	14.52095			
135	302.8284	1143	53.39682	303.681	1.14E+03	53.532					
139	212.132	1150.5	212.132	212.917	1.15E+03	212.915	15	14.29001	176.7146	163.8251	-7.29397
137	212.132	1135.5	212.132	212.908	1.13E+03	212.899					
138	206.8287	1143	206.8287	207.768	1.14E+03	207.769	15	14.59681			
136	217.4353	1143	217.4353	218.091	1.14E+03	218.089					
184	52.09445	1150.5	295.4423	52.2478	1.15E+03	296.569	15	14.3502	176.7146	163.6963	-7.36682
182	52.09445	1135.5	295.4423	52.2404	1.13E+03	296.494					
183	50.79209	1143	288.0563	51.0419	1.14E+03	289.403	15	14.52417			
181	53.39682	1143	302.8284	53.5379	1.14E+03	303.711					
102	295.4423	850.5	52.09445	295.982	849.15	52.1732	15	14.37108	176.7146	163.2373	-7.62661
100	295.4423	835.5	52.09445	296.029	834.779	52.1879					
101	288.0563	843	50.79209	288.893	841.973	50.9349	15	14.46238			

103	302.8284	843	53.39682	303.132	842.022	53.4665				
107	212.132	850.5	212.132	212.554	849.172	212.547	15	14.326	176.7146	162.7181	-7.92039
105	212.132	835.5	212.132	212.546	834.846	212.549				
106	206.8287	843	206.8287	207.444	841.994	207.428	15	14.46175		
104	217.4353	843	217.4353	217.663	841.985	217.661				
168	52.09445	850.5	295.4423	52.1656	849.149	296.053	15	14.33211	176.7146	163.2819	-7.60135
166	52.09445	835.5	295.4423	52.1817	834.817	295.999				
167	50.79209	843	288.0563	50.9049	842.01	288.88	15	14.50568		
165	53.39682	843	302.8284	53.436	841.946	303.163				
126	295.4423	550.5	52.09445	295.646	549.877	52.1043	15	14.16509	176.7146	159.8782	-9.52747
124	295.4423	535.5	52.09445	295.685	535.712	52.1363				
125	288.0563	543	50.79209	288.586	542.876	50.877	15	14.37077		
127	302.8284	543	53.39682	302.741	542.784	53.3562				
131	212.132	550.5	212.132	212.348	549.893	212.33	15	14.2545	176.7146	160.1329	-9.38334
129	212.132	535.5	212.132	212.261	535.639	212.249				
130	206.8287	543	206.8287	207.227	542.791	207.243	15	14.30338		
128	217.4353	543	217.4353	217.347	542.765	217.351				
180	52.09445	550.5	295.4423	52.1153	549.913	295.675	15	14.254	176.7146	160.3339	-9.26958
178	52.09445	535.5	295.4423	52.1227	535.659	295.671				
179	50.79209	543	288.0563	50.8783	542.717	288.616	15	14.32183		
177	53.39682	543	302.8284	53.3643	542.826	302.72				

Appendix II

Percentage Change of the Cross-sectional Area of the Cutaneous Blood Vessels

	23mmHg	46mmHg	92mmHg	137mmHg
Average Dermis	-1.205	-2.384	-4.698	-6.954
Average Hypodermis	-6.146	-11.718	-21.398	-29.507
Average All	-5.048	-9.644	-17.687	-24.495
A1	-1.219	-2.426	-4.743	-7.011
B1	-1.197	-2.389	-4.739	-6.972
C1	-1.196	-2.386	-4.657	-6.883
D1	-1.203	-2.394	-4.679	-6.978
E1	-1.230	-2.373	-4.763	-7.039
F1	-1.207	-2.397	-4.744	-6.991
A2	-1.198	-2.383	-4.654	-6.875
B2	-1.196	-2.381	-4.648	-6.932
C2	-1.194	-2.369	-4.607	-6.874
D2	-1.209	-2.406	-4.686	-6.982
E2	-1.219	-2.413	-4.782	-7.035
F2	-1.189	-2.293	-4.672	-6.870
A3	-6.028	-11.466	-20.931	-28.831
B3	-5.938	-11.390	-20.924	-28.952
C3	-6.332	-12.079	-22.114	-30.513
D3	-6.177	-11.816	-21.470	-29.545
E3	-5.943	-11.324	-20.841	-28.783
F3	-6.090	-11.654	-21.200	-29.212
A4	-6.316	-12.042	-22.044	-30.422
B4	-6.066	-11.639	-21.286	-29.533
C4	-6.114	-11.580	-21.105	-29.110
D4	-6.323	-12.044	-21.974	-30.271
E4	-6.026	-11.557	-21.089	-29.236
F4	-6.256	-11.863	-21.657	-29.969
A5	-6.148	-11.773	-21.565	-29.656
B5	-5.955	-11.473	-20.978	-28.905
C5	-6.119	-11.709	-21.258	-29.237

D5	-6.114	-11.693	-21.341	-29.403
E5	-6.043	-11.509	-21.131	-29.217
F5	-6.020	-11.454	-20.914	-28.767
A6	-6.345	-12.016	-21.946	-30.265
B6	-6.158	-11.741	-21.488	-29.572
C6	-6.343	-12.018	-21.756	-29.859
D6	-6.444	-12.203	-22.294	-30.714
E6	-6.015	-11.513	-20.930	-28.777
F6	-6.254	-11.895	-21.727	-29.840
A7	-6.097	-11.611	-21.212	-29.160
B7	-6.149	-11.723	-21.416	-29.649
C7	-6.370	-12.127	-22.161	-30.529
D7	-6.216	-11.762	-21.319	-29.380
E7	-5.941	-11.333	-20.680	-28.603
F7	-6.124	-11.650	-21.187	-29.089
A8	-5.953	-11.351	-20.768	-28.679
B8	-6.003	-11.457	-21.006	-29.068
C8	-6.035	-11.478	-20.917	-28.762
D8	-6.091	-11.637	-21.309	-29.466
E8	-5.836	-11.169	-20.532	-28.503
F8	-6.124	-11.663	-21.286	-29.323
A9	-6.299	-12.009	-21.947	-30.289
B9	-6.267	-11.941	-21.815	-30.066
C9	-6.391	-12.155	-22.155	-30.486
D9	-6.225	-11.865	-21.631	-29.764
E9	-6.224	-11.876	-21.733	-30.000
F9	-6.239	-11.890	-21.690	-29.872

Appendix III

Results from Laser Doppler Measurements

Volunteer 1

Newton	0	0.5	1	1.5	2	2.5
1	13.3	5.3	5.4	3.1	2.4	1.8
2	11.1	5.9	5.2	3.1	2.5	2.1
3	16.7	6.5	5.6	3.5	2.8	1.7
4	14.1	6.6	6	2.9	2.6	1.9
5	13	6.8	5.3	3.2	2.7	1.7
6	14.2	7	5.1	2.8	2.3	1.8
7	7	7.8	5.3	3.2	2.3	1.9
8	11.5	6.6	5.8	3	2.5	2.2
9	9.3	6.5	5.2	3.5	2.3	1.8
Average	12.357	6.557	5.400	3.143	2.471	1.857

Volunteer 2

Newton	0	0.5	1	1.5	2	2.5
1	104	31.4	37.9	9	11.9	6.8
2	107	41.6	16.6	9.4	6	7.9
3	105	37.7	15.6	13.8	5.7	7.3
4	102	28.4	17.8	10.9	8.1	6.8
5	40.8	28.2	16	12.5	6.2	7.5
6	87.3	36.2	15.5	45.7	6.3	8.3
7	104	33.8	13.7	25.7	5.6	6.1
8	105	38.1	16	15.9	6.7	6.9
9	107	45.2	21	16.2	6	7.7
Average	100.723	35.314	16.929	14.914	6.429	7.271

Volunteer 3

Newton	0	0.5	1	1.5	2	2.5
1	76	62.7	79.2	19.1	16.8	8.2
2	79.7	49.4	44.2	33.5	13.2	12.3
3	75	56.9	36.7	47.4	32.2	5.5
4	73.7	72.7	43.5	31	25.5	7.3
5	71.7	45.2	38.9	24.8	25.2	6.2
6	74	54.9	37	22.7	22.8	9.3
7	73.7	61.2	43.4	33.9	27.1	9.6

8	71.8	51.2	41	27.8	19.1	6.2
9	72.2	66.8	57.5	31.1	14	7.2
Average	73.482	57.586	43.643	29.257	21.500	7.714

Appendix IV

A Selection of Publications Resulting from this Project

- **Book Chapter**
    - o **"The Effects of Pressure and Friction to skin"** Fleming L., Leung P. H. 2018 In Press
- **Journal Article**
    - o **"Development of a Model to Demonstrate the Effects of Friction and Pressure on Skin in Relation to Pressure Ulcer Formation**" Leung, P. H., Fleming, L., Walton, K., Barrans, S. & Ousey, K. 15 Apr 2017 In: Wear. 376-377, Part A, p. 266-271 6 p. ISSN 0043-1648
    - o **"Finite Element Analysis to model ischemia experienced in the development of device related pressure ulcers**" Leung, I. P. H., Fleming, L. T., Walton, K., Barrans, S. M., & Ousey, K. (2019) *Proceedings of the Institution of Mechanical Engineers, Part H: Journal of Engineering in Medicine, 233*(7), 745-753. doi:10.1177/0954411919851387
- **Conference Podium Presentation**
    - o **"Development of a Model to Demonstrate the Effects of Friction and Pressure on Skin in Relation to Pressure Ulcer Formation**" Leung, P. H., Fleming, L., Walton, K., Barrans, S. & Ousey, K. 26- 30 Mar 2017, Wear of Material 2017: 21st International Conference on Wear of Materials, Hilton Long Beach, California, USA
    - o **"Metrology Strategies for Use as an Evidence Base in Device Evaluations**" Leung, P. H., Fleming, L. T. 21 Jun 2017, 1st Wound Care: From Innovations to Clinical Trails, Manchester, UK
    - o **"Standardising Surfaces Evaluations**" Fleming, L. T., Leung, P. H., 11-12 Sep 2017, Stryker Pressure Care Symposium, Nottingham, UK
- **Conference Poster Presentation**
    - o **"The Needs of Having a Standardised Procedures for Surface Measurement**" Leung, P. H., Fleming, L., Ousey, K., 20-22 Sept 2017, EPUAP the 19th Annual Meeting of the European Pressure Ulcer Advisory Panel, Belfast, Northern Ireland.

Development of a model to demonstrate the effects of friction and pressure on skin in relation to pressure ulcer formation

Isaac P.H. Leung [a,*], Leigh Fleming [a], Karl Walton [a], Simon Barrans [c], Karen Ousey [b]

[a] Centre for Precision Technology, University of Huddersfield, UK
[b] Institute of Skin Integrity and Infection Prevention, University of Huddersfield, UK
[c] Turbocharger Research Institute, University of Huddersfield, UK

ARTICLE INFO

ABSTRACT

Pressure ulcers are a common injury of the skin which leads to pain and potential infection for patients and financial burden to the healthcare providers across the global due to treatment costs, litigation and extended hospital stays. The current study focuses on one of the causes of pressure ulcer formation, ischemia. Blood vessels are deemed to be deformed and blood flow restricted when skin is subjected to external mechanical loads including friction, pressure and the combination of both. Hence, normal oxygen delivery to cells or metabolic waste removal are locally stopped which causes cells deaths and ultimately pressure ulcers.

The current study proposes a 3D finite element analysis model which is capable of demonstrating the effect of friction, pressure and the combination of both to the deformation of blood vessels. The results of simulation suggested that applied pressure collapsed the blood vessels while friction opened up the blood vessels. However, as a combination effect of pressure and friction, the cross-sectional areas of blood vessels were reduced significantly. This model is clinically and physiologically relevant in terms of loading regime and blood vessels structures. The model with further development can be adopted to be an effective tool to evaluate the effects of medical devices to the possibility of pressure ulcer formation.

© 2017 The Authors. Published by Elsevier B.V. This is an open access article under the CC BY license (http://creativecommons.org/licenses/by/4.0/).

1. Introduction

The aim of the study is to develop a Finite element analysis (FEA) model to predict the effect of friction and pressure on skin in relation to pressure ulcer (PU) formation. There are two main reasons which are known to increase the possibility of PU formation; ischemia and excessive amounts of internal strain resulting in deep tissue injury [1,2]. The current study focuses on the condition of ischemia resulting from external friction and pressure. Skin and soft tissue becomes distorted when external friction and/ or pressure are applied to skin surface, this results in compression of the blood vessels. This phenomenon has a physiological effect restricting blood flow, with the restriction in blood flow, perfusion of oxygen is limited and removal of metabolic waste is inhibited which leads to cells death in the affected area resulting in ischemia followed by PU formation [3,4]. The proposed model in the current study demonstrates the effect of friction and pressure to the reduction of cross-sectional areas of blood vessels in the different layers of skin including the dermis and hypodermis. This initial model is simplified and the skin is modelled to be isotropic and non-viscoelastic. These initial simplified models are clinically and biologically relevant in terms of skin and blood vessels structures. The loading conditions have been developed by conducting pressure mapping of support surfaces with healthy volunteers in a clinical setting to ensure validity of the loading regimes used. It is proposed that this model with further development could be used to predict the effects of medical devices on the change in blood vessel dimensions whilst indicating the probability of PU formation.

Skin is the biggest organ and often not given the attention that it deserves as one of the most important. It serves to protect the internal organs, prohibit external hazards affecting the body, regulate temperature and absorb shocks. The stratum corneum, epidermis, dermis and hypodermis/ subcutaneous fat are the key layers of the skin Fig. 1. Each of these layers is unique, with different mechanical properties and varying distribution and configuration of blood vessels. This versatile organ can be subjected to various injuries and trauma, one severe instance which causes loss of integrity in the skin as a barrier to bacteria and infection is pressure Ulcers (PU) and friction blister formation.

Pressure ulcers are a skin injury that used to be labelled as "bedsores" or "pressure sores". They can be just a minor

* Corresponding author.
E-mail address: pakhung.leung@hud.ac.uk (I.P.H. Leung).

Finite element analysis to model ischemia experienced in the development of device related pressure ulcers

Isaac PH Leung[1], Leigh T Fleming[2], Karl Walton[1], Simon M Barrans[3] and Karen Ousey[4]

Abstract

Pressure ulcers are a common occurrence of damage to skin. Severity ranges from slightly discoloured skin to full thickness tissue damage which can be fatal in some cases. Engineering effort, typically developing computational models had made significant progress in the understanding and demonstration of the formation mechanism of pressure ulcers with the aetiology of excessive stress; however, relatively limited attempts had been made to develop relevant models for pressure ulcers caused by ischemia. The aim of this article is to present evidence of a computational model developed to simulate ischemic pressure ulcer formation and demonstrate the established relationship between the computational data and the acquired clinically relevant experimental data by utilising Laser Doppler Velocimetry. The application of the presented computational model and the established relationship allows the evaluation of the effect of a mechanical loading to the cutaneous blood flow velocity which is a step closer to understand and evaluate a mechanical load to the formation of pressure ulcers caused by ischemia.

Introduction

Skin is a large and multifunctional organ of human body which acts as a barrier to prevent harmful pathogens and chemicals from entering the body; it regulates body temperature, and also absorbs shock.[1] A pressure ulcer (PU) can be described as localised skin damage which is a significant, health risk to patients, in most serious cases can be fatal through complications such as infection due to loss of skin integrity as a barrier and in most occurrences reduces the quality of life outcomes for patients. There is also a serious financial burden to health care providers and funding bodies. A PU is officially defined as follows:

> A PU is localised damage to the skin and/or underlying tissue, usually over a bony prominence (or related to a medical or other device), resulting from sustained pressure (including pressure associated with shear). The damage can be present as intact skin or an open ulcer and may be painful. (NHSi, 2018)[2]

The financial and social burden of pressure ulceration is a global challenge, with the Department of Health & Human Services of the United States, stating there are 2.5 million patients suffering from PUs and 60,000 patients dead as a direct result of a PU with more than 17,000 lawsuits which are PU related each year.[3] The prevalence rate of PUs for 186,000 patients from a range of healthcare settings in one large cohort study was reported as 4.36% from July 2017 to July 2018 (NHS Safety Thermometer).[4] PUs are categorised into four different stages by the wound depth. Category I

[1]Centre for Precision Technologies (CPT), School of Computing and Engineering, University of Huddersfield, Huddersfield, UK
[2]Materials and Engineering Research Institute (MERI), Department of Engineering and Mathematics, Sheffield Hallam University, Sheffield, UK
[3]Turbocharger Research Institute, University of Huddersfield, Huddersfield, UK
[4]Institute of Skin Integrity and Infection Prevention, University of Huddersfield, Huddersfield, UK

Corresponding author:
Isaac PH Leung, Centre for Precision Technologies (CPT), School of Computing and Engineering, University of Huddersfield, Huddersfield HD1 3DH, UK.
Email: P.akhung.leung@hud.ac.uk

Development of a model to demonstrate the effects of friction and pressure on skin in relation to pressure ulcer formation
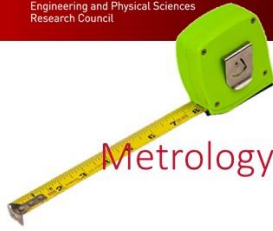
[1]Centre for Precision Technology, University of Huddersfield, UK

[2]Turbocharger Research Institute, University of Huddersfield, UK

[3]Institute of Skin Integrity and Infection Prevention, University of Huddersfield, UK

[1]Isaac Leung, [1]Leigh Fleming, [1]Karl Walton, [2]Simon Barrens, [3]Karen Ousey

"**Metrology Strategies for Use as an Evidence Base in Device Evaluations**" Leung, P. H., Fleming, L. T. 21 Jun 2017, 1st Wound Care: From Innovations to Clinical Trails, Manchester, UK

"**Standardising Surfaces Evaluations**" Fleming, L. T., Leung, P. H., 11-12 Sep 2017, Stryker Pressure Care Symposium, Nottingham, UK

The Needs of Having a Standardised Procedures for Surface Measurement

Isaac Leung, Leigh Fleming, Karen Ousey

Centre for Precision Technology, University of Huddersfield, UK
Institute of Skin Integrity and Infection Prevention, University of Huddersfield, UK

The Future Metrology Hub

Aim:

Standardising the measurement protocol of conducting pressure mapping measurements for mattresses.

Rationale:

There are many devices available reporting to relieve pressure. The standardisation of measurement would allow clinicians and manufacturers to make more reliable comparisons in their decision making process. This study highlights the need for standardisation in measurement practice for pressure care products.

Without Standardisation:

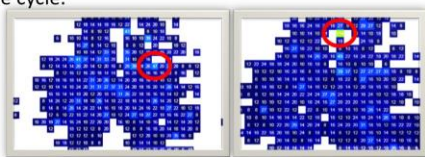The duration for the dynamic mattresses to complete one cycle.

Figure 1 Two pressure mapping results for a dynamic mattress

There was 142% difference between 2 measurements showed in Figure 1. They were conducted with the same mattress, same volunteer, same backrest incline angle but at different instants of the operating cycle.

Current Standardisation Regarding to PU:

✓ Practice guide line from EPUAP and NPUAP
✓ Terminologies from NPUAP (S3I)
✓ PU grading systems from EPUAP and NPUAP

Standardisation for Surface Measurements:

This good practice of pressure evaluation needs to translate to international standards for measurement methodology so there can be comparison of function and performance of pressure care devices.

ISO **BSi British Standards**

Control Variables:

For investigating the function and performance of mattresses alone, factors that need to be considered in order to have comparable, scientific and unbiased measurements.

For Static Mattress
- Volunteers' BMI
- Volunteers' Posture
- Pressure Mapping Equipment
- Multiple Measurements
- Backrest Inclining Angle

For Dynamic Mattress
- All factors for static mattress
- Cycling Duration
- Settling Time
- Operation Mode

With Standardisation and Careful Consideration:

Static Mattress Study

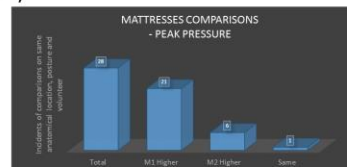A pressure mapping study had been conducted with 2 generations of mattress provided by the same company.

Figure 2 Graph of comparison for 2 mattresses

With careful consideration and standardised measurement procedures, there were 28 valid comparisons. A good percentage of the comparisons indicated that the magnitudes of peak pressure were usually lower on one mattress. **A clear conclusion of lower pressure mattress could be drawn.**

Dynamic Mattress Study

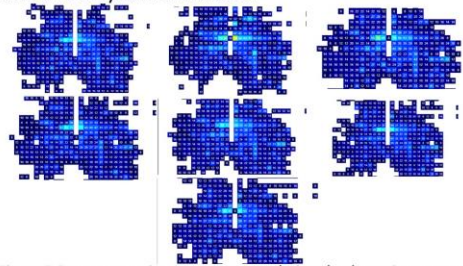Ten measurements were conducted over the cycling period of a dynamic mattress.

Figure 3 Seven successive measurements during the dynamic mattress cycle

Even though the dynamic mattress meant to redistribute the pressure during the operating cycle. It showed in 7 successive measurements that the peak pressure had insignificant change in magnitudes and remained at the same anatomical location. **Measurements were concluded that the dynamic mattress was capable to redistribute the pressure but only to a small extent. Different phenomena can be recognised when measurements were conducted with standardised procedures.**

Acknowledgements

EPSRC Pioneering research and skills **University of HUDDERSFIELD** **The University Of Sheffield.** **Loughborough University** **UNIVERSITY OF BATH**

"**The Needs of Having a Standardised Procedures for Surface Measurement**" Leung, P. H., Fleming, L., Ousey, K., 20-22 Sept 2017, EPUAP the 19th Annual Meeting of the European Pressure Ulcer Advisory Panel, Belfast, Northern Ireland